Acta Biomed. - Vol. 91 - Suppl. 8 - July 2020 | ISSN 0392 - 4203

ACTA BIOMEDICA SUPPLEMENT

ATENEI PARMENSIS | FOUNDED 1887

Official Journal of the Society of Medicine and Natural Sciences of Parma and Centre on health systems' organization, quality and sustainability, Parma, Italy

The Acta Biomedica is indexed by Index Medicus / Medline Excerpta Medica (EMBASE), the Elsevier BioBASE, Scopus (Elsevier) and Bibliovigilance

Diagnostic and Interventional Radiology: an update

Guest Editors: Andrea Giovagnoni, Chiara Floridi, Marina Carotti

Free on-line www.actabiomedica.it

Mattioli 1885

Pubblicazione trimestrale - Poste Italiane s.p.a. - Sped. in A.P. - D.L. 353/2003 (conv. in L. 27/02/2004 n. 46) art. 1, comma 1, DCB Parma - Finito di stampare Ju2y 2020

Acta Bio Medica

Atenei parmensis
founded 1887

Official journal of the Society of Medicine and Natural Sciences of Parma and Centre on Health System's Organization, Quality and Sustainability, Parma, Italy

free on-line: www.actabiomedica.it

EDITORIAL OFFICE MANAGER
Valeria Ceci
Mattioli 1885 srl - Casa Editrice
Strada di Lodesana 649/sx, Loc. Vaio
43036 Fidenza (PR), Italy
Tel. ++39 0524 530383
Fax ++39 0524 82537
contact@actabiomedica.it

Francesco Covino
Società di Medicina e Scienze Naturali
Azienda Ospedaliero-Universitaria
di Parma - Cattani Building, 2nd floor
Via Gramsci, 14 - Parma, Italy
Tel./Fax ++39 0521 033730
francesco.covino@unipr.it

PUBLISHER
Mattioli 1885 srl Casa Editrice
Strada di Lodesana, 649/sx, Loc. Vaio
43036 Fidenza (PR), Italy
Tel. ++39 0524 530383
Fax ++39 0524 82537
E-mail: edit@mattioli1885.com

Mattioli 1885
srl- Strada di Lodesana 649/sx
43036 Fidenza (Parma)
tel 0524/530383
fax 0524/82537
www.mattioli1885.com

Index

Volume 91 / Suppl. 8 July 2020

Acta Biomed 2020; Vol. 91, Supplement 8: 5-8 DOI: 10.23750/abm.v91i8-S.9995

Editorial

Diagnostic and interventional radiology: an update

Andrea Giovagnoni[1], *Massimo De Filippo*[2], *Antonio Barile*[3]

[1] Department of Clinical, Special and Dental Sciences, University Politecnica delle Marche, Ancona, AN, Italy; [2] Department of Medicine and Surgery (DiMec), Section of Radiology, University of Parma, Maggiore Hospital, Parma, Italy; [3] Department of Biotechnology and Applied Clinical Sciences, University of L'Aquila, L'Aquila, Italy

In recent years, radiology has undergone revolutionary changes in all aspects of the discipline (1-10). The progressive and rapid innovation of technology has led on the one hand to ever more significant and new applications in the diagnostic field; on the other hand, it has opened up to interventional radiology therapeutic possibilities that are radically changing the clinical approach to numerous pathologies (11-15). Furthermore, the advent of artificial intelligence is unveiling a new scenario with which the radiologist of the future will have to confront, and which will undoubtedly lead to important implications in the conception of radiology (16-18). In this context of innovation, the clinical and - above all - global approach of radiology remains fundamental (19-21); it is for this reason that with this Special Issue entitled "Diagnostic and interventional radiology: an update" we wanted to deal with some focuses that summarized the foundations of diagnostic and interventional radiology topics in light of the relative "state of the art".

In the first part of the volume, dedicated to abdominal imaging (22-24), the first two articles, "Hepatic tumors: pitfalls in diagnostic imaging" and "The role of imaging in surgical planning for liver resection" represent a guide to the radiologist who have to integrate the different and multimodal diagnostic techniques, to confront and being a point of reference for the clinicians and the surgeons in the patient's therapeutic management (25-27).

The third article by Reginelli et al., "MRI of perianal fistulas in Chron's disease", also deals with a very frequent pathology, for which a precise and therapy-oriented imaging diagnosis is fundamental. In particular, the authors provide valuable notions of anatomy and study technique, essential for the formulation of an exhaustive diagnosis (28).

Another contribution by Reginelli et al., "Extranodal lymphomas: a pictorial review for CT and MRI classification", focuses on the study of the imaging classification of a pathology in which staging and treatment are primarily clinical, but supported by careful imaging study.

In the second section, we focused on thoracic and cardiovascular radiology topics (29-31). The article "Anterior chest wall non-traumatic diseases: a road map for the radiologist" is an accurate focus on the pathology of the chest wall, a topic for which the radiologist can often find difficulties about the information to provide to the clinician, and for which knowledge of anatomy and possible pathological pictures is of fundamental importance.

Following the recent tragic pandemic outbreak of Coronavirus pneumonia, Floridi et al. discuss, with a "practical guide", the fundamental role of diagnostic imaging in the approach and management of patients with COVID-19.

The last article of the thoracic section is the contribution of Pradella et al., "Masses in right side of the heart: spectrum of imaging findings", dedicated to cardiac radiology, in which the authors provide an overview of the radiological characteristics - either with coronary CT and with cardiac MRI – of cardiac tumors and masses.

The next section is dedicated to the great chapter of interventional radiology, of which we have collected some insights. The work by Ierardi et al., "Basic em-

bolization techniques: tips and tricks" is a handy guide to the interventional radiologist, more or less expert, providing practical indications on the techniques and materials for one of the leading and most crucial interventional radiology endovascular procedures (32).

Another technique for which interventional radiology has become a fundamental prerogative is biopsy. Pagnini et al. discuss about it in their contribution "Imaging guided percutaneous renal biopsy", underlining the importance of the knowledge of imaging in such a demanding approach as that of renal biopsy.

Turning to extravascular interventional neuroradiology, Negro et al., in their article "Predictive factors of volumetric reduction in lumbar disc herniation treated by O2-O3 chemiodiscolysis", present an original study dealing with a popular, effective and minimally invasive technique for the treatment of low back pain (33, 34).

The recent innovations applied to diagnostic and interventional radiology have led to significant changes also in the field of musculoskeletal radiology (35-39). In the article "Advanced diagnostic imaging and intervention in tendon diseases", Bruno et al. describe the application of advanced MRI and US techniques in the study of degenerative tendon pathology, together with the description of the main imaging-guided interventional techniques (40).

More focused on diagnostics, the contribution of Acanfora et al. on the spectrum of synovial pathology describes the most frequent inflammatory, degenerative, and pseudotumoral pathology (41, 42).

Dual-energy technology in CT imaging has been introduced recently (43); one of the most interesting and useful applications is the study of joint gouty crystals, described by Carotti et al. in the work "Clinical utility of Dual energy Computed Tomography in gout: current concepts and applications".

The last two articles of the volume are dedicated to neuroradiology (44-48). The contribution of Palumbo et al. is a comprehensive review of the clinical, diagnostic, and therapeutic features of spondylodiscitis. In the article "Diagnosis and management of intralabyrinthine schwannoma: case series and review of the literature", Di Lullo et al. integrate the clinical and imaging aspects of this pathology, with the consequent implications in therapeutic management.

Despite the difficulty in the exhaustive treatment of such vast and complex topics, we believe that the proposed works can be essential and useful targeted insights for radiologists of different subspecialties.

A heartfelt thanks to all the authors who made the realization of this project possible.

Conflict of interest: Authors declare that they have no commercial associations (e.g. consultancies, stock ownership, equity interest, patent/licensing arrangement etc.) that might pose a conflict of interest in connection with the submitted article.

References

1. Barile A, Bruno F, Arrigoni F, et al. Emergency and Trauma of the Ankle. Semin Musculoskelet Radiol 2017; 21: 282- 89.
2. Barile A, Conti L, Lanni G, et al. Evaluation of medial meniscus tears and meniscal stability: weight-bearing MRI vs arthroscopy. Eur J Radiol 2013; 82(4): 633-9.
3. Floridi C, Radaelli A, Pesapane F, et al. Clinical impact of cone beam computed tomography on iterative treatment planning during ultrasound-guided percutaneous ablation of liver malignancies. Medical oncology 2017; 34: art n° 113
4. Di Geso L, Zardi EM, Afeltra A, et al. Comparison between conventional and automated software-guided ultrasound assessment of bilateral common carotids intima-media thickness in patients with rheumatic diseases. Clin Rheumatol 2012; 31: 881-4.
5. Manetta R, Palumbo P, Gianneramo C, et al. Correlation between ADC values and Gleason score in evaluation of prostate cancer: multicentre experience and review of the literature. Gland Surg 2019; 8: S216-s22.
6. Cortellini A, Bozzetti F, Palumbo P, et al. Weighing the role of skeletal muscle mass and muscle density in cancer patients receiving PD-1/PD-L1 checkpoint inhibitors: a multicenter real-life study. Sci Rep 2020; 10: 1456.
7. Mungai F, Pasquinelli F, Mazzoni LN, et al. Diffusion-weighted magnetic resonance imaging in the prediction and assessment of chemotherapy outcome in liver metastases. Radiol Med 2014; 119: 625-33
8. Agostini A, Kircher MF, Do R, et al. Magnetic Resonance Imaging of the Liver (Including Biliary Contrast Agents) Part 1: Technical Considerations and Contrast Materials. Seminars in roentgenology 2016; 51: 308-316
9. Salvati F, Rossi F, Limbucci N, et al. Mucoid metaplastic-degeneration of anterior cruciate ligament. The Journal of sports medicine and physical fitness 2008; 48: 483-487.
10. Barile A, Bruno F, Mariani S, et al. What can be seen after rotator cuff repair: a brief review of diagnostic imaging findings. Musculoskelet Surg 2017; 101: (Suppl1): 3-14
11. Masciocchi C, Arrigoni F, Ferrari F, et al. Uterine fibroid therapy using interventional radiology mini-invasive treatments: current perspective. Med Oncol 2017; 34: 52.

12. Zoccali C, Rossi B, Zoccali G, et al. A new technique for biopsy of soft tissue neoplasms: a preliminary experience using MRI to evaluate bleeding. Minerva Med 2015; 106: 117-120.
13. Carrafiello G, D'Ambrosio A, Mangini M, et al. Percutaneous cholecystostomy as the sole treatment in critically ill and elderly patients. Radiol Med 2012; 117: 772-9.
14. Ierardi AM, Tsetis D, Ioannou C, et al. Ultra-low profil polymer-filled stent graft for abdominal aortic aneurysm treatment: a two-year follow-up. Radiol Med 2015; 120: 542-8.
15. Dialetto G, Reginelli A, Cerrato M, et al. Endovascular stent graft treatment of thoracic aortic syndromes: a 7-year experience. European journal of radiology 2007; 64 (1): 65-72.
16. Nardone V, Reginelli A, Guida C, et al. Delta-radiomics increases multicentre reproducibility: a phantom study. Med Oncol 2020; 37: 38.
17. Grassi R, Miele V, Giovagnoni A. Artificial intelligence: a challenge for third millennium radiologist. Radiol Med 2019; 124: 241-42.
18. Neri, E., Coppola, F., Miele, V. et al. Artificial intelligence: Who is responsible for the diagnosis?. Radiol med 2020 125, 517–521
19. Mariani S, La Marra A, Arrigoni F, et al. Dynamic measurement of patello-femoral joint alignment using weight-bearing magnetic resonance imaging (WB-MRI). European journal of radiology 2015; 84: 2571-8
20. Scaglione M, Salvolini L, Casciani E, Giovagnoni A, Mazzei MA, Volterrani L. The many faces of aortic dissections: Beware of unusual presentations. Eur J Radiol 2008;65: 359-64.
21. Mascalchi M, Maddau C, Sali L, et al. Circulating tumor cells and microemboli can differentiate malignant and benign pulmonary lesions. Journal of Cancer 2017; 8: 2223-2230.
22. Pinto A, Lanza C, Pinto F, et al. Role of plain radiography in the assessment of ingested foreign bodies in the pediatric patients. Semin Ultrasound CT MR 2015; 36: 21-7.
23. Reginelli A, Capasso R, Ciccone V, et al. Usefulness of triphasic CT aortic angiography in acute and surveillance: Our experience in the assessment of acute aortic dissection and endoleak. Int J Surg 2016; 33 Suppl 1: S76-84
24. Reginelli A, Russo A, Iasiello F, et al. [Role of diagnostic imaging in the diagnosis of acute appendicitis: a comparison between ultrasound and computed tomography]. Recenti Prog Med 2013; 104: 597-600.
25. Panfili E, Nicolini D, Polverini V, Agostini A, Vivarelli M, Giovagnoni A. Importance of radiological detection of early pulmonary acute complications of liver transplantation: analysis of 259 cases. Radiol Med 2015; 120: 413-20.
26. Borgheresi A, Gonzalez-Aguirre A, Brown KT, et al. Does Enhancement or Perfusion on Preprocedure CT Predict Outcomes After Embolization of Hepatocellular Carcinoma? Acad Radiol 2018; 25: 1588-94.
27. Mungai F, Pasquinelli F, Mazzoni LN, et al. Diffusion-weighted magnetic resonance imaging in the prediction and assessment of chemotherapy outcome in liver metastases. Radiol Med 2014; 119: 625-33.
28. Iacobellis F, Berritto D, Fleischmann D, et al. CT findings in acute, subacute, and chronic ischemic colitis: suggestions for diagnosis. Biomed Res Int 2014; 2014: 895248.
29. Agliata G, Schicchi N, Agostini A, et al. Radiation exposure related to cardiovascular CT examination: comparison between conventional 64-MDCT and third-generation dualsource MDCT. Radiol Med 2019; 124: 753-61.
30. Di Cesare E, Patriarca L, Panebianco L, et al. Coronary computed tomography angiography in the evaluation of intermediate risk asymptomatic individuals. Radiol Med 2018; 123: 686-94.
31. Pescarolo M, Sverzellati N, Verduri A, et al. How much do GOLD stages reflect CT abnormalities in COPD patients? Radiol Med 2008; 113: 817-29.
32. Ierardi AM, Piacentino F, Fontana F, et al. The role of endovascular treatment of pelvic fracture bleeding in emergency settings. Eur Radiol 2015; 25: 1854-64.
33. Perri M, Grattacaso G, di Tunno V, et al. T2 shine-through phenomena in diffusion-weighted MR imaging of lumbar discs after oxygen-ozone discolysis: a randomized, double-blind trial with steroid and O2-O3 discolysis versus steroid only. Radiol Med 2015; 120: 941-50.
34. Patriarca L, Letteriello M, Di Cesare E, Barile A, Gallucci M, Splendiani A. Does evaluator experience have an impact on the diagnosis of lumbar spine instability in dynamic MRI? Interobserver agreement study. Neuroradiol J 2015; 28: 341-6.
35. Masciocchi C, Arrigoni F, La Marra A, Mariani S, Zugaro L, Barile A. Treatment of focal benign lesions of the bone: MRgFUS and RFA. Br J Radiol 2016; 89: 20150356.
36. Zoccali C, Arrigoni F, Mariani S, Bruno F, Barile A, Masciocchi C. An unusual localization of chondroblastoma: The triradiate cartilage; from a case report a reconstructive technique proposal with imaging evolution. J Clin Orthop Trauma 2017; 8: S48-s52.
37. De Filippo M, Pesce A, Barile A, et al. Imaging of postoperative shoulder instability. Musculoskelet Surg 2017; 101: 15-22.
38. Pogliacomi F, De Filippo M, Paraskevopoulos A, Alesci M, Marenghi P, Ceccarelli F. Mini-incision direct lateral approach versus anterior mini-invasive approach in total hip replacement: results 1 year after surgery. Acta Biomed 2012; 83: 114-21.
39. Barile A, Arrigoni F, Bruno F, et al. Present role and future perspectives of interventional radiology in the treatment of painful bone lesions. Future Oncol 2018; 14: 2945-55.
40. Arrigoni F, Napoli A, Bazzocchi A, et al. Magnetic-resonance- guided focused ultrasound treatment of non-spinal osteoid osteoma in children: multicentre experience. Pediatr Radiol 2019; 49: 1209-16.
41. Carotti M, Salaffi F, Di Carlo M, Giovagnoni A. Relationship between magnetic resonance imaging findings, radiological grading, psychological distress and pain in patients with symptomatic knee osteoarthritis. Radiol Med 2017; 122: 934-43.

42. Bruno F, Arrigoni F, Palumbo P, et al. New advances in MRI diagnosis of degenerative osteoarthropathy of the peripheral joints. Radiol Med 2019; 124: 1121-27.
43. Agostini A, Mari A, Lanza C, et al. Trends in radiation dose and image quality for pediatric patients with a multidetector CT and a third-generation dual-source dual-energy CT. Radiol Med 2019; 124: 745-52.
44. Paonessa A, Limbucci N, Tozzi E, et al. Radiological strategy in acute stroke in children. Eur J Radiol 2010; 74: 77-85
45. Tamburrini S, Solazzo A, Sagnelli A, et al. Amyotrophic lateral sclerosis: sonographic evaluation of dysphagia. Radiol Med 2010; 115: 784-93.
46. Varrassi M, Cobianchi Bellisari F, Bruno F, et al. High-resolution magnetic resonance imaging at 3T of pituitary gland: advantages and pitfalls. Gland Surg 2019; 8: S208-s15.
47. D'Orazio F, Splendiani A, Gallucci M. 320-Row Detector Dynamic 4D-CTA for the Assessment of Brain and Spinal Cord Vascular Shunting Malformations. A Technical Note. Neuroradiol J 2014; 27: 710-7.
48. Scoccianti S, Simontacchi G, Greto D, et al. Dosimetric Predictors of Acute and Chronic Alopecia in Primary Brain Cancer Patients Treated With Volumetric Modulated Arc Therapy. Front Oncol 2020; 10: 467.
49. Michelini G, Corridore A, Torlone S, et al. Dynamic MRI in the evaluation of the spine: state of the art. Acta Biomed 2018; 89: 89-101
50. Perri M, Grattacaso G, Di Tunno V, et al. MRI DWI/ADC signal predicts shrinkage of lumbar disc herniation after O2- O3 discolysis. Neuroradiol J 2015; 28: 198-204
51. Splendiani A, Bruno F, Patriarca L, et al. Thoracic spine trauma: advanced imaging modality. Radiol Med 2016; 121: 780-92.

Received: 20 May
Accepted: 10 June
Correspondence:
Antonio Barile
Department of Biotechnology and Applied Clinical Sciences, University of L'Aquila, L'Aquila, Italy
Via Vetoio 1, 67100 – L'Aquila, Italy
E-mail: antonio.barile@univaq.it

Acta Biomed 2020; Vol. 91, Supplement 8: 9-17 DOI: 10.23750/abm.v91i8-S.9969

Review

Hepatic tumors: pitfalls in diagnostic imaging

Giulia Grazzini[1], Diletta Cozzi[1], Federica Flammia[1], Roberta Grassi[2], Andrea Agostini[3,4], Maria Paola Belfiore[2], Alessandra Borgheresi[4], Maria Antonietta Mazzei[5], Chiara Floridi[3,4], Gianpaolo Carrafiello[6], Andrea Giovagnoni[3,4], Silvia Pradella[1], Vittorio Miele[1]

[1] Department of Radiology, Careggi University Hospital, Florence, Italy; [2] Department of Precision Medicine, University of Campania "L. Vanvitelli", Naples, Italy; [3] Department of Clinical, Special and Dental Sciences, University Politecnica delle Marche, Ancona, Italy; [4] Division of Special and Pediatric Radiology, Department of Radiology, University Hospital "Umberto I - Lancisi - Salesi", Ancona, Italy; [5] Unit of Diagnostic Imaging, Department of Medical, Surgical and Neuro Sciences and of Radiological Sciences, University of Siena, Azienda Ospedaliero-Universitaria Senese, Siena, Italy; [6] Radiology Department, Fondazione IRCCS Cà Granda, Ospedale Maggiore Policlinico, Milan, Italy

Summary. On computed tomography (CT) and magnetic resonance imaging (MRI), hepatocellular tumors are characterized based on typical imaging findings. However, hepatocellular adenoma, focal nodular hyperplasia, and hepatocellular carcinoma can show uncommon appearances at CT and MRI, which may lead to diagnostic challenges. When assessing focal hepatic lesions, radiologists need to be aware of these atypical imaging findings to avoid misdiagnoses that can alter the management plan. The purpose of this review is to illustrate a variety of pitfalls and atypical features of hepatocellular tumors that can lead to misinterpretations providing specific clues to the correct diagnoses. (www.actabiomedica.it)

Keywords: CT, MRI, hepatocellular tumors, hepatocellular adenoma, focal nodular hyperplasia, hepatocellular carcinoma

Introduction

According to the classification of hepatocellular nodules by the International Working Party in 1995 and further elaboration by the International Consensus Group for Hepatocellular Neoplasia in 2009, hepatocellular nodules are divided into regenerative lesions including focal nodular hyperplasia (FNH), and dysplastic or neoplastic lesions, which comprise hepatocellular adenoma (HCA), dysplastic nodule (DN), and hepatocellular carcinoma (HCC) (1). Diagnostic imaging is a fundamental step for characterizing a wide range of pathologies (2-12), and in the abdominal field, we can take advantage of a multiparametric assessment through ultrasound, computed tomography (CT) and magnetic resonance imaging (MRI) (13-21). Typical imaging features of hepatocellular nodular lesions are well known (22). However, FNH, HCA, and HCC can show unusual findings or share an overlap in radiological characteristics leading to diagnostic challenges. Differentiation of benign from malignant lesions is essential for an appropriate management plan (23-25).

In this review, we profile both typical and atypical imaging features of hepatocellular tumors on CT and MRI for being aware of radiologic pitfalls and for achieving the correct diagnosis.

Focal Nodular Hyperplasia

FNH is the most common benign hepatocellular lesion (up to 8% of all liver neoplasms), occurs primarily in women of reproductive age (80% of cases), and is often discovered incidentally (26-28). FNH is thought to arise from a vascular anomaly leading to a hyperplastic response with disorganized growth of hepatocytes and bile ducts. As the FNH management is usually

conservative, a definitive diagnosis should be obtained by imaging in order to avoid biopsy. However, atypical imaging FNH presentations can occur so that diagnosis could be a challenge. Typical FNHs are solitary, non-capsulated with a central fibrous scar (53% of FNHs overall), and are usually smaller than 5cm (27). On non-enhanced CT, FNH is usually iso- or hypodense to the adjacent liver parenchyma. Thanks to its multiparametric properties, MRI is highly sensitive and specific for the characterization of focal liver lesions (29). On unenhanced MRI, FNH is typically iso- or moderate hypointense on T1-weighted images and iso- or moderate hyperintense on T2-weighted images (30). The central scar appears as a thin band hypointense on T1 and hyperintense on T2-weighted images **(fig. 1)** (31). On contrast-enhanced CT and MRI, FNHs typically undergo immediate, intense, homogeneous enhancement on arterial phase and enhancement similar to the liver on portal venous and delayed phases **(fig. 1)** (30). The central scar is characterized by a delayed enhancement due to fibrotic content (32, 33).

In literature, the prevalence of atypical FNHs varies from 10% to 50%, and a wide range of atypical imaging findings have been described (26). On T1-weighted images, FNHs can appear hyperintense due to intralesional steatosis, hemorrhage, copper accumulation, or peliosis (26). In 10-37% of cases, FNHs show a pseudocapsule that results from compression of the adjacent hepatic parenchyma leading to differential diagnosis with HCC (26).

The primary differential diagnosis of the typical FNH includes HCA, which demonstrates a similar enhancement pattern. Usually, the diagnosis of FNH or HCA is possible thanks to characteristic lesion features such as the central scar in FNHs or the heterogeneous appearance due to intralesional hemorrhage in HCA (34). However, in up to 50% of cases, FNHs do not exhibit the central scar, especially in lesions smaller than 3cm, and, also, they can occasionally show heterogeneous signal on MRI (35). Therefore, hepatobiliary (HB) contrast-enhanced MRI is mandatory to differentiate FNHs from HCAs. MRI performed with HB contrast agent (the most common are Gd-BOPTA, MultiHance, Bracco, Milan, Italy and Gd-EOB-DTPA, Primovist; Bayer Schering Pharma, Germany) is considered the gold standard in imaging FNH (32, 34). Furlan A. et al., in their study on FNHs occurred after chemotherapy treatment, demonstrated that typical MRI

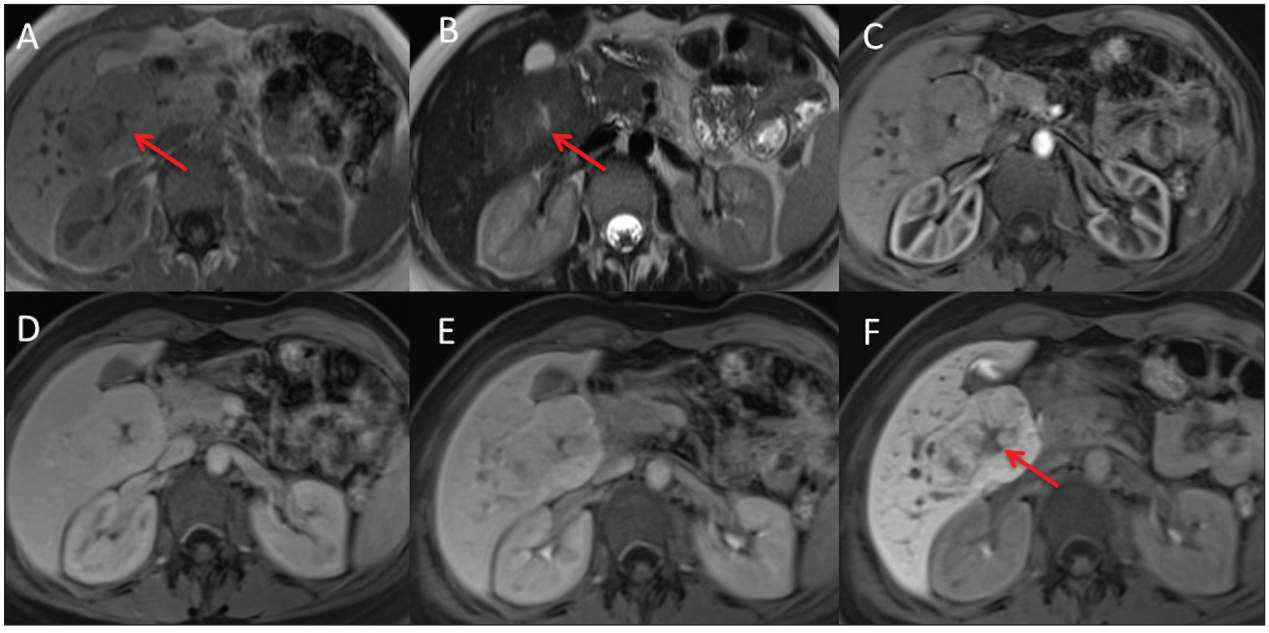

Figure 1. FNH with the central scar on Gd-EOB-DTPA-enhanced MRI. The typical FNH shows a central scar (arrows) that appears as a hypointense band on T1 (A) and hyperintense on T2-weighted images (B). On contrast-enhanced MRI, FNH undergoes immediate enhancement on arterial phase (C) and enhancement similar to the liver on portal venous and late, delayed phases (D-E). In the hepatocyte phase, FNH shows isointensity with the central scar hypointense (F)

appearance might avoid unnecessary biopsy or surgery (36). A particular finding of FNHs is iso- or hyperintensity in the hepatocyte phase with the central scar hypointense **(fig. 1)** (37, 38). On the contrary, in HCAs, the failure uptake of HB contrast agents on hepatocyte phase leads to hypointensity relative to a background enhanced normal liver parenchyma (34, 35).

The central fibrous scar is not specific for FNH, and other lesions, such as haemangiomas and fibrolamellar HCCs, may show it (32). Fibrolamellar HCC is a variant that usually occurs in young adults without chronic liver disease. The clues to the correct diagnosis of fibrolamellar HCCs are features such as hypointensity of the central scar on both T1- and T2-weighted images and hypointensity on the HB phase, different from FNHs (38).

In the cirrhotic liver, especially in patients with alcoholic cirrhosis or in liver showing hemodynamic changes, such as Budd Chiari syndrome, hyperplastic nodules called FNH- like nodules (FNH-LNs) has been reported. These hypervascular lesions may mimic tumors such as metastasis, HCA, or HCC. FNH-LN can show marked arterial enhancement or a wash-out and capsule appearance on CT or MRI, as HCC dose (39, 40). However, as FNH, FNH-LNs uptake HB contrast agents on hepatocyte phase showing iso- or hyperintensity (39).

Hepatocellular Adenoma

HCA is an uncommon benign tumor (annual incidence of 3-4/100000) that usually affects young females with a history of prolonged oral contraceptive use (41). Recent studies suggest obesity and metabolic syndrome as emerging risk factors for HCA, too (41). HCA is characterized by cords of well-differentiated hepatocytes separated by sinusoids lacking portal triad and interlobular bile ducts (27, 28).

The most common complication of HCA is bleeding with the risk of hemorrhagic rupture, while malignant degeneration occurs in a small subset of HCAs (around 4-5% of HCAs) (27).

According to 2010 WHO classification, four subtypes of HCA are described based on their genetic and pathologic features: inflammatory HCA (I-HCA), hepatocyte nuclear factor (HNF)-1α-inactivated HCA, β-catenin-mutated HCA (β-HCA), and unclassified HCA (U-HCA) (28, 37). These subtypes show noticeable differences in imaging features. The latest 2017 Genotype/Phenotype Classification of HCAs categorized HCAs into eight major subtypes. The four additional subtypes were previously within the U-HCA category, and they have not yet been associated with specific diagnostic imaging features (41).

MRI plays a crucial role in the diagnosis and subtype characterization of HCAs, helping to differentiate HCAs from HCCs and FNHs (41, 42). Bise S. et al. analyzed MRI features of 116 HCAs reporting that MRI can identify up to 88% of the two main HCA subtypes (I-HCA and HNF1α-HCA). However, they demonstrated that MRI cannot classify HCAs when necrotic/hemorrhagic changes cover > 50% of the lesion, HNF1α-HCAs does not show steatosis and when HCA subtype is β-HCA or U-HCAs (43).

Typical imaging findings of HCA are heterogeneous signal intensity on T1- and T2-weighted images and heterogeneous iso or hypodensity on unenhanced CT due to the presence of hemorrhage, necrosis, or intralesional fat **(fig. 2)**. On contrast-enhanced imaging, HCA typically demonstrates moderate to intense enhancement in the arterial phase and prolonged mild enhancement or washing out on the portal venous phase. On hepatocyte phase images of HB contrast-enhanced MRI, HCA typically appears hypointense compared to the adjacent liver parenchyma (35, 38).

I-HCA is the most common subtype representing 30%-50% of HCAs. The hallmark feature for I-HCA is the "atoll sign" on T2-weighted images described as a band of peripheral T2 hyperintense signal. I-HCA may show imaging features that overlap with FNH. They are hypervascular masses that demonstrate intense arterial enhancement with persistent enhancement on portal venous and delayed phases. Different from other adenoma subtypes, on HB phase I-HCAs can appear iso- to hyperintense compared to the background parenchyma probably due to retention of contrast material within dilated intratumoral sinusoids. The clue to differentiate I-HCA from FNH is the signal intensity on the HB phase not as homogeneous as FNH, and often the hyperenhancement is only peripheral (42). T2 signal hyperintensity associated with strong arterial phase enhancement and delayed persistent enhancement on

MRI enable diagnosis of I-HCA with a sensitivity of 85–88% and a specificity of 88–100% (41).

HNF1α-HCA is the second most common subtype, and histologically is characterized by intracellular fat deposition. Therefore, a signal dropout on opposed- compared with in-phase T1-weighted images had a reported sensitivity of 86% and a specificity of 100% for HNF1α-HCA (42).

β-HCA is less common (approximately 10% of all HCAs) and occurs more in men. This subtype has a higher risk of malignant transformation. The imaging features of β-HCA are not specific and mimic HCCs. On contrast-enhanced MRI, β-HCAs demonstrate homogenous or heterogeneous arterial phase hyperenhancement with possible wash-out on portal venous phase. Also, these tumors can show a capsule appearance as HCC. On diffusion-weighted imaging (DWI), the absence of restriction can be useful to distinguish benign lesions from HCC **(fig. 2),** although also HCA could sometimes show restricted diffusion (42). Besides, these tumors can show a vaguely demarcated central scar and appear iso- to hyperintense relative to the liver parenchyma on the HB phase, so that the differential diagnosis from FNH could be a challenge.

Finally, no specific imaging features have been described for unclassified HCA (41, 42).

In conclusion, in the absence of typical features of HCA on MRI, a tumor biopsy should be proposed to rule out malignancy (27).

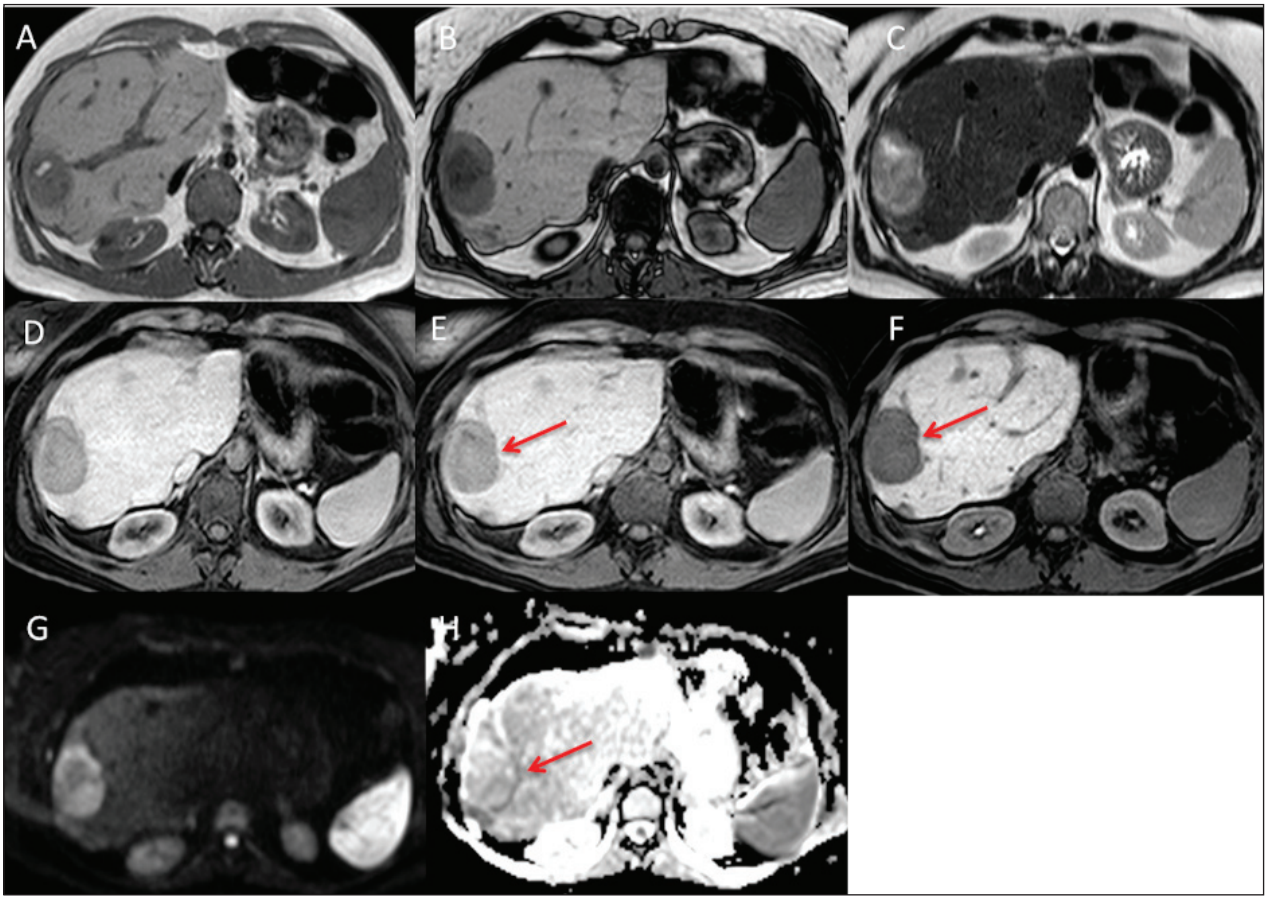

Figure 2. β-HCA on Gd-BOPTA-enhanced MRI. β-HCA shows heterogeneous signal intensity on T1- (A) and T2-weighted (C) with a signal dropout on opposed-phase T1-weighted image (B) due to the presence of hemorrhage and intralesional fat. On contrast-enhanced imaging, β-HCA demonstrates moderate enhancement in the arterial phase (D) and prolonged mild enhancement on the portal venous phase (E). On hepatocyte phase (F), β-HCA appears hypointense compared to the adjacent liver parenchyma. The presence of a capsule appearance (arrows) leads to differential diagnosis from HCC. On DWI (G-H) the absence of diffusion restriction is useful to distinguish β-HCA from HCC

Hepatocellular Carcinoma

HCC is the most common primary hepatic malignant tumor and typically develops in a cirrhotic liver (42, 44). According to international guidelines, including those of the European Association for the Study of the Liver and the American Association for the Study of Liver Disease, HCC can be diagnosed noninvasively using contrast-enhanced CT or MRI based on its typical vascular pattern (37, 45). Imaging modalities also play a fundamental role in guiding interventional radiology procedures, as well as in surgical planning and follow-up (46-57). The hallmark imaging features of HCC are arterial phase hyperenhancement (wash-in) and hypoenhancement on portal or delayed phase images (wash-out) (42, 58, 59). However, approximately 40% of HCC nodules show atypical imaging features, so that diagnosis remains a challenge for radiologists (42).

The typical enhancement pattern of HCCs is due to a multistep process of arterialization of the nodule. During the multistep process of hepatocarcinogenesis, a sequential decrease in the portal blood supply and development of neoangiogenesis with an increase in the hepatic arterial blood supply occurs (58, 60). The imaging features of HCC vary significantly with the histological classification and with the size of the lesion. Typically HCCs are hypointense on T1- weighted images and hyperintense on T2-weighted images. However, early HCCs (defined as a well-differentiated tumor <2 cm in size) can show iso- or hyperintensity on T1-weighted images because of the accumulation of fat, glycoproteins, or copper (42, 60, 61). Large HCCs may have a mosaic pattern with areas of variable signal intensities on T1- and T2-weighted images and heterogeneous enhancement on contrast-enhanced images during the arterial phase (60). Poorly differentiated and undifferentiated HCCs may show a tumor capsule that appears hypointense on both T1- and T2-weighted images. The tumor capsule appears as a peripheral rim enhancement on the portal venous phase that has to be differentiated from arterial rim enhancement, which is common in intrahepatic cholangiocarcinoma (ICC) or metastases from adenocarcinoma (42, 60, 62).

Early HCCs are hypovascular nodule due to decreased portal venous blood supply and insufficient neovascularization. As a result, 10-20% of HCCs do not show typical arterial phase wash-in and are detected only in the portal venous or delayed phase as hypoenhancing nodules **(fig. 3)**. The differential diagnosis of hypovascular HCC from DN is a challenge, but several studies have reported that features as hypointensity on T1-weighted imaging, hyperintensity on T2-weighted imaging, and diffusion restriction on DWI help in distinguishing early HCCs from DNs (42, 58, 63). Several studies have demonstrated that HB contrast agents represent useful tools for the detection and characterization of atypical HCC nodules, such as hypovascular HCC (64). HB contrast agents are transported into the hepatocytes through the molecular transporter organic anion-transporting polypeptide 8 (OATP8) that are downregulated in HCC nodules. Therefore, hypointensity on the HB phase is strongly suggestive of almost all HCCs and some high-grade DNs (58, 64). Recent studies reported that the decreased expression of OATP8 precedes the neoangiogenesis among these nodules demonstrating that hepatobiliary phase imaging improves the diagnosis of HCCs (58). Galia M. et al. analyzed 69 indeterminate hepatocellular nodules demonstrating that hepatobiliary phase hypointensity is weakly associated with

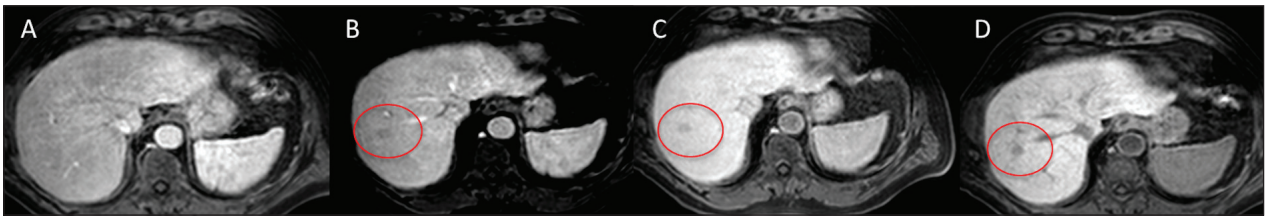

Figure 3. Atypical HCC on Gd-BOPTA-enhanced MRI. Hypovascular HCC does not show typical arterial phase wash-in (A), but it is detected in the portal venous (B) and delayed phase (C) as a hypoenhancing nodule (circle). On the hepatobiliary phase, hypovascular HCC appears hypointense (D)

HCC development (65). In this setting, the Asian Pacific Association for the Study of the Liver and the Korean Liver Cancer Study Group and the National Cancer Center guidelines suggest hypointensity on hepatobiliary phase as an alternative sign to wash-out on the portal venous phase (42). Nevertheless, a minority of HCCs (approximately 5–12%) appears iso or hyperintense relative to background parenchyma in the hepatocyte phase for increased expression of OATP8 in well- or moderately-differentiated lesions (35, 37, 66). Iannicelli E. et al., in their study on 120 suspected hepatic nodules in patients with chronic liver disease, reported two lesions appearing hyperintense in the hepatobiliary phase images; these nodules were well-differentiated HCCs at histological examination (58). Radiologists need to be familiar with this diagnostic pitfall to differentiate atypical HCCs from FNHs (67). The clues to the correct diagnosis of HCCs may be ancillary features such as a hypointense rim on the HB phase and absence of a central scar **(fig. 4)** (42).

When MRI is performed with gadoxetate disodium (Eovist Bayer HealthCare; Primovist, Bayer Schering Pharma) as HB contrast agent, the radiologist must pay attention to the "pseudo-washout" phenomenon (68). When this HB contrast agent is used, hemangiomas appear hypointense compared to the surrounding parenchyma in the equilibrium phase due to rapid contrast uptake by the adjacent normal parenchyma. This is known as the "pseudo-washout" phenomenon and lead to differentiate especially high-flow hemangioma from hypervascular hepatic tumors, such as HCC (68, 69). The keys to differentiate hemangiomas from malignant lesions are very high signal on T2- and heavily T2-weighted images and no restriction on DWI. Finally, the diagnosis can be confirmed with CT or with MRI performed with an extracellular contrast agent (35, 63, 68).

Small HCCs often do not show portal or delayed phase wash-out at dynamic CT or MR images appearing isointense. This atypical enhancement pattern causes difficult differential diagnoses with non-neoplastic arterial-enhancing pseudolesions commonly found in cirrhotic liver, such as arterioportal shunts. DWI and MR hepatobiliary contrast agents may be helpful because arterioportal shunts usually show no diffusion restriction and are isointense on hepatobiliary phase, instead of HCC. The nodule-in-nodule is another atypical radiologic feature of HCC. It is defined as a tumor focus within a high-grade dysplastic nodule. On enhanced CT o MR images, the central HCC focus appears as

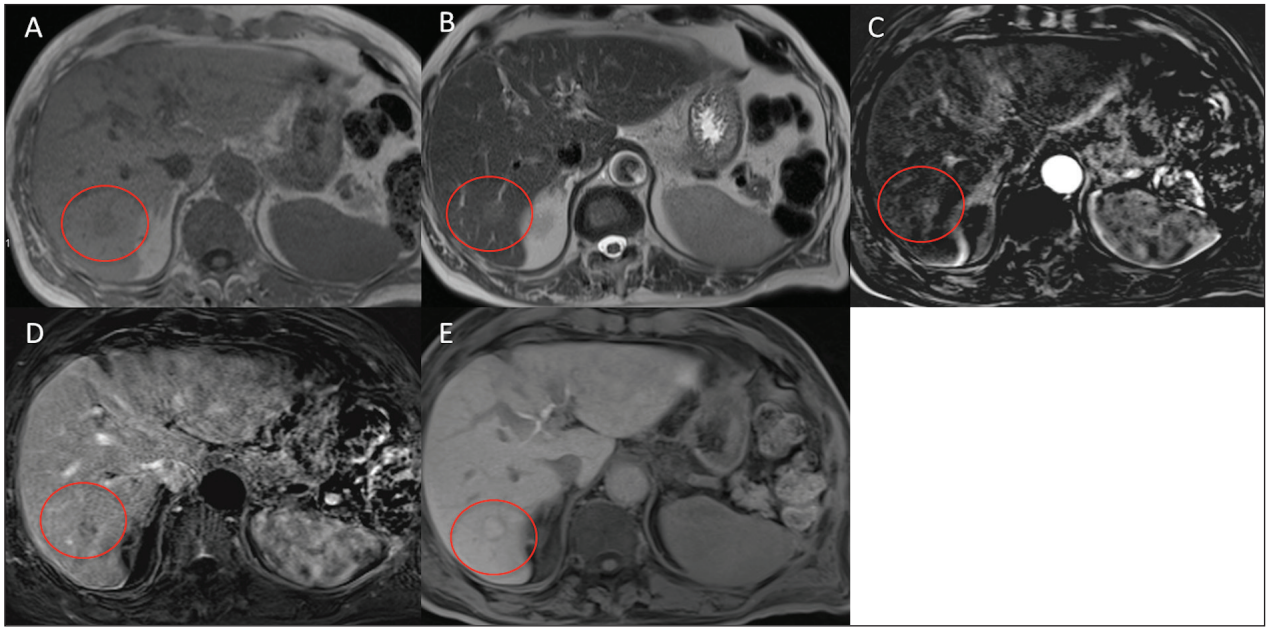

Figure 4. Well-differentiated HCC on Gd-BOPTA-enhanced MRI. HCC (circle) shows a slight hypointensity on T1-weighted image (A), slight hyperintensity on T2-weighted image (B), and typical arterial wash-in (C) and wash-out on portal phase (D). HCC appears hyperintense relative to background parenchyma in the hepatocyte phase (E) with a hypointense peripheral rim

a focus of arterial phase hyperenhancement inside a less enhancing nodule. On T1-weighted images, the background nodule often has a higher signal intensity, while on T2-weighted images the inner focus of HCC is hyperintense. The inner HCC focus shows diffusion restriction on DWI (42, 63).

Approximately 7-13% of HCCs do not appear as a nodule but as a mass with ill-defined and invasive borders, and they are called infiltrative HCCs. Portal vein tumor thrombosis is often a primary imaging feature of these atypical HCCs and can affect the hemodynamics of the tumor so that infiltrative HCCs may not exhibit the hallmark imaging features of wash in and wash-out. In this setting, the correct diagnosis is difficult, and the differential diagnosis should include ICC. Multidisciplinary discussion and laboratory data, such as elevated alpha-fetoprotein levels, may help diagnose infiltrative HCCs correctly (42).

Among the HCC variants, those with targetoid appearance include scirrhous HCCs and large HCCs (≥5 cm) with central necrosis/ischemia. The enhancement pattern of scirrhous HCCs is determined by central fibrosis within the tumor. On dynamic CT and MRI, scirrhous HCCs show peripheral rim enhancement on the arterial phase with a delayed enhancement of the central region. Also, scirrhous HCCs often showed the targetoid appearance on the HB phase, defined as peripheral hypointensity. Therefore, it is critical to differentiate scirrhous HCCs from ICCs characterized by the targetoid appearance on dynamic or HB imaging as well as on DWI. Ancillary features such as heterogeneous hyperintensity with central dark area on T2-weighted images or a capsule are more favorable for scirrhous HCCs in comparison with ICCs. On the contrary, the absence of the wash-out appearance, surface retraction, and presence of bile duct dilatation is helpful features in distinguishing ICCs from scirrhous HCCs. According to the Liver Imaging Reporting and Data System (LI-RADS), hepatic tumors with arterial rim enhancement should be categorized as probably or definitely malignant but not HCC specific, and liver biopsy is warranted for a confirmative diagnosis (42).

In conclusion, a definitive diagnosis of HCC cannot be made with dynamic CT or MRI without the hallmark features. Therefore the majority of international guidelines recommend liver biopsy in atypical HCC nodules larger than 1cm (65).

Conflict of interest: Authors declare that they have no commercial associations (e.g. consultancies, stock ownership, equity interest, patent/licensing arrangement etc.) that might pose a conflict of interest in connection with the submitted article.

References

1. Lo RC, Ng IO. Hepatocellular tumors: immunohistochemical analyses for classification and prognostication. Chin J Cancer Res 2011; 23: 245-53.
2. Mazzei MA, Squitieri NC, Sani E, et al. Differences in perfusion CT parameter values with commercial software upgrades: a preliminary report about algorithm consistency and stability. Acta Radiol 2013; 54: 805-11.
3. Hori M, Murakami T, Kim T, Tomoda K, Nakamura H. CT Scan and MRI in the Differentiation of Liver Tumors. Dig Dis. 2004;22:39-55.
4. Nowicki TK, Markiet K, Izycka-Swieszewska E, Dziadziuszko K, Studniarek M, Szurowska E. Efficacy comparison of multi-phase CT and hepatotropic contrast-enhanced MRI in the differential diagnosis of focal nodular hyperplasia: a prospective cohort study. BMC Gastroenterol. 2018;18:10.
5. Pesapane F, Patella F, Fumarola EM, et al. Intravoxel Incoherent Motion (IVIM) Diffusion Weighted Imaging (DWI) in the Periferic Prostate Cancer Detection and Stratification. Med Oncol 2017; 34: 35.
6. Zhang YD, Zhu FP, Xu X, et al. Liver Imaging Reporting and Data System:Substantial Discordance Between CT and MR for Imaging Classification of Hepatic Nodules. Acad Radiol. 2016;23:344-352.
7. Marampon F, Gravina GL, Popov VM, et al. Close correlation between MEK/ERK and Aurora-B signaling pathways in sustaining tumorigenic potential and radioresistance of gynecological cancer cell lines. Int J Oncol 2014; 44: 285-94.
8. Chou R, Cuevas C, Fu R, et al. Imaging Techniques for the Diagnosis of Hepatocellular Carcinoma: A Systematic Review and Meta-analysis. Ann Intern Med. 2015;162:697-711.
9. Kurucay M, Kloth C, Kaufmann S, et al. Multiparametric imaging for detection and characterization of hepatocellular carcinoma using gadoxetic acid-enhanced MRI and perfusion-CT: which parameters work best?. Cancer Imaging. 2017;17:18.
10. Agliata G, Schicchi N, Agostini A, et al. Radiation exposure related to cardiovascular CT examination: comparison between conventional 64-MDCT and third-generation dual-source MDCT. Radiol Med 2019; 124: 753-61.
11. Lamba R, Fananapazir G, Corwin MT, Khatri VP. Diagnostic imaging of hepatic lesions in adults. Surg Oncol Clin N Am. 2014;23:789-820

12. Reginelli A, Silvestro G, Fontanella G, et al. Performance status versus anatomical recovery in metastatic disease: The role of palliative radiation treatment. Int J Surg 2016; 33 Suppl 1: S126-31.
13. Barabino M, Gurgitano M, Fochesato C, et al. LI-RADS to categorize liver nodules in patients at risk of HCC: tool or a gadget in daily practice?. Radiol Med. 2020;10.1007s11547-020-01225-8.
14. Baker FA, Zeina AR, Mouch SA, Mari A. Benign Hepatic Tumors: From Incidental Imaging Finding to Clinical Management. Korean J Fam Med. 2020;10.4082/kjfm.18.0188.
15. Alenezi AO, Krishna S, Mendiratta-Lala M, Kielar AZ. Imaging and Management of Liver Cancer. Semin Ultrasound CT MR. 2020;41:122-138.
16. Hartke J, Johnson M, Ghabril M. The diagnosis and treatment of hepatocellular carcinoma. Semin Diagn Pathol.2017;34:153-159.
17. Wu M, Li L, Wang J, et al. Contrast-enhanced US for characterization of focal liver lesions: a comprehensive meta-analysis. Eur Radiol. 2018;28:2077-2088.
18. Battaglia V, Cervelli R. Liver investigations: Updating on US technique and contrast-enhanced ultrasound (CEUS). Eur J Radiol. 2017;96:65-73
19. Donato H, França M, Candelária I, Caseiro-Alves F. Liver MRI: From basic protocol to advanced techniques. Eur J Radiol. 2017;93:30-39.
20. Haimerl M, Wächtler M, Platzek I, et al. Added value of Gd-EOB-DTPA-enhanced Hepatobiliary phase MR imaging in evaluation of focal solid hepatic lesions. BMC Med Imaging. 2013;13:41.
21. Agostini A, Mari A, Lanza C, et al. Trends in radiation dose and image quality for pediatric patients with a multidetector CT and a third-generation dual-source dual-energy CT. Radiol Med 2019; 124: 745-52.
22. Curtis WA, Fraum TJ, An H, Chen Y, Shetty AS, Fowler KJ. Quantitative MRI of Diffuse Liver Disease: Current Applications and Future Directions. 2019, Radiology. 290(1):23-30
23. Elsayes KM, Menias CO, Morshid AI, et al. Spectrum of Pitfalls, Pseudolesions, and Misdiagnoses in Noncirrhotic Liver. AJR Am J Roentgenol 2018; 211: 97-108.
24. Ito K, Honjo K, Fujita T, et al. Liver neoplasms: diagnostic pitfalls in cross-sectional imaging. Radiographics 1996; 16: 273-93.
25. Hoodeshenas S, Yin M, Venkatesh SK. Magnetic Resonance Elastography of Liver: Current Update. Top Magn Reson Imaging. 2018 27(5):319-333
26. Asbach P, Klessen C, Koch M, Hamm B, Taupitz M. Magnetic resonance imaging findings of atypical focal nodular hyperplasia of the liver. Clin Imaging 2007; 31: 244-52.
27. Roncalli M, Sciarra A, Tommaso LD. Benign hepatocellular nodules of healthy liver: focal nodular hyperplasia and hepatocellular adenoma. Clin Mol Hepatol 2016; 22: 199-211.
28. Husainy MA, Sayyed F, Peddu P. Typical and atypical benign liver lesions: A review. Clin Imaging 2017; 44: 79-91.
29. Cellina M, Oliva G, Menozzi A, Soresina M, Martinenghi C, Gibelli D. Non-contrast Magnetic Resonance Lymphangiography: an emerging technique for the study of lymphedema. Clin Imaging 2019; 53: 126-33.
30. Alobaidi M, Shirkhoda A. Benign focal liver lesions: discrimination from malignant mimickers. Curr Probl Diagn Radiol 2004; 33: 239-53.
31. Marin D, Brancatelli G, Federle MP, et al. Focal nodular hyperplasia: typical and atypical MRI findings with emphasis on the use of contrast media. Clin Radiol 2008; 63: 577-85.
32. Vernuccio F, Ronot M, Dioguardi Burgio M, et al. Uncommon evolutions and complications of common benign liver lesions. Abdom Radiol (NY) 2018; 43: 2075-96.
33. Scialpi M, Palumbo B, Pierotti L, et al. Detection and characterization of focal liver lesions by split-bolus multidetector-row CT: diagnostic accuracy and radiation dose in oncologic patients. Anticancer Res 2014; 34: 4335-44.
34. Grazioli L, Morana G, Kirchin MA, Schneider G. Accurate differentiation of focal nodular hyperplasia from hepatic adenoma at gadobenate dimeglumine-enhanced MR imaging: prospective study. Radiology 2005; 236: 166-77.
35. Scali EP, Walshe T, Tiwari HA, Harris AC, Chang SD. A Pictorial Review of Hepatobiliary Magnetic Resonance Imaging With Hepatocyte-Specific Contrast Agents: Uses, Findings, and Pitfalls of Gadoxetate Disodium and Gadobenate Dimeglumine. Can Assoc Radiol J 2017; 68: 293-307.
36. Furlan A, Brancatelli G, Dioguardi Burgio M, et al. Focal Nodular Hyperplasia After Treatment With Oxaliplatin: A Multiinstitutional Series of Cases Diagnosed at MRI. AJR Am J Roentgenol 2018; 210: 775-79.
37. Agostini A, Kircher MF, Do RK, et al. Magnetic Resonanance Imaging of the Liver (Including Biliary Contrast Agents)-Part 2: Protocols for Liver Magnetic Resonanance Imaging and Characterization of Common Focal Liver Lesions. Semin Roentgenol 2016; 51: 317-33.
38. Murakami T, Tsurusaki M. Hypervascular benign and malignant liver tumors that require differentiation from hepatocellular carcinoma: key points of imaging diagnosis. Liver Cancer 2014; 3: 85-96.
39. Kim MJ, Lee S, An C. Problematic lesions in cirrhotic liver mimicking hepatocellular carcinoma. Eur Radiol 2019; 29: 5101-10.
40. Carrafiello G, Fontana F, Cotta E, et al. Ultrasound-guided thermal radiofrequency ablation (RFA) as an adjunct to systemic chemotherapy for breast cancer liver metastases. Radiol Med 2011; 116: 1059-66.
41. Zulfiqar M, Sirlin CB, Yoneda N, et al. Hepatocellular adenomas: Understanding the pathomolecular lexicon, MRI features, terminology, and pitfalls to inform a standardized approach. J Magn Reson Imaging 2019;
42. Kim JH, Joo I, Lee JM. Atypical Appearance of Hepatocellular Carcinoma and Its Mimickers: How to Solve Challenging Cases Using Gadoxetic Acid-Enhanced Liver Magnetic Resonance Imaging. Korean J Radiol 2019; 20: 1019-41.
43. Bise S, Frulio N, Hocquelet A, et al. New MRI features improve subtype classification of hepatocellular adenoma. Eur Radiol 2019; 29: 2436-47.

44. Petrillo M, Patella F, Pesapane F, et al. Hypoxia and tumor angiogenesis in the era of hepatocellular carcinoma transarterial loco-regional treatments. Future Oncol 2018; 14: 2957-67.
45. Agostini A, Kircher MF, Do R, et al. Magnetic Resonance Imaging of the Liver (Including Biliary Contrast Agents) Part 1: Technical Considerations and Contrast Materials. Semin Roentgenol 2016; 51: 308-16.
46. Nicolini D, Agostini A, Montalti R, et al. Radiological response and inflammation scores predict tumour recurrence in patients treated with transarterial chemoembolization before liver transplantation. World J Gastroenterol 2017; 23: 3690-701.
47. Floridi C, Radaelli A, Pesapane F, et al. Clinical impact of cone beam computed tomography on iterative treatment planning during ultrasound-guided percutaneous ablation of liver malignancies. Med Oncol 2017; 34: 113.
48. Panfili E, Nicolini D, Polverini V, Agostini A, Vivarelli M, Giovagnoni A. Importance of radiological detection of early pulmonary acute complications of liver transplantation: analysis of 259 cases. Radiol Med 2015; 120: 413-20.
49. Greco F, Autorino R, Altieri V, et al. Ischemia Techniques in Nephron-sparing Surgery: A Systematic Review and Meta-Analysis of Surgical, Oncological, and Functional Outcomes. Eur Urol 2019; 75: 477-91.
50. Ingraham C, Johnson G, Padia SA, Vaidya S. Interventional Radiology for Liver Lesions. Semin Roentgenol. 2016;51:367-377.
51. Cornelis FH, Borgheresi A, Petre EN, Santos E, Solomon SB, Brown K. Hepatic Arterial Embolization Using Cone Beam CT with Tumor Feeding Vessel Detection Software: Impact on Hepatocellular Carcinoma Response. Cardiovasc Intervent Radiol 2018; 41: 104-11.
52. Gonzalez-Guindalini FD, Botelho MP, Harmath CB, et al. Assessment of liver tumor response to therapy: role of quantitative imaging. Radiographics. 2013;33:1781-1800.
53. Carrafiello G, D'Ambrosio A, Mangini M, et al. Percutaneous cholecystostomy as the sole treatment in critically ill and elderly patients. Radiol Med 2012; 117: 772-9.
54. Carrafiello G, Ierardi AM, Piacentino F, Cardim LN. Percutaneous transhepatic embolization of biliary leakage with N-butyl cyanoacrylate. Indian J Radiol Imaging 2012; 22: 19-22.
55. Lucchina N, Tsetis D, Ierardi AM, et al. Current role of microwave ablation in the treatment of small hepatocellular carcinomas. Ann Gastroenterol 2016; 29: 460-65.
56. Ippolito D, Inchingolo R, Grazioli L, et al. Recent advances in non-invasive magnetic resonance imaging assessment of hepatocellular carcinoma. World J Gastroenterol. 2018;24:2413-2426.
57. Belfiore MP, Reginelli A, Maggialetti N, et al. Preliminary results in unresectable cholangiocarcinoma treated by CT percutaneous irreversible electroporation: feasibility, safety and efficacy. Med Oncol 2020; 37: 45.
58. Iannicelli E, Di Pietropaolo M, Marignani M, et al. Gadoxetic acid-enhanced MRI for hepatocellular carcinoma and hypointense nodule observed in the hepatobiliary phase. Radiol Med 2014; 119: 367-76.
59. Borgheresi A, Gonzalez-Aguirre A, Brown KT, et al. Does Enhancement or Perfusion on Preprocedure CT Predict Outcomes After Embolization of Hepatocellular Carcinoma? Acad Radiol 2018; 25: 1588-94.
60. Jeong YY, Yim NY, Kang HK. Hepatocellular carcinoma in the cirrhotic liver with helical CT and MRI: imaging spectrum and pitfalls of cirrhosis-related nodules. AJR Am J Roentgenol 2005; 185: 1024-32.
61. Venturini M, Angeli E, Maffi P, et al. Liver focal fatty changes at ultrasound after islet transplantation: an early sign of altered graft function? Diabet Med 2010; 27: 960-4.
62. Vernuccio F, Cannella R, Porrello G, et al. Uncommon imaging evolutions of focal liver lesions in cirrhosis. Abdom Radiol (NY) 2019; 44: 3069-77.
63. Elsayes KM, Chernyak V, Morshid AI, et al. Spectrum of Pitfalls, Pseudolesions, and Potential Misdiagnoses in Cirrhosis. AJR Am J Roentgenol 2018; 211: 87-96.
64. Bargellini I, Battaglia V, Bozzi E, Lauretti DL, Lorenzoni G, Bartolozzi C. Radiological diagnosis of hepatocellular carcinoma. J Hepatocell Carcinoma 2014; 1: 137-48.
65. Galia M, Agnello F, Sparacia G, et al. Evolution of indeterminate hepatocellular nodules at Gd-EOB-DPTA-enhanced MRI in cirrhotic patients. Radiol Med 2018; 123: 489-97.
66. Park HJ, Choi BI, Lee ES, Park SB, Lee JB. How to Differentiate Borderline Hepatic Nodules in Hepatocarcinogenesis: Emphasis on Imaging Diagnosis. Liver Cancer 2017; 6: 189-203.
67. Pinto A, Caranci F, Romano L, Carrafiello G, Fonio P, Brunese L. Learning from errors in radiology: a comprehensive review. Semin Ultrasound CT MR 2012; 33: 379-82.
68. Doo KW, Lee CH, Choi JW, Lee J, Kim KA, Park CM. "Pseudo wash-out" sign in high-flow hepatic hemangioma on gadoxetic acid contrast-enhanced MRI mimicking hypervascular tumor. AJR Am J Roentgenol 2009; 193: W490-6.
69. Pradella S, Lucarini S, Colagrande S. Liver lesion characterization: the wrong choice of contrast agent can mislead the diagnosis of hemangioma. AJR Am J Roentgenol 2012; 199: W662.

Received: 20 May 2020
Accepted: 10 June 2020
Correspondence:
Giulia Grazzini
Department of Radiology, Careggi University Hospital
L.go Brambilla, 3
50134 – Florence – Italy
E-mail: grazzini.giulia@gmail.com

Acta Biomed 2020; Vol. 91, Supplement 8: 18-26 DOI: 10.23750/abm.v91i8-S.9938

Review

The role of imaging in surgical planning for liver resection: what the radiologist needs to know

Andrea Agostini[1,2], Alessandra Borgheresi[2], Chiara Floridi[1,2], Marina Carotti[1,2], Giulia Grazzini[3], Francesco Pagnini[4], Susanna Guerrini[5], Pierpaolo Palumbo[6], Silvia Pradella[3], Gianpaolo Carrafiello[7,8], Marco Vivarelli[1,9], Andrea Giovagnoni[1,2]

[1]Department of Clinical, Special and Dental Sciences, University Politecnica delle Marche, Ancona, AN, Italy; [2]Division of Special and Pediatric Radiology, Department of Radiology, University Hospital "Umberto I – Lancisi – Salesi", Ancona, AN, Italy; [3]Department of Radiology, Careggi University Hospital, Florence, Italy; [4]Department of Medicine and Surgery, Unit of Radiology, University of Parma, Parma, Italy; [5]Unit of Diagnostic Imaging, Department of Radiological Sciences, University of Siena, Azienda Ospedaliero-Universitaria Senese, Siena, Italy; [6]Department of Biotechnology and Applied Clinical Sciences, University of L'Aquila, L'Aquila, Italy; [7]Radiology Department, Fondazione IRCSS Ca Granda, Ospedale Maggiore Policlinico, Milan, Italy; [8]Department of Health Sciences, Università degli Studi di Milano, Milan, Italy; [9]University Hospital "Umberto I – Lancisi – Salesi", Division of Hepatobiliary and Transplant Surgery, Ancona, Italy

Summary. The management of patients undergoing surgical resection for liver malignancies requires a multidisciplinary team, including a dedicated radiologist. In the preoperative workup, the radiologist has to provide precise, relevant information to the surgeon. This requires the radiologist to know the basics of surgical techniques as well as liver surgical anatomy in order to help to avoid unexpected surgical scenarios and complications. Moreover, virtual resections and volumetries on radiological images will be discussed, and basic concepts of postoperative liver failure, regeneration, and methods for hypertrophy induction will be provided. (www.actabiomedica.it)

Keywords: Imaging, liver malignancies, liver resection, surgical planning, MRI, CT, US

Introduction

Surgical resection often represents the only curative treatment in patients with liver malignancies. In the last 50 years, from a pioneering surgery, the liver resections have pushed up its limits with remarkable achievements in terms of effectiveness, clinical outcomes, and safety (1-3).

The reasons of these achievements rely in part on the evolution of surgical and anesthetic techniques; on the other side, the advances in cross-sectional imaging provided a significant contribution in the preoperative workup allowing a better treatment allocation and safety (1, 4). The management of these complex patients requires a multidisciplinary team, including dedicated radiologists with specific skills and knowledge. Cross-sectional imaging (MRI, CT, and US) techniques gained extensive application in gastrointestinal radiology; they are advised as first-line techniques in the diagnosis, staging, and follow-up in many diseases (5-11).

In this paper, we will provide an overview of the main concepts the radiologist needs to know to manage a presurgical workup of a patient with liver lesions. In particular, the present review will discuss: 1. the basics of surgical anatomy and terminology; 2. the relevant anatomical variants in liver resections; 3. The role of imaging, with a focus on virtual resections and volumetric estimations (the advanced techniques for the evaluation of diffuse disease go beyond the scope of this review); 4. The pathophysiological elements of liver regeneration, liver failure, and techniques for induction of liver hypertrophy.

Liver surgical anatomy and resections

Couinaud's segmentation

The modern techniques for liver resections rely on Couinaud's segmental anatomy of the liver: each segment is fed by an independent portal branch (12). The main anatomical landmarks are the hepatic veins (right, middle, and left), each of them lying in the so-called "portal scissurae" (12). The main portal scissura includes the middle hepatic vein, which corresponds to the Cantlie's line (Fig. 1). The right portal scissura contains the right hepatic vein and divides the right hemiliver into two sectors: right postero-lateral and right antero-medial. The two right sectors are further divided into two segments each (respectively to the hilar plane): segments VII and VI laterally, and segment V and VIII medially. The left hemiliver is divided into two sectors by the left portal scissura (containing the left hepatic vein). The left anterior sector contains segments IV and III, while segment II is in the left posterior sector. The Spigel lobe (segment I) has autonomous feeding vessels (Fig. 1) (12).

Liver surgical resections

The modern surgical terminology considers the anatomic and non-anatomic resections (respectively AR and NAR) of the liver.

In AR, one or more Couinaud's segments are removed together with the inside tumor and relative portal pedicles (13). The rationale is the oncological effectiveness assuming that hepatic tumors spread through portal branches. The actual definitions of AR refer to the "Brisbane 2000 Terminology of Liver anatomy and Resections" proposed by the International Hepato-Pancreato-Biliary Association (IHPBA) (14). This classification uses a modified version of Couinaud's segmental anatomy: the term sector is replaced with "section," and the left lateral section is composed of the Couinaud's segments II and III (13, 14). The IHPBA define AR in relation to the order of portal divisions:

1. Hepatectomy (first-order): the two hemilivers are divided by the Cantlie's line (Couinaud's middle hepatic scissura);
2. Sectionectomy (second-order): the right sections correspond to Couinaud's. The left medial section is segment IV, and the left lateral section includes segments II+III. The Counauds terminology and segmentation are retained as an alternative.
3. Segmentectomy (third-order): resection of one or more of Couinaud's segments.

In NAR, also named atypical or wedge resections, a portion of hepatic parenchyma (with the tumor inside) is resected independently of vascular segmental anatomy. The rationale is the parenchymal sparing, which balances the oncological effectiveness in patients with underlying chronic liver disease (4).

Anatomical variants of surgical relevance

The normal vascular and biliary anatomy is present in up to 70% of cases, and anatomical variants

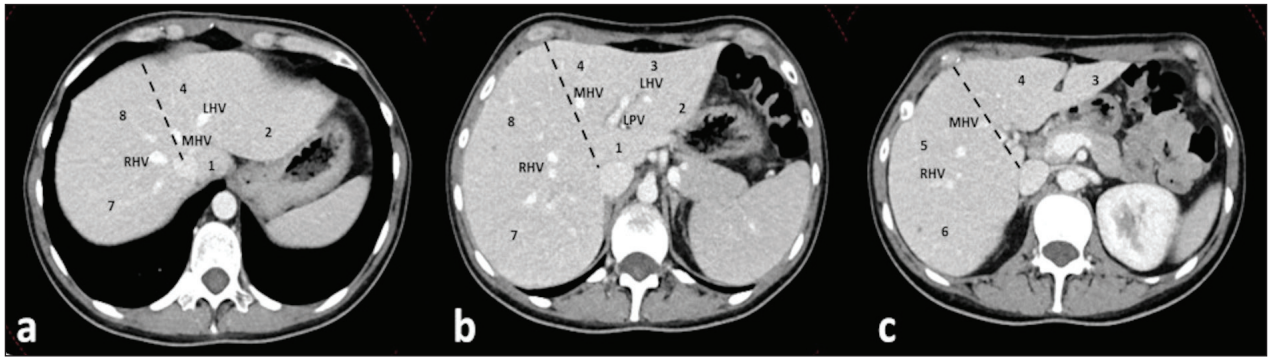

Figure 1. Normal segmental anatomy of the liver. a, b, c, cranio-caudal axial CT slices, portal venous phase. Dashed line: Cantlie's line dividing the two hemilivers. RHV: right hepatic vein; MHV: middle hepatic vein; LHV: left hepatic vein; LPV: left portal vein. Arabic numbers: Couinaud's segments.

are relatively commons (15). The radiologist has to recognize the relevant anatomical variants for surgery, keeping in mind two concepts: an unexpected vascular injury leads to significant bleeding, and the remnant liver needs vascular and biliary structures to work properly.

Hepatic Artery

Several variants of the hepatic artery (HA) have surgical relevance and need to be reported (16). Besides the normal anatomy (HA originating from the celiac trunk), the significant variants involve the "accessory" or "replaced" arteries from other vessels than the celiac trunk. The critical factor to be considered is the spatial relationship between the vessel and the type of resection, to prevent injuries to the aberrant branch and irrorated liver (e.g. left aberrant hepatic arteries are relevant for left hepatectomy) (Fig. 2a) (15, 16).

Portal Vein

Typically, the portal vein bifurcates at the hilum to feed the left and right hemi-livers in 65% of cases (17), respectively. The relevant portal variants to be recognized to avoid accidental ligation involve the bifurcation of the main portal trunk. The most frequent are the portal trifurcation and the so-called "Z-type" portal vein, where the right portal vein is absent, and right sectorial branches originate from the main trunk (Fig. 2b). Other relevant variants involve the segment VIII fed by the left portal vein (16,17).

Hepatic Veins

The importance of hepatic vein variants relies on the drained territories and the potential congestive status of the remnant liver after ligation of an aberrant vessel. The classification of hepatic veins is more complex: the right hepatic vein has four variants, while the middle and left hepatic veins are classified into three variants each (18-20). Usually, the right hepatic vein drains the segments V, VI, and VII; if a variant drains the entire right hemiliver, the middle hepatic vein can be removed during left hepatectomy (18). An accessory right hepatic vein with caval confluence of at least 20 mm caudally to the right hepatic vein may allow for resection of segment VII and VIII together with the right hepatic vein (fig. 2c) (18). The middle and left hepatic veins present a common trunk in 65-85% of cases with difficult selective clamping of the middle hepatic vein alone (19,20). The relevant variants

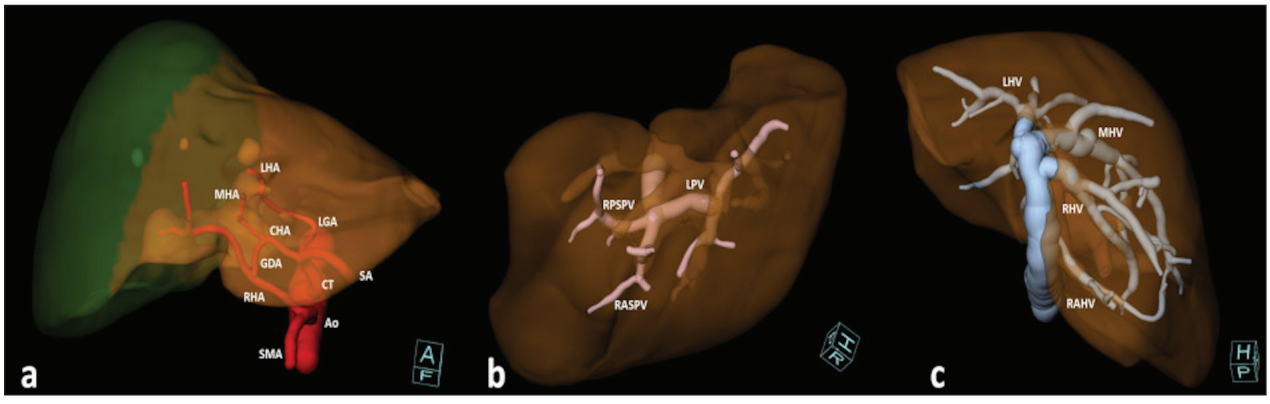

Figure 2. Volume Rendering (VR) reconstructions of relevant vascular variants for surgery. A: antero-inferior view of a variant of the hepatic artery (red). Replaced left hepatic artery from the left gastric artery, middle hepatic artery from common hepatic artery, and replaced right hepatic artery from the superior mesenteric artery. Variants of the left hepatic artery are relevant in left hepatectomies (brown hemiliver), while variants of the right hepatic artery are relevant for right hepatectomies (green hemiliver). Ao: aorta. CT: celiac trunk. SMA: superior mesenteric artery. CHA: common hepatic artery. SA: splenic artery. LGA: left gastric artery. GDA: gastro-duodenal artery. LHA: left hepatic artery. MHA: middle hepatic artery. RHA: right hepatic artery. B: portal trifurcation (pink), cranial-right view. RPSPV: right posterior sectorial portal vein. RASPV: right anterior sectorial portal vein. LPV: left portal vein. C: variants of hepatic veins (blue) with right accessory hepatic vein, cranio-posterior view. RAHV: right accessory hepatic vein. RHV: right hepatic vein. MHV: middle hepatic vein. LHV: left hepatic vein.

of middle and left hepatic veins regard the drainage of segments V, VIII, and IV to be evaluated before the ligation of the left or the middle hepatic vein (18).

Biliary Tree

In the normal biliary anatomy, the confluence of the right and left hepatic duct makes the main hepatic duct at the hilum (80% of cases) (21). Even though systematic correlations between biliary and vascular variants have not been demonstrated (21), a not-recognized biliary variant may lead to postoperative leakage or biliary obstruction in a portion of the remnant liver (16). The most relevant biliary variants involve a segment or sector drained contralaterally or in an ectopic way; these frequently involve the right posterior sectorial duct draining into the left hepatic duct, in the main hepatic duct or the cystic duct (16, 21).

Imaging techniques

Ultrasound

Transabdominal liver ultrasound (US) is generally the first level for the evaluation of a focal liver lesion; elastography techniques are used for the evaluation of liver fibrosis (22, 23). It is fast, diffuse and cheap, but is not panoramic and strongly dependent on the operator. With the administration of contrast material (CEUS), it may be helpful in the characterization of liver lesions (24).

Conversely, the US plays a fundamental role in intraoperative imaging, allowing for an accurate evaluation of the lesions, vascular pedicles, and their relationships and is also helpful in the evaluation of segmental anatomy (e.g., the US finger compression) (25).

Computer Tomography

The Computer Tomography (CT) examination is fundamental in the preoperative evaluation and the administration of intravenous contrast material is mandatory. A post-contrast triphasic protocol is necessary for an accurate evaluation of the arterial vessels, the intrahepatic portal and venous vessels as well as for detection, localization and characterization of the liver lesions (16). Adequate dose of contrast material and bolus tracking techniques are recommended for optimal acquisition timing and adequate contrast resolution between the vascular pedicles, the lesions, and the liver parenchyma (26). Advanced techniques, such as Dual-Energy CT, allow for further optimization of contrast administration (27, 28). The purpose of the radiological report is to help the surgeon to decide whether the procedure is indicated and, eventually, to choose the best surgical method. The report should include the size, number, and location of the lesions, including their relationship with the vessels and biliary tree, by using the Couinaud's landmarks. The relevant anatomical variants with potential influence on the surgical technique (see the previous section) need to be reported. Moreover, the patency of the vascular pedicles, as well as the presence of neoplastic portal thrombus, need to be reported (4).

The radiologist should highlight potential contraindications to surgery, such as radiological signs of portal hypertension (i.e., ascites, splenomegaly, patency of umbilical vein, and abdominal varices), associated with a higher rate of perioperative complications (4).

Furthermore, the radiologist should recognize and report signs of chronic liver disease (cirrhosis and steatosis) or the presence of biliary dilatation / obstructive jaundice suggesting an impairment of the function of the relative parenchyma (29).

Compared to MRI, CT provides a relatively poor representation of the biliary duct system but is faster and provides a higher spatial resolution of the vascular structures. This is relevant for 3D reconstructions of the liver parenchyma and vessels provided for the multidisciplinary evaluation and surgical planning. A further step is the virtual resections with volumetric estimations, discussed in the next sections (4).

Finally, the evaluation of diffuse liver disease with advanced techniques such as Dual-Energy is not fully standardized and validated (30).

Magnetic Resonance Imaging

Magnetic Resonance Imaging (MRI) represents the gold-standard for the evaluation of the liver focal and diffuse disease and the biliary tree. In this regard,

MRI has assumed a primary role in the study of various districts and pathologies, thanks to its high contrast resolution and the absence of ionizing radiations compared to CT (31-34).

An adequate MRI protocol should include the basic sequences (axial and coronal T2-weighted turbo spin-echo, axial T1-weighted gradient-echo in- and out-of-phase with eventual Dixon technique) together with Diffusion-Weighted imaging (DWI), magnetic resonance cholangiopancreatography (MRCP) and post-contrast acquisitions (35, 36).

The DWI is helpful in the detection and characterization of focal lesions and eventual neoplastic portal vein thromboses (35, 37).

The first advantage of hepatobiliary contrast agents (HCA) is the remarkably high accuracy in detection and mapping of focal lesions, in particular the smaller ones (<1 cm); this is cost-effective by reducing the rate of inadequate surgical treatments in patients with colorectal liver metastases (38). Moreover, the evaluation of the biliary tree in the excretory phase, integrated with MRCP, may be helpful for the evaluation of eventual lesions or variants of the biliary tract and the spatial relations with hepatic nodules (35).

The advanced techniques, such as MR Elastography, Proton Density Fat Fraction (PDFF), the evaluation of iron overload, and the T1 mapping with hepatobiliary contrast agents for liver function, can provide valuable information on liver parenchyma, though not widely available (35).

Quantitative evaluation: the role of Virtual Resections

The remnant liver and the Post-Hepatectomy Liver Failure (PHLF)

The curative effectiveness of a major liver resection needs to be balanced with the amount of remnant liver parenchyma. In the postoperative period, the remnant liver has contemporarily to sustain liver regeneration (induced by the increased sinusoidal shear stress) and metabolic functions. In the case of imbalance between the metabolic and regenerating functions, the functional reserve, and the volume of the remnant liver, the post-hepatectomy liver failure (PHLF) occurs (29).

There are several definitions of PHLF; a widely accepted one describes the PHLF as the postoperative impairment of metabolic functions of the remnant liver with hyperbilirubinemia and increased INR (with or without clinical symptoms) on or after postoperative day 5 (29, 39). The PHLF may present with different grades of severity, with variable mortality up to 54% (39).

The portal hyperperfusion of the remnant liver (because of the loss of vascular space after resection), the imbalance of the metabolism of biliary salts, dysregulation of the innate hepatic immune system and the presence of underlying chronic liver disease (e.g., steatosis or cirrhosis) are the major pathophysiological factors of PHLF. Thus, the combination of patient's and hepatic intrinsic factors (e.g., cirrhosis) and operative factors (e.g., loss of vascular) are responsible for the occurrence of PHLF (29, 40).

Virtual Resections

Cross-sectional imaging plays a pivotal role in the estimation of the postoperative liver remnant (Future Liver Remnant, FLR). The FLR is a percentage of the estimated remnant liver volume (RLV) over the estimated preoperative total liver volume (TLV) (41).

The RLV is accurately calculated on CT or MRI images following the Couinaud's landmarks with dedicated software. A relevant technical factor is the slice thickness, responsible for partial volume artifacts: acceptable values are below 6 mm in CT and below 8 mm in MRI (easily achieved with modern scanners) (42).
The recent advances in artificial intelligence allow for segmentation of big volumes (TLV) in short time with no more needs for calculation of standard liver volumes from anthropometric data; moreover, tumoral lesions are easily segmented (Tumor volume, TuV) (43). Thus, the FLR can be easily calculated as a fraction of the RLV on the Functional Liver Volume (FLV=TLV-TuV) (Fig. 3) (41):

The estimation of FLR does not consider the presence of underlying liver disease that has to be estimated separately. If a cutoff of FLR=25-30% can be considered as safe in patients without chronic liver diseases, higher thresholds (more than 40%) are neces-

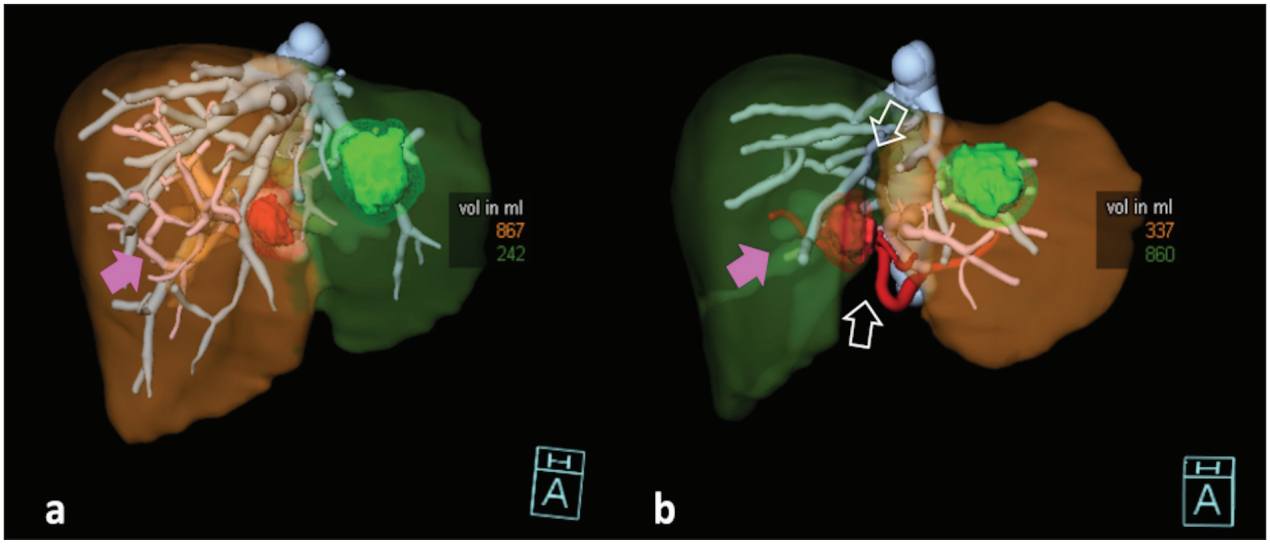

Figure 3. Associating Liver Partition and Portal vein ligation for Staged hepatectomy (ALPPS), Volume rendering reconstructions (VR). Hepatic artery: red. Hepatic veins: blue. Portal vein: pink. Red lesion: tumor. Green lesion: cyst. A: Baseline CT before step 1: simulation of right hepatectomy extended to segment 4. Green liver: Remnant Liver Volume (RLV) including Couinaud's segments 1, 2, 3. Brown Liver: resected liver (segments 4, 5, 6, 7, 8). The RLV had a volume of 242 ml and 230 ml without the cyst. The calculated future liver remnant was 21% (fraction of RLV on Functional Liver), below the safe threshold for resection (FLR>=25%). The patient was candidate to ALPPS. B: follow-up CT on 7° post-operative day after ALPPS step 1. The RLV (brown liver) increased from 242 ml to 337 ml (equal to 325 ml without the cyst). The calculated FLR was 28%, and the patient underwent to right hepatectomy extended to segment 4 on the following day. The procedures performed in step 1 can be observed: the right portal vein was ligated (not visible in b, pink arrows), and the in-situ splitting was performed (empty white arrows).

sary in the presence of steatosis, cirrhosis, or obstructive jaundice (29, 41). Thus, the volumetric estimations from virtual resections need to be integrated with clinical data (e.g., MELD Score, Child-Pugh, Indocyanine test, and eventual liver biopsy) in a multidisciplinary environment (4, 29).

Induction of liver hypertrophy

It is possible to increase a not-sufficient FLR by induction of liver hypertrophy with selective occlusion of portal branches with different techniques (44).

The portal vein embolization (PVE) is an interventional technique for percutaneous occlusion of portal branches, with a reported mean increase in FLR of nearly 38% at 4-weeks CT (44). The relatively low invasiveness needs to be balanced with a relatively low increase of FLR and long times with a reported 20% drop-out rate because of tumor progression (44, 45).

The portal vein ligation (PVL) is usually associated with wedge resections in two-stage hepatectomies in colorectal liver metastases: a hemiliver is debulked, and the contralateral portal branch is ligated for subsequent hepatectomy (46). The data available do not suggest significant differences between the outcomes of PVE and PVL (44).

The ALPPS (Associating Liver Partition and Portal Vein Ligation for Staged Hepatectomy) is a two-stage hepatectomy with several variants (47, 48). The first step includes the portal ligation together with the partial or total liver transection to avoid portal shunts (47). After a median time of 7-9 days, a mean increase in FLR of 69-75% has been reported on CT studies, and the hepatectomy can be safely performed in the 2nd step (Fig. 3) (44, 47). The absence of almost null tumor progression needs to be balanced with a reported higher mortality rate (49).

Conclusions

In this overview, we provided a basic discussion on the surgical techniques and the underlying anatomical concepts the radiologist needs to be aware of.

The patients with hepatobiliary malignancies require a multidisciplinary approach in which radiology plays a pivotal role in qualitative and quantitative evaluations.

Conflict of interest: Authors declare that they have no commercial associations (e.g. consultancies, stock ownership, equity interest, patent/licensing arrangement etc.) that might pose a conflict of interest in connection with the submitted article.

References

1. Kokudo N, Takemura N, Ito K, Mihara F. The history of liver surgery: Achievements over the past 50 years. Ann Gastroenterol Surg 2020; 4: 109-17.
2. Calise F, Giuliani A, Sodano L, et al. Segmentectomy: is minimally invasive surgery going to change a liver dogma? Updates Surg 2015; 67: 111-5.
3. Marte G, Scuderi V, Rocca A, Surfaro G, Migliaccio C, Ceriello A. Laparoscopic splenectomy: a single center experience. Unusual cases and expanded inclusion criteria for laparoscopic approach. Updates Surg 2013; 65: 115-9.
4. Shin DS, Ingraham CR, Dighe MK, et al. Surgical resection of a malignant liver lesion: what the surgeon wants the radiologist to know. AJR Am J Roentgenol 2014; 203: W21-33.
5. Belfiore MP, Reginelli A, Maggialetti N, et al. Preliminary results in unresectable cholangiocarcinoma treated by CT percutaneous irreversible electroporation: feasibility, safety and efficacy. Med Oncol 2020; 37: 45.
6. Giannitto C, Campoleoni M, Maccagnoni S, et al. Unindicated multiphase CT scans in non-traumatic abdominal emergencies for women of reproductive age: a significant source of unnecessary exposure. Radiol Med 2018; 123: 185-90.
7. Petrillo M, Patella F, Pesapane F, et al. Hypoxia and tumor angiogenesis in the era of hepatocellular carcinoma transarterial loco-regional treatments. Future Oncol 2018; 14: 2957-67.
8. Cornelis FH, Borgheresi A, Petre EN, Santos E, Solomon SB, Brown K. Hepatic Arterial Embolization Using Cone Beam CT with Tumor Feeding Vessel Detection Software: Impact on Hepatocellular Carcinoma Response. Cardiovasc Intervent Radiol 2018; 41: 104-11.
9. Borgheresi A, Gonzalez-Aguirre A, Brown KT, et al. Does Enhancement or Perfusion on Preprocedure CT Predict Outcomes After Embolization of Hepatocellular Carcinoma? Acad Radiol 2018; 25: 1588-94.
10. Belfiore G, Belfiore MP, Reginelli A, et al. Concurrent chemotherapy alone versus irreversible electroporation followed by chemotherapy on survival in patients with locally advanced pancreatic cancer. Med Oncol 2017; 34: 38.
11. Carrafiello G, Fontana F, Cotta E, et al. Ultrasound-guided thermal radiofrequency ablation (RFA) as an adjunct to systemic chemotherapy for breast cancer liver metastases. Radiol Med 2011; 116: 1059-66.
12. Couinaud C. Liver anatomy: portal (and suprahepatic) or biliary segmentation. Dig Surg 1999; 16: 459-67.
13. Bismuth H. Revisiting liver anatomy and terminology of hepatectomies. Ann Surg 2013; 257: 383-6.
14. Strasberg SM, Belghiti J, Clavien PA, et al. The Brisbane 2000 Terminology of Liver Anatomy and Resections. Hpb 2000; 2: 333-39.
15. Lopez-Andujar R, Moya A, Montalva E, et al. Lessons learned from anatomic variants of the hepatic artery in 1,081 transplanted livers. Liver Transpl 2007; 13: 1401-4.
16. Catalano OA, Singh AH, Uppot RN, Hahn PF, Ferrone CR, Sahani DV. Vascular and biliary variants in the liver: implications for liver surgery. Radiographics 2008; 28: 359-78.
17. Covey AM, Brody LA, Getrajdman GI, Sofocleous CT, Brown KT. Incidence, patterns, and clinical relevance of variant portal vein anatomy. AJR Am J Roentgenol 2004; 183: 1055-64.
18. Barbaro B, Soglia G, Alvaro G, et al. Hepatic veins in presurgical planning of hepatic resection: what a radiologist should know. Abdom Imaging 2013; 38: 442-60.
19. Reichert PR, Renz JF, D'Albuquerque LA, et al. Surgical anatomy of the left lateral segment as applied to living-donor and split-liver transplantation: a clinicopathologic study. Ann Surg 2000; 232: 658-64.
20. Masselot R, Leborgne J. Anatomical study of hepatic veins. Anat Clin 1978; 1: 109–25.
21. Macdonald DB, Haider MA, Khalili K, et al. Relationship between vascular and biliary anatomy in living liver donors. AJR Am J Roentgenol 2005; 185: 247-52.
22. Rodgers SK, Fetzer DT, Gabriel H, et al. Role of US LIRADS in the LI-RADS Algorithm. Radiographics 2019; 39: 690-708.
23. Kennedy P, Wagner M, Castera L, et al. Quantitative Elastography Methods in Liver Disease: Current Evidence and Future Directions. Radiology 2018; 286: 738-63.
24. Burrowes DP, Medellin A, Harris AC, Milot L, Wilson SR. Contrast-enhanced US Approach to the Diagnosis of Focal Liver Masses. Radiographics 2017; 37: 1388-400.
25. Torzilli G, Makuuchi M. Ultrasound-guided finger compression in liver subsegmentectomy for hepatocellular carcinoma. Surg Endosc 2004; 18: 136-9.
26. Ichikawa T, Erturk SM, Araki T. Multiphasic contrast-enhanced multidetector-row CT of liver: contrast-enhancement theory and practical scan protocol with a combination of fixed injection duration and patients' body-weight-tailored dose of contrast material. Eur J Radiol 2006; 58: 165-76.
27. Agostini A, Borgheresi A, Mari A, et al. Dual-energy CT: theoretical principles and clinical applications. Radiol Med 2019; 124: 1281-95.
28. Agostini A, Mari A, Lanza C, et al. Trends in radiation dose and image quality for pediatric patients with a multidetector CT and a third-generation dual-source dual-energy CT. Radiol Med 2019; 124: 745-52.
29. Guglielmi A, Ruzzenente A, Conci S, Valdegamberi A,

Iacono C. How much remnant is enough in liver resection? Dig Surg 2012; 29: 6-17.
30. Agostini A, Borgheresi A, Mari A, et al. Dual-energy CT: theoretical principles and clinical applications. Radiol Med 2019
31. Mungai F, Pasquinelli F, Mazzoni LN, et al. Diffusion-weighted magnetic resonance imaging in the prediction and assessment of chemotherapy outcome in liver metastases. Radiol Med 2014; 119: 625-33.
32. Carrafiello G, Ierardi AM, Piacentino F, Cardim LN. Percutaneous transhepatic embolization of biliary leakage with Nbutyl cyanoacrylate. Indian J Radiol Imaging 2012; 22: 19-22.
33. Carrafiello G, D'Ambrosio A, Mangini M, et al. Percutaneous cholecystostomy as the sole treatment in critically ill and elderly patients. Radiol Med 2012; 117: 772-9.
34. Calistri L, Castellani A, Matteuzzi B, Mazzoni E, Pradella S, Colagrande S. Focal Liver Lesions Classification and Characterization: What Value Do DWI and ADC Have? J Comput Assist Tomogr 2016; 40: 701-8.
35. Agostini A, Kircher MF, Do RK, et al. Magnetic Resonanance Imaging of the Liver (Including Biliary Contrast Agents)-Part 2: Protocols for Liver Magnetic Resonanance Imaging and Characterization of Common Focal Liver Lesions. Semin Roentgenol 2016; 51: 317-33.
36. Agostini A, Kircher MF, Do R, et al. Magnetic Resonance Imaging of the Liver (Including Biliary Contrast Agents) Part 1: Technical Considerations and Contrast Materials. Semin Roentgenol 2016; 51: 308-16.
37. Liver EAftSot. EASL Clinical Practice Guidelines: Management of hepatocellular carcinoma. Journal of hepatology 2018; 69: 182-236.
38. Zech CJ, Grazioli L, Jonas E, et al. Health-economic evaluation of three imaging strategies in patients with suspected colorectal liver metastases: Gd-EOB-DTPA-enhanced MRI vs. extracellular contrast media-enhanced MRI and 3-phase MDCT in Germany, Italy and Sweden. Eur Radiol 2009; 19 Suppl 3: S753-63.
39. Rahbari NN, Garden OJ, Padbury R, et al. Posthepatectomy liver failure: a definition and grading by the International Study Group of Liver Surgery (ISGLS). Surgery 2011; 149: 713-24.
40. van Mierlo KM, Schaap FG, Dejong CH, Olde Damink SW. Liver resection for cancer: New developments in prediction, prevention and management of postresectional liver failure. J Hepatol 2016; 65: 1217-31.
41. Schindl MJ, Redhead DN, Fearon KC, et al. The value of residual liver volume as a predictor of hepatic dysfunction and infection after major liver resection. Gut 2005; 54: 289-96.
42. Reiner CS, Karlo C, Petrowsky H, Marincek B, Weishaupt D, Frauenfelder T. Preoperative liver volumetry: how does the slice thickness influence the multidetector computed tomography- and magnetic resonance-liver volume measurements? J Comput Assist Tomogr 2009; 33: 390-7.
43. Chlebus G, Schenk A, Moltz JH, van Ginneken B, Hahn HK, Meine H. Automatic liver tumor segmentation in CT with fully convolutional neural networks and object-based postprocessing. Sci Rep 2018; 8: 15497.
44. Pandanaboyana S, Bell R, Hidalgo E, et al. A systematic review and meta-analysis of portal vein ligation versus portal vein embolization for elective liver resection. Surgery 2015; 157: 690-8.
45. van Lienden KP, van den Esschert JW, de Graaf W, et al. Portal vein embolization before liver resection: a systematic review. Cardiovasc Intervent Radiol 2013; 36: 25-34.
46. Popescu I, Alexandrescu ST. Surgical options for initially unresectable colorectal liver metastases. HPB Surg 2012; 2012: 454026.
47. Schnitzbauer AA, Lang SA, Goessmann H, et al. Right portal vein ligation combined with in situ splitting induces rapid left lateral liver lobe hypertrophy enabling 2-staged extended right hepatic resection in small-for-size settings. Ann Surg 2012; 255: 405-14.
48. Vivarelli M, Vincenzi P, Montalti R, et al. ALPPS Procedure for Extended Liver Resections: A Single Centre Experience and a Systematic Review. PLoS ONE 2015; 10: e0144019.
49. Olthof PB, Coelen RJS, Wiggers JK, et al. High mortality after ALPPS for perihilar cholangiocarcinoma: case-control analysis including the first series from the international ALPPS registry. HPB (Oxford) 2017; 19: 381-87.

Received: 20 May 2020
Accepted: 10 June 2020
Correspondence:
Alessandra Borgheresi
University Hospital "Umberto I – Lancisi – Salesi"
Department of Radiology – Division of Special and Pediatric Radiology
Via Conca 71, 60126 Ancona (AN)
Phone: +39 071 596 4078
Office: +39 071 5964085
E-mail: alessandra.borgheresi@gmail.com

Acta Biomed 2020; Vol. 91, Supplement 8: 27-33 DOI: 10.23750/abm.v91i8-S.9970

Review

MRI of perianal fistulas in Crohn's disease

Alfonso Reginelli[1], Giovanna Vacca[1], Sabrina Giovine[2], Andrea Izzo[1], Andrea Agostini[3], Maria Paola Belfiore[1], Michaela Cellina[4], Chiara Floridi[3], Alessandra Borgheresi[3], Pierpaolo Palumbo[5], Andrea Giovagnoni[3], Salvatore Cappabianca[1], Roberto Grassi[1]

[1] Department of Precision Medicine, University of Campania "L. Vanvitelli," Naples, Italy; [2] Department of Radiology, SG Moscati Hospital, ASL Caserta, Aversa, Italy; [3] Department of Clinical, Special and Dental Sciences, University Politecnica delle Marche, Ancona, AN, Italy; [4] Department of Radiology, Ospedale Fatebenefratelli, ASST Fatebenefratelli Sacco, Milan,Italy; [5] Department of Biotechnology and Applied Clinical Sciences, University of L'Aquila, L'Aquila, Italy

Summary. Perianal fistulas represent one of the most critical complications of Crohn's disease (CD). Management and treatment need a multidisciplinary approach with an accurate description of imaging findings. *Aim.* This study aspires to assess the significative role of Magnetic Resonance Imaging (MRI) in the study of perianal fistulas, secondary extensions, and abscess in patients with CD. Therefore it is essential to standardize an appropriate protocol of sequences that allow the correct evaluation of disease activity and complications. *Methods*: We selected and reviewed ten recent studies among the most recent ones present in literature exclusively about pelvic MRI imaging and features in CD. We excluded studies that weren't in the English language. *Conclusions:* MRI has a crucial role in the evaluation and detection of CD perianal fistulas because, thanks to its panoramic and multiplanar view, it gives excellent anatomic detail of the anal sphincters. Today MRI is the gold standard imaging technique for the evaluation of perianal fistulas, mainly because this technique shows higher concordance with surgical findings than does any other imaging evaluation. Surgical treatment is often required in the management of perianal fistula in patients with CD, which often have complex perineal findings. (www.actabiomedica.it)

Keywords: Magnetic Resonance Imaging, Crohn, Fistula in ano, Perianal disease.

Introduction

Perineal manifestation in patients with CD includes skin tags, hemorrhoids, anal fissures, rectal ulcers, perianal fistulas and abscesses (1).

The cumulative incidence of perianal fistulas in patients with Crohn's disease range is from 13% to 27% (2-4). The significant risk factors are the inflammatory colonic CD and the active rectal involvement (2-6). Still, the type of fistulas (simple or complicated) (Fig 1) and the presence of an abscess may influence the course of the disease. Complicated fistula is more often seen in CD (1), having one or more secondary tracts and abscess. The patient frequently refers perianal swelling, fever, drainage of pus, or blood, and in a long time, also fecal incontinence may occur. For those reasons, it can be possible to develop also psychiatric diseases like anxiety and depression (7). The treatment is the same as the other CD locations and usually requires a combined surgical and medical approach.

Pathogenesis & Pathology

Currently, the central hypothesis about the origin of CD is represented by a disorder of the mucosal barrier that activates innate immunity in people with genetic predisposition and alteration of the microbiota

(8). After the initial trigger, there is massive recruitment of leukocyte and inappropriate stimulation of the immune system. Fistulas originate by an epithelial defect caused by inflammation whose repair is impaired because of the migratory potential of colonic lamina propria fibroblasts (9). Another hypothesis is represented by the migration of the intestinal epithelial cells and the transformation, lead by the TGF-Beta, into myofibroblasts. This process is called epithelial-to-mesenchymal transition. Another critical factor in the pathogenesis of CD is the up-regulation of the matrix metalloproteinases (MMP) such as MMP-9 and MMP-3.

Another hypothesis consists in the“ cryptoglandular hypothesis”: anomalous drainage of the anal glands located within the intersfinteric space may start the inflammatory process, passing through a perianal abscess acutely and a fistulous tract in a second time (87% of patients with an abscess may develop a fistula) (Fig 2) (10).

Available data indicate that CD-associated fistulas start from an epithelial defect that may be caused by ongoing inflammation. Often CD fistulas penetrate the gut wall surrounded by acute and chronic cells. Perianal fistulas in CD have a high grade of recurrence. In this regards, MRI has assumed a primary role over CT in the study of various district and pathologies, thanks to its high contrast resolution its excellent soft tissue contrast and multiplanar capability (11-16).

MRI imaging is the gold standard for the evaluation of perianal disease and allows us to classify fistula correctly to choose the type of treatment (9).

Classification of perianal fistulas

Incorrect classification and/or determination of extent increases the risk of incomplete healing, recurrent fistula, and inadvertent sphincter injury.

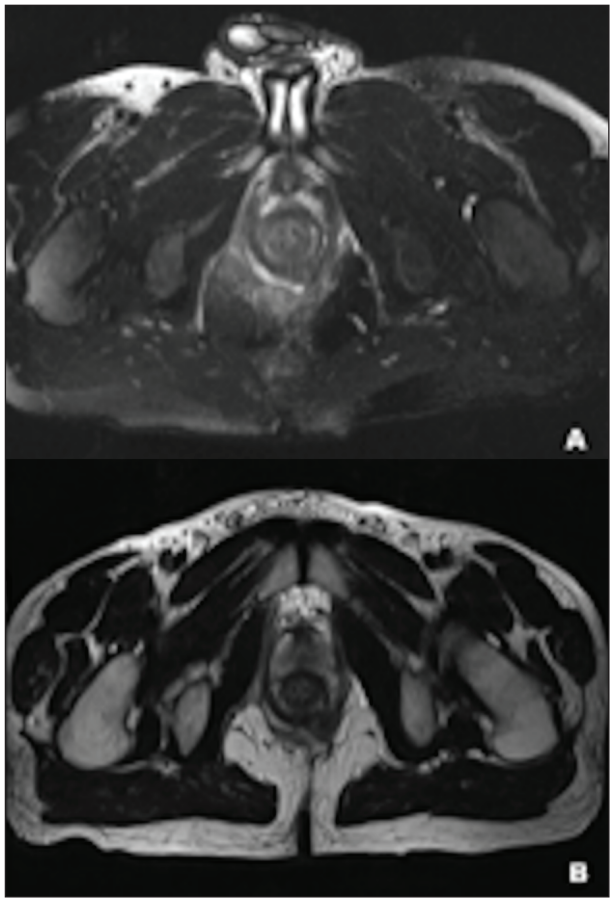

Figure 1 An oblique axial T2w fat-sat (a) and T2w (b) images show a complex transphinteric fistulous tract with an “horseshoe” feature

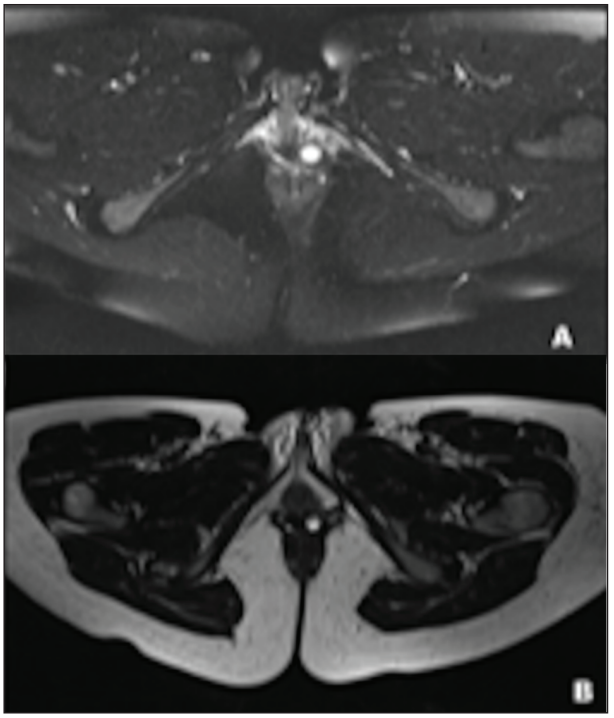

Figure 2. An oblique axial T2w fat sat (a) and T2w (b) images show an inflammatory collection at the level of the external anal sphincter

There are two main classification systems for perianal fistulas: Parks classification and St.James's University Hospital classification. Both are based on the relationship between the primary track and the sphincter muscles.

Parks classification gives central importance to the external sphincter and proposes a division into four groups:

- Intersphincteric fistulas involve only in the intersphincteric space and may reach the perianal skin through or medial to the subcutaneous external sphincter.
- Transsphincteris fistulas pass through the external sphincter into the ischiorectal fossa.
- Suprasphincteric fistulas travel upward into the intersphincteric space, passes over the top of the puborectalis muscle, then descends through the levator plate to the ischio-rectal fossa and then to the skin.
- Extrasphincteric fistula travel outside the external sphincter space without touching the anal canal.

St.James's University Hospital classification has been composed of radiologists, giving an essential role to MRI imaging, especially to landmarks that can be seen in the axial plane. The classification is composed five grade for the fistulas:

- Grade 1: Simple linear intersphincteric fistula.
- Grade 2: Intersphincteric fistula with an abscess or secondary track.
- Grade 3: Transsphincteric fistula
- Grade 4: Transsphincteric fistula with an abscess or secondary track in the ischiorectal or ischio-anal fossa.
- Grade 5: Supraelevator and Translevator Disease (17).

MRI technique

Today MRI is the gold standard imaging technique for the evaluation of perianal fistulas, mainly because it shows higher concordance with surgical findings than does any other imaging evaluation (18).

It has a high-resolution contrast and, thanks to its panoramic and multiplanar view, it gives excellent anatomic detail of the anal sphincters. It has to be performed with body or phased-array coils and not require special preparation.

The imaging plans have to be oriented perpendicular (for the axial acquisition) and parallel (for the coronal acquisition) to the long axis of the anal canal to evaluate the source of the fistulous tract including all the levator plate and the entire perineum to identify areas of sepsis and infected tract that may lead to recurrence.

For transverse image, it's better to use FOV that should extend from L5 to the anus, and for the sagittal plane, it should include both acetabula (19).

First, the operator has to perform a TSE T2w in the sagittal plane, providing an overview of the pelvis and the anal canal. After that, the appropriate protocol consists in:

1. Oblique Axial T1w FSE
2. Oblique Axial T2w FSE
3. Oblique Axial and oblique coronal fat-suppressed T1w FSE with gadolinium-based contrast material.

The saturation of fat may be obtained either with short time inversion-recovery (STIR) or frequency-selective fat saturated T2-weighted FSE.

Three-dimension (3D) T2w TSE sequences can provide source data for post-processing reformation in any plane (17). Another new tool for the diagnosis of fistulas is the MR fistulography: it is based on the presence of the wall enhancement after the injection of contrast material with digital subtraction MR (17). It is a 3D T1w gradient-echo sequence with digital subtraction, and it appears useful in the diagnosis of fistulas.

Diffusion Imaging sequence DWI/ADC is used for the study of CD fistulas, particularly in patients unable to receive intravenous contrast material.

Dynamic contrast-enhanced MR imaging with 2D T1w sequences permit to create a time-signal intensity curve and the misuration of the volume of enhancing pixels (17).

Intravenous injection of gadolinium could be performed, especially in the first MR imaging assessment of perianal CD or in case of doubts in the precontrast sequences (20).

The last development of pelvic MRI consists of the possibility of use in clinical practice higher-field-strength MR with the 3.0 T imaging. A better signal-to-noise ratio can be used to allow decreasing imaging time and maximize spatial resolution with

a better chance of characterization of perianal fistulas (1). Therefore few papers are published about the use of 3T MRI for studying patients affected by CD. Some studies are focused on pediatric patients showing more accuracy for diagnosing IBD in children and can detect perianal disease (PAD) with high specificity and moderate sensitivity (21).

MRI findings

Three pelvic spaces are present at the level of the rectum: the peritoneal space, the supra levator, and the infraelevator space, divided by the levator ani muscle. Perirectal fascia splits the supraelevator space in perirectal (medial, containing fat) and pararectal (lateral, including connective tissue and ureters). The levator ani has a V-shaped aspect on the coronal plane and a linear hypointensity on the sagittal one (19).

The first sequences of the protocol have to be an unenhanced T1w image for an anatomy overview of the pelvis. We can identify the ischiorectal fossa, the levator plate, the sphincter complex. If there is a fistula, the T1w image shows the fistulous tract as an area of low/intermediate signal similar to the typical anatomical structures of the pelvis. An advantage of using T1W sequences is in the postoperative assessment because it's possible to see hemorrhage as areas with high signal intensity.

T2w before and after contrast-enhancement signal within the fistula correlate directly with the state of flogosis (22). Therefore T2w imaging, especially with fat suppression sequences, shows the active fistula and abscesses as areas with high signal instead of chronic fistulous tract, which have low signal both in T1w and T2w.

T1w imaging after the injection of gadolinium-based contrast material help to identify small lesion and secondary tracts, particularly in recent surgical intervention. With fat suppression, we can obtain a better visualization of the fistulous track both in T1w and T2w imaging and, in T1w images, the extensions and the relationship to the anal canal mainly to the external sphincter (1). Abscesses show a central area of low signal intensity due to pus and/or air that is surrounded by intense ring enhancement. In order to avoid post-operative incontinence is helpful to establish a relationship between the primary track and the sphincter complex before treatment planning (22-24).

In another study it has been demonstrated that fistulae are more often present in patient with CD than in patients with hidradenitis suppurativa and they also communicate more often with anal sphincters. It is possible to make also a specific differential diagnosis searching features' predominance in perianal area, absence of rectal wall thickening and bilaterality of features that are more common in hidradenitis suppurativa (25).

It is also important to give information about the extension of fistulous tracts into the supraelevator space because it may change the surgical treatment: if a fistula develops both under and above the levator ani muscle, it must be managed from both sides of it to be radical (19).

Medical Treatment

Patients suffering from Crohn's disease often experience perianal disease and have complex perianal sepsis requiring repeated treatments (11).

Today the treatment of perianal fistulas in patient with CD is based on combined medical and surgical therapy. First of all antibiotics, such as ciprofloxacin and/or metronidazole are used as first line. Remission and response with this antibiotics is reported in several studies. Antibiotics have also been studied as bridges or adjuvant therapy to immunomodulators or biologics. Recent European guidelines show that antibiotics therapy must be added both in medical and surgical treatment in order to avoid local sepsis and to maintain clinical response. Immunosuppressors such as 6-mercaptopurine and azathioprine are often proposed for treatment of luminal CD but they did not demostrate significant efficacy in perianal disease (1).

Nowadays medical management of CD is based on anti-tumor necrosis factor alpha agents. The mechanism of action in unknown but it is proposed a probable down regolation of pro-infiammatory cytokine (26,27). The benefit of the treatment with infliximab, adalimumab and certolizumab pegol in the maintenance of remission is demostrated in many studies.

Partricularly, infliximab mainteinance therapy prolongs the clinical response (1). According to the Italian group for the study of infiammatory bowel disease IG-IBD, anti-TNF should be used as the first choice of medical treatment in CD (28).

Surgical Treatment

Surgical treatment is often required in the managment of perianal fistula.

Complex fistula need often a surgical approach. Initially, conservative sphincter-sparing techniques are preferred. However, because of the probable recurrence with these procedures these patients often need multiple interventions. Recurrence is usually due to infection that has gone undetected and untreated. In CD, the primary objective of initial surgery is the dreinage of abscesses to control perianal sepsis in the least invasive way possible. The secondary aim of surgery performed at a later stage is to cure the fistula while preserving continence (1).

The placement of non-cutting setons combined with medical treatment is a right solution for the treatment of complex fistula or fistula involving a significant part of the anal sphincter. This approach has shown optimal results in several studies thanks to the closure of the external opening and the minimal risk of incontinence (1). Fistulotomy allow the healing by secondary intention. Still, this treatment is used for superficial intersphincteric or transphinteric fistula, so it is fit only for few patients with CD. Biomaterials like fibrin glue can be injected into the external opening of the fistula for the treatment of complex fistula to avoid fecal incontinence or recurrence. Ligation of the intersphincteric fistula tract (LIFT) is a new surgical approach that consists of a ligature of the intersphincteric tract close to the internal opening removing all the granulation tissue. Video-assisted anal fistula treatment is another minimally invasive sphincter-sparing technique, but it needs no perineal wound.

Other surgical options are represented by a rectal mucosal advancement flap or a curvilinear flap made with mucosa, submucosa, and sometimes the muscle may be considered when sphincter function could be lost by fistulotomy (1).

When conservative therapies are not possible, fecal diversion is required packing a loop ileostomy .

An Italian group studied the use of autologous bone marrow-derived mesenchymal stromal cells and report a feasible, safe, and beneficial therapy in refractory cases (29).

Conclusions

Today pelvic MRI is the gold standard for the evaluation and quantification of perianal disease in patients with CD. Classification systems such as Parks and St James ones help the choice of the best surgical treatment and the assessment of the activity of the fistula. Thanks to MRI imaging is possible to assess the timing of the surgery accurately. Radiologists have to be familiar with perianal CD findings and complications for the central role of MRI in the management of these patients.

Acknoledgments

Thanks to the Research Program "Valere" supported by the University of Campania "L.Vanvitelli."

Conflict of interest: Authors declare that they have no commercial associations (e.g. consultancies, stock ownership, equity interest, patent/licensing arrangement etc.) that might pose a conflict of interest in connection with the submitted article.

References

1. Sheedy SP, Bruining DH, Dozois EJ, Faubion WA, Fletcher JG. MR Imaging of Perianal Crohn Disease. Radiology 2017; 282: 628-645.
2. Tang LY, Rawsthorne P, Bernstein CN. Are perineal and luminal fistulas associated in Crohn's disease? A population-based study. Clinical gastroenterology and hepatology: the official clinical practice journal of the American Gastroenterological Association 2006; 4: 1130-4.
3. Schwartz DA, Loftus EV, Jr., Tremaine WJ, et al. The natural history of fistulizing Crohn's disease in Olmsted County, Minnesota. Gastroenterology 2002; 122: 875-80.
4. Eglinton TW, Barclay ML, Gearry RB, Frizelle FA. The spectrum of perianal Crohn's disease in a population-based cohort. Diseases of the colon and rectum 2012; 55: 773-7.
5. Hellers G, Bergstrand O, Ewerth S, Holmstrom B. Occur

rence and outcome after primary treatment of anal fistulae in Crohn's disease. Gut 1980; 21: 525-7.
6. Ingle SB, Loftus EV, Jr. The natural history of perianal Crohn's disease. Digestive and liver disease : official journal of the Italian Society of Gastroenterology and the Italian Association for the Study of the Liver 2007; 39: 963-9.
7. Maconi G, Gridavilla D, Viganò C, et al. Perianal disease is associated with psychiatric co-morbidity in Crohn's disease in remission. International journal of colorectal disease 2014; 29:
8. Silva FAR, Rodrigues BL, Ayrizono MdLS, Leal RF. The Immunological Basis of Inflammatory Bowel Disease. Gastroenterology research and practice 2016; 2016: 2097274.
9. Scharl M, Rogler G. Pathophysiology of fistula formation in Crohn's disease. World J Gastrointest Pathophysiol 2014; 5: 205-212.
10. Parks AG, Gordon PH, Hardcastle JD. A classification of fistula-in-ano. The British journal of surgery 1976; 63: 1-12.
11. Agostini A, Kircher MF, Do R, et al. Magnetic Resonance Imaging of the Liver (Including Biliary Contrast Agents) Part 1: Technical Considerations and Contrast Materials. Seminars in roentgenology 2016; 51: 308-316.
12. Agostini A, Kircher MF, Do RK, et al. Magnetic Resonanance Imaging of the Liver (Including Biliary Contrast Agents)-Part 2: Protocols for Liver Magnetic Resonanance Imaging and Characterization of Common Focal Liver Lesions. Seminars in roentgenology 2016; 51: 317-333.
13. Somma F, Faggian A, Serra N, et al. Bowel intussusceptions in adults: the role of imaging. La Radiologia medica 2015; 120: 105-17.
14. Dionigi G, Dionigi R, Rovera F, et al. Treatment of high output entero-cutaneous fistulae associated with large abdominal wall defects: single center experience. International journal of surgery (London, England) 2008; 6: 51-6.
15. Maggialetti N, Capasso R, Pinto D, et al. Diagnostic value of computed tomography colonography (CTC) after incomplete optical colonoscopy. International journal of surgery (London, England) 2016; 33 Suppl 1: S36-44.
16. Reginelli A, Russo A, Iasiello F, et al. [Role of diagnostic imaging in the diagnosis of acute appendicitis: a comparison between ultrasound and computed tomography]. Recenti progressi in medicina 2013; 104: 597-600.
17. de Miguel Criado J, del Salto LG, Rivas PF, et al. MR imaging evaluation of perianal fistulas: spectrum of imaging features. Radiographics : a review publication of the Radiological Society of North America, Inc 2012; 32: 175-94.
18. Morris J, Spencer JA, Ambrose NS. MR imaging classification of perianal fistulas and its implications for patient management. Radiographics : a review publication of the Radiological Society of North America, Inc 2000; 20: 623-35; discussion 635-7.
19. O'Donovan AN, Somers S, Farrow R, Mernagh JR, Sridhar S. MR imaging of anorectal Crohn disease: a pictorial essay. Radiographics : a review publication of the Radiological Society of North America, Inc 1997; 17: 101-7.
20. Vernuccio F, Picone D, Midiri F, Salerno S, Lagalla R, Lo Re G. MR Imaging of Perianal Crohn Disease: The Role of Contrast- enhanced Sequences. Radiology 2017; 284: 921-922.
21. Ziech ML, Hummel TZ, Smets AM, et al. Accuracy of abdominal ultrasound and MRI for detection of Crohn disease and ulcerative colitis in children. Pediatric radiology 2014; 44: 1370-8.
22. Oliveira IS, Kilcoyne A, Price MC, Harisinghani M. MRI features of perianal fistulas: is there a difference between Crohn's and non-Crohn's patients? Abdominal radiology (New York) 2017; 42: 1162-1168.
23. O'Malley RB, Al-Hawary MM, Kaza RK, Wasnik AP, Liu PS, Hussain HK. Rectal imaging: part 2, Perianal fistula evaluation on pelvic MRI--what the radiologist needs to know. AJR. American journal of roentgenology 2012; 199: W43-53.
24. Beets-Tan RG, Beets GL, van der Hoop AG, et al. Preoperative MR imaging of anal fistulas: Does it really help the surgeon? Radiology 2001; 218: 75-84.
25. Monnier L, Dohan A, Amara N, et al. Anoperineal disease in Hidradenitis Suppurativa : MR imaging distinction from perianal Crohn's disease. European radiology 2017; 27: 4100-4109.
26. Berra-Romani R, Raqeeb A, Torres-Jacome J, et al. The mechanism of injury-induced intracellular calcium concentration oscillations in the endothelium of excised rat aorta. Journal of vascular research 2012; 49: 65-76.
27. Moccia F, Zuccolo E, Poletto V, et al. Targeting Stim and Orai Proteins as an Alternative Approach in Anticancer Therapy. Current medicinal chemistry 2016; 23: 3450-3480.
28. Marzo M, Felice C, Pugliese D, et al. Management of perianal fistulas in Crohn's disease: an up-to-date review. World journal of gastroenterology 2015; 21: 1394-1403.
29. Ciccocioppo R, Bernardo ME, Sgarella A, et al. Autologous bone marrow-derived mesenchymal stromal cells in the treatment of fistulising Crohn's disease. Gut 2011; 60: 788-98.

Received: 20 May 2020
Accepted: 10 June 2020
Correspondence:
Alfonso Reginelli
Department of Precision Medicine, University of Campania "L. Vanvitelli," Naples, Italy
E-mail: alfonso.reginelli@hotmail.com

Acta Biomed 2020; Vol. 91, Supplement 8: 34-42 DOI: 10.23750/abm.v91i8-S.9971

Review

Extranodal lymphomas: a pictorial review for CT and MRI classification

Alfonso Reginelli[1], Fabrizio Urraro[1], Angelo Sangiovanni[1], Gaetano Maria Russo[1], Carolina Russo[1], Roberta Grassi[1], Andrea Agostini[2], Maria Paola Belfiore[1], Michaela Cellina[3], Chiara Floridi[2], Andrea Giovagnoni[2], Antonello Sica[4], Salvatore Cappabianca[1]

[1] Department of Precision Medicine, University of Campania Luigi Vanvitelli, Naples, Italy; [2] Department of Clinical, Special and Dental Sciences, University Politecnica delle Marche, Ancona, AN, Italy; [3] Department of Radiology, Ospedale Fatebenefratelli, ASST Fatebenefratelli Sacco, Milan, Italy; [4] Oncology and Hematology Unit, Department of Precision Medicine, University of Campania; "Luigi Vanvitelli", Naples, Italy

Summary. Extranodal lymphomas represent an extranodal location of both non-Hodgkin and Hodgkin lymphomas. This study aims to evaluate the role of CT and MRI in the assessment of relationships of extranodal lymphomas with surrounding tissues and in the characterization of the lesion. We selected and reviewed ten recent studies among the most recent ones present in literature exclusively about CT and MRI imaging of extranodal lymphomas. Contrast-enhanced computed tomography (CT) is usually the first-line imaging modality in the evaluation of extranodal lymphomas, according to Lugano classification. However, MRI has a crucial role thanks to the superior soft-tissue contrast resolution, particularly in the anatomical region as head and neck. (www.actabiomedica.it)

Keywords: Extranodal lymphomas, Computed Tomography, Magnetic Resonance Imaging.

Introduction

Lymphoma is a neoplastic proliferation of lymphoid cells in lymph nodes and lymphatic tissues primarily, with bone marrow, spleen, and thymus involvement in many cases (1). In addition to lymphoid organs and tissues, lymphomas can have an extranodal location, with or without contextual nodal involvement (2). This presentation can be primitive or secondary to hematogenous spread from nodal site to extranodal site (3). The extranodal engagement occurred more frequently for non-Hodgkin lymphomas (NHL, 25-40%) than for Hodgkin lymphomas (HL, 1%). Approximately one-third of non-Hodgkin lymphomas (NHL) arise from sites other than lymph nodes, spleen, or the bone marrow (4). The median age at diagnosis for patients with NHL is 67.2 years; however, because of AIDS and organ transplantation increase, lymphoma may become more prevalent in middle-aged patients (5). The most common types of extranodal lymphomas (ENL) are diffuse large B-cell lymphoma (DLBCL) and Malt lymphoma (6).

In 43% of cases, extranodal involvement is localized in the gastrointestinal tract, followed by head and neck with 14% of cases, lung (2%), skin (7%), bone (5%), and brain (6-7%) (7). The head and neck localization represent the second most common malignant neoplasm of these anatomical regions, involving nodal and extranodal sites or both (8, 9), and Waldayer's ring is most frequently involved (10).

Diagnosis and accurate localization and staging are fundamental to choosing the best treatment strategy (11); to this end, PET/CT role has become increasingly important in recent years (12, 13) thanks to the ability to identify metabolically active tumors. At the same time, as regards ENLs and the relationships that lesions contract with surrounding tissues and organs, an accurate morphological characterization is essential, therefore the use of methods such as CT and MRI for the study of these pathologies and many

others remains fundamental. Cross-sectional imaging (MRI, CT and US) techniques gained large application in radiology; in the setting of inflammatory and oncological diseases, they are advised as techniques in the diagnosis, staging and follow-up (14-20).

The purpose of our study was to illustrate, with a pictorial review based on our case studies, typical characteristics of extranodal lymphomas found with CT and MRI, site by site.

Role of Imaging

Contrast-enhanced computed tomography (CT) is usually the first-line imaging modality for newly diagnosed neck masses to determine lesion extent and bony involvement, according to Lugano classification (21). CT diagnostic criteria for characterizing ENL include two diameters measurement (longest and shortest diameter) (22), although an interobserver variation up to 15% was observed, caused by lesions irregularity or an inferior lesion to background contrast (23). Intravenous contrast medium is fundamental, and an optimal bowel opacification is necessary for abdomen evaluation (22). ENL in CT images is reported in **Figures 1 and 2**.

Magnetic resonance imaging (MRI) provides more excellent soft-tissue contrast. It is crucial in accurately determining invasion of sophisticated anatomical planes and skull base, besides evaluating spinal or intracranial extension (**Figures 3 and 4**). Generally, the soft-tissue contrast resolution of MRI is superior to that of CT; however, ENLs MRI in the detailed region as head and neck, have been reported to show variable homogeneity and signal intensity of tumor on both T1WIs and T2WIs (24). After intravenous contrast medium administration, ENL lesions have homogeneous diffuse enhancement, predominantly peripheral thick band-like enhancement and marginal septal enhancement in 68%, 21%, and 11%, respectively, as shown by Chun et al. (25). CT and MRI play a crucial role in clinical staging, assessment of prognosis, and treatment planning for ENLs and other various pathologies (26-33).

ENLs should be in the imaging differential of any soft tissue mass showing (10): imaging homoge-

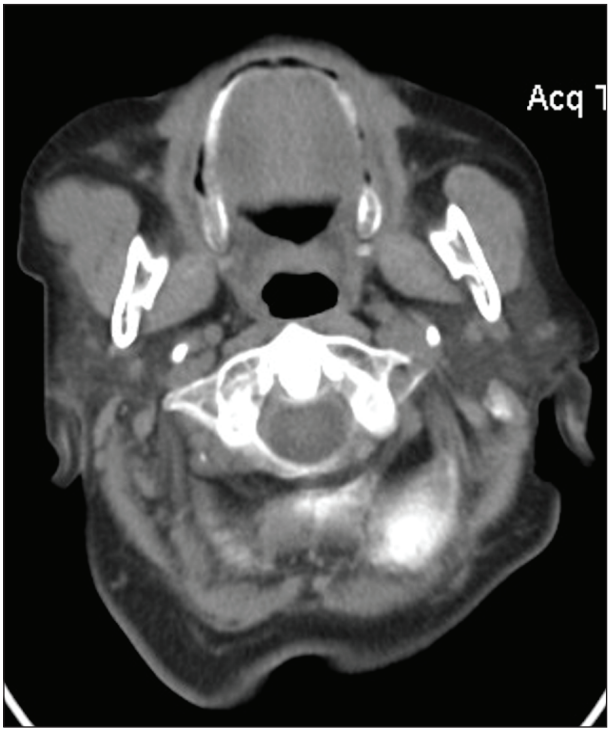

Figure 1. CT shows a rounded lesion at the level of the anterior margin of the right maxillary muscle

Figure 2. CECT shows a rounded lesion at the level of left parotid gland with inhomogeneus ce and shaded margins

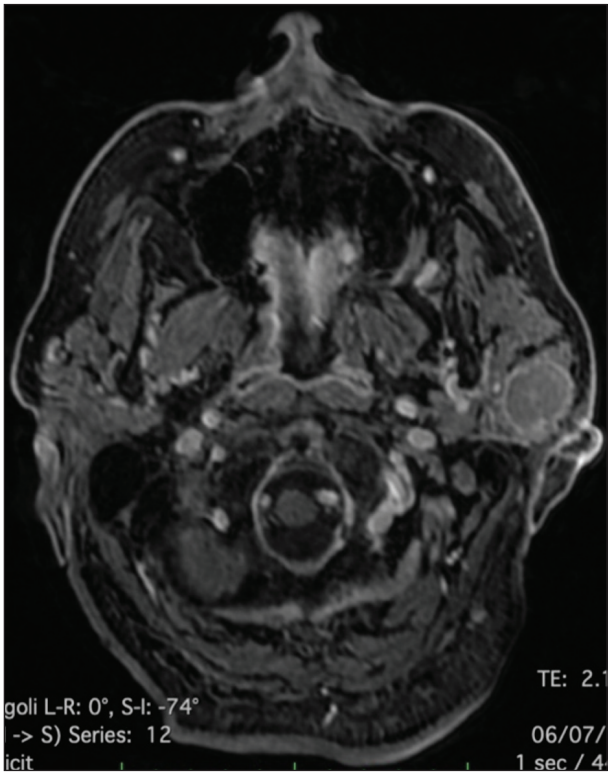

Figure 3. MRI with contrast enhancment show rounded nodular lesion in the context of the left parotid gland with shaded margins and peripheral enhancement.

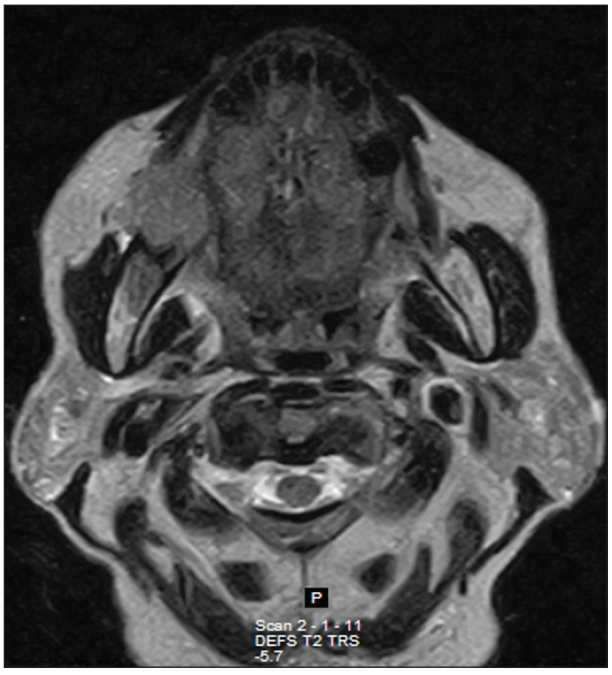

Figure 4. MRI T2w with nodular solid lesion right mandibula inhomogeneously hypointense with lobulated margins.

nous attenuation or signal; absence of calcification; hemorrhage or significant necrosis or cystic changes; the intermediate-to-low signal on fluid-sensitive MRI sequences, and marked diffusion restriction (hypercellular nature of the mass); encasement of vessels without luminal compression and moderate to intense homogenous enhancement. Whatever organs are involved by ENL, these lesions show standard features that suggest diagnosis and indicated that biopsy samples should be taken, avoiding unnecessary surgery, as in many others tumors (34). For this reason, imaging has a vital role in direct diagnosis trough imaging-guided biopsy, with accuracy at around 90% (35).

Head and neck

Lymphomas arising in the head and neck area constitute the second most frequent extranodal site after the gastrointestinal tract (36). Hereafter we will analyze ENLs characteristics in the individual subsites.

Waldeyer's ring

Waldeyer's ring is the most common site where the extranodal disease occurs in head and neck lymphomas. Together with the paranasal sinuses and the nasal cavity, Waldeyer's ring is the most frequently extranodal sites involved. More often, there are more sections of involvement within the ring, and their appearance can identify the extranodal lesions; in fact, Waldeyer's ring looks like squamous carcinoma (37). In MRI, the classical imaging appearance of the EHNLs in the Waldeyer's ring is a well-demarcated mass that shows the T2w intermediate signal conformed to space/surrounding structures with a smooth interface in contrast to epithelial malignancies. T1w shows an isointense signal, and the enhancement is homogenous (10, 38, 39). The margins are sharply demarcated also in the invasion of the adjacent spaces. Multiple subsite involvement is frequently, such as the lack of skull base destruction and unilateral or bilateral non-necrotic lymphadenopathy (40). In order of frequency, the common subsites of Waldayer's ring are (38): palatine tonsils, nasopharyngeal tonsil (or adenoids), lingual tonsils; most Waldeyer's ring lymphomas are of B-Cell

origin, and more than half occur in the palatine tonsil (41, 42). Symptoms are similar to squamous cell carcinoma in these locations. Still, on clinical inspection, the EHNLs is not ulcerated mucosal masses like in the squamous cell carcinoma, and they appear mostly submucosal (43). Clinical symptoms depending on the area involved: f.e., sore throat or tonsillar swelling are present in tonsils involving; nasal obstruction, cervical mass, obstruction of Eustachian tube with decreased hearing in nasopharyngeal tonsil (40); foreign body sensation in lingual tonsils. EHNLs of Waldeyer's ring is associated with gastric disease in 10 percent of patients (43). The appearance of Waldeyer's ring ENLs is shown in **Figure 5**.

Sinonasal region

Sinonasal lymphomas are very rare; they affect less than 1 percent of all malignant tumors of the head and neck and are mainly non-Hodgkin lymphomas (44).

They are divided into two groups that have different symptoms, prognosis, and treatment: B-cell lymphomas, more frequent, less aggressive but with better prognosis; T/NK cell lymphomas: rarer but most found in the nasal cavity (45).

Regarding symptoms, high-grade lymphomas are aggressive with a non-healing ulcer, pain, cranial nerve manifestations, facial swelling, and epistaxis. Low-grade lymphomas present with a sinonasal mass associated with obstructive symptoms, meanwhile high-grade diffuse large B-cell tumors are used to present with bone or soft tissue destruction; T-cell lymphomas are associated with perforation or damage of the nasal septum (44, 46).

In imaging, they are bulky masses with intermediate signal intensity on MRI with moderate contrast improvement. ENL is presented as a destructive soft tissue mass that can mimic squamous cell carcinoma but tends to be more homogeneous in T2 imaging with less intense carcinoma enhancement. Although the areas of development are different, lymphomas are more frequent in the nasal cavity or the maxillary sinus, and the lesions can reshape or erode adjacent bones. Sites like frontal or sphenoid sinuses or the ethmoid are infrequent (47) (**Figure 6)**.

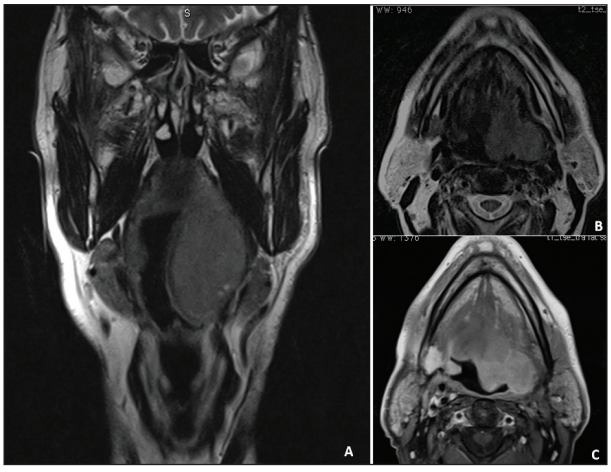

Figure 5. (a-b) Waldeyer's ring lesion. MRI T2w. Nodular capsulated solid lesion in the left parapharyngeal space with reduction of the pharyngeal airspace. (c) After i.v administration the lesion show midly inhomogeneous enhancement.

Figure 6. CT of a bulky masses inhomogeneous hypodensity. The CT show a destructive soft tissue mass can mimic squamous cell carcinoma.

Thyroid

Primary thyroid lymphoma is a rare tumor accounting for 1 to 5% of all thyroid malignancies and approximately 2% of all malignant extranodal lymphomas (48). Pure thyroid MALT lymphomas comprise about 6 to 28% of primary thyroid lymphomas and are recognized as extranodal marginal zone B-cell lymphomas (49, 50). Thyroid lymphoma is a rare pathology associated with about 80 % by cases with Hashimoto thyroiditis and more frequent in women, especially between 70 and 80 years (51, 52). The most frequent sign is a palpable mass with neck enlargement, but patients may also present a cold thyroid nodule or symptoms as dysphagia, hoarseness, and suffocation. Primary thyroid lymphoma can be confused radiologically with anaplastic thyroid carcinoma; however, these lesions are characterized by typical features, classified into three types detectable in CT and MRI exams (53):

- type 1 is a solitary nodule surrounded by healthy thyroid tissue, which rapidly enlarges the mass by imitating anaplastic thyroid carcinoma or other aggressive carcinomas;
- type 2 consists of several thyroid nodules that mimic the goiter;
- type 3 shows a homogeneous enlargement of both thyroid lobes with reduced attenuation, with or without peripheral hyper-attenuating thyroid tissue.

A difference between thyroid lymphoma and carcinoma is the presence on transverse imaging of a more homogeneous signal, whereas the lack of calcification, cystic degeneration, or necrosis distinguishes it from goiter (52).

Tongue

Extranodal lymphomas of the tongue are a very rare disease. The alterations are identifiable with the physical examination, while MRI is useful for defining exact disease extension.

Salivary gland

Primary salivary gland lymphoma represents 2-5% of all salivary gland neoplasms, involving parotid gland (70%) and submandibular gland more frequently (54). The diagnosis of primary lymphomatous involvement of the parotid gland requires that three criteria must be fulfilled: involvement of organ is the first disease manifestation; disease must involve gland parenchyma and not adjacent nodes; lymphoid infiltrate is malignant (55). For instrumental diagnosis, CECT should be performed from skull base to clavicles for intraparotid lesions to evaluate the extent of cervical disease fully. In the case of NHL clinical suspicion, special attention must be paid as they may be isodense and, therefore, invisible in CECT. If MRI performed, T2 MR, FS, or STIR make intraparotid lesions more conspicuous; a single unilateral mass of relative soft-tissue homogeneity with a poorly defined margin was thought to be the most common sign of a parotid lymphoma (56). Diffusion-weighted imaging is beneficial in unusual cases with shallow apparent diffusion coefficient values.

Cranial vault and skull base

THE primary NHL of calvarial bones is extremely rare. If present, initial symptoms, and signs usually include painless scalp nodules, headaches, convulsions, or focal neurological deficits, also not to be forgotten as a complication is cerebrospinal fluid diffusion. In the imaging findings of the cranial vault, lymphoma may be present cerebral infiltration and orbital involvement (57, 58). Even though CT is superior to assess cortical bony destruction, MRI allows for better soft tissue characterization, the extent of involvement, and marrow infiltration. Although MRI cannot diagnose lymphoma with certainty, its inclusion in the differential can be critical, since the surgical approach can be very different.

In the skull base, ENLs mainly involve clivus, and principal CT is permeative bony destruction. Other less common imaging features include destructive lytic pattern, sclerosis, or bone expansion beyond cortex, or "traversing" bone lesion with preserved cancellous bone and minimal attenuation of the cortex. Typically, the injury is often isointense to the gray matter on T1WI and intermediate signal on T2WI.

Acknoledgements

Thanks to the Research Program "Valere" supported by the University of Campania "L.Vanvitelli."

Conflict of interest: Authors declare that they have no commercial associations (e.g. consultancies, stock ownership, equity interest, patent/licensing arrangement etc.) that might pose a conflict of interest in connection with the submitted article.

References

1. Guermazi A, Brice P, de Kerviler EE, et al. Extranodal Hodgkin disease: spectrum of disease. Radiographics : a review publication of the Radiological Society of North America, Inc 2001; 21: 161-79.
2. Gurney KA, Cartwright RA. Increasing incidence and descriptive epidemiology of extranodal non-Hodgkin lymphoma in parts of England and Wales. The hematology journal : the official journal of the European Haematology Association 2002; 3: 95-104.
3. Even-Sapir E, Lievshitz G, Perry C, Herishanu Y, Lerman H, Metser U. Fluorine-18 fluorodeoxyglucose PET/CT patterns of extranodal involvement in patients with Non -Hodgkin lymphoma and Hodgkin's disease. Radiologic clinics of North America 2007; 45: 697-709, vii.
4. Groves FD, Linet MS, Travis LB, Devesa SS. Cancer surveillance series: non-Hodgkin's lymphoma incidence by histologic subtype in the United States from 1978 through 1995. Journal of the National Cancer Institute 2000; 92: 1240-51.
5. Zucca E, Conconi A, Cavalli F. Treatment of extranodal lymphomas. Best practice & research. Clinical haematology 2002; 15: 533-47.
6. Vannata B, Zucca E. Primary extranodal B-cell lymphoma: current concepts and treatment strategies. Chinese clinical oncology 2015; 4: 10.
7. Paes FM, Kalkanis DG, Sideras PA, Serafini AN. FDG PET/CT of extranodal involvement in non-Hodgkin lymphoma and Hodgkin disease. Radiographics : a review publication of the Radiological Society of North America, Inc 2010; 30: 269-91.
8. Thomas AG, Vaidhyanath R, Kirke R, Rajesh A. Extranodal lymphoma from head to toe: part 1, the head and spine. AJR. American journal of roentgenology 2011; 197: 350-6.
9. Urquhart A, Berg R. Hodgkin's and non-Hodgkin's lymphoma of the head and neck. The Laryngoscope 2001; 111: 1565-9.
10. Watal P, Bathla G, Thaker S, Sato TS, Moritani T, Smoker WRK. Multimodality Imaging Spectrum of the Extranodal Lymphomas in the Head and Neck-A Pictorial Review. Current problems in diagnostic radiology 2018; 47: 340-352.
11. Glass AG, Karnell LH, Menck HR. The National Cancer Data Base report on non-Hodgkin's lymphoma. Cancer 1997; 80: 2311-20.
12. Kostakoglu L, Goldsmith SJ. Fluorine-18 fluorodeoxyglucose positron emission tomography in the staging and follow- up of lymphoma: is it time to shift gears? European journal of nuclear medicine 2000; 27: 1564-78.
13. Das J, Ray S, Sen S, Chandy M. Extranodal involvement in lymphoma - A Pictorial Essay and Retrospective Analysis of 281 PET/CT studies. Asia Oceania journal of nuclear medicine & biology 2014; 2: 42-56.
14. Agliata G, Schicchi N, Agostini A, et al. Radiation exposure related to cardiovascular CT examination: comparison between conventional 64-MDCT and third-generation dual-source MDCT. La Radiologia medica 2019; 124: 753-761.
15. Floridi C, Radaelli A, Pesapane F, et al. Clinical impact of cone beam computed tomography on iterative treatment planning during ultrasound-guided percutaneous ablation of liver malignancies. Medical oncology (Northwood, London, England) 2017; 34: 113.
16. Agostini A, Kircher MF, Do R, et al. Magnetic Resonance Imaging of the Liver (Including Biliary Contrast Agents) Part 1: Technical Considerations and Contrast Materials. Seminars in roentgenology 2016; 51: 308-316.
17. Panfili E, Nicolini D, Polverini V, Agostini A, Vivarelli M, Giovagnoni A. Importance of radiological detection of early pulmonary acute complications of liver transplantation: analysis of 259 cases. La Radiologia medica 2015; 120: 413-20.
18. Agostini A, Mari A, Lanza C, et al. Trends in radiation dose and image quality for pediatric patients with a multidetector CT and a third-generation dual-source dual-energy CT. La Radiologia medica 2019; 124: 745-752.
19. Agostini A, Kircher MF, Do RK, et al. Magnetic Resonanance Imaging of the Liver (Including Biliary Contrast Agents)-Part 2: Protocols for Liver Magnetic Resonanance Imaging and Characterization of Common Focal Liver Lesions. Seminars in roentgenology 2016; 51: 317-333.
20. Paolicchi F, Bastiani L, Guido D, Dore A, Aringhieri G, Caramella D. Radiation dose exposure in patients affected by lymphoma undergoing repeat CT examinations: how to manage the radiation dose variability. La Radiologia medica 2018; 123: 191-201.
21. Cheson BD, Fisher RI, Barrington SF, et al. Recommendations for initial evaluation, staging, and response assessment of Hodgkin and non-Hodgkin lymphoma: the Lugano classification. Journal of clinical oncology : official journal of the American Society of Clinical Oncology 2014; 32: 3059-68.
22. Regacini R, Puchnick A, Luisi FAV, Lederman HM. Can diffusion-weighted whole-body MRI replace contrast-enhanced CT for initial staging of Hodgkin lymphoma in children and adolescents? Pediatric radiology 2018; 48: 638-647.
23. Hopper KD, Kasales CJ, Van Slyke MA, Schwartz TA, TenHave TR, Jozefiak JA. Analysis of interobserver and intraobserver variability in CT tumor measurements. AJR. American journal of roentgenology 1996; 167: 851-4.
24. Matsuzaki H, Hara M, Yanagi Y, et al. Magnetic resonance imaging (MRI) and dynamic MRI evaluation of extranodal non-Hodgkin lymphoma in oral and maxillofacial regions. Oral surgery, oral medicine, oral pathology and oral radiology 2012; 113: 126-133.
25. Chun CW, Jee WH, Park HJ, et al. MRI features of skeletal

muscle lymphoma. AJR. American journal of roentgenology 2010; 195: 1355-60.
26. Muccio CF, Di Blasi A, Esposito G, Brunese L, D'Arco F, Caranci F. Perfusion and spectroscopy magnetic resonance imaging in a case of lymphocytic vasculitis mimicking brain tumor. Polish journal of radiology 2013; 78: 66-9.
27. Cozzi D, Dini C, Mungai F, Puccini B, Rigacci L, Miele V. Primary pulmonary lymphoma: imaging findings in 30 cases. La Radiologia medica 2019; 124: 1262-1269.
28. Marampon F, Gravina GL, Popov VM, et al. Close correlation between MEK/ERK and Aurora-B signaling pathways in sustaining tumorigenic potential and radioresistance of gynecological cancer cell lines. International journal of oncology 2014; 44: 285-94.
29. d'Amuri FV, Maestroni U, Pagnini F, et al. Magnetic resonance imaging of adrenal gland: state of the art. Gland surgery 2019; 8: S223-s232.
30. Bevilacqua A, D'Amuri FV, Pagnini F, et al. Percutaneous needle biopsy of retroperitoneal lesions: technical developments. Acta bio-medica : Atenei Parmensis 2019; 90: 62-67.
31. D'Amico G, Di Crescenzo V, Muto M, et al. Cytological diagnosis of limph nodes by instrumental guide: Ultrasonography and CT. Recenti progressi in medicina 2013; 104: 367-370.
32. Cipriani P, Di Benedetto P, Ruscitti P, et al. Perivascular Cells in Diffuse Cutaneous Systemic Sclerosis Overexpress Activated ADAM12 and Are Involved in Myofibroblast Transdifferentiation and Development of Fibrosis. J Rheumatol 2016; 43: 1340-9.
33. Giacomelli R, Liakouli V, Berardicurti O, et al. Interstitial lung disease in systemic sclerosis: current and future treatment. Rheumatology international 2017; 37: 853-863.
34. Frampas E. Lymphomas: Basic points that radiologists should know. Diagnostic and interventional imaging 2013; 94: 131-44.
35. Hesselmann V, Zahringer M, Krug B, et al. Computed-tomography- guided percutaneous core needle biopsies of suspected malignant lymphomas: impact of biopsy, lesion, and patient parameters on diagnostic yield. Acta radiologica (Stockholm, Sweden : 1987) 2004; 45: 641-5.
36. Frata P, Buglione M, Grisanti S, et al. Localized Extranodal Lymphoma of the Head and Neck: Retrospective Analysis of a Series of 107 Patients from a Single Institution. Tumori 2005; 91: 456-62.
37. Lee YY, Van Tassel P, Nauert C, North LB, Jing BS. Lymphomas of the head and neck: CT findings at initial presentation. AJR. American journal of roentgenology 1987; 149: 575-81.
38. Aiken AH, Glastonbury C. Imaging Hodgkin and non -Hodgkin lymphoma in the head and neck. Radiologic clinics of North America 2008; 46: 363-78, ix-x.
39. Kato H, Kanematsu M, Kawaguchi S, Watanabe H, Mizuta K, Aoki M. Evaluation of imaging findings differentiating extranodal non-Hodgkin's lymphoma from squamous cell carcinoma in naso- and oropharynx. Clinical imaging 2013; 37: 657-63.
40. King AD, Lei KI, Richards PS, Ahuja AT. Non-Hodgkin's lymphoma of the nasopharynx: CT and MR imaging. Clinical radiology 2003; 58: 621-5.
41. Nayak LM, Deschler DG. Lymphomas. Otolaryngologic clinics of North America 2003; 36: 625-46.
42. Yuen A, Jacobs C. Lymphomas of the head and neck. Seminars in oncology 1999; 26: 338-45.
43. Aviles A, Delgado S, Ruiz H, de la Torre A, Guzman R, Talavera A. Treatment of non-Hodgkin's lymphoma of Waldeyer's ring: radiotherapy versus chemotherapy versus combined therapy. European journal of cancer. Part B, Oral oncology 1996; 32b: 19-23.
44. Abbondanzo SL, Wenig BM. Non-Hodgkin's lymphoma of the sinonasal tract. A clinicopathologic and immunophenotypic study of 120 cases. Cancer 1995; 75: 1281-91.
45. Van Prooyen Keyzer S, Eloy P, Delos M, Doyen C, Bertrand B, Rombaux P. Sinonasal lymphomas. Case report. Acta oto-rhino-laryngologica Belgica 2000; 54: 45-51.
46. Yasumoto M, Taura S, Shibuya H, Honda M. Primary malignant lymphoma of the maxillary sinus: CT and MRI. Neuroradiology 2000; 42: 285-9.
47. Das S, Kirsch CF. Imaging of lumps and bumps in the nose: a review of sinonasal tumours. Cancer imaging : the official publication of the International Cancer Imaging Society 2005; 5: 167-77.
48. Pedersen RK, Pedersen NT. Primary non-Hodgkin's lym phoma of the thyroid gland: a population based study. Histopathology 1996; 28: 25-32.
49. Jaffe ES, Harris NL, Diebold J, Muller-Hermelink HK. World Health Organization classification of neoplastic diseases of the hematopoietic and lymphoid tissues. A progress report. American journal of clinical pathology 1999; 111: S8-12.
50. Thieblemont C, Mayer A, Dumontet C, et al. Primary thyroid lymphoma is a heterogeneous disease. The Journal of clinical endocrinology and metabolism 2002; 87: 105-11.
51. Kim HC, Han MH, Kim KH, et al. Primary thyroid lymphoma: CT findings. European journal of radiology 2003; 46: 233-9.
52. Widder S, Pasieka JL. Primary thyroid lymphomas. Current treatment options in oncology 2004; 5: 307-13.
53. Matsuzuka F, Miyauchi A, Katayama S, et al. Clinical aspects of primary thyroid lymphoma: diagnosis and treatment based on our experience of 119 cases. Thyroid : official journal of the American Thyroid Association 1993; 3: 93-9.
54. Wolvius EB, van der Valk P, van der Wal JE, et al. Primary non-Hodgkin's lymphoma of the salivary glands. An analysis of 22 cases. Journal of oral pathology & medicine : official publication of the International Association of Oral Pathologists and the American Academy of Oral Pathology 1996; 25: 177-81.
55. Hirokawa N, Hareyama M, Akiba H, et al. Diagnosis and Treatment of Malignant Lymphoma of the Parotid Gland. Japanese Journal of Clinical Oncology 1998; 28: 245-249.
56. Zhu L, Wang P, Yang J, Yu Q. Non-Hodgkin lymphoma involving the parotid gland: CT and MR imaging findings. Dentomaxillofac Radiol 2013; 42: 20130046-20130046.

57. Kantarci M, Erdem T, Alper F, Gundogdu C, Okur A, Aktas A. Imaging characteristics of diffuse primary cutaneous B-cell lymphoma of the cranial vault with orbital and brain invasion. AJNR. American journal of neuroradiology 2003; 24: 1324-6.
58. Jamjoom AB, Jamjoom ZA, Naim Ur R, Cheema MA. Primary midline cranial vault lymphoma simulating a parasagittal meningioma: the role of angiography in preoperative diagnosis. Neurosurgical review 1998; 21: 202-5.

Received: 20 May 2020
Accepted: 10 June 2020
Correspondence:
Alfonso Reginelli
Department of Precision Medicine,
University of Campania
"L. Vanvitelli," Naples, Italy
E-mail: alfonso.reginelli@hotmail.com

Acta Biomed 2020; Vol. 91, Supplement 8: 43-50 DOI: 10.23750/abm.v91i8-S.9972

Review

Anterior chest wall non-traumatic diseases: a road map for the radiologist

Susanna Guerrini[1], Giulio Bagnacci[2], Antonio Barile[3], Ernesto La Paglia[4], Francesco Gentili[5], Luca Luzzi[6], Nicola Giordano[7], Antonella Fioravanti[8], Francesca Bellisai[8], Luca Cantarini[8], Luca Volterrani[2], Bruno Frediani[8], Maria Antonietta Mazzei[2]

[1] Unit of Diagnostic Imaging, Department of Radiological Sciences, University of Siena, Azienda Ospedaliero-Universitaria Senese, Siena, Italy; [2] Unit of Diagnostic Imaging, Department of Medical, Surgical and Neuro Sciences and of Radiological Sciences, University of Siena, Azienda Ospedaliero-Universitaria Senese, Siena, Italy; [3] Department of Biotechnology and Applied Clinical Sciences, University of L'Aquila, L'Aquila, Italy; [4] Unit of Diagnostic Imaging, Humanitas Cellini, Torino, Italy; [5] Section of Radiology, Department of Medicine and Surgery, Azienda Ospedaliera Universitaria di Parma, Parma, Italy; [6] Thoracic Surgery Unit, Department of Medical, Surgical and Neuro Sciences, University of Siena, Azienda Ospedaliero-Universitaria Senese, Siena, Italy; [7] Scleroderma Unit, Internal Medicine, Department of Medical, Surgical and Neuro Sciences, University of Siena, Azienda Ospedaliero-Universitaria Senese, Siena, Italy; [8] Unit of Rheumatology, Department of Medical, Surgical and Neuro Sciences, University of Siena, Azienda Ospedaliero-Universitaria Senese, Siena, Tuscany, Italy

Summary. The anterior chest wall (AWC) non-traumatic pathologies are largely underestimated, and early detection through imaging is becoming increasingly important. This paper aims to review the major non-traumatic ACW pathologies, with a particular interest in imaging features and differential diagnosis. (www.actabiomedica.it)

Keywords: anterior chest wall, ultrasound, magnetic resonance imaging, computed tomography, DECT, sternocostoclavicular joint.

Introduction

The anterior chest wall (AWC) non-traumatic pathologies are largely underestimated. Both the ACW joints and bone structures can be subject to infective, degenerative, inflammatory, malformative, or oncologic diseases, that could present with the same symptoms (1-5). In this context, early detection through imaging is becoming increasingly important. This paper aims to review the major non-traumatic ACW pathologies, with a particular interest in imaging features and differential diagnosis.

Essential Anatomy of Anterior Chest Wall

Knowledge of the anatomy of the ACW is fundamental for a correct interpretation of imaging features. *Sternocostal Joint (SCOJ)* is composed of the costochondral cartilage from the second rib and their articulation with the sternum (manubrium and body). It contains an interarticular ligament and two synovial membranes, similar to the costovertebral joints (6).

Manubriosternal Joint (MSJ) is an amphiarthrodial joint comprising two hyaline cartilage-covered surfaces separated by a fibrocartilaginous disk that is anchor by dorsal and ventral ligaments covering the surfaces of the joint. In about 30% of people, the absorption of the disk results in synovial joint conversion (6).

Sternoclavicular Joint (SCJ) is a diarthrodial saddle-shaped synovial joint composed by the sternal end of the clavicle, the clavicular notch of the manubrium, and the cartilage of the first rib (7). Between the two articular surfaces, there is a fibrocartilaginous disk that separates the joint into two distinct synovial cavities (8). The joint capsule consists of a fibrous outer layer and an inner synovial membrane (7, 8).

Imaging

Imaging is becoming increasingly important in the early diagnosis, to start a customized treatment, and during follow-up of ACW pathologies (9, 10). Multimodality imaging may be required in some cases for a proper assessment of different pathological features (11-15). Due to its wide availability and low costs (16-17), X-Ray (XR) represents the first-line imaging investigation, with standard and special projections (above all Rockwood or serendipity) that can assess bone structural changes, even if limited by the overlapping of vertebrae and ribs, the congenital oblique orientation of SCJ and the inability to delineate the soft tissues (6, 18). *Digital tomography (DT),* using a single pass of the radiographic generator over a digital detector, obtains a sequence of multiple digital X-ray images (9) of the ACW overcoming both overlapping phenomena and limitations caused by congenital oblique orientation. Even if XR/DT permit a differential diagnosis with unilateral involvement and could demonstrate the enlargement of the articular cavity (suggestive for inflammatory disease) or the presence of cortical bone interruption (suggestive for neoplastic lesion), other imaging modalities are often necessary (18). *Ultrasound (US)* and *Magnetic Resonance Imaging (MRI)* have focused on the demonstration/quantification of pathologies affecting the synovia and allow early diagnosis of inflammatory arthropathies (9, 19-20). These imaging methods can also be applied for interventional purposes (21-25); for example, aspiration of the joint under US can help to isolate organisms or demonstrating crystals. Moreover, *contrast-enhanced US (CEUS)* and MRI can demonstrate the presence of active inflammation and quantify inflammation or neoplastic processes (2, 26,27). MRI seems to be superior to US/CEUS in the assessment of bone tissue inflammation (marrow edema and osteitis), bone erosion, and cartilage loss in association with its panoramic view (26,28,29). *Computed Tomography (CT)* is most indicated for bone destruction/ossification or in cases of malformations (30,31). However, thanks to the introduction of *Dual-Energy CT (DECT)* technology, it could also identify/quantify marrow edema, allowing to demonstrate active inflammation and accurate differential diagnosis in crystal-deposition arthropathy (presence and type of crystal) (32-35).

Whole-body bone scintigraphy (58), using technetium 99m-labeled diphosphonate, provides information about the whole skeleton in a single examination, and it is usually used to diagnose inflammatory changes in the ACW when there is a suspicion about the involvement of other areas (6, 36).

Medical History

ACW can be affected alone or in systemic pathologies; for this reason, a complete medical history including laboratory tests should be made, before any imaging evaluation, in order to contribute the differential diagnosis (**tab. 1**) (8, 18).

Major pathologies of the anterior thoracic wall

Osteoarthritis

Osteoarthritis (OA) is the most common condition affecting the SCJ, less frequently the MSJ, presenting with local pain/swelling and limited motion of arms/shoulders (particularly high elevation with crepitus) (8). OA is typically bilateral and asymmetric, with right-sided predominance (7). It is common in advanced age; however, there are some predisposing factors, such as manual labor (8). XR/DT and CT (more sensitive) can demonstrate subchondral sclerosis, cysts, osteophytes, and joint space narrowing (37, 38). US highlights the presence of joint distention, hyperemia, and cortical irregularity. The matches findings on MRI are low-signal intensity on all sequences in the areas of subchondral sclerosis and foci of hyperintense signal on T2-weighted images (T2WI) in the areas of cystic changes and edema (26).

Rheumatoid Arthritis

The SCJ rate of involvement in patients affected by rheumatoid arthritis (RA) is variable (1% to 43%), whereas the MSJ rate is about 27%, according to the percentage of synovial conversion (6, 8). Symptoms include swelling, tenderness, crepitus, and painful limitation of movements; the diagnosis is confirmed by

Table 1. Main features of non-traumatic ACW diseases

Disease	*Sex*	*Age (y)*	*Site*	*Side*	*Pain*	*Laboratory*	***Radiographic changes***
Osteoarthritis	M=F	>40	SCJ	B	+	Normal	Sclerosis, osteophytes
Rheumatoid arthritis	F>M	Any	SCJ, MSJ	B	+	+RF, +ANA	Often unremarkable
Seronegative spondyloarthropathies	M>F	<40	SCJ, MSJ	U	Not frequent	+HLA-B27	Erosions, cysts
Sonozaki syndrome	M>F	<40	SCJ, SCOJ	U	Not frequent	–HLA-B27	Diffuse sclerosis
SAPHO syndrome	M>F	30-60	SCJ, SCOJ, MSJ	B	+	↑ESR, –reumatologic marker	Sclerosis, enthesopathic bone formation
Crystal Deposition Arthropathy	M>F	>40	SCJ	U	+++	+BRFC, –BRFC	Calcification of soft tissue
Condensing osteitis	F>M	25-40	Medial end of the clavicle	U	+	Normal	Medial clavicle enlargement, marrow obliteration
Friedrich's disease	F>M	Any	Medial end of the clavicle	U	+	Normal	Irregular end of medial clavicle
Tietze's syndrome	F>M	20-50	II-IV costochondral junctions	U	+	Oten normal	hypertrophy and calcification of the costal cartilages
Septic Artritis	M=F	Any	SCJ	U	+++	↑WBC, ↑ESR, ↑CRP	Sclerotic, lytic, or mixed lesions
Neoplasm	M=F	Any	Any	U	+	Normal, ↑neoplastic markers	Bone enlargement, mass, cortical bone interruption

B = bilateral, U = unilateral, ANA = antinuclear antibodies, BRFC = birefringent crystals, CRP = C-reactive protein, ESR = erythrocyte sedimentation rate, RF = rheumatoid factor, WBC = white blood cell count, + = elevated levels or presence of, ++ = moderate elevation, +++ = marked elevation, – = not seen or absence of.

anti-cyclic citrullinated peptide serum testing (37, 39, 40). Isolated involvement is not impossible; however, polyarticular disease and bilaterality are common. The pathologic process of RA includes synovial inflammation, pannus formation, bony erosions, degeneration of the intra-articular disk, and joint space narrowing (8). In the very early phase of involvement, XR is generally unremarkable, whereas US could detect synovial inflammation, pannus formation (hypoechoic and non-compressible), and intraarticular synovial blood perfusion using the power Doppler technique; it could also detect irregularity of cortical bone surface (41, 42). Contrast-enhancement MRI (CE-MRI), is the primary technique in the early phase of the disease, demonstrating marrow edema (a factor strictly related with prognosis), synovial inflammation with joint effusions containing rice bodies (suggestive of RA). CT shows tiny bony erosions and joint destruction in the full-blown disease but could also be useful in the early phase if performed with DECT technique (35).

Seronegative Spondyloarthropathies

The ACW can also be affected in seronegative spondyloarthropathies (SSpA) (38). The prevalence of the involvement and the site may vary according to the type of SSpA: *psoriatic arthritis* has a predilection for the SCJ (50% of cases), whereas MSJ has a high incidence involvement (80%) in *ankylosis spondylitis* (6, 7). The onset is usually before age 40 years, and diagnosis could be confirmed by the detection of HLA-B27 in association with a clinical history of dermatologic/ gastrointestinal symptoms and absence of serum autoantibodies. Symptoms are usually unilateral (swelling, tenderness, and pain) (8). Structural changes (osseous hyperostosis, enthesophytes) can be detected by XR or CT. CT could demonstrate marginal erosions of the sternum, clavicle, or both, as well as subchondral erosion and sclerosis, whereas MRI is needed for detecting early changes, such as marrow edema and enthesitis (**fig. 1**). MRI is also useful in the follow-up of patients to differentiate

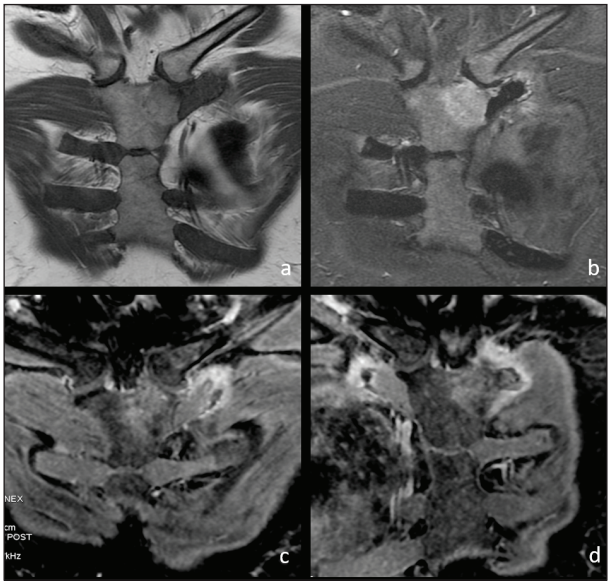

Figure 1. MRI examination of a 38y old female with psoriasis and pain and swelling of the left SCJ. She told the same symptoms a few years earlier, at the controlateral SCJ. MRI showed fat deposition (T1 weighted image, a) and marrow edema (T2 weighted image, b) of the subchondral bone of the manubrium and signs of enthesitis on the costochondral cartilage of the first rib and on the inner portion of the end of the clavicle (T2 weighted image, b, and T1 gradient echo image with fat saturation after contrast media administration, c and d). Signs of enthesitis were also present on the costochondral cartilage of the first rib on the right side (d). The MRI diagnosis, confirmed by clinical and laboratory data, was AWC involvement in psoriatic arthritis.

active from chronic forms and to manage other joints involvement (axial skeleton or sacroiliac joints) (28, 43, 44). The end-stage appearance of the SCJ consists of ankylosis of the sternoclavicular or costosternal joints (45). The *Sonozaki syndrome* (SS), also known as pustulotic arthro-osteitis (PAO), belongs to the group of psoriatic arthritis; however, no relation with antigen HLA-B27 was observed (46). CT could detect the periosteal reaction of the clavicles in the early phase, inflammatory enthesopathy of the costoclavicular ligament, arthritis of the SCJ, and erosive and sclerotic processes of the MSJ. MRI and DECT can quantify the activity of the inflammation, better characterizing soft-tissue and bone involvement (47). Whether the SAPHO (Synovitis–acne–pustulosis–hyperostosis–osteitis) syndrome represents a clinical entity by itself or should be considered a subset within the family of SSpA [due to the frequent affliction of the axial skeleton (91%), enthesitis, and inflammatory bowel diseases], is still unknown (7, 48, 49). It includes symptoms of the Sonozaki syndrome, chronic recurrent multifocal osteomyelitis of bone marrow and bones (CRMO), focused acne, and others (7). SCJ, SCOJ, and MSJ are most commonly affected (70 to 90%); bilateral involvement is the most frequent, but symptoms can be unilateral. The middle-aged women are preferred (49). In adults after at least three months of disease, XR findings can be characteristic represented by expanded bone, sclerosis, osteolysis, periosteal reaction, and enthesopathic new bone formation; MRI might be required to detect subclinical lesions (low signal intensity corresponding to the sclerotic bone and areas of high signal intensity on T2WI due to marrow edema/osteitis) (48, 49).

Crystal Deposition Arthropathy

Both gout and calcium pyrophosphate dehydrate deposition (CPPD) disease can involve the SCJ (37). Symptoms can be acute pain and swelling; sometimes, it can present with swelling alone, mimicking a tumor (7). Aspiration of swollen joint and following evaluation under polarizing light microscopy allows the correct diagnosis (50). The prevalence of CPPD crystal deposition in the SCJ is 17% and increases with patient age (50). XR is often negative in the early phase of the disease. In the superficial portion of the joint, US is sensitive in the individuation of CPPD (fibrocartilages and tendons crystal deposition) and gouty tophi in subcutaneous tissues or tendons that appear as hyperechoic with a heaped-up appearance (37). MRI is used to assess inflammation, bone erosions, cartilage damage, and tophi, with low signal intensity on T1WI and iso- to high signal intensity on T2WI (7). DECT represents the best imaging modality to diagnose crystal deposition arthropathy differentiating the type of crystal by analyzing specific attenuation characteristics, and showing marrow edema and/or erosions (34, 51).

Condensing osteitis

Condensing osteitis (CO), also known as aseptic enlarging osteosclerosis, is a rare condition character-

ized by sclerosis and enlargement of the medial end of the clavicle not involving the SCJ (52). Predisposing factors are mechanical stress, trauma, infections, and female sex (20–60 years of age) (8). Symptoms are local swelling, with no inflammatory skin changes, and pain on arm abduction with typical unilateral involvement. CO does not affect other anterior chest wall joints, thus differentiating it from SAPHO (7). XR and CT findings include homogeneous dense sclerotic patch and enlargement in the medial end of the clavicle, limited to the inferior margin, with sparing of the SCJ, without periosteal reaction or bony erosion (52). On MRI, it presents low-signal intensity on T1WI and low or intermediate signal on T2WI with occasionally interspersed areas of bright signal and bone/peri-osseous enhancement.

Tietze's syndrome

Tietze's syndrome (TS), also known as costochondritis, affects from the second to fourth costochondral junctions (rarely the SCJ and the SCOJ) with hypertrophy and calcification of the costal cartilages (in most cases only one costal cartilage is involved) (7). TS is defined as a benign, painful, non-suppurative, self-limiting (resolve within days to weeks) disease, with localized swelling over the interested area (Tietze's area) (53). Females are affected more than males (2:1 ratio) between twenty and fifty years of age. The diagnosis is primarily clinical however MRI is the imaging of choice to show cartilaginous, joints and bone abnormalities (focal cartilage enlargement and edema of both cartilage and subchondral bone, vivid and rapid contrast enhancement of the cartilage and peri-articular structures involved) and to exclude other differential diagnoses (8, 53). XR and CT can show hypertrophy and calcification of the costal cartilages, but they are less accurate than MRI.

Septic arthritis

Septic arthritis (SA) of the SCJ is frequently associated with a preexisting disease or risk factors (sepsis, infected subclavian central lines, recent sternal trauma, diabetes mellitus, human immunodeficiency virus (HIV) infection, renal dialysis, and intravenous drug abuse); it is rarely isolated (1% of all SA). Most patients are male (8). Symptoms are pain, swelling, and tenderness, associated with fever, chills, or night sweats. SA can rapidly evolve with severe complications (osteomyelitis, abscess or phlegmon and mediastinitis), and the most common isolated organism is Staphylococcus aureus, followed by Pseudomonas, Brucella, and E.Coli (7). A culture of aspirate/tissue sample with imaging gives the diagnosis. XR may highlight the presence of sclerotic, lytic, or mixed lesions but may be less sensitive than DECT that can show erosions, widening, periosteal reaction, and marrow edema in the acute phase, or sclerosis, in chronic phase. MRI and US are more specific and should be considered the imaging modality of choice; US can guide fluid aspiration (8).

Other non-traumatic pathologies involving the ACW

Among less common diseases, particular attention should be given to primary or secondary tumors such as Ewings sarcoma, lymphomas, fibrous tumors, and metastases (54). Rare benign conditions are hemophilic pseudotumor, a complication of hemophilia that may affect the proximal clavicle, Paget's disease, neuropathic arthropathy of the SCJ, secondary to syringomyelia, Friedrich's disease (or spontaneous aseptic osteonecrosis of the medial end of the clavicle), synovial osteochondromatosis and ganglion cysts. SCJ changes have also been described with other systemic pathologies such as polymyalgia rheumatica, primary and secondary hyperparathyroidism (with the erosion of the medial clavicle) and hemodialysis-related amyloidosis (6, 8, 55). Congenital deformities can also affect the ACW and are caused by anomalies of chest wall growth, leading to sternal depression or protrusion, or related to failure of the normal spine or rib development (56). Patients should be first imaged with XR or directly address to the best diagnostic techniques, CT or MRI, for assessing the degree of the involvement, the differential diagnosis, and treatment planning (56).

Conclusion

The ACW can be affected by multiple non-traumatic diseases, and most of these conditions present with the same symptoms. The radiologists should be aware of the AWC anatomy, prevalence, and site of involvement, as well as imaging features and possibilities.

Conflict of interest: Authors declare that they have no commercial associations (e.g. consultancies, stock ownership, equity interest, patent/licensing arrangement etc.) that might pose a conflict of interest in connection with the submitted article.

References

1. Zappia M, Maggialetti N, Natella R, et al. Diagnostic imaging: pitfalls in rheumatology. Radiol Med 2019; 124: 1167-74.
2. Bruno F, Arrigoni F, Palumbo P, et al. New advances in MRI diagnosis of degenerative osteoarthropathy of the peripheral joints. Radiol Med 2019; 124: 1121-27.
3. Salaffi F, Carotti M, Bosello S, et al. Computer-aided quantification of interstitial lung disease from high resolution computed tomography images in systemic sclerosis: correlation with visual reader-based score and physiologic tests. Biomed Res Int 2015; 2015: 834262.
4. Salaffi F, Carotti M, Di Carlo M, Farah S, Gutierrez M. Adherence to Anti-Tumor Necrosis Factor Therapy Administered Subcutaneously and Associated Factors in Patients With Rheumatoid Arthritis. J Clin Rheumatol 2015; 21: 419-25.
5. Vitali C, Carotti M, Salaffi F. Is it the time to adopt salivary gland ultrasonography as an alternative diagnostic tool for the classification of patients with Sjogren's syndrome? Comment on the article by Cornec et al. Arthritis Rheum 2013; 65: 1950.
6. Rennie WJ, Jans L, Jurik AG, Sudol-Szopinska I, Schueller- Weidekamm C, Eshed I. Anterior Chest Wall in Axial Spondyloarthritis: Imaging, Interpretation, and Differential Diagnosis. Semin Musculoskelet Radiol 2018; 22: 197-206.
7. Edwin J, Ahmed S, Verma S, Tytherleigh-Strong G, Karuppaiah K, Sinha J. Swellings of the sternoclavicular joint: review of traumatic and non-traumatic pathologies. EFORT Open Rev 2018; 3: 471-84.
8. Higginbotham TO, Kuhn JE. Atraumatic disorders of the sternoclavicular joint. J Am Acad Orthop Surg 2005; 13: 138-45.
9. Salaffi F, Carotti M, Barile A. Musculoskeletal imaging of the inflammatory and degenerative joints: current status and perspectives. Radiol Med 2019; 124: 1067-70.
10. Bruno F, Arrigoni F, Mariani S, et al. Advanced magnetic resonance imaging (MRI) of soft tissue tumors: techniques and applications. Radiol Med 2019; 124: 243-52.
11. Scaglione M, Salvolini L, Casciani E, Giovagnoni A, Mazzei MA, Volterrani L. The many faces of aortic dissections: Beware of unusual presentations. Eur J Radiol 2008; 65: 359-64.
12. Agostini A, Kircher MF, Do RK, et al. Magnetic Resonanance Imaging of the Liver (Including Biliary Contrast Agents)-Part 2: Protocols for Liver Magnetic Resonanance Imaging and Characterization of Common Focal Liver Lesions. Semin Roentgenol 2016; 51: 317-33.
13. Agostini A, Kircher MF, Do R, et al. Magnetic Resonance Imaging of the Liver (Including Biliary Contrast Agents) Part 1: Technical Considerations and Contrast Materials. Semin Roentgenol 2016; 51: 308-16.
14. Agliata G, Schicchi N, Agostini A, et al. Radiation exposure related to cardiovascular CT examination: comparison between conventional 64-MDCT and third-generation dualsource MDCT. Radiol Med 2019; 124: 753-61.
15. Agostini A, Mari A, Lanza C, et al. Trends in radiation dose and image quality for pediatric patients with a multidetector CT and a third-generation dual-source dual-energy CT. Radiol Med 2019; 124: 745-52.
16. Russo S, Lo Re G, Galia M, et al. Videofluorography swallow study of patients with systemic sclerosis. Radiol Med 2009; 114: 948-59.
17. Pinto A, Lanza C, Pinto F, et al. Role of plain radiography in the assessment of ingested foreign bodies in the pediatric patients. Semin Ultrasound CT MR 2015; 36: 21-7.
18. Tytherleigh-Strong G, Mulligan A, Babu S, See A, Al-Hadithy N. Digital tomography is an effective investigation for sternoclavicular joint pathology. Eur J Orthop Surg Traumatol 2019; 29: 1217-21.
19. Carotti M, Salaffi F, Di Carlo M, Giovagnoni A. Relationship between magnetic resonance imaging findings, radiological grading, psychological distress and pain in patients with symptomatic knee osteoarthritis. Radiol Med 2017; 122: 934-43.
20. Barile A, Bruno F, Mariani S, et al. What can be seen after rotator cuff repair: a brief review of diagnostic imaging findings. Musculoskelet Surg 2017; 101: 3-14.
21. Dialetto G, Reginelli A, Cerrato M, et al. Endovascular stent-graft treatment of thoracic aortic syndromes: a 7-year experience. Eur J Radiol 2007; 64: 65-72.
22. Ierardi AM, Tsetis D, Ioannou C, et al. Ultra-low profile polymer- filled stent graft for abdominal aortic aneurysm treatment: a two-year follow-up. Radiol Med 2015; 120: 542-8.
23. Cazzato RL, Arrigoni F, Boatta E, et al. Percutaneous management of bone metastases: state of the art, interventional strategies and joint position statement of the Italian College of MSK Radiology (ICoMSKR) and the Italian College of Interventional Radiology (ICIR). Radiol Med 2019; 124: 34- 49.

24. Zoccali C, Rossi B, Zoccali G, et al. A new technique for biopsy of soft tissue neoplasms: a preliminary experience using MRI to evaluate bleeding. Minerva Med 2015; 106: 117-20.
25. Masciocchi C, Arrigoni F, La Marra A, Mariani S, Zugaro L, Barile A. Treatment of focal benign lesions of the bone: MRgFUS and RFA. Br J Radiol 2016; 89: 20150356.
26. Bellelli A, Silvestri E, Barile A, et al. Position paper on magnetic resonance imaging protocols in the musculoskeletal system (excluding the spine) by the Italian College of Musculoskeletal Radiology. Radiol Med 2019; 124: 522-38.
27. Di Cesare E, Cademartiri F, Carbone I, et al. [Clinical indications for the use of cardiac MRI. By the SIRM Study Group on Cardiac Imaging]. Radiol Med 2013; 118: 752-98.
28. Gentili F, Cantarini L, Fabbroni M, et al. Magnetic resonance imaging of the sacroiliac joints in SpA: with or without intravenous contrast media? A preliminary report. Radiol Med 2019; 124: 1142-50.
29. La Paglia E, Zawaideh JP, Lucii G, Mazzei MA. MRI of the axial skeleton: differentiating non-inflammatory diseases and axial spondyloarthritis: a review of current concepts and applications : Special issue on "musculoskeletal imaging of the inflammatory and degenerative joints: current status and perspectives". Radiol Med 2019; 124: 1151-66.
30. D'Orazio F, Splendiani A, Gallucci M. 320-Row Detector Dynamic 4D-CTA for the Assessment of Brain and Spinal Cord Vascular Shunting Malformations. A Technical Note. Neuroradiol J 2014; 27: 710-7.
31. Mazzei MA, Contorni F, Gentili F, et al. Incidental and Underreported Pleural Plaques at Chest CT: Do Not Miss Them-Asbestos Exposure Still Exists. Biomed Res Int 2017; 2017: 6797826.
32. Biondi M, Vanzi E, De Otto G, et al. Water/cortical bone decomposition: A new approach in dual energy CT imaging for bone marrow oedema detection. A feasibility study. Phys Med 2016; 32: 1712-16.
33. Mazzei MA, Volterrani L. Errors in multidetector row computed tomography. Radiol Med 2015; 120: 785-94.
34. Carotti M, Salaffi F, Beci G, Giovagnoni A. The application of dual-energy computed tomography in the diagnosis of musculoskeletal disorders: a review of current concepts and applications. Radiol Med 2019; 124: 1175-83.
35. Agostini A, Borgheresi A, Mari A, et al. Dual-energy CT: theoretical principles and clinical applications. Radiol Med 2019; 124: 1281-95.
36. Reginelli A, Capasso R, Petrillo M, et al. Looking for Lepidic Component inside Invasive Adenocarcinomas Appearing as CT Solid Solitary Pulmonary Nodules (SPNs): CT Morpho-Densitometric Features and 18-FDG PET Findings. Biomed Res Int 2019; 2019: 7683648.
37. Li M, Wang B, Zhang Q, et al. Imageological measurement of the sternoclavicular joint and its clinical application. Chin Med J (Engl) 2012; 125: 230-5.
38. Lawrence CR, East B, Rashid A, Tytherleigh-Strong GM. The prevalence of osteoarthritis of the sternoclavicular joint on computed tomography. J Shoulder Elbow Surg 2017; 26: e18-e22.
39. Giacomelli R, Afeltra A, Alunno A, et al. Guidelines for biomarkers in autoimmune rheumatic diseases - evidence based analysis. Autoimmun Rev 2019; 18: 93-106.
40. Mascalchi M, Maddau C, Sali L, et al. Circulating tumor cells and microemboli can differentiate malignant and benign pulmonary lesions. J Cancer 2017; 8: 2223-30.
41. Rodriguez-Henriquez P, Solano C, Pena A, et al. Sternoclavicular joint involvement in rheumatoid arthritis: clinical and ultrasound findings of a neglected joint. Arthritis Care Res (Hoboken) 2013; 65: 1177-82.
42. Filippucci E, Cipolletta E, Mashadi Mirza R, et al. Ultrasound imaging in rheumatoid arthritis. Radiol Med 2019; 124: 1087-100.
43. Marchesoni A, D'Angelo S, Anzidei M, et al. Radiologistrheumatologist multidisciplinary approach in the management of axial spondyloarthritis: a Delphi consensus statement. Clin Exp Rheumatol 2019; 37: 575-84.
44. Conticini E, Di Martino V, De Stefano R, Frediani B, Volterrani L, Mazzei MA. Crowned Dens Syndrome Presenting as Hemiplegia and Hypoesthesia. J Clin Rheumatol 2019;
45. Guglielmi G, Scalzo G, Cascavilla A, Salaffi F, Grassi W. Imaging of the seronegative anterior chest wall (ACW) syndromes. Clin Rheumatol 2008; 27: 815-21.
46. Brzezinska-Wcislo L, Bergler-Czop B, Lis-Swiety A. Sonozaki syndrome: case report and review of literature. Rheumatol Int 2012; 32: 473-7.
47. Hyodoh K, Sugimoto H. Pustulotic arthro-osteitis: defining the radiologic spectrum of the disease. Semin Musculoskelet Radiol 2001; 5: 89-93.
48. Rukavina I. SAPHO syndrome: a review. J Child Orthop 2015; 9: 19-27.
49. Fioravanti A, Cantarini L, Burroni L, Mazzei MA, Volterrani L, Galeazzi M. Efficacy of alendronate in the treatment of the SAPHO syndrome. J Clin Rheumatol 2008; 14: 183-4.
50. Richman KM, Boutin RD, Vaughan LM, Haghighi P, Resnick D. Tophaceous pseudogout of the sternoclavicular joint. AJR Am J Roentgenol 1999; 172: 1587-9.
51. Chhana A, Doyle A, Sevao A, et al. Advanced imaging assessment of gout: comparison of dual-energy CT and MRI with anatomical pathology. Ann Rheum Dis 2018; 77: 629- 30.
52. Cone RO, Resnick D, Goergen TG, Robinson C, Vint V, Haghighi P. Condensing osteitis of the clavicle. AJR Am J Roentgenol 1983; 141: 387-8.
53. Volterrani L, Mazzei MA, Giordano N, Nuti R, Galeazzi M, Fioravanti A. Magnetic resonance imaging in Tietze's syndrome. Clin Exp Rheumatol 2008; 26: 848-53.
54. Gentili F, Pelini V, Lucii G, et al. Update in diagnostic

imaging of the thymus and anterior mediastinal masses. Gland Surg 2019; 8: S188-S207.
55. Levy M, Goldberg I, Fischel RE, Frisch E, Maor P. Friedrich's disease. Aseptic necrosis of the sternal end of the clavicle. J Bone Joint Surg Br 1981; 63B: 539-41.
56. Mak SM, Bhaludin BN, Naaseri S, Di Chiara F, Jordan S, Padley S. Imaging of congenital chest wall deformities. Br J Radiol 2016; 89: 20150595.

Received: 20 May 2020
Accepted: 10 June 2020
Correspondence:
Susanna Guerrini
Unit of Diagnostic Imaging, Department of Radiological Sciences, University of Siena,
Azienda Ospedaliero-Universitaria Senese, Siena, Italy
Viale Bracci 16, 53100, Siena, Italy.
Tel. +39 3273512629 - Fax +39 0577 586147
E-mail: guerrinisus@gmail.com

Acta Biomed 2020; Vol. 91, Supplement 8: 51-59 DOI: 10.23750/abm.v91i8-S.9973

Review

Radiological diagnosis of coronavirus disease 2019 (COVID-19): a practical guide

Chiara Floridi[1,2], Marco Fogante[2], Andrea Agostini[1,2], Alessandra Borgheresi[2], Michaela Cellina[3], Raffaele Natella[4], Federico Bruno[5], Diletta Cozzi[6], Nicola Maggialetti[7], Pierpaolo Palumbo[5], Vittorio Miele[6], Marina Carotti[2], Andrea Giovagnoni[1,2]

[1] University Politecnica delle Marche, Department of Clinical, Special and Dental Sciences; [2] Division of Special and Pediatric Radiology, Department of Radiology, University Hospital "Umberto I – Lancisi – Salesi" Ancona, AN, Italy; [3] Department of Radiology, ASST Fatebenefratelli Sacco, Milan, Italy; [4] Department of Precision Medicine, University of Campania "Luigi Vanvitelli", Naples, Italy; [5] Department of Biotecnology and Applied Clinical Sciences, University of L'Aquila, L'Aquila, Italy; [6] Department of Radiology, Azienda Ospedaliero-Universitaria Careggi, Florence, Italy; [7] Department of Medicine and Health Sciences "V. Tiberio", University of Molise, Campobasso, Italy.

Summary. Novel beta-coronavirus (2019-nCoV) is the cause of Coronavirus disease-19 (COVID-19), and on March 12th 2020, the World Health Organization defined COVID-19 as a controllable pandemic. Currently, the 2019 novel coronavirus (SARS-CoV-2) can be identified by virus isolation or viral nucleic acid detection; however, false negatives associated with the nucleic acid detection provide a clinical challenge. Imaging examination has become the indispensable means not only in the early detection and diagnosis but also in monitoring the clinical course, evaluating the disease severity, and may be presented as an important warning signal preceding the negative RT-PCR test results. Different radiological modalities can be used in different disease settings. Radiology Departments must be nimble in implementing operational changes to ensure continued radiology services and protect patients and staff health. (www.actabiomedica.it)

Keywords: SARS-CoV-2, COVID-19, chest CT, chest x-ray, lung US

Introduction

Novel beta-coronavirus (2019-nCoV) is the cause of Coronavirus disease-19 (COVID-19), and on March 12th 2020, the World Health Organization defined COVID-19 as a controllable pandemic.

Person-to-person virus transmission occurs primarily through droplets or via direct contact from an infected individual. Clinical common symptoms are fever, cough, dyspnea, and muscle aches (1). The mortality rate is about 3.0%, and male gender, age ≥60 years, delay in diagnosis, and severe pneumonia are associated with increased mortality rates (2).

COVID-19 is highly contagious, and early diagnosis is mandatory to isolate suspected cases and contacts to control the outbreak. Real-time polymerase chain reaction (RT-PCR) is the standard diagnostic method to detect viral nucleotides from the oropharyngeal or nasopharyngeal swab, but it has a sensitivity of 60-71%; hence, at present, the diagnosis of COVID-19 is mainly based on epidemiological history, clinical symptoms and chest imaging findings (3).

Chest imaging plays an essential role in the detection, evaluation of severity, and follow-up of the disease (4), and healthcare workers in Radiology Departments are exposed to patients with COVID-19 and are at high risk of being infected (5).

The aim of this work is to provide a Practical Guide that summarized the Radiology Department preparedness, the choice of best imaging modalities, the main radiological findings, and differential diagnosis of COVID-19.

Radiology Department Preparedness

The novel coronavirus can be transmitted through respiratory droplets, that may travel up to 183cm from their source, or via direct contact and probably could be transmitted via touching a surface or item that is contaminated with the virus. For all these reasons, the healthworkers exposed to Covid-19 have a high risk of being infected and need strict precautions also in the Radiology Department.

If possible, it is preferable to use the diagnostic imaging portable X-ray equipment to reduce the transportation of the patients. For this purpose, the presence of a portable x-ray equipment in each covid-department is desirable. If the Covid-patients need to be transported to the Radiology department to perform a radiological exam (especially CT and MR examinations) (6-12), they should avoid the conventional routes but use dedicated elevators and designated routes, avoiding to stay in the waiting area. Moreover, if possible, it should be expected a dedicated CT scanner for infected patients. During Covid-patients radiological exams, all the radiologic personal should wear adequate personal protective equipment (PPE), and at the end of radiological exams, they should be able to remove the PPE using a specific room, in order to avoid contamination of themselves or their colleagues. The computed tomography (CT) scanner, the image workstation, mouse, and keyboards need to be disinfected after every contact with suspected and infected patients. Environmental services staff need to have guidelines and to be specifically trained for the professional cleaning of the potentially contaminated surfaces after each high-risk patient contact.

If appropriately prepared, the Radiology Department Personnel can reduce and manage the coronavirus outbreak impact on the facility and the staff (13).

Imaging modalities

Chest X-ray

Chest X-ray (CXR) is the first imaging modality used in clinical suspicion of infective lung disease to detect lung abnormalities, to assess the extension and complications, and to rule out alternative diagnosis. Pulmonary signs usually compared on the CXR within 12 hours of the onset of symptoms (14).

Suggested Indications in COVID-19

CXR is suggested in the detection of lung abnormalities, with clinical suspicion and waiting for the RT-PCR outcome (30). CXR is suggested in the routine follow-up to obviate the need for computed tomography (CT) and to reduce the burden on CT units (15). The main advantages are the low cost, especially in the settings of limited medical resources, the possibility of bedside examination with a dedicated portable CXR machine, the reduction of the risk of cross-infection related to patients' transport (16). The main disadvantages are the low sensibility in the detection of lung abnormalities in the early stage and the possibility that the radiological findings do not correlate with disease progression (16).

Chest CT

Chest CT, particularly high-resolution CT (HRCT), is the more sensitive imaging modality in the detection of lung infection abnormalities. HRCT is useful in clinical suspicion of pneumonia with normal or nonspecific CXR findings, to assess the extension and complications, to rule out underlying lesions, and to evaluate patients with persistent or recurrent pulmonary opacities (14).

Suggested Indications in COVID-19

Chest CT is suggested for early diagnosis with clinical suspicions, normal or non-definitive lung abnormalities in CXR, and with RT-PCR outcome unavailable or negative (17). Chest CT is suggested in clinical deterioration unaccompanied with CXR worsening and in the follow-up of severe cases to evaluate permanent lung damage (19). The main advantages are the high sensitivity for the detection of lung abnormalities that could be helpful in rectifying RT-PCR false negatives and the high performance in the evaluation of different stages of disease severity (19). The main disadvantages are the risk of transporting critical pa-

tients, the necessity to decontaminate the scan room, the time-consuming of the organization (20) and the higher radiation exposure (21).

Lung ultrasound

Lung ultrasound (LUS) initially seemed to be unsuitable for the study of lung parenchyma and was mainly used to guide puncture of pleural effusion. With advances in ultrasound technology, LUS has been gradually used successfully in the diagnosis and monitoring of infective lung disease (22).

Suggested Indications in COVID-19

LUS is suggested in the serial monitoring of lung aeration in the intensive care unit (ICU) to evaluate lung excursion and compliance to regulate the intensity of respiratory support (23). LUS is suggested to evaluate the re-expansion of the atelectasis areas and to guide invasive diagnostic procedures (23). The main advantages are the possibility of bedside examination, the reduction of radiation exposure, the reduction of the risk of cross-infection related to patients' transport, the real-time images, the opportunity of serial monitoring, and the reduction of healthcare workers exposed during the investigation (24). The main disadvantages are the operator-dependent image interpretation, the necessity of experience to generate high quality and reproducible images, the time-consuming examinations due to the evaluation of many lung regions and the necessity for the clinician to implement personal safety procedures (24).

PET-CT

Positron emission tomography with 2-deoxy-2-[fluorine-18] fluoro D-glucose integrated with computed tomography (18F-FDG PET-CT) imaging has the ability to delineate infective lung disease quantitatively. In inflammatory conditions, glycolytic metabolism is elevated in the region of leukocyte infiltration associated with inflammatory processes, and consequently, FDG uptake is increased (25).

Suggested Indications in COVID-19

PET-CT is suggested at the early stages of the disease when clinical symptoms are not specific, and differential diagnosis between benignant and malignant lesions is challenging (25). The main advantages are the possibility to reflect in changes in uptake patterns and locations during virus exposure and to evaluate all the body when a viral infection causes the damage of other organs and/or it is associated with other diseases (26). The main disadvantages are the limited use in an emergency setting, the complexity of images interpretation, time-consuming of the procedure, the risk of transporting critical patients, and the necessity to decontaminate room (26). Suggested indications for each imaging modalities are summarized in **Table 1**.

Table 1. Suggested Indications of imaging modalities in COVID-19.

Imaging Modalities	Suggested Indications
CXR	• detection of lung abnormalities, with clinical suspicion and waiting the RT-PCR outcome. • routinely follow-up to obviate the need for a CT and to reduce the burden on CT units.
Chest CT	• early diagnosis with clinical suspicions, normal or non-definitive lung abnormality in CXR and with RT-PCR outcome unavailable or negative. • clinical deterioration unaccompanied with CXR worsening. • follow-up of severe cases to evaluate permanent lung damage.
Lung US	• serial monitoring of lung aeration in ICU to evaluate lung excursion and compliance to regulate the intensity of respiratory support. • to evaluate the re-expansion of the atelectasis areas. • to guide invasive diagnostic procedures.
PET-CT	• differential diagnosis between benign and malignant lesions

Abbreviations. COVID-19: coronavirus disease-19; CXR: chest X-ray; CT: computed tomography; US: ultrasound, PET: positron emission tomography; RT-PCR: real time-polymerase chain reaction; ICU: invasive care unit.

Imaging Features

Chest X-ray

The main imaging abnormalities are patchy or diffuse asymmetric focal or multifocal unilateral ill-defined areas and airspace opacity with peripheral distribution in the middle and lower peripheral lung zones (**fig. 1**). As the disease progress, compared multifocal consolidation involving one or both lungs with extension into the perihilar and upper lobes. Rarely the opacities are focal and unilateral.

The imaging findings of unfavorable outcomes are the presence of diffuse and confluent airspace opacities that involved four or more lung zones, and the blunting of the costophrenic angles resulting from pleural effusion (27).

Chest CT

The imaging abnormalities increased in number and severity in the first period with a short plateau phase and a gradual decrease. The initial stage (0-4 days after onset of the initial symptoms) is characterized by bilateral, peripheral, and sub-pleural or peribronchovascular areas of patchy or segmental pure ground-glass opacities (GGOs) (**fig. 3**) with the involvement of lower lobes, rare consolidations, reverse halo sign and vascular dilatation. The progressive stage (5-8 days after the onset of the initial symptom) is characterized by diffuse GGOs, consolidations, interlobular septal thickening, and sometimes crazy-paving pattern. The peak stage (9-13 days after the onset of the initial symptom) is characterized by diffuse consolidations, parenchymal bands, and marked interlobular septal thickening. The

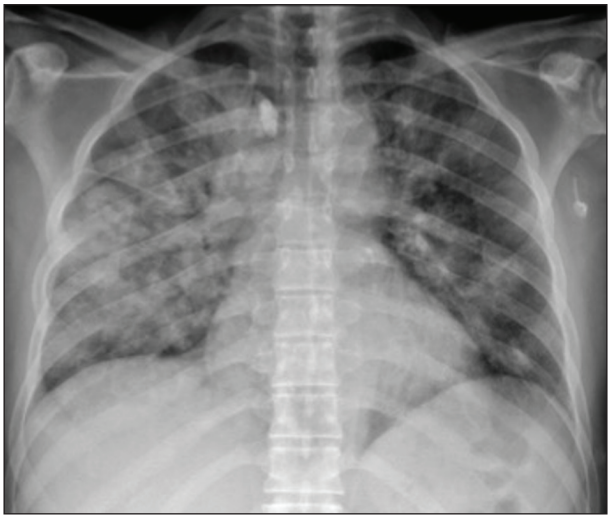

Figure 1. 65-year-old man patient with fever and respiratory failure (RT-PCR test positive): the chest x-ray image shows diffuse multifocal consolidation involving both lungs.

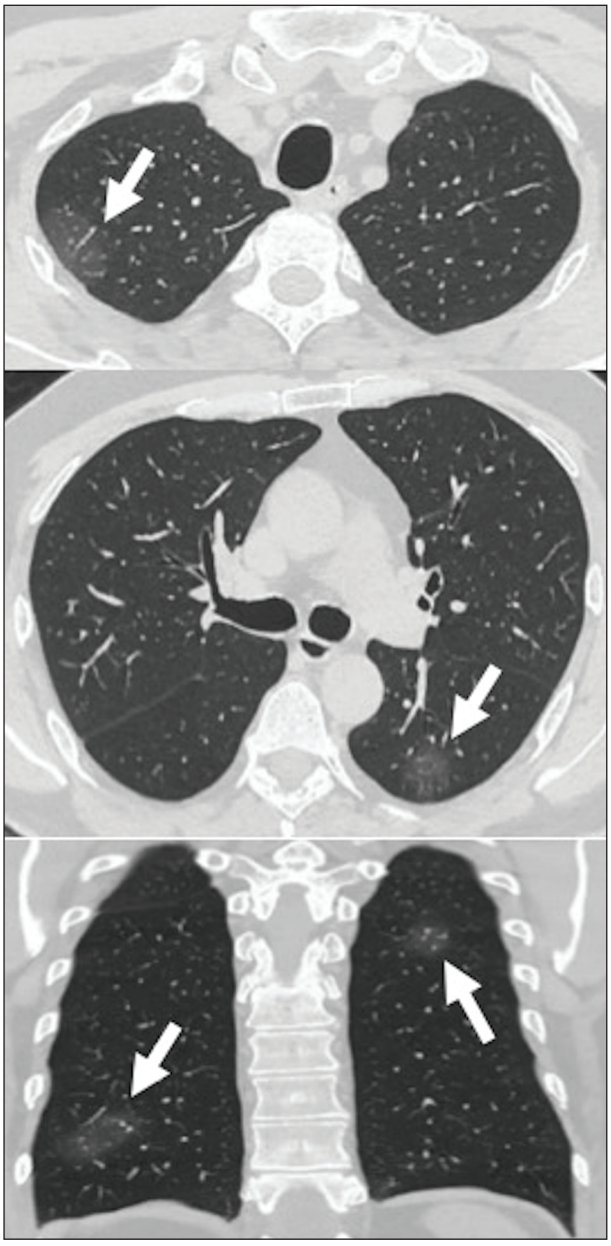

Figure 2. 54-year-old man patient with fever and diffuse thoracic pain (RT-PCR test positive): the multiplanar chest CT images show multifocal and bilateral peripheral areas of patchy pure ground-glass opacities (white arrows).

Figure 3. 81-year-old man patient with fever, cough and respiratory failure (RT-PCR test positive): the axial image of chest CT shows multiple bilateral ground-glass areas with marked interlobular septal thickenin.

absorption stage (14-30 days after the onset of the initial symptom) is characterized by rare consolidations and diffuse GGOs due to the consolidation absorption. Nodules, tree-in-bud opacities, honeycombing, traction bronchiectasis, cavitation, and lymphadenopathy (defined as lymph node size of ≥10 mm in short-axis dimension) are rare. The imaging findings of unfavorable outcomes are greater involvement of the lungs, pleural effusion, and diffuse fibrosis (28-30). Chest CT findings are summarized in **Table 2**.

Lung Ultrasound

The main imaging abnormalities are vertical hyperechoic artifacts that depart from the pleural line directed in depth, called B lines, and consolidations. If ≤ 3 B lines on a scan are physiological, especially in the middle-basal fields, the presence of a higher number is pathological, and the number of B lines correlates with disease severity. In the early stages, B lines are confined and mainly detected in the subpleural regions of one or both lungs. In the advanced stages, several B lines involve multiple lobes with diffuse consolidations. The imaging findings of unfavorable outcomes are diffuse consolidations in both lungs without a base–apex gradient, irregularity of the pleural line, multiple and diffuse B lines, and the presence of pleural effusion (31).

PET-TC

The main imaging abnormalities are lesions with high 18F-FDG uptake accompanied by an increased

Table 2. Chest CT imaging findings at different stages in COVID-19.

Findings	Stage			
	Initial	**Progressive**	**Peak**	**Absorption**
Days after initial symptoms	0-4	5-8	9-13	14-30
GGO	+++	+++	++	+++
Consolidation	+	++	+++	+
Reverse halo sign	++	+	+	++
Interlobular septal thickening	Rare	++	+++	++
Crazy paving	+	++	+++	Absent
Localization	Bilateral	Bilateral	Bilateral	Bilateral
	Lower lobes	Multiple lobes	Multiple lobes	Lower lobes
	Peripheral and subpleural	Diffuse	Diffuse	Peripheral and subpleural
Bronchiectasis	Rare	Rare	+	Absent
Fibrosis	Rare	Rare	+	++
Honeycombing	Rare	Rare	+	Absent
Vascular dilatation	++	++	++	++
Pleural effusion	Rare	Rare	+	+
Lymphadenopathy	Rare	Rare	Rare	Rare

Abbreviations. COVID-19: coronavirus disease-19; CT: computed tomography; GGO: ground glass opacity.

nodal FDG uptake without evidence of disseminated disease. Although a bilateral involvement of the lung parenchyma can be observed in several benign and malignant lung diseases, tumors presenting as GGOs are unlikely to be FDG-avid (32, 33).

Differential diagnosis

To optimize patient management, medical care, and disease control, it is important to distinguish COVID-19 from other pathologies. Diagnostic imaging (MRI, CT, and US) techniques, gained large application in thoracic and general radiology; they are advised as first-line techniques helping diagnosis, staging, and follow-up (34-43). Compared to non-COVID-19 pneumonia, COVID-19 pneumonia have GGOs, peripheral distribution, reverse halo sign, and vascular dilatation; on the contrary, pleural effusion and lymphadenopathy are rare (44).

The CT appearance of COVID-19 shares some similarities especially with those of the same viral family: Middle East respiratory syndrome (MERS) and severe acute respiratory syndrome (SARS). They manifest similar lung involvement with a peripheral GGOs predominance and crazy-paving pattern. MERS demonstrated a tendency to have subpleural distribution at the lower lobes, and after recovery, airspace disease showed marked improvement but with often residual fibrotic changes. Furthermore, the absence of pulmonary cavitation, pleural effusions, and lymphadenopathy are also characteristic of SARS. Differently with 2019-nCoV, SARS involvement is more common unilateral, and compared to patients with SARS and MERS, COVID-19 progression is relatively slow. Other non-COVID-19 viral pneumonia mainly manifest as peribronchial and perivascular interstitial inflammation; they show multiple interlaced or parallel high-attenuation fibrous streaks and high attenuation reticular patterns caused by infiltration of the interlobular septa. If the pneumonia is secondary to bronchitis and does not involve the alveoli, CT images show bronchioles partially or entirely blocked, tree-in-bud pattern, and localized atelectasis (45).

COVID-19 needs to be differentiated from bacterial pneumonia, mycoplasma pneumonia, and chlamydia pneumonia. Bacterial pneumonia occurs in the lung parenchyma and mainly manifests as bronchial pneumonia or lobar pneumonia with many inflammatory secretions in the bronchioles and alveoli. Patchy consolidations are frequent, and GGOs are less common. Mycoplasma pneumonia and Chlamydia Pneumonia commonly occur in school-age children and adolescents but rarely occurs in adults. It shows mostly centrilobular nodules and bronchial wall thickening. The proportion of lung consolidation is less in COVID-19 than that in Mycoplasma Pneumonia and Chlamydia Pneumonia.

Also, COVID-19 needs to be differentiated from heart disease. Heart-failure induced pulmonary edema manifests differently with two subtypes: pulmonary alveolar edema and interstitial pulmonary edema. The first one is characterized by local or multiple GGOs, which typically exhibit the high attenuation butterfly sign with both hila as the center, accompanied by signs of interstitial pulmonary edema such as sporadic or local interlobular septal thickening. The second one shows extensive or local interlobular septal thickening in both lungs, peribronchial cuffing, and redistribution of blood flow in both lungs and could be accompanied by GGOs (46). Principal differential diagnoses are summarized in **Table 3**.

Table 3. Differential diagnosis with COVID-19.

MERS
Rapid progression
SARS
Unilateral
Rapid Progression
Viral non COVID
Interstitial peribronchial thickening
Interstitial interlobular thickening
Hilar lesions
Bacterial Pneumonia
Patchy consolidations
Chlamydia and Mycoplasma pneumonia
Centrilobular nodules
Bronchial wall thickening
Lung disease from heart failure
Butterfly sign
Interlobular septal thickening

Abbreviations. COVID-19: coronavirus disease-19; MERS: Middle East respiratory syndrome; SARS: severe acute respiratory syndrome.

Conclusions

Radiologists have a primary role in the COVID-19 early detection of lung abnormality, in the suggestion of disease severity, and potential progression to acute respiratory distress syndrome, and in the detection of possible co-infection in hospitalized patients. Guidelines are necessary to manage patients with known or suspected infection of 2019-nCoV and to minimize the risk of infection in the Radiology Department. The correct management and the rapid and early diagnosis of new cases are a great benefit not only for the patient but also for public health surveillance.

Conflict of interest: Authors declare that they have no commercial associations (e.g. consultancies, stock ownership, equity interest, patent/licensing arrangement etc.) that might pose a conflict of interest in connection with the submitted article.

References

1. Sun P, Qie S, Liu Z, et al. Clinical characteristics of hospitalized patients with SARS-CoV-2 infection: A single arm meta-analysis. Journal of medical virology 2020.
2. Borges do Nascimento IJ, Cacic N, Abdulazeem HM, et al. Novel Coronavirus Infection (COVID-19) in Humans: A Scoping Review and Meta-Analysis. Journal of clinical medicine 2020; 9.
3. Kim H. Outbreak of novel coronavirus (COVID-19): What is the role of radiologists? European radiology 2020.
4. Yang W, Sirajuddin A, Zhang X, et al. The role of imaging in 2019 novel coronavirus pneumonia (COVID-19). European radiology 2020.
5. Tsou IYY, Liew CJY, Tan BP, et al. Planning and coordination of the radiological response to the coronavirus disease 2019 (COVID-19) pandemic: the Singapore experience. Clinical radiology 2020.
6. Panfili E, Nicolini D, Polverini V, et al. Importance of radiological detection of early pulmonary acute complications of liver transplantation: analysis of 259 cases. La Radiologia medica 2015; 120: 413-20.
7. Mascalchi M, Maddau C, Sali L, et al. Circulating tumor cells and microemboli can differentiate malignant and benign pulmonary lesions. Journal of Cancer 2017; 8: 2223- 2230.
8. Salaffi F, Carotti M, Bosello S, et al. Computer-aided quantification of interstitial lung disease from high resolution computed tomography images in systemic sclerosis: correlation with visual reader-based score and physiologic tests. BioMed research international 2015; 2015: 834262.
9. Salaffi F, Carotti M, Di Carlo M, et al. Adherence to Anti-Tumor Necrosis Factor Therapy Administered Subcutaneously and Associated Factors in Patients With Rheumatoid Arthritis. Journal of clinical rheumatology : practical reports on rheumatic & musculoskeletal diseases 2015; 21: 419-25.
10. Carrafiello G, Lagana D, Nosari AM, et al. Utility of computed tomography (CT) and of fine needle aspiration biopsy (FNAB) in early diagnosis of fungal pulmonary infections. Study of infections from filamentous fungi in haematologically immunodeficient patients. La Radiologia medica 2006; 111: 33-41.
11. Cozzi D, Dini C, Mungai F, et al. Primary pulmonary lymphoma: imaging findings in 30 cases. La Radiologia medica 2019; 124: 1262-1269.
12. Mazzei MA, Contorni F, Gentili F, et al. Incidental and Underreported Pleural Plaques at Chest CT: Do Not Miss Them-Asbestos Exposure Still Exists. BioMed research international 2017; 2017: 797826.
13. Mossa-Basha M, Meltzer CC, Kim DC, et al. Radiology Department Preparedness for COVID-19: Radiology Scientific Expert Panel. Radiology 2020; 200988.
14. Franquet T. Imaging of Community-acquired Pneumonia. Journal of thoracic imaging 2018; 33: 282-294.
15. Wong HYF, Lam HYS, Fong AH, et al. Frequency and Distribution of Chest Radiographic Findings in COVID-19 Positive Patients. Radiology 2019; 201160.
16. Jacobi A, Chung M, Bernheim A, Eber C. Portable chest X-ray in coronavirus disease-19 (COVID-19): A pictorial review. Clinical imaging 2020; 64: 35-42.
17. Li Y, Xia L. Coronavirus Disease 2019 (COVID-19): Role of Chest CT in Diagnosis and Management. AJR. American journal of roentgenology 2020; 1-7.
18. Ai T, Yang Z, Hou H, et al. Correlation of Chest CT and RTPCR Testing in Coronavirus Disease 2019 (COVID-19) in China: A Report of 1014 Cases. Radiology 2020; 200642.
19. Fang Y, Zhang H, Xie J, et al. Sensitivity of Chest CT for COVID-19: Comparison to RT-PCR. Radiology 2020; 200432.
20. Xie X, Zhong Z, Zhao W, Zheng C, Wang F, Liu J. Chest CT for Typical 2019-nCoV Pneumonia: Relationship to Negative RT-PCR Testing. Radiology 2020; 200343.
21. Agostini A, Floridi C, Borgheresi A, et al. Proposal of a low-dose, long-pitch, dual-source chest CT protocol on third-generation dual-source CT using a tin filter for spectral shaping at 100 kVp for CoronaVirus Disease 2019 (COVID-19) patients: a feasibility study. La Radiologia medica 2020; 125: 365-373.
22. Ye X, Xiao H, Chen B, Zhang S. Accuracy of Lung Ultrasonography versus Chest Radiography for the Diagnosis of Adult Community-Acquired Pneumonia: Review of the Literature and Meta-Analysis. PloS one 2015; 10: e0130066.
23. Vetrugno L, Bove T, Orso D, et al. Our Italian experience using lung ultrasound for identification, grading and serial follow-up of severity of lung involvement for management of patients with COVID-19. Echocardiography (Mount Kisco, N.Y.) 2020; 37: 625-627.
24. Soldati G, Smargiassi A, Inchingolo R, et al. Is There a Role for Lung Ultrasound During the COVID-19 Pandemic?

Journal of ultrasound in medicine : official journal of the American Institute of Ultrasound in Medicine 2020;
25. Bomanji J, Almuhaideb A, Zumla A. Combined PET and X-ray computed tomography imaging in pulmonary infections and inflammation. Current opinion in pulmonary medicine 2011; 17: 197-205.
26. Deng Y, Lei L, Chen Y, Zhang W. The potential added value of FDG PET/CT for COVID-19 pneumonia. European journal of nuclear medicine and molecular imaging 2020;
27. Yoon SH, Lee KH, Kim JY, et al. Chest Radiographic and CT Findings of the 2019 Novel Coronavirus Disease (COVID-19): Analysis of Nine Patients Treated in Korea. Korean journal of radiology 2020; 21: 494-500.
28. Pan F, Ye T, Sun P, et al. Time Course of Lung Changes On Chest CT During Recovery From 2019 Novel Coronavirus (COVID-19) Pneumonia. Radiology 2020; 200370.
29. Wu J, Wu X, Zeng W, et al. Chest CT Findings in Patients With Coronavirus Disease 2019 and Its Relationship With Clinical Features. Investigative radiology 2020; 55: 257-261.
30. Bernheim A, Mei X, Huang M, et al. Chest CT Findings in Coronavirus Disease-19 (COVID-19): Relationship to Duration of Infection. Radiology 2020; 200463.
31. Sofia S, Boccatonda A, Montanari M, et al. Thoracic ultrasound and SARS-COVID-19: a pictorial essay. Journal of ultrasound 2020;
32. Qin C, Liu F, Yen TC, Lan X. (18)F-FDG PET/CT findings of COVID-19: a series of four highly suspected cases. European journal of nuclear medicine and molecular imaging 2020; 47: 1281-1286.
33. Xu X, Yu C, Qu J, et al. Imaging and clinical features of patients with 2019 novel coronavirus SARS-CoV-2. European journal of nuclear medicine and molecular imaging 2020; 47: 1275-1280.
34. Carrafiello G, Mangini M, Fontana F, et al. Microwave ablation of lung tumours: single-centre preliminary experience. La Radiologia medica 2014; 119: 75-82.
35. Ianniello S, Piccolo CL, Buquicchio GL, Trinci M, Miele V. First-line diagnosis of paediatric pneumonia in emergency: lung ultrasound (LUS) in addition to chest-X-ray (CXR) and its role in follow-up. The British journal of radiology 2016; 89: 20150998.
36. Cortellini A, Bozzetti F, Palumbo P, et al. Weighing the role of skeletal muscle mass and muscle density in cancer patients receiving PD-1/PD-L1 checkpoint inhibitors: a multicenter real-life study. Scientific reports 2020; 10: 1456.
37. Splendiani A, Bruno F, Patriarca L, et al. Thoracic spine trauma: advanced imaging modality. La Radiologia medica 2016; 121: 780-92.
38. Cipriani P, Berardicurti O, Masedu F, et al. Biologic therapies and infections in the daily practice of three Italian rheumatologic units: a prospective, observational study. Clinical rheumatology 2017; 36: 251-260.
39. Ruscitti P, Iacono D, Ciccia F, et al. Macrophage Activation Syndrome in Patients Affected by Adult-onset Still Disease: Analysis of Survival Rates and Predictive Factors in the Gruppo Italiano di Ricerca in Reumatologia Clinica e Sperimentale Cohort. J Rheumatol 2018; 45: 864-872.
40. Ruscitti P, Cipriani P, Ciccia F, et al. Prognostic factors of macrophage activation syndrome, at the time of diagnosis, in adult patients affected by autoimmune disease: Analysis of 41 cases collected in 2 rheumatologic centers. Autoimmunity reviews 2017; 16: 16-21.
41. Cipriani P, Di Benedetto P, Ruscitti P, et al. Perivascular Cells in Diffuse Cutaneous Systemic Sclerosis Overexpress Activated ADAM12 and Are Involved in Myofibroblast Transdifferentiation and Development of Fibrosis. J Rheumatol 2016; 43: 1340-9.
42. Giacomelli R, Liakouli V, Berardicurti O, et al. Interstitial lung disease in systemic sclerosis: current and future treatment. Rheumatology international 2017; 37: 853-863.
43. Reginelli A, Capasso R, Petrillo M, et al. Looking for Lepidic Component inside Invasive Adenocarcinomas Appearing as CT Solid Solitary Pulmonary Nodules (SPNs): CT Morpho-Densitometric Features and 18-FDG PET Findings. BioMed research international 2019; 2019: 7683648.
44. Bai HX, Hsieh B, Xiong Z, et al. Performance of radiologists in differentiating COVID-19 from viral pneumonia on chest CT. Radiology 2020; 200823.
45. Chung M, Bernheim A, Mei X, et al. CT Imaging Features of 2019 Novel Coronavirus (2019-nCoV). Radiology 2020; 295: 202-207.
46. Dai WC, Zhang HW, Yu J, et al. CT Imaging and Differential Diagnosis of COVID-19. Canadian Association of Radiologists journal = Journal l'Association canadienne des radiologistes 2020; 71: 195-200.

Received: 20 May 2020
Accepted: 10 June 2020
Correspondence:
Marco Fogante
University Hospital "Umberto I – Lancisi – Salesi"
Department of Radiology –
Division of Special and Pediatric Radiology
Via Conca 71, 60126 Ancona (AN)
Phone: +39 071 596 4078
E-mail: marco.fogante89@gmail.com

Acta Biomed 2020; Vol. 91, Supplement 8: 60-70 DOI: 10.23750/abm.v91i8-S.9940

Review

Masses in right side of the heart: spectrum of imaging findings

Silvia Pradella[1], Giulia Grazzini[1], Mayla Letteriello[1], Cristian De Amicis[1], Roberta Grassi[2], Nicola Maggialetti[3], Mattia Carbone[4], Pierpaolo Palumbo[5], Marina Carotti[6,7], Ernesto Di Cesare[8], Andrea Giovagnoni,[6,7] Diletta Cozzi[1], Vittorio Miele[1]

[1]Department of Radiology, Careggi University Hospital, Florence, Italy; [2]Department of Precision Medicine, University of Campania "Luigi Vanvitelli", Naples, Italy; [3]Department of Medicine and Health Sciences "V. Tiberio", University of Molise, Campobasso, Italy; [4]Department of Radiology, S. Giovanni and Ruggi D'Aragona Hospital, Salerno, Italy; [5]Department of Biotechnology and Applied Clinical Sciences, University of L'Aquila, L'Aquila, Italy; [6]Department of Clinical, Special and Dental Sciences, University Politecnica delle Marche, Ancona, AN, Italy; [7]University Hospital "Umberto I-Lancisi-Salesi", Department of Radiology, Ancona, Italy; [8]Department of Life, Health & Environmental Sciences, University of L'Aquila, L'Aquila, Italy

Summary. Primary heart tumors are rare, benign tumors represent the majority of these. If a cardiac mass is found, the probability that it is a metastasis or a so-called "pseudo-mass" is extremely higher than a primary tumor. The detection of a heart mass during a transthoracic echocardiography (TE) is often unexpected. The TE assessment can be difficult, particularly if the mass is located at the level of the right chambers. Cardiac Computed Tomography (CCT) can be useful in anatomical evaluation and Cardiac Magnetic Resonance (CMR) for masses characterization as well. We provide an overview of right cardiac masses and their imaging futures. (www.actabiomedica.it)

Keywords: Cardiac masses, right heart, tumors, MRI, CT

Right sided cardiac masses: introduction and overview of imaging modalities

Primary cardiac tumors are very rare and even less common are the malignant ones (about 25 percent of all) (1). Primary cardiac neoplasms count approximately 0.02 to 0.1% of autopsy (1, 2). In young people rhabdomyoma and fibromas are most common although in adults myxomas and sarcomas are more frequent(3, 4).Approximately 75% of myxomas arise from left atrium (LA) and only about 20% of cases from right atrium (RA), whereas cardiac sarcomas, most frequently diagnosed as angiosarcoma, occur predominantly in the right atrium (5). As reported in literature, intracardiac masses are most likely to be found in the LA and more unlikely in the right ventricle (RV) (1). Neoplastic masses include benign, malignant tumors and metastatic tumors (6). Metastases are the most common cardiac neoplasms (7). Counting all cardiac masses, thrombus is the most common entity (8). Clinical manifestations of heart masses depend on the size and location of the tumor and the infiltration of adjacent structures rather than the nature of the tumor itself (9). Cross-sectional imaging as Magnetic Resonance (MR) and Computed Tomography (CT) techniques, gained large application in the day practice, particularly in cardiovascular radiology. Right-sided cardiac masses do not have a uniform clinical presentation. Pulmonary embolization may occur as the initial clinical manifestation for right myxoma (10-29). Non-invasive imaging plays a central role in the diagnosis and management pathway of cardiac masses (8). Transthoracic echocardiography (TE) remains the first-line modality of investigation to evaluate a cardiac mass because of its availability, capability to get dynamic assessment of lesions, non-invasiveness, absence

of contrast material or radiation exposure (30). However, echocardiography provides limited assessment of soft-tissue characteristics and extracardiac structures, it may be limited by poor acoustic windows, particularly for right chambers evaluation mostly in obese patients and the uncooperative ones.

Different imaging modalities are available for anatomical evaluation and characterization of tissues and masses in various district, including the heart (31-50). Multimodality imaging such as cardiac MR prevents misdiagnosis which often leads to unnecessary cardiac surgery (51). Cardiac CT (CCT), CMR, and 18F-FDG PET/CT work synergistically with echocardiography. Non-invasive imaging can distinguish tumor from "tumor like" mass and highlight typical characteristics of benign tumors differentiating them from malignant ones (8). CMR is fundamental to differentiate malignant from benign tumors through the use of multiparametric sequences (52). CCT has a limited role in tissue characterization compared to the CMR imaging; but both can be used synergistically with echocardiography to detect the mass, define its exact location and its anatomical relationships with adjacent structures(6). Appropriate Use Criteria for CMR and CCT provide specific guidance on the approach to cardiac masses. Since CMR does not require the use of ionizing radiation, it is the modality of choice particularly for pediatric patients, along with echocardiography(4). CMR quality images is dependent on patient cooperation. Additionally, CMR is specifically contraindicated in patients with claustrophobia and implanted unsafe magnetic devices. Also, CMR may be inadequate for evaluating small mobile masses (e.g., papillary fibroelastoma or valvular vegetations) due to limitations in spatial resolution. CCT provides an optimal anatomical evaluation and, in the presence of ECG-gating, a detailed assessment of the coronary arteries, fundamental prior to surgery. ECG gating, however, it is used to reduce motion artifacts, which can preclude detecting small lesions and cause blurring of the margins of larger lesions. Prospective ECG-gating is preferred because it allows lesion mobility through the reconstruction of cine images. To obtain an appropriate opacification in the right heart chambers (not so dense as to create streak artifacts) is indicated an intravenous infusion of iodinated contrast medium (for adults about 60-70 mL at 5 mL/s) followed by a 50%:50% contrast: saline flush. A delayed phase (obtained 2–3 min later without additional contrast injection) can be performed to help with tissue characterization. Considering that the radiation dose is very low with the latest CT generation, the CT can be a valid alternative to CMR (53, 54). Transesophageal echocardiography (TEE), like three-dimensional studies, can be a useful tool in addition to TE to clarify cardiac mass lesions characteristics in selected patients (8).

Right sided cardiac masses: lesion characteristics and imaging approach

In clinical practice, whenever a cardiac mass is detected on echocardiography, a reasonable approach is to focus on the location first, and then on the imaging characteristics **(Table 1)**. The clinical context and symptom presentation must guide us into getting the correct diagnosis. Embolic phenomena into the pulmonary circulation are an example of right sided lesions symptom onset. A reduction of cardiac output can result from an intracavity obstruction or valvular dysfunction caused by a tumor hemodynamically expressive. Generally, features that suggest a malignant lesion include myocardium and pericardium invasion resulting in arrhythmias, heart failure and pericardial effusions. Features that suggest a benign lesion include a well-defined and single mass that involves a single cardiac chamber (more frequent left than right); small size (<5 cm) and smooth margin; the presence of a narrow transition zone or pedunculated appearance; absent or minimal enhancement; absence of local invasion, metastasis and pericardial effusion; rare calcification (except for small foci in fibroma, myxoma, or teratoma) **(Table 2)** (6, 55).

Primary cardiac tumors

Benign Cardiac tumors

-Myxoma. Approximately, myxomas have an incidence of 0.0017% in the general population and they count 25–50% of all primary cardiac tumors. They are most common from the third to sixth decade of life. Myxoma can arise in the LA (75%), but they may arise

Table 1. Right sided cardiac most common masses- main characteristics

Cardiac masses	Lesion category	Age and sex	Incidence	Common location	Imaging typical features
Myxoma	Benign tumor	Adult, female-to-male ratio 2.7:1	Most common primary cardiac tumor (50% of benign tumors)	Atria (95%): left (75%) right (20%	Spherical, mobile, hyperintense on T2 w CMR images, 10 % calcified
Papillary fibroelastoma	Benign tumor	Adult, female-to-male ratio 1:1	Third in the prevalence of benign cardiac tumors	Predominantly from the aortic or mitral valve (usually tricuspid valve)	Pedunculated usually mobile, solitary, small (10 mm), smooth, hyperintense on T2 w CMR images
Lipoma	Benign tumor	Middle-aged and older adults, female-to-male ratio 1:1	About 8% of primary cardiac tumors approximately 14% of benign cardiac masses	Any chamber, intra-myocardial or intracavitary	Encapsulated, well-circumscribed, may be mobile, signal dropout on STIR CMR sequences. Low-attenuation on CT
Rhabdomyoma	Benign tumor	Children	The most common benign pediatric cardiac tumor	Left ventricle and septum (70%), right ventricle and atrial wall (30%)	Single or multiple well circumscribed, hyperintense on T2w CMR images, no or minimal enhancement
Angiosarcoma	Malignant tumor	Adult, female-to-male ratio 1:2-3	Rare, 0.0001% in autopsy series	Right atrium	Broad base, irregular, heterogeneous, infiltrative, pericardial effusion, metastatic. Heterogeneous signal on CMR: isointense on T1w and hyperintense on T2w. Heterogenous CE with a "sun ray appearance"
Lymphoma	Malignant tumor	Adult, median age 60 years old (range of 13–90 years old)	Secondary cardiac involvement by lymphoma 25% of patients, primary cardiac lymphoma 2% of cardiac primary tumors	Right atrium	Ill-defined, infiltrative (encasing adjacent structures), often pericardial effusion. On CMR: isointense on T1 w and hyperintense on T2 w. Homogenous CE
Metastases	Malignant tumors	Adult, female-to-male ratio 1:1	9 % in patients with metastatic cancer. Intracavitary metastases are rare, making up 3% to 5% of cardiac metastases	Pericardial. Any one of the heart chambers (if intracavitary)	CMR: hypointense on T1 w and hyperintense on T2 w. Heterogenous CE
Right Intracardiac thrombus	Non-neoplastic	Any age and sex; depend on underlying cardiac disorder	Intracardiac thrombi are found in about 10% of cases of pulmonary thromboembolism (PTE).	Right atrium, right ventricle, or main pulmonary artery	Intracavitary and freely mobile, especially if recently formed thrombi. No CE in early contrast phases
Prominent crista terminalis	Non-neoplastic	Any age and sex	Occasional finding	Right atrium	A well-defined fibromuscular ridge on the posterolateral wall of the right atrium

Table 2. Suggestive lesion features

Mass characteristics	Benign	Malignant
Location	Left > right	Right > left
Dimension	Small (<5 cm), single mass	Large (>5 cm), several masses
Calcification (if present)	Small	Large
Shape	Well defined margins, pedunculate	Irregular margins, broad base, signs of infiltration
Contrast Enhancement	Usually absent	Weak to intense

in other sites, such as the right side of the heart (5-20%), especially the RA (56). The sizes of these tumors vary from 1 to 15 cm and, usually, they appear as well defined, smooth and lobular mass, pedunculated.

On CMR images, myxomas have a typical heterogeneous appearance with variable iso- or hypointensity on T1-weighted sequences and hyperintensity on T2-weighted sequences due to their water content **(Fig.1).** Their heterogeneous appearance is due to the presence of intralesional hemorrhagic foci, cysts, necrosis, fibrosis, and calcification. Myxomas show heterogeneous enhancement mostly hypointense on first-pass perfusion sequences, with areas iso- or hyperintense on late gadolinium enhancement (LGE) sequences (4, 30).

On CT images myxomas appear as a lobular mass with low attenuation (usually like water attenuation values) with intralesional calcification, especially in myxoma localized in the RA. After the administration of contrast medium, they show heterogeneous contrast enhancement (CE) (6, 57).

-Papillary fibroelastoma. Papillary fibroelastoma (PF) has an incidence of up to 0.33 % in autopsy series and it is the third most common primary benign cardiac tumor (58). PFs are more frequent among the 4th and 8th decades of life. PFs are most commonly on the surface of the valves (80%) and consist of connective tissue (58). All heart valves can be affected, though the aortic valve is the most frequently involved, followed by the mitral valve. Gowda et al. (58) reported in a review of 725 cases of PFs that tricuspid valve was involved in 11% of cases, and pulmonary valve in 7%; while in the 4% of the cases PFs arise from endocardial surface of right atrium, right ventricle, right atrial appendage and Eustachian valve. Most of the patients are asymptomatic and PFs are diagnosed accidentally; however, they can be associated with valve dysfunction, embolization from attached thrombi and fragmentation (59). They are usually small (average diameter of 10 mm) and they appear as pedunculated or mobile masses (59). PFs are not always easily visible on

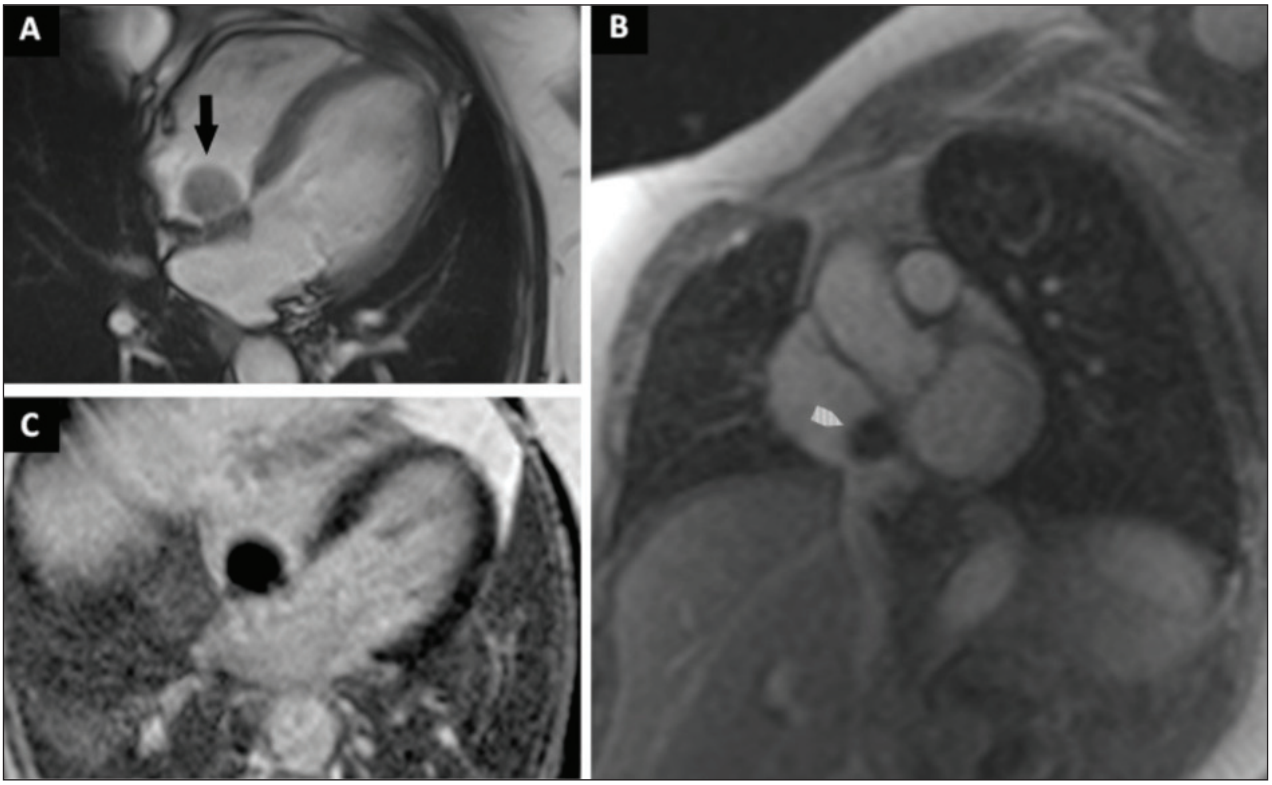

Figure 1. Right atrium myxoma- 70-year-old female. Rounded and well-defined mass (diameter about 22 mm) mobile, isointense to myocardial tissue on Trufi cine sequence (black arrow) (A), hypointense on first-pass perfusion sequences (white arrowhead) (B) and isointense to myocardial on LGE (C).

CMR due to the small size. On CMR cine-sequences they appear as small mobile and homogeneous valvular mass surrounding turbulent flow, with isointense T1 and hyperintense T2 signal intensity. Fat-saturation sequences are useful to differentiate fibroelastomas from lipomas, because the first one has no signal loss dropout. In cardiac CT, they appear small, hypodense attached through a thin stalk to valve surface (6).

-Lipoma. Lipomas represent about 8% of primary cardiac tumors and approximately 14% of benign cardiac masses, with an incidence of 0.2 and 0.4% reported in autopsy studies. Lipomas can occur in all age groups, but they're most likely to be found in the fifth and sixth decades of life(60). Lipomas are encapsulated and well-defined tumors containing neoplastic adipocytes (6). Typically, lipomas are localized in the RA and the left ventricle (LV) (60). In most cases, cardiac lipomas are discovered accidentally and the patients are asymptomatic. Rarely, very large lipomas can lead to symptomatic obstruction of the tricuspid valve or vena cava resulting in heart failure. They can be multiple in patients with tuberous sclerosis (61). On CMR they appear slightly hyperintense on T2-weighted, homogeneous hyperintense on T1-weighted, with loss of signal on fat suppression sequences, and with no CE (30). On CT imaging they appear with a homogeneous fat attenuation (density<-50 Hounsfield units), without CE (6).

-Rhabdomyoma. Rhabdomyoma is the most common benign pediatric cardiac tumor, frequently associated with tuberous sclerosis. These tumors involve children from fetal age to early infancy and tend to regress spontaneously (56). They are multiple in 90% of cases and most commonly localized in the LV and ventricular septum, although up to 30% of cases the atrial wall or RV are involved (62). These tumors may present clinically with arrhythmia and heart failure. Usually, echocardiography is adequate for making the diagnosis, but CMR can be useful in atypical presentations or for surgical planning (4). On imaging, they appear as single or multiple well-circumscribed, intramural or intracavitary masses. On CMR images, rhabdomyomas are homogeneous on all sequences, isointense to normal myocardium on T1-weighted images and hyperintense on T2-weighted images, and they show no or minimal enhancement on first-pass perfusion imaging and iso-intensity on LGE images (4). CCT is rarely performed because the affected population is mainly pediatric.

-Fibroma. Fibroma is the second most common type of pediatric cardiac tumor (63). It occurs rarely in adolescents or adults (about 15 %) (56). Cardiac fibromas typically arise in the LV (63). Although, cases of fibromas located in the RV (30%) and RA (10%) have been reported (64). The average diameter of this tumor is 5 cm and the clinical onset depends upon their location and size. On CMR imaging fibromas are slightly hypointense on T2-weighted images and isointense on T1-weighted images relative to muscle, due to their dense and fibrous nature. They have well-defined borders; little or no CE during the early phases, hyperenhancement on LGE and high extracellular volume (ECV) values (63, 64). On CT, fibroma appears as a homogeneous mass, with low attenuation and no or minimal enhancement. The characteristic presence of central calcification (patchy hypointense foci within the lesion) is useful to differentiate it from rhabdomyoma (6).

-Hemangioma. Hemangioma is a rare benign vascular tumor (2,8 % of primary cardiac tumors) that can arise from any cardiac chamber, with a predilection of RA and interventricular septum. In a review of 200 cases of hemangiomas, Weidong Li (65) reported that in the 44.1% of cases the right heart was involved (including RA, RV, tricuspid valve, and pulmonary valve). The average age of patients was 43 years old; however, pre-natal cases are also described with a range from the 20th gestational week up to 86 years (65). Hemangioma can be symptomatic in case of bleeding (56). On CMR images, hemangiomas appear heterogeneous with intermediate signal on T1 images and inhomogeneous hyperintense T2 images because of the presence of calcification and fibrous septa; after administration of gadolinium the mass shows intense enhancement due to its vascular structures. In the same way, on CT images hemangioma appears heterogeneous with intense enhancement (65).

Malignant cardiac tumors

-Sarcomas. Sarcomas are mesenchymal tumors and they are the most common cardiac primary malig-

nant neoplasms (3, 56). Usually, males are affected more often than females with a ratio of 2–3/1. The patients younger than 65 years old are the most affected (66).

Any type of sarcoma can affect the heart but angiosarcoma is the most frequent in the right chambers, especially in the RA (80% of cardiac angiosarcomas); while leiomyosarcoma, osteosarcoma and malignant fibrous histiocytoma are the most common in the left chambers. Sarcomas are generally large and they can frequently infiltrate adjacent structures (56). Hemorrhagic pericardial effusion is frequently present. Dyspnea is the most common presenting symptom; however, the patient may also present chest pain, embolic phenomena, peripheral edema, arrhythmias, syncope and sudden death (1). At the time of diagnosis patients can have metastases, most commonly to lungs, lymph nodes, bone and liver (56). CT shows the presence of large lesion, typically with a broad-based attachment and heterogenous CE because are present hemorrhagic and necrosis areas (6, 57).

On CMR T1-weighted images, the mass appears predominantly isointense to myocardium, eventually with areas of high signal due to the presence of intralesional hemorrhage. On T2-weighted images, especially angiosarcoma shows a heterogeneous predominantly hyperintense appearance **(Fig. 2)**. On LGE sequences the tumor has a "sunrise appearance" (peripheral enhancement and central areas of necrosis) (30, 67).

-Lymphoma. Cardiac primary lymphoma is generally a non-Hodgkin type. Secondary cardiac involvement by lymphoma is about 25% of patients with a disseminated lymphoma, while primary cardiac lymphoma is 2% of cardiac primary tumors. The age range of presentation is between 13–90 years old (56). Most commonly lymphomas arise from the right heart chambers, particularly the RA, followed by the RV

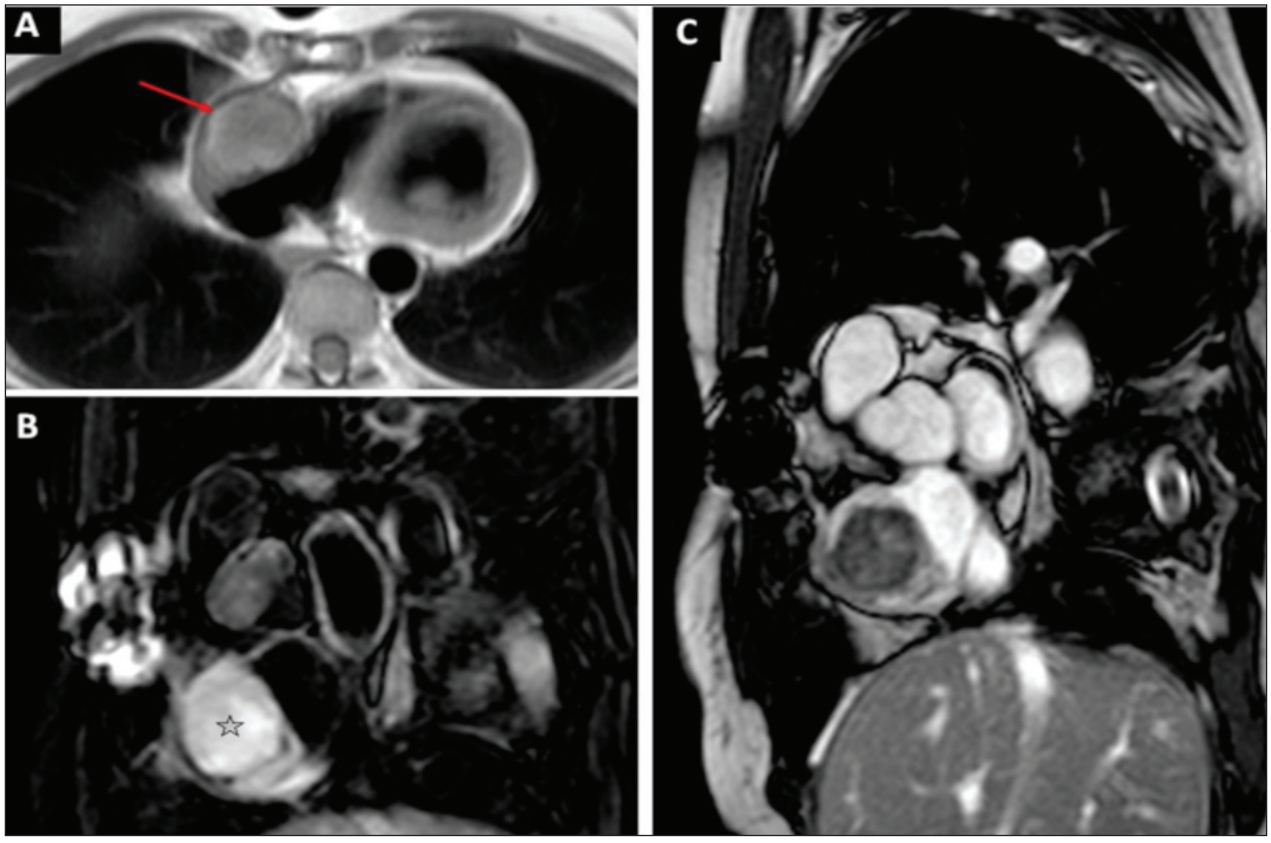

Figure 2. Right atrium angiosarcoma treated with radiotherapy- 57-year-old female. Large with a broad-based mass into the right atrium associated to thickening of the pericardium (red arrow), predominantly isointense to myocardium on T1-weighted image (A). On T2-weighted image, SPIR, the mass shows a typical and high signal hyperintensity (star) (B); heterogenous appearance on balance cine sequences (C).

(56). Often it is associated with pericardium effusion and invasion of the pericardium is frequent. On CT images lymphoma appears or as multiple solid masses attached to the myocardium, or, more commonly, as myocardial or epicardial infiltrative large mass, hypodense or isodense related to the myocardium; with a slight CE. A peculiar characteristic of lymphoma is its diffusion along the surface of the adjacent structures enclosing them (68). On CMR usually, lymphomas are homogeneous relatively hypointense on T1-weighted images and hyperintense on T2-weighted images. CE may be homogeneous or heterogeneous, but not so intense as other malignant tumors (30). The absence of necrosis or hemorrhage areas is useful to distinguish cardiac lymphoma from angiosarcoma.

-Metastasis. Cardiac metastases are more frequent than primary cardiac malignancy(30). Malignant tumors can metastasize to the heart through the direct extension of adjacent organs (lung, esophagus), or through blood vessels dissemination (melanoma) or venous extension into the right atrium within the inferior vena cava (renal cell carcinoma and hepatocellular carcinoma) and via mediastinal lymphatics. The most frequent location of metastasis is the pericardium (64-69%), followed by epicardium (25-34%) and myocardium (30%). Intracavitary metastases are rare, making up 3% to 5% of cardiac metastases **(Fig. 3)** (69). Usually, the imaging features of metastatic disease are not specific, but generally, they have heterogeneous CE, low signal intensity on CMR T1-weighted images and high signal intensity on T2-weighted images. The only exception is reserved for melanoma metastases which appear hyperintense on T1 because of the presence of melanin pigment and also hemorrhagic lesions can show hyperintense areas on T1- weighted images due to the blood degradation products. (30, 67).

Cardiac pseudo-masses

-Thrombosis. Thrombi are the most common intracavitary masses. Thrombus can occur in any of the

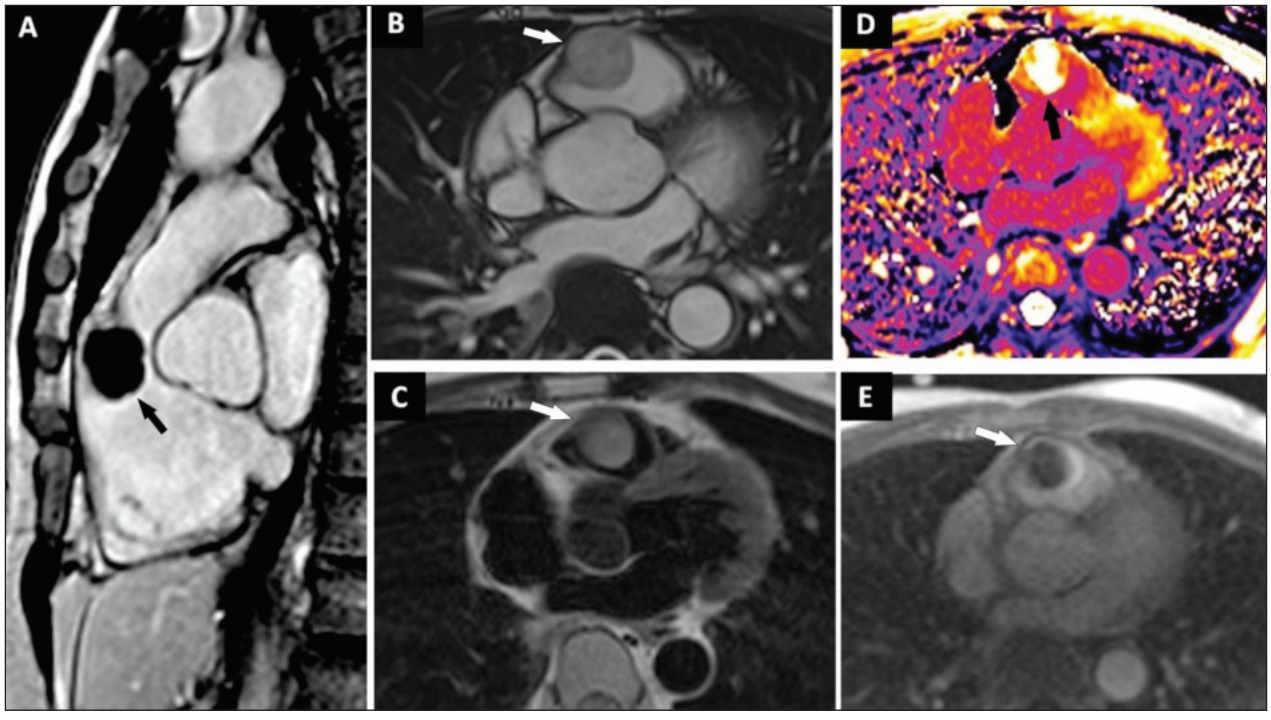

Figure 3. Right ventriculus chordoma metastasis -69-year-old male, with a history of sacral chordoma surgically removed about 10 years before. On TE accidentally discovered a mass in the right ventricular outflow tract (RVOT) (black arrow) (A). CMR shows a solid and rounded mass with regular edges, about 3 cm, intracavitary, slightly inhomogeneous on Trufi cine sequence (white arrow) (B); slightly hyperintense to myocardium on T2- STIR sequence (white arrow) (C). The mass shows different values on T1 map compared to normal adjacent myocardium (black arrow) (D) and progressive CE (white arrow) (E).

cardiac chambers but are typically found in the LA in patients with atrial fibrillation. However, they develop in the region where the flow is slowed or around foreign bodies (for example central venous catheter tip) **(Fig. 4)**. Thrombus is easily detected on CCT image, especially on delayed imaging, as a low-attenuation mass, without CE. Chronic thrombi may present peripheral enhancement because of the presence of a fibrous pseudo-capsule and may develop spotty calcifications. On CMR first pass enhancement images and LGE thrombus show no CE (30, 55).

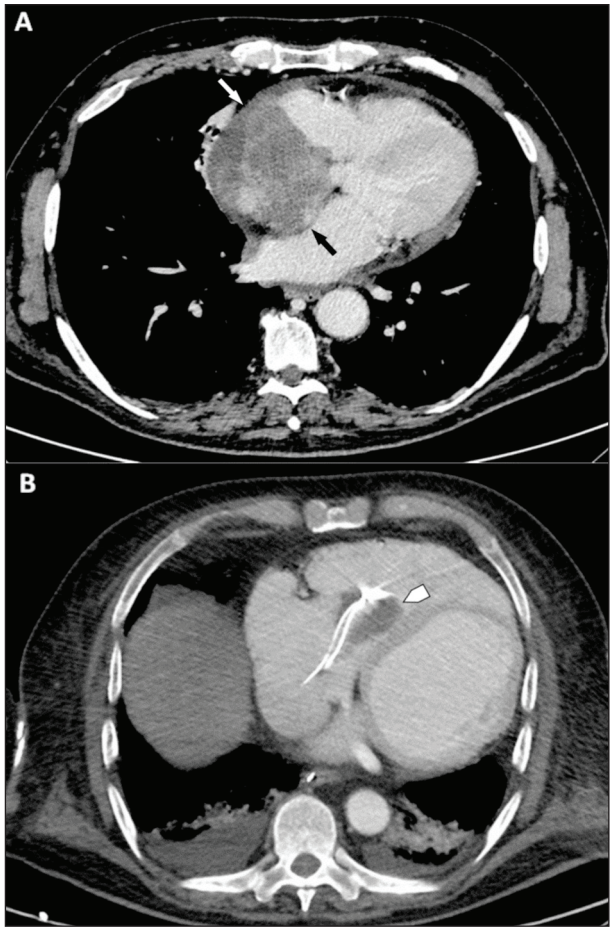

Figure 4. Voluminous sarcoma arising from the right atrium (A) vs thrombus in the right ventricle (B). In A the mass shows invasion of inter-atrial septum (black arrow), inferior vena cava, and pericardium (white arrow) (which appears thickened with a thin pericardial effusion); on CT venous phase, the mass shows heterogenous enhancement. In B in the right ventricle a catheter tip-related thrombosis (white arrowhead) shows hypodensity without CE on CT venous phase (B).

Pseudo-masses. Pseudo masses are normal structures misinterpreted as pathological findings. The orifice of the inferior vena cava (Eustachian valve) can simulate a mass. Into RA the "crista terminalis" or hypertrophic or accessories trabeculae (into RA and RV) may appear as a thrombus or as a mass. Also, lipomatous hypertrophy of the interatrial septum (LHIS) can simulate a tumor (70). LHIS is indistinguishable from lipoma except that the formers occur in the atrial septum with a typical distribution (generally sparing the fossa ovalis). They are asymptomatic and do not require resection (71, 72).

Conflict of interest: Authors declare that they have no commercial associations (e.g. consultancies, stock ownership, equity interest, patent/licensing arrangement etc.) that might pose a conflict of interest in connection with the submitted article.

References

1. Paraskevaidis IA, Michalakeas CA, Papadopoulos CH, Anastasiou-Nana M. Cardiac tumors. ISRN Oncol 2011; 2011: 208929.
2. Robertson R. Primary cardiac tumours; surgical treatment. American journal of surgery 1957; 94: 183-93.
3. Basso C, Rizzo S, Valente M, Thiene G. Cardiac masses and tumours. Heart (British Cardiac Society) 2016; 102: 1230-45.
4. Ghadimi Mahani M, Lu JC, Rigsby CK, Krishnamurthy R, Dorfman AL, Agarwal PP. MRI of pediatric cardiac masses. AJR. American journal of roentgenology 2014; 202: 971-81.
5. Bovet P, Paccaud F. Body-mass index and mortality. Lancet (London, England) 2009; 374: 113; author reply 114.
6. Kassop D, Donovan MS, Cheezum MK, et al. Cardiac Masses on Cardiac CT: A Review. Current cardiovascular imaging reports 2014; 7: 9281.
7. Lichtenberger JP, 3rd, Reynolds DA, Keung J, Keung E, Carter BW. Metastasis to the Heart: A Radiologic Approach to Diagnosis With Pathologic Correlation. AJR. American journal of roentgenology 2016; 207: 764-772.
8. Susic L, Baraban V, Vincelj J, et al. Dilemma in clinical diagnosis of right ventricular masses. Journal of clinical ultrasound : JCU 2017; 45: 362-369.
9. Obeid AI, al Mudamgha A, Smulyan H. Diagnosis of right atrial mass lesions by transesophageal and transthoracic echocardiography. Chest 1993; 103: 1447-51.
10. Agliata G, Schicchi N, Agostini A, et al. Radiation exposure related to cardiovascular CT examination: comparison between conventional 64-MDCT and third-generation

dual-source MDCT. La Radiologia medica 2019; 124: 753-761.
11. Rahouma M, Arisha MJ, Elmously A, et al. Cardiac tumors prevalence and mortality: A systematic review and meta-analysis. Int J Surg. 2020;76:178-189.
12. Agostini A, Kircher MF, Do R, et al. Magnetic Resonance Imaging of the Liver (Including Biliary Contrast Agents) Part 1: Technical Considerations and Contrast Materials. Seminars in roentgenology 2016; 51: 308-316.
13. Malik SB, Chen N, Parker RA 3rd, Hsu JY. Transthoracic Echocardiography: Pitfalls and Limitations as Delineated at Cardiac CT and MR Imaging. Radiographics. 2017;37:383-406.
14. Agostini A, Mari A, Lanza C, et al. Trends in radiation dose and image quality for pediatric patients with a multidetector CT and a third-generation dual-source dual-energy CT. La Radiologia medica 2019; 124: 745-752.
15. Díaz Angulo C, Méndez Díaz C, Rodríguez García E, Soler Fernández R, Rois Siso A, Marini Díaz M. Imaging findings in cardiac masses (Part I): study protocol and benign tumors. Radiologia. 2015;57:480-488.
16. Zhu D, Yin S, Cheng W, et al. Cardiac MRI-based multimodality imaging in clinical decision-making: Preliminary assessment of a management algorithm for patients with suspected cardiac mass. Int J Cardiol. 2016;203:474-481
17. Rajiah P, MacNamara J, Chaturvedi A, Ashwath R, Fulton NL, Goerne H. Bands in the Heart: Multimodality Imaging Review. Radiographics. 2019;39:1238-1263.
18. Maleszewski JJ, Anavekar NS, Moynihan TJ, Klarich KW. Pathology, imaging, and treatment of cardiac tumours. Nat Rev Cardiol. 2017;14:536-549.
19. Tower-Rader A, Kwon D. Pericardial Masses, Cysts and Diverticula: A Comprehensive Review Using Multimodality Imaging. Prog Cardiovasc Dis. 2017;59:389-397.
20. Zoccali C, Rossi B, Zoccali G, et al. A new technique for biopsy of soft tissue neoplasms: a preliminary experience using MRI to evaluate bleeding. Minerva medica 2015; 106: 117-20.
21. Hong YJ, Hur J, Han K, et al. Quantitative Analysis of a Whole Cardiac Mass Using Dual-Energy Computed Tomography: Comparison with Conventional Computed Tomography and Magnetic Resonance Imaging. Sci Rep. 2018;8:15334.
22. Schiattarella GG, Cerulo G, De Pasquale V, et al. The Murine Model of Mucopolysaccharidosis IIIB Develops Cardiopathies over Time Leading to Heart Failure. PloS one 2015; 10: e0131662.
23. Tumma R, Dong W, Wang J, Litt H, Han Y. Evaluation of cardiac masses by CMR-strengths and pitfalls: a tertiary center experience. Int J Cardiovasc Imaging. 2016;32:913-920.
24. Ma G, Wang D, He Y, Zhang R, Zhou Y, Ying K. Pulmonary embolism as the initial manifestation of right atrial myxoma: A case report and review of the literature. Medicine (Baltimore). 2019;98:e18386.
26. Di Cesare E, Patriarca L, Panebianco L, et al. Coronary computed tomography angiography in the evaluation of intermediate risk asymptomatic individuals. La Radiologia medica 2018; 123: 686-694.
27. de Roos A, Higgins CB. Cardiac radiology: centenary review. Radiology. 2014; 273(2 Suppl):S142-59
28. Ren DY, Fuller ND, Gilbert SAB, Zhang Y. Cardiac Tumors: Clinical Perspective and Therapeutic Considerations. Curr Drug Targets. 2017;18:1805-1809.
29. Abbasi Tashnizi M, Soltani G, Mehrabi Bahar M, Ahmadi M, Golmakani E, Saremi E. Right Atrium Myxoma After Lung Adenocarcinoma. Iranian Red Crescent medical journal 2015; 17: e19656.
30. Motwani M, Kidambi A, Herzog BA, Uddin A, Greenwood JP, Plein S. MR imaging of cardiac tumors and masses: a review of methods and clinical applications. Radiology 2013; 268: 26-43.
31. Krumm P, Mangold S, Gatidis S, et al. Clinical use of cardiac PET/MRI: current state-of-the-art and potential future applications. Jpn J Radiol. 2018;36:313-323.
32. Zhou W, Srichai MB. Multi-modality Imaging Assessment of Pericardial Masses. Curr Cardiol Rep. 2017;19:32.
33. Schindler TH. Cardiovascular PET/MR imaging: Quo Vadis?. J Nucl Cardiol. 2017;24:1007-1018.
34. Kim J, Da Nam B, Hwang JH, et al. Primary cardiac angiosarcoma with right atrial wall rupture: A case report. Medicine (Baltimore). 2019;98:e15020.
35. Di Cesare E, Cademartiri F, Carbone I, et al. Clinical indications for the use of cardiac MRI. By the SIRM Study Group on Cardiac Imaging. La Radiologia medica 2013; 118: 752-98.
36. Rinuncini M, Zuin M, Scaranello F, et al. Differentiation of cardiac thrombus from cardiac tumor combining cardiac MRI and 18F-FDG-PET/CT Imaging. Int J Cardiol. 2016;212:94-96.
37. Yılmaz R, Demir AA, Önür İ, Yılbazbayhan D, Dursun M. Cardiac calcified amorphous tumors: CT and MRI findings. Diagn Interv Radiol. 2016;22:519-524.
38. Tarantini G, Favaretto E, Napodano M, et al. Design and methodologies of the POSTconditioning during coronary angioplasty in acute myocardial infarction (POST-AMI) trial. Cardiology 2010; 116: 110-6.
39. Liddy S, McQuade C, Walsh KP, Loo B, Buckley O. The Assessment of Cardiac Masses by Cardiac CT and CMR Including Pre-op 3D Reconstruction and Planning. Curr Cardiol Rep. 2019;21:103.
40. Scaglione M, Salvolini L, Casciani E, Giovagnoni A, Mazzei MA, Volterrani L. The many faces of aortic dissections: Beware of unusual presentations. European journal of radiology 2008; 65: 359-64.
41. Chan AT, Plodkowski AJ, Pun SC, et al. Prognostic utility of differential tissue characterization of cardiac neoplasm and thrombus via late gadolinium enhancement cardiovascular magnetic resonance among patients with advanced systemic cancer. J Cardiovasc Magn Reson. 2017;19:76.

42. Furlow B. Computed Tomography of Cardiac Malignancies. Radiol Technol. 2016;87:529CT-45CT.
43. Abrams HL. History of cardiac radiology. AJR Am J Roentgenol. 1996;167(2):431-8
44. Colin GC, Gerber BL, Amzulescu M, Bogaert J. Cardiac myxoma: a contemporary multimodality imaging review. Int J Cardiovasc Imaging. 2018;34:1789-1808.
45. Quarta G, Aquaro GD, Pedrotti P, et al. Cardiovascular magnetic resonance imaging in hypertrophic cardiomyopathy: the importance of clinical context. European heart journal cardiovascular Imaging 2018; 19: 601-610.
46. Wu CM, Bergquist PJ, Srichai MB. Multimodality Imaging in the Evaluation of Intracardiac Masses. Curr Treat Options Cardiovasc Med. 2019;21:55.
47. Ruscitti P, Cipriani P, Masedu F, et al. Increased Cardiovascular Events and Subclinical Atherosclerosis in Rheumatoid Arthritis Patients: 1 Year Prospective Single Centre Study. PloS one 2017; 12: e0170108.
48. Patel R, Lim RP, Saric M, et al. Diagnostic Performance of Cardiac Magnetic Resonance Imaging and Echocardiography in Evaluation of Cardiac and Paracardiac Masses. Am J Cardiol. 2016;117:135-140.
49. Di Cesare E, Battisti S, Di Sibio A, et al. Early assessment of sub-clinical cardiac involvement in systemic sclerosis (SSc) using delayed enhancement cardiac magnetic resonance (CE-MRI). European journal of radiology 2013; 82: e268-73.
50. Barone-Rochette G, Jankowski A, Rodiere M. Cardiac magnetic resonance imaging and cardiac computed tomography in clinical practice. Rev Med Interne. 2014;35(11):742-51
51. Glockner JF. Magnetic Resonance Imaging and Computed Tomography of Cardiac Masses and Pseudomasses in the Atrioventricular Groove. Canadian Association of Radiologists journal = Journal l'Association canadienne des radiologistes 2018; 69: 78-91.
52. Mousavi N, Cheezum MK, Aghayev A, et al. Assessment of Cardiac Masses by Cardiac Magnetic Resonance Imaging: Histological Correlation and Clinical Outcomes. Journal of the American Heart Association 2019; 8: e007829.
53. Schicchi N, Fogante M, Esposto Pirani P, et al. Third-generation dual-source dual-energy CT in pediatric congenital heart disease patients: state-of-the-art. La Radiologia medica 2019; 124: 1238-1252.
54. Agostini A, Borgheresi A, Mari A, et al. Dual-energy CT: theoretical principles and clinical applications. La Radiologia medica 2019; 124: 1281-1295.
55. Hoey E, Ganeshan A, Nader K, Randhawa K, Watkin R. Cardiac neoplasms and pseudotumors: imaging findings on multidetector CT angiography. Diagnostic and interventional radiology (Ankara, Turkey) 2012; 18: 67-77.
56. Grebenc ML, Rosado de Christenson ML, Burke AP, Green CE, Galvin JR. Primary cardiac and pericardial neoplasms: radiologic-pathologic correlation. Radiographics : a review publication of the Radiological Society of North America, Inc 2000; 20: 1073-103; quiz 1110-1, 1112.
57. Young PM, Foley TA, Araoz PA, Williamson EE. Computed Tomography Imaging of Cardiac Masses. Radiologic clinics of North America 2019; 57: 75-84.
58. Gowda RM, Khan IA, Nair CK, Mehta NJ, Vasavada BC, Sacchi TJ. Cardiac papillary fibroelastoma: a comprehensive analysis of 725 cases. American heart journal 2003; 146: 404-10.
59. Howard RA, Aldea GS, Shapira OM, Kasznica JM, Davidoff R. Papillary fibroelastoma: increasing recognition of a surgical disease. The Annals of thoracic surgery 1999; 68: 1881-5.
60. D'Souza J, Shah R, Abbass A, Burt JR, Goud A, Dahagam C. Invasive Cardiac Lipoma: a case report and review of literature. BMC cardiovascular disorders 2017; 17: 28.
61. Malik SB, Kwan D, Shah AB, Hsu JY. The right atrium: gateway to the heart--anatomic and pathologic imaging findings. Radiographics : a review publication of the Radiological Society of North America, Inc 2015; 35: 14-31.
62. Kondo T, Niida Y, Mizuguchi M, Nagasaki Y, Ueno Y, Nishimura A. Autopsy case of right ventricular rhabdomyoma in tuberous sclerosis complex. Legal medicine (Tokyo, Japan) 2019; 36: 37-40.
63. Sargar KM, Sheybani EF, Shenoy A, Aranake-Chrisinger J, Khanna G. Pediatric Fibroblastic and Myofibroblastic Tumors: A Pictorial Review. Radiographics : a review publication of the Radiological Society of North America, Inc 2016; 36: 1195-214.
64. Gravina M, Casavecchia G, Totaro A, et al. Left ventricular fibroma: what cardiac magnetic resonance imaging may add? International journal of cardiology 2014; 176: e63-5.
65. Li W, Teng P, Xu H, Ma L, Ni Y. Cardiac Hemangioma: A Comprehensive Analysis of 200 Cases. The Annals of thoracic surgery 2015; 99: 2246-52.
66. Hamidi M, Moody JS, Weigel TL, Kozak KR. Primary cardiac sarcoma. The Annals of thoracic surgery 2010; 90: 176-81.
67. Hoey ET, Shahid M, Ganeshan A, Baijal S, Simpson H, Watkin RW. MRI assessment of cardiac tumours: part 2, spectrum of appearances of histologically malignant lesions and tumour mimics. Quantitative imaging in medicine and surgery 2014; 4: 489-97.
68. Jeudy J, Kirsch J, Tavora F, et al. From the radiologic pathology archives: cardiac lymphoma: radiologic-pathologic correlation. Radiographics : a review publication of the Radiological Society of North America, Inc 2012; 32: 1369-80.
69. Goldberg AD, Blankstein R, Padera RF. Tumors metastatic to the heart. Circulation 2013; 128: 1790-4.
70. Rangel-Hernandez MA, Aranda-Fraustro A, Melendez-Ramirez G, Espinola-Zavaleta N. Misdiagnosis for right atrial mass: a case report. European heart journal. Case reports 2018; 2: yty004.
71. Bielicki G, Lukaszewski M, Kosiorowska K, Jakubaszko J, Nowicki R, Jasinski M. Lipomatous hypertrophy of the atrial septum - a benign heart anomaly causing unexpected

surgical problems: a case report. BMC cardiovascular disorders 2018; 18: 152.
72. Carino D, Agostinelli A, Ricci M, Romano G, Nicolini F, Gherli T. A rare case of gint lipomatous hypertrophy of the atrial septum. Acta bio-medica : Atenei Parmensis 2018; 89: 114-116.

Received: 20 May 2020
Accepted: 10 June 2020
Correspondence:
Diletta Cozzi, MD
Department, of Radiology, Careggi University Hospital
L.go G.A. Brambilla, 3 - 50134 Florence – Italy
E-mail: dilettacozzi@gmail.com

Acta Biomed 2020; Vol. 91, Supplement 8: 71-80 DOI: 10.23750/abm.v91i8-S.9974

Review

Basic embolization techniques: tips and tricks

Anna Maria Ierardi[1], Filippo Piacentino[2], Filippo Pesapane[3], Aldo Carnevale[4], Marco Curti[2], Federico Fontana[2], Massimo Venturini[2], Antonio Pinto[5], Francesco Gentili[6], Susanna Guerrini[7], Massimo De Filippo[6], Melchiore Giganti[8], Gianpaolo Carrafiello[1,9]

[1] Radiology Department, Fondazione IRCCS Cà Granda, Ospedale Maggiore Policlinico, Milan, Italy; [2] Department of Diagnostic and Interventional Radiology, University of Insubria, Ospedale di Circolo e Fondazione Macchi, Varese, Italy; [3] Breast Imaging Unit, IEO European Institute of Oncology IRCCS, Milan, Italy; [4] University Radiology Unit, Radiology Department, Arcispedale Sant'Anna, Ferrara, Italy; [5] Department of Radiology, CTO Hospital, Azienda dei Colli, Naples, Italy; [6] Section of Radiology, Unit of Surgical Sciences, Department of Medicine and Surgery, Azienda Ospedaliero-Universitaria di Parma, University of Parma, Parma, Italy; [7] Department of Radiological Sciences, Diagnostic Imaging Unit, Azienda Ospedaliera Universitaria Senese, Siena, Italy; [8] Department of Morphology, Surgery and Experimental Medicine, Radiology Section, University of Ferrara, Ferrara, Italy; [9] Department of Health Sciences, Università degli Studi di Milano, Milan, Italy

Summary. Good knowledge of the various approaches of embolization of peripheral bleedings and different embolic materials available is of paramount importance for successful and safe embolization. We review and illustrate the main endovascular and percutaneous techniques used for embolization, along with the characteristics of the different embolic materials, and the potential complications. (www.actabiomedica.it)

Keywords: embolization, interventional radiology, sac packing, sandwich technique

Introduction

In recent years, radiology has been one of the medical branches that has experienced the most important technological revolution and expansion, both in diagnostic (1-3) and interventional applications. In the interventional setting, numerous and different techniques have been introduced (4-7), allowing the treatment of several medical (8) and surgical (9-11) conditions in practically all body areas (12-19). In this context, embolization has become a major arm of modern interventional radiology practice, with growing scope and complexity in diverse clinical scenarios. The goal of embolization is to obtain the occlusion or decrease of the blood/ lymph flow through the endovascular application of different agents or materials. Over the past decades, endovascular embolization has witnessed an increasing use because of a combination of the trend towards conservative treatment protocols, advances in catheter technology, the introduction of new embolic agents, and improvements in digital imaging (20, 21).

Different endovascular procedures have been applied for previously unsolvable problems, replacing open surgery in many settings thanks to their low invasiveness, reduced morbidity and mortality rates, shortened hospital stay and recovery time, and an overall positive impact on the health system economics (20, 21).

After the first intuition in 1953 by Seldinger, of a simple technique allowing the percutaneous catheter replacement of a needle or trocar, Dotter described, in the early 1960s, the possibility of using catheters to perform intravascular surgery; however, only in the mid-1970s, transcatheter therapeutic procedures started to become popular (22). Since then, embolization has become a fundamental procedure and has been included in the treatment protocols for a wide variety of conditions: trauma, emergency bleeding; non-traumatic hemorrhage including hemoptysis or

gastro-intestinal bleeding; cancer care, through direct therapy delivery and solid tumor chemoembolization, preoperative devascularization, hepatic growth stimulation before surgery; congenital or acquired vascular malformations and aneurysms; treatment of uterine myomas and other benign conditions (23-32).

A comprehensive understanding and practical knowledge of these techniques are essential for the optimal and safe use in different scenarios. In this work, we describe different approaches of embolization with a focus on "tips and tricks" of each modality, providing interventional strategies for avoiding and managing procedure-related complications.

Endovascular Approach

The endovascular approach is the most used, with different available techniques.

Proximal Embolization

Proximal embolization (PE) is recommended in cases of multifocal injury or in cases of contrast blush detected at CT-angiography, without clear evidence of bleeding with catheter angiography. This approach requires a proper planning in the different vascular areas, to assess the presence of "good" collaterals to the target tissue, and thus preventing ischemic lesions (33).

Spleen

PE plays a crucial role in the management of traumatic splenic lesions, decreasing the perfusion pressure within the splenic parenchyma, and maintaining the collateral flow to preserve long-term splenic function. PE of splenic artery reduces the risk of acute rupture, infarction, and abscess formation. Splenic PE is performed mainly using endovascular plugs and coils, to spare the origin of the dorsal pancreatic artery and great pancreatic artery, and to maintain the collateral flow (34, 35).

Proximal splenic embolization, if permed in selected patients, is also an efficient treatment for hypersplenism, increasing white blood cells (WBC) and platelets count in these patients (36).

Liver

Blunt liver trauma are more frequently associated with venous injuries, commonly treated conservatively. In case of arterial lesions in hemodynamically stable patients, the endovascular approach is recommended; this can be performed through permanent and distal embolization (e.g., coils) if the bleeding site is easily evidenced by angiogram; otherwise temporary embolization (usually with gelfoam) should be chosen for "shower" embolization, distally to the origin of the gastro-duodenal artery. Procedural complications include liver necrosis and abscess formations (37, 38).

Renal artery embolization

Renal artery embolization (RAE) is recommended in various pathologic conditions, including traumatic or iatrogenic vascular injuries, and reports have described good preservation of renal function after embolization. RAE should always be performed as selective as possible in order to reduce the risk of loss of nephrons and renal function (39). Some authors stated that detachable coils are safer than liquid embolizing agents (40), because they allow a more reliable controlled release (**fig. 1**).

Recently, Jardinet et al. (41) proposed the use of microvascular plugs as embolic agents in case of renal bleeding; they reported a superselective embolization with a minimal resulting renal infarction volume.

Pelvic Trauma

In case of active arterial bleeding from pelvic fractures or organ injuries (muscle laceration), endovascular embolization is nowadays considered a safe option in order to stabilize a patient with polytrauma (33, 42, 43). Internal iliac artery (IIA) branches are the most common source of pelvic bleeding followed by branches of the external iliac and common femoral arteries. In pelvic trauma, both proximal and distal embolization were described (44, 45).

Proximal embolization is usually adopted in patients with multiple lesions and/or unstable patients. As hemodynamic stabilization should be considered the main purpose of TAE, the operator may also use

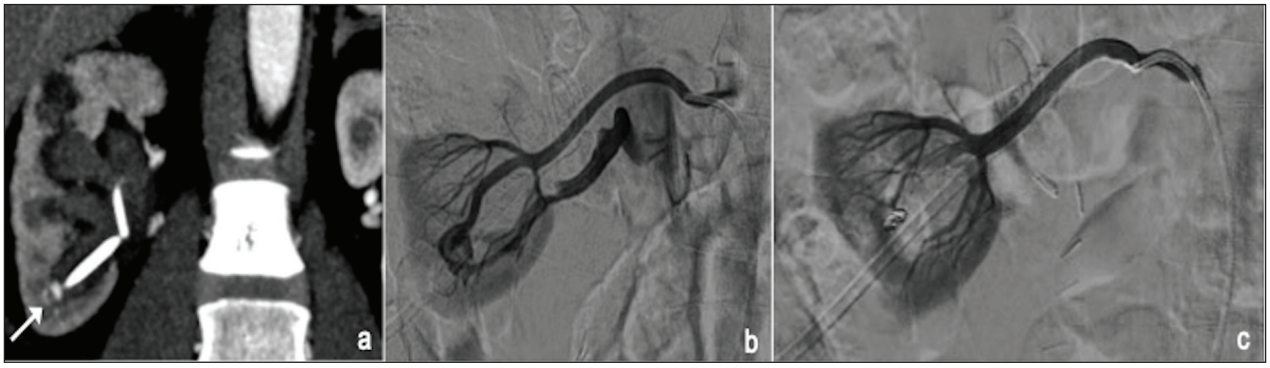

Figure 1. CT coronal view shows pseudoaneurysm (PSA) after nephrostomy (a); arteriogram confirms PSA and reveals an arteriovenous fistula also (b); final angiogram after embolization with coil (c).

temporary embolic materials to save valuable time in hemodynamically unstable patients.

Selective embolization is preferred in stable patients and when one or more bleeding point are clearly visualized at preliminary angiogram (33, 45).

In literature, both mechanical and liquid embolic agents were described as effective and safe (46, 47). Gelfoam and coils seem to be the most used materials, often used in combination. Gelfoam is a biodegradable gelatine sponge, lasts for 7–21 days, and it is relatively manageable and economical. Furthermore, no long or short-term complications were associated with its use (46). Coils are commonly used for more specific and selective embolization, allowing a fast mechanical occlusion. However, multiple coils are often necessary to obtain the complete bleeding control. Liquid agents, including adhesive (glue) or non-adhesive (Onyx), represent interesting tools for very distal vessels, and can also be used in cases of rebleeding. The main limitations of liquid embolising agents are the costs, the lack of controlling the amount used and the risk of back-flow (45).

Lower gastrointestinal bleeding

Embolization is currently proposed as the first step in the treatment of acute, life-threatening LGIB, when an endoscopic approach is not possible or unsuccessful (48). Despite the high success rate, some complications like rebleeding and bowel infarction are reported in literature. Due to the terminal bowel vascular branches with no collateral circulation, the ideal area to perform LGIB embolization is at the level of vasa recta. The ideal embolic agent should also be characterized by controlled release to reduce the risk of extravasation in the marginal vessels. Some Authors (49) suggested the use of selective flow-directed particles; however, these cannot be visualized or precisely deposited and may reflux into non-target arteries. Better results, in terms of rebleeding rates, were achieved with cyanoacrylates, despite their use require experienced operator, due to the increased risk of non-targeted embolization and microcatheter entrapment (50). To overcome this limitation, detachable coils were introduced, allowing a safe and selective embolization also in cases in which vessels are thin and/or tortuous. Liquid embolic (LE) materials like non-adhesive agents, such as ethylene-vinyl alcohol co-polymer (EVOH), are characterized by controlled release, non-adherence, progressive solidification, cohesiveness, high vascular penetration, and a weak inflammatory effect on the endothelium.

Moreover, they polymerize gradually from the periphery out towards the center. This represents a great difference from cyanoacrylates, which polymerize instantaneously. Furthermore, another advantage is that LE is displaced by pressure applied by the operator on the syringe and is not blood-flow dependent. Consequently, the procedure is safer and allows to leave the distal tip of the catheter in situ, thus permitting selective angiographic control after some minutes.

Bronchial artery hypertrophy embolization

Bronchial artery embolization is the recommended treatment for hemoptysis in case of airways bleeding. Both mechanical and liquid agents could be used. Among the mechanical ones, the most used are particles and coils (**fig. 2**). The particles are highly effective on the distal microcirculation (51). Coils represent a safer alternative, with high success rates, however, in case of large-caliber bronchial artery with tortuous course (V-shaped), the use of coils can be problematic. Liquid embolic agents overcame those limitations, the most used being n-Butyl-2-cyanoacrylate (NBCA). Nevertheless, liquid embolizing agents have some limitations such as the need of compatible microcatheters, the cost and the mandatory use of dimethyl sulfoxide DMSO, which can cause vasospasm, endothelial wall damage and pain (52).

Sac packing

In case of aneurysm or pseudoaneurysm, a sac packing (SP) technique can be used for embolization (53). This procedure implies coils placement in a vascular sac until it is obliterated or excluded from the circulation. This technique is well suited for saccular aneurysms with a narrow neck, allowing retention of the coils in the sac and preserving the parent vessel flow to the visceral end-organ (54-56) (**fig. 3**). Balloon assisted SP, bare metal stent-assisted SP and percutaneous SP cast forming may also be considered techniques to fill the sac with one or more embolic agents. This technique consists in the coaxial positioning of an inflated balloon, in order to reduce the risk of spillage of the embolic agent; moreover, in the event of intraprocedural acute aneurysm rupture, the balloon could be used as a fast hemostatic agent (57).

Bare metal stent-assisted SP, always used in combination with coils, aims to avoid the coils migration and, at the same time, maintain the patency of the treated vessel (58, 59).

Percutaneous direct puncture of the sac may be considered when the endovascular approach is not feasible or unsuccessful. Of course, the sac must be accessible with the percutaneous approach; imaging guidance must be usable (ultrasound, CT, Cone Beam CT, fluoroscopic). The sac may be filled with one or more embolic agents using more than one imaging technique as guidance.

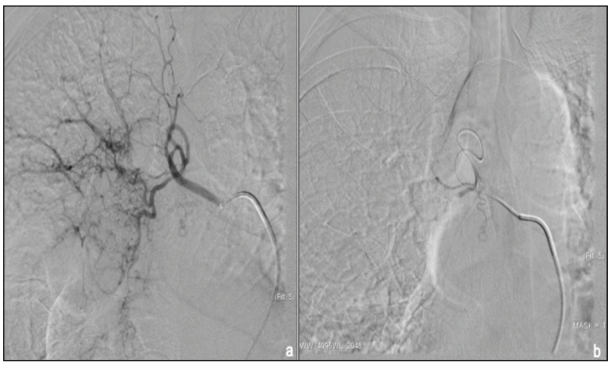

Figure 2. selective arteriogram of the right hypertrophic bronchial artery (a); final angiogram after embolization performed with particles (b).

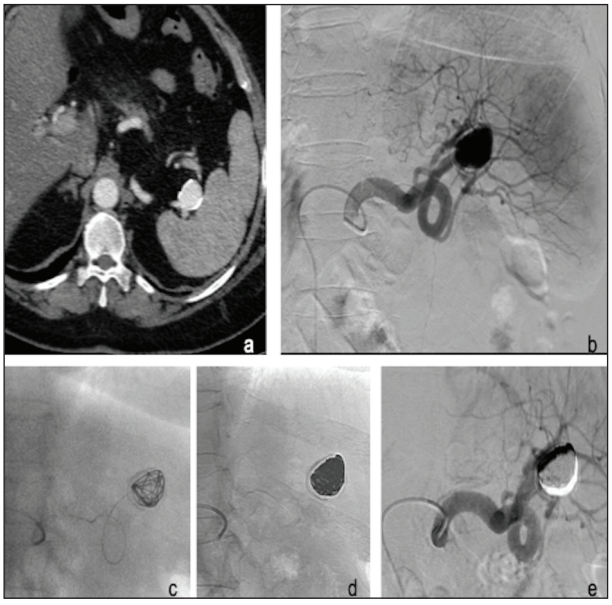

Fig 3. 52 years old female with incidental finding of distal splenic artery aneurysm. Axial CT acquisition shows a distal splenic artery aneurysm with a diameter of cm 3 (a); Digital Substruction Angiography (DSA) confirms the arterial dilation of the distal part of the splenic artery (b). Super-selective arteriogram performed with microcatheter with the distal end inside the aneurysmal sac (c). Single shot acquisition demonstrates coils compacted in the aneurysm (d). Post procedural DSA corfims regular patency of the splenic artery with the complete exclusion of the distal splenic artery aneurysm (e).

Sandwich Technique

The sandwich technique implicates embolization of both the afferent and efferent vessels to completely remove all portions of a target lesion from the circulation. Such a method is usually preferred in patients in whom collateral flow could "flow back" into the lesion if only one segment of the vessel is occluded (60). Sandwich technique is indicated in peripheral embolization, especially in districts in which backflow from collaterals should be fill the bleeding site (**fig. 4**). A clear understanding of the target vessel is critical, especially if it contains extensive collateral supply (e.g., via muscular branches) as these can provide distal flow and supply to the bleeding vessel and therefore result in continued bleeding if they are not also embolized. Accordingly, both proximal and distal segments to the site of injury of the artery, are routinely embolized to prevent this complication (61). The intraprocedural impossibility to reach the distal branch during an endovascular exclusion of a PSA represents an example of a condition that is a common challenge. An example of sandwich technique application is that of embolization of splenic artery aneurysm/pseudoaneurysm that could be evidenced in the setting of pancreatitis, splenic trauma, or mycotic infection of the arterial wall. As with most pseudoaneurysms, there is a high risk of rupture without appropriate management, and all splenic lesions should be treated regardless of size or clinical manifestation (62). Such proper management is usually a coil embolization or a stent-graft placement across the lesion when the anatomy allows (for instance, more proximal lesions and non-tortuous arterial segments to facilitate device passage).

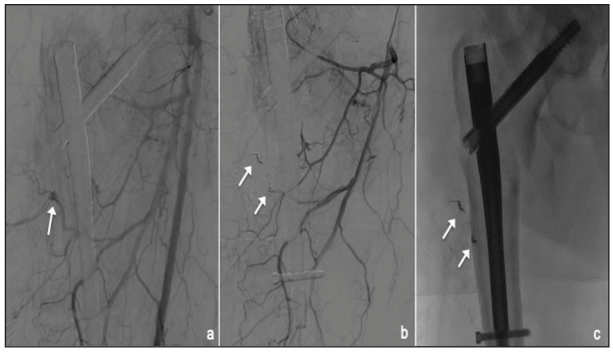

Figure 4. small pseudoaneurysm (PSA) of the profunda femoral artery (white arrow,a); angiogram at the end of the embolization with sandwich technique performed with 2 microcoils (white arrows, b); single shot confirms the presence of 2 coils (white arrows, c).

Distal and proximal embolization (sandwich technique) across the aneurysm neck is typically required to prevent collateral circulation resulting in continued sac pressurization. Since the aneurysm sac could continue to be pressurized through short gastric or distal pancreatic arteries acting as retrograde-filling collateral vessel, embolization of only the feeding-afferent artery would be unsatisfactory indeed. The "back door", also named the efferent artery, is usually closed first, followed by the "front door", namely the afferent artery. Alternatively, a sac-packing technique with coils or parent artery glue embolization has also been used. Intentional embolization of the entire splenic artery may be required in complex, high-risk splenic pseudoaneurysms (63).

The sandwich technique may also be applied in more complex settings of multiple afferent or efferent vessels.

Stent placement

Aneurysm and PSA with wide neck have an increased risk of migration of embolic material. To avoid this complication, stent-graft (covered stent) placement, stent-assisted coiling and balloon remodeling techniques are useful (53). These techniques also help in preserving the patency of parent artery. Recently, flow diverting multi-layered bare stents are available, which facilitate slowing the blood flow within the visceral artery aneurysms and maintaining patency of the parent artery as well as any branches arising from or proximal to the aneurysm. Although it is used in the treatment of true aneurysms, its use in pseudoaneurysms is limited, as thrombosis occurs slowly and there is a possibility of rupture in the interim (53).

Percutaneous approach

It is usually used for cases of failed endovascular approach or pseudoaneurysms or bleeding not accessible endovascularly, PSA with narrow neck or localized in solid organs. Bleeding sites must be visible with imaging guides. More often, ultrasound or CT guidance is used as imaging guidance; cone-beam CT may be used as well. More rarely, operator may take advantage from the stasis of the contrast media into the pseudoaneurysm after angiogram acquisition; after realizing the impossibility to reach the bleeding site by endovascular route, fluoroscopic guidance may be successfully used. Multiple projections are usually necessary to guide the needle. Its correct position may be confirmed with the injection of contrast media; once in the desired location, the embolic agent is injected under fluoroscopic guidance until the embolization in completed

The pseudoaneurysm is usually punctured using a 22 G Chiba needle. Care should be taken to keep the tip of the needle away from the neck, to avoid non-target embolization. Once within the pseudoaneurysm, embolization is performed as described above, until thrombosis of the pseudoaneurysm occurs (**fig. 5**). Thrombin, glue and occasionally coils are used as embolic materials. Complications include rupture of the pseudoaneurysm, non- target embolization, and recurrence (64, 65).

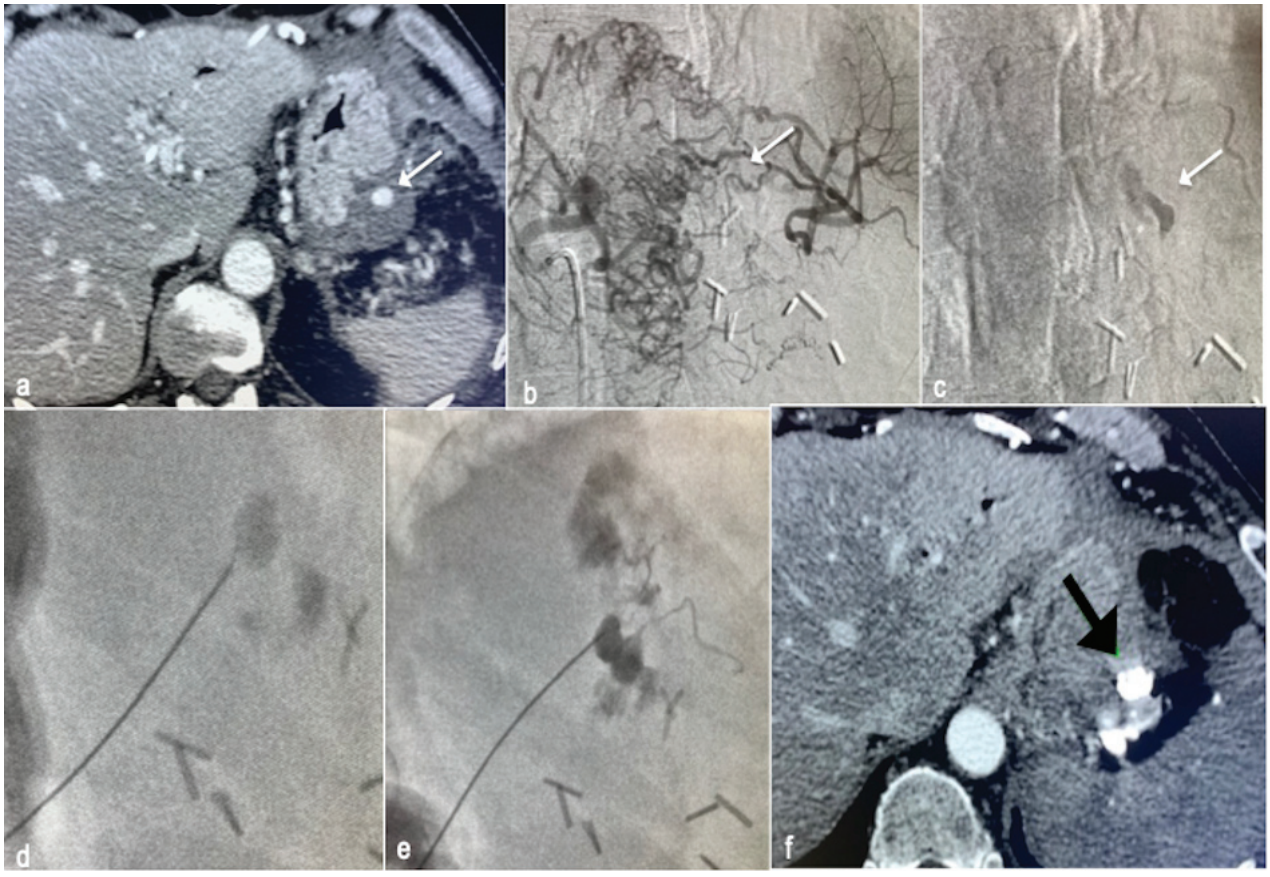

Figure 5. CT scan reveals gastric pseudoaneurysm (PSA) (a); arteriogram of the celiac trunk shows occlusion of the splenic artery and the PSA filled by small vessels, impossible to catheterize (b); contrast medium remained in the PSA (white arrow,c); percutaneous puncture was performed under fluoroscopic guidance (d); glue was used as embolic agent (e); CT was performed to check the complete embolization of the PSA (black arrow, f).

Complications

Complications may be divided into complications of the puncture site, of the embolization site and post-embolization (64). Complications of the puncture site occur in approximately 10-20% of cases and they are usually classified as minor complications (pain, bleeding and hematoma) that may be easily managed intraprocedurally (66). Infection or, rarely, pseudoaneurysm at the puncture site can be managed with supportive care, percutaneous drainage, or other non-invasive management.

Complications related to the embolization are essentially the inadvertent distal infarction of nonexpendable vessels and damages in the adjacent organs (67).

For this reason, a clear understanding of the target vessel is critical, especially if it contains extensive collateral supply, as these can provide flow to the bleeding vessel. Therefore, routinely both segments of the artery proximal and distal to the site of injury, are embolised.

A technically successful embolization requires the catheter tip to be placed so that embolic material is deposited only in blood vessels that serve the abnormal area, preventing injury to healthy tissue. This can be technically impossible in a small percentage of cases (68).

Post-embolization complications include the post-embolization syndrome, which is one of the most common side effects of such procedure and it is more often associated with large fibroids or large tumors or solid organ embolization. This includes fever, nausea and/or vomiting, and pain. It is often a self-limiting phenomenon and usually occurs within the first 72 hours after the procedure and generally starting to subside after 72 hours. Although the etiology of the post-embolization syndrome is partially unknown, it was hypothesized that tissue hypoxia and cell death lead to the release of tissue breakdown products, inflammatory mediators, and vasoactive substances from the tumor and or adjacent healthy tissues. Early imaging following embolization, either by ultrasound or CT, may reveal intralesional gas. This is not to be mistaken for abscess without additional factors (69).

Post-embolization syndrome usually is self-limiting, and treatment is symptomatic with analgesics and intravenous fluids. Prophylactic use of antipyretic and antiemetic therapy may be considered prior to the embolization of large tumors/fibroids (70).

Another complication that may follow embolization procedures is the continued bleeding distal to the point of embolization secondary to collateral flow.

In general, up to 85% of complications of embolization can be managed with only supportive care, percutaneous drainage, or other non-invasive management (64, 66, 67).

Conflict of interest: Authors declare that they have no commercial associations (e.g. consultancies, stock ownership, equity interest, patent/licensing arrangement etc.) that might pose a conflict of interest in connection with the submitted article.

References

1. D'Orazio F, Splendiani A, Gallucci M. 320-Row Detector Dynamic 4D-CTA for the Assessment of Brain and Spinal Cord Vascular Shunting Malformations. A Technical Note. Neuroradiol J 2014; 27: 710-7.
2. Mazzei MA, Gentili F, Mazzei FG, et al. High-resolution MR lymphangiography for planning lymphaticovenous anastomosis treatment: a single-centre experience. Radiol Med 2017; 122: 918-27.
3. Carrafiello G, Lagana D, Recaldini C, et al. Comparison of contrast-enhanced ultrasound and computed tomography in classifying endoleaks after endovascular treatment of abdominal aorta aneurysms: preliminary experience. Cardiovasc Intervent Radiol 2006; 29: 969-74.
4. Gatta G, Parlato V, Di Grezia G, et al. Ultrasound-guided aspiration and ethanol sclerotherapy for treating endometrial cysts. Radiol Med 2010; 115: 1330-9.
5. Carrafiello G, Fontana F, Mangini M, et al. Initial experience with percutaneous biopsies of bone lesions using XperGuide cone-beam CT (CBCT): technical note. Radiol Med 2012; 117: 1386-97.
6. Perri M, Grattacaso G, di Tunno V, et al. T2 shine-through phenomena in diffusion-weighted MR imaging of lumbar discs after oxygen-ozone discolysis: a randomized, double blind trial with steroid and O2-O3 discolysis versus steroid only. Radiol Med 2015; 120: 941-50.
7. Belfiore G, Belfiore MP, Reginelli A, et al. Concurrent chemotherapy alone versus irreversible electroporation followed by chemotherapy on survival in patients with locally advanced pancreatic cancer. Med Oncol 2017; 34: 38.
8. Carrafiello G, Mangini M, Fontana F, et al. Suprarenal inferior vena cava filter implantation. Radiol Med 2012; 117: 1190-8.
9. Carrafiello G, Piffaretti G, Lagana D, et al. Endovascular

treatment of ruptured abdominal aortic aneurysms: aorto-uniiliac or bifurcated endograft? Radiol Med 2012; 117: 410-25.
10. Carrafiello G, D'Ambrosio A, Mangini M, et al. Percutaneous cholecystostomy as the sole treatment in critically ill and elderly patients. Radiol Med 2012; 117: 772-9.
11. Carrafiello G, Dionigi G, Ierardi AM, et al. Efficacy, safety and effectiveness of image-guided percutaneous microwave ablation in cystic renal lesions Bosniak III or IV after 24 months follow up. Int J Surg 2013; 11 Suppl 1: S30-5.
12. Barile A, Arrigoni F, Bruno F, et al. Present role and future perspectives of interventional radiology in the treatment of painful bone lesions. Future Oncol 2018; 14: 2945-55.
13. Belfiore MP, Reginelli A, Maggialetti N, et al. Preliminary results in unresectable cholangiocarcinoma treated by CT percutaneous irreversible electroporation: feasibility, safety and efficacy. Med Oncol 2020; 37: 45.
14. Detti B, Baki M, Becherini C, et al. High-dose intensitymodulated radiation therapy as primary treatment of prostate cancer: genitourinary/gastrointestinal toxicity and outcomes, a single-institution experience. Radiol Med 2019; 124: 422-31.
15. Consoli A, Grazzini G, Renieri L, et al. Effects of hyperearly (<12 hours) endovascular treatment of ruptured intracranial aneurysms on clinical outcome. Interv Neuroradiol 2013; 19: 195-202.
16. Barile A, Quarchioni S, Bruno F, et al. Interventional radiology of the thyroid gland: critical review and state of the art. Gland Surg 2018; 7: 132-46.
17. Masciocchi C, Arrigoni F, La Marra A, Mariani S, Zugaro L, Barile A. Treatment of focal benign lesions of the bone: MRgFUS and RFA. Br J Radiol 2016; 89: 20150356.
18. Zoccali C, Rossi B, Zoccali G, et al. A new technique for biopsy of soft tissue neoplasms: a preliminary experience using MRI to evaluate bleeding. Minerva Med 2015; 106: 117-20.
19. Arrigoni F, Gregori LM, Zugaro L, Barile A, Masciocchi C. MRgFUS in the treatment of MSK lesions: a review based on the experience of the University of L'Aquila, Italy. Translational Cancer Research 2014; 3: 442-48.
20. Tsetis D, Uberoi R, Fanelli F, et al. The Provision of Interventional Radiology Services in Europe: CIRSE Recommendations. Cardiovasc Intervent Radiol 2016; 39: 500-6.
21. Carnevale A, Pellegrino F, Cossu A, et al. Current concepts in ablative procedures for primary benign liver lesions: a step forward to minimize the invasiveness of treatment when deemed necessary. Med Oncol 2020; 37: 31.
22. Murphy TP, Soares GM. The evolution of interventional radiology. Semin Intervent Radiol 2005; 22: 6-9.
23. Chakraverty S, Flood K, Kessel D, et al. CIRSE guidelines: quality improvement guidelines for endovascular treatment of traumatic hemorrhage. Cardiovasc Intervent Radiol 2012; 35: 472-82.
24. Borgheresi A, Gonzalez-Aguirre A, Brown KT, et al. Does Enhancement or Perfusion on Preprocedure CT Predict Outcomes After Embolization of Hepatocellular Carcinoma? Acad Radiol 2018; 25: 1588-94.
25. Cornelis FH, Borgheresi A, Petre EN, Santos E, Solomon SB, Brown K. Hepatic Arterial Embolization Using Cone Beam CT with Tumor Feeding Vessel Detection Software: Impact on Hepatocellular Carcinoma Response. Cardiovasc Intervent Radiol 2018; 41: 104-11.
26. Masciocchi C, Arrigoni F, Ferrari F, et al. Uterine fibroid therapy using interventional radiology mini-invasive treatments: current perspective. Med Oncol 2017; 34: 52.
27. Arrigoni F, Bruno F, Zugaro L, et al. Developments in the management of bone metastases with interventional radiology. Acta Biomed 2018; 89: 166-74.
28. Angileri SA, Mailli L, Raspanti C, Ierardi AM, Carrafiello G, Belli AM. Prophylactic occlusion balloon placement in internal iliac arteries for the prevention of postpartum haemorrhage due to morbidly adherent placenta: short term outcomes. Radiol Med 2017; 122: 798-806.
29. Campobasso D, Marchioni M, Altieri V, et al. GreenLight Photoselective Vaporization of the Prostate: One Laser for Different Prostate Sizes. J Endourol 2020; 34: 54-62.
30. Castellani D, Cindolo L, De Nunzio C, et al. Comparison Between Thulium Laser VapoEnucleation and GreenLight Laser Photoselective Vaporization of the Prostate in Real-Life Setting: Propensity Score Analysis. Urology 2018; 121: 147-52.
31. Floridi C, Radaelli A, Pesapane F, et al. Clinical impact of cone beam computed tomography on iterative treatment planning during ultrasound-guided percutaneous ablation of liver malignancies. Med Oncol 2017; 34: 113.
32. Nicolini D, Agostini A, Montalti R, et al. Radiological response and inflammation scores predict tumour recurrence in patients treated with transarterial chemoembolization before liver transplantation. World J Gastroenterol 2017; 23: 3690-701.
33. Ierardi AM, Duka E, Lucchina N, et al. The role of interventional radiology in abdominopelvic trauma. Br J Radiol 2016; 89: 20150866.
34. Mangini M, Lagana D, Fontana F, et al. Use of Amplatzer Vascular Plug (AVP) in emergency embolisation: preliminary experience and review of literature. Emerg Radiol 2008; 15: 153-60.
35. Lagana D, Carrafiello G, Mangini M, et al. Indications for the use of the Amplatzer vascular plug in interventional radiology. Radiol Med 2008; 113: 707-18.
36. Quencer KB, Smith TA. Review of proximal splenic artery embolization in blunt abdominal trauma. CVIR Endovasc 2019; 2: 11.
37. Martin JG, Shah J, Robinson C, Dariushnia S. Evaluation and Management of Blunt Solid Organ Trauma. Tech Vasc Interv Radiol 2017; 20: 230-36.
38. Carrafiello G, Ierardi AM, Piacentino F, Cardim LN. Percutaneous transhepatic embolization of biliary leakage with N-butyl cyanoacrylate. Indian J Radiol Imaging 2012; 22: 19-22.
39. Ginat DT, Saad WE, Turba UC. Transcatheter renal artery embolization: clinical applications and techniques. Tech Vasc Interv Radiol 2009; 12: 224-39.

40. Ierardi AM, Floridi C, Fontana F, et al. Transcatheter embolisation of iatrogenic renal vascular injuries. Radiol Med 2014; 119: 261-8.
41. Jardinet T, Bonne L, Oyen R, Maleux G. Initial Experience With the Microvascular Plug in Selective Renal Artery Embolization. Vasc Endovascular Surg 2020; 54: 240-46.
42. Carrafiello G, Ierardi AM, Duka E, et al. Usefulness of Cone-Beam Computed Tomography and Automatic Vessel Detection Software in Emergency Transarterial Embolization. Cardiovasc Intervent Radiol 2016; 39: 530-7.
43. Ierardi AM, Piacentino F, Fontana F, et al. The role of endovascular treatment of pelvic fracture bleeding in emergency settings. Eur Radiol 2015; 25: 1854-64.
44. Barentsz MW, Vonken EP, van Herwaarden JA, Leenen LP, Mali WP, van den Bosch MA. Clinical outcome of intraarterial embolization for treatment of patients with pelvic trauma. Radiol Res Pract 2011; 2011: 935484.
45. Awwad A, Dhillon PS, Ramjas G, Habib SB, Al-Obaydi W. Trans-arterial embolisation (TAE) in haemorrhagic pelvic injury: review of management and mid-term outcome of a major trauma centre. CVIR Endovasc 2018; 1: 32.
46. Frevert S, Dahl B, Lonn L. Update on the roles of angiography and embolisation in pelvic fracture. Injury 2008; 39: 1290-4.
47. Travis T, Monsky WL, London J, et al. Evaluation of short-term and long-term complications after emergent internal iliac artery embolization in patients with pelvic trauma. J Vasc Interv Radiol 2008; 19: 840-7.
48. Ierardi AM, Urbano J, De Marchi G, et al. New advances in lower gastrointestinal bleeding management with embolotherapy. Br J Radiol 2016; 89: 20150934.
49. Urbano J, Manuel Cabrera J, Franco A, Alonso-Burgos A. Selective arterial embolization with ethylene-vinyl alcohol copolymer for control of massive lower gastrointestinal bleeding: feasibility and initial experience. J Vasc Interv Radiol 2014; 25: 839-46.
50. Venturini M, Lanza C, Marra P, et al. Transcatheter embolization with Squid, combined with other embolic agents or alone, in different abdominal diseases: a single-center experience in 30 patients. CVIR Endovasc 2019; 2: 8.
51. Woo S, Yoon CJ, Chung JW, et al. Bronchial artery embolization to control hemoptysis: comparison of N-butyl-2-cyanoacrylate and polyvinyl alcohol particles. Radiology 2013; 269: 594-602.
52. Izaaryene J, Vidal V, Bartoli JM, Gaubert JY. Multiple bronchial artery aneurysms: Successful treatment with ethylenevinyl alcohol copolymer (Onyx(R)). Diagn Interv Imaging 2016; 97: 125-7.
53. Madhusudhan KS, Venkatesh HA, Gamanagatti S, Garg P, Srivastava DN. Interventional Radiology in the Management of Visceral Artery Pseudoaneurysms: A Review of Techniques and Embolic Materials. Korean J Radiol 2016; 17: 351-63.
54. Loffroy R, Rao P, Ota S, et al. Packing technique for endovascular coil embolisation of peripheral arterial pseudoaneurysms with preservation of the parent artery: safety, efficacy and outcomes. Eur J Vasc Endovasc Surg 2010; 40: 209-15.
55. Briganti F, Leone G, Ugga L, et al. Mid-term and longterm follow-up of intracranial aneurysms treated by the p64 Flow Modulation Device: a multicenter experience. J Neurointerv Surg 2017; 9: 70-76.
56. Briganti F, Leone G, Ugga L, et al. Safety and efficacy of flow re-direction endoluminal device (FRED) in the treatment of cerebral aneurysms: a single center experience. Acta Neurochir (Wien) 2016; 158: 1745-55.
57. Hobo R, Sybrandy JE, Harris PL, Buth J, Collaborators E. Endovascular repair of abdominal aortic aneurysms with concomitant common iliac artery aneurysm: outcome analysis of the EUROSTAR Experience. J Endovasc Ther 2008; 15: 12-22.
58. Oderich GS, Ricotta JJ, 2nd. Novel surgeon-modified hypogastric branch stent graft to preserve pelvic perfusion. Ann Vasc Surg 2010; 24: 278-86.
59. Tang H, Tang X, Fu W, et al. Coil embolization of renal artery bifurcation and branch aneurysms with flow preservation. J Vasc Surg 2018; 68: 451-58 e2.
60. Jesinger RA, Thoreson AA, Lamba R. Abdominal and pelvic aneurysms and pseudoaneurysms: imaging review with clinical, radiologic, and treatment correlation. Radiographics 2013; 33: E71-96.
61. Ierardi AM, Petrillo M, Bacuzzi A, et al. Endovascular retreatment of a splenic artery aneurysm refilled by collateral branches of the left gastric artery: a case report. J Med Case Rep 2014; 8: 436.
62. Mandel SR, Jaques PF, Sanofsky S, Mauro MA. Nonoperative management of peripancreatic arterial aneurysms. A 10-year experience. Ann Surg 1987; 205: 126-8.
63. Loffroy R, Guiu B, Cercueil JP, et al. Transcatheter arterial embolization of splenic artery aneurysms and pseudoaneurysms: short- and long-term results. Ann Vasc Surg 2008; 22: 618-26.
64. Filippiadis DK, Binkert C, Pellerin O, Hoffmann RT, Krajina A, Pereira PL. Cirse Quality Assurance Document and Standards for Classification of Complications: The Cirse Classification System. Cardiovasc Intervent Radiol 2017; 40: 1141-46.
65. Ierardi AM, Pesapane F, Rivolta N, et al. Type 2 endoleaks in endovascular aortic repair: cone beam CT and automatic vessel detection to guide the embolization. Acta Radiol 2018; 59: 681-87.
66. Ptohis ND, Charalampopoulos G, Abou Ali AN, et al. Contemporary Role of Embolization of Solid Organ and Pelvic Injuries in Polytrauma Patients. Front Surg 2017; 4: 43.
67. Ekeh AP, Khalaf S, Ilyas S, Kauffman S, Walusimbi M, McCarthy MC. Complications arising from splenic artery embolization: a review of an 11-year experience. Am J Surg 2013; 205: 250-4; discussion 54.
68. Pesapane F, Nezami N, Patella F, Geschwind JF. New concepts in embolotherapy of HCC. Med Oncol 2017; 34: 58.
69. Ganguli S, Faintuch S, Salazar GM, Rabkin DJ. Postembolization syndrome: changes in white blood cell counts im-

mediately after uterine artery embolization. J Vasc Interv Radiol 2008; 19: 443-5.
70. Pesapane F, Leenknegt B, Ammar T, Panella S, Garzillo G, Huang DY. Intraoperative microvascular assessment with contrast-enhanced ultrasound (CEUS) during uterine artery embolisation (UAE): a case report and literature review. J Ultrasound 2020;

Received: 20 May 2020
Accepted: 10 June 2020
Correspondence:
Anna Maria Ierardi
Radiology Department, Fondazione IRCCS Cà Granda, Ospedale Maggiore Policlinico, Milan, Italy
Tel. +39 349 0897140
E-mail: amierardi@yahoo.it

Acta Biomed 2020; Vol. 91, Supplement 8: 81-88 DOI: 10.23750/abm.v91i8-S.9940 © Mattioli 1885

Review

Imaging guided percutaneous renal biopsy: do it or not?

Francesco Pagnini[1], Eleonora Cervi[1], Umberto Maestroni[2], Andrea Agostini[3,4], Alessandra Borgheresi[4], Filippo Piacentino[5], Salvatore Alessio Angileri[6], Anna Maria Ierardi[6], Chiara Floridi[3,4], Mattia Carbone[7], Francesco Ziglioli[2], Massimo De Filippo[1]

[1] Department of Medicine and Surgery, Unit of Radiology, University of Parma, Parma, Italy; [2] Department of Urology, Azienda Ospedaliero-Universitaria di Parma, University of Parma, Parma, Italy; [3] Department of Clinical, Special and Dental Sciences, University Politecnica delle Marche, Ancona, Italy; [4] Department of Radiology - Division of Special and Pediatric Radiology, University Hospital "Umberto I - Ancona, Italy; [5] Department of Diagnostic and Interventional Radiology, University of Insubria, Ospedale di Circolo e Fondazione Macchi, Varese, Italy; [6] Radiology Department, Fondazione IRCCS Ca' Granda Ospedale Maggiore Policlinico di Milano, Milan, Italy; [7] Department of Radiology, San Giovanni E Ruggi D'Aragona Hospital, Salerno, Italy.

Summary. Since its first reported application, renal biopsy became an important part of the diagnostic algorithm, considered advantages and risks, to better manage therapeutic options. The biopsy can be performed with different techniques (open, laparoscopic, transjugular, transurethral and percutaneous). Currently, the percutaneous approach is the modality of choice. Percutaneous biopsy can be performed under CT or US guidance, but critical benefits and disadvantages have to be considered. Core needle biopsy is usually preferred to fine-needle aspiration because of the sample quality, usually obtaining multiple cores, especially in heterogeneous tumors. Principal complications are hematuria (1-10%), perinephric hematoma (10-90%), pneumothorax (0,6%), clinically significant pain (1,2%). (www.actabiomedica.it)

Keywords: percutaneous renal biopsy, small renal mass, renal cell carcinoma, US-guided biopsy, CT-guided biopsy, coaxial technique.

Introduction

Interventional radiology techniques have been developed and used widely, becoming critical both for the diagnosis and therapeutic management of many diseases (1-15). The first renal biopsy approach was surgical, performed by Gwyn (16). More recently, different methods (open, laparoscopic, transjugular, transurethral, and percutaneous) (17, 18) and improvements have been made (19). Nowadays, the percutaneous approach (Percutaneous Renal Biopsy or PRB) is considered the modality of choice, but in case of failure or major contraindication, other methods could be preferred. The transjugular approach, even in consideration of its disadvantages, allows multiorgan biopsies during the same procedure, and it can be recommended in case of failure of PRB and in patients with severe coagulopathies since it gives the possibility to perform a selective embolization in case of bleeding. The transurethral biopsy may be considered in case of patients undergoing a cystoscopic examination and do not wish to undergo PRB separately, or when there is the suspected involvement of upper urinary tract.

Indications

The main indications to perform a renal biopsy, following nephrologists recommendation, are cases of idiopathic nephritic and nephrotic syndromes and the diagnosis of unknown primary lesions (20). Renal biopsy could also be useful in detecting acute or chronic renal allograft rejection (in presence of increasing serum creatinine levels) or in order to evaluate the response to antirejection therapy.

Timing and utility of the biopsy are still debated even in presence of an unknown primary lesion,

though the consensus on the need of tissue sampling if the management could be conditioned. Different theories explain the poor adoption of renal tumor biopsy as a standard of care for small renal masses (SRMs, size <4 cm), but none is well-supported by studies reported over the past years (21, 22). Safety, discordance with diagnosis after surgery, low diagnostic rates, and lack of perceived impact on clinical management are reported as the leading causes for the low consensus between specialists for practicing renal tumor biopsy (RTB) (23). Despite these concerns, the number of renal biopsies is grown thanks to the fact that procedural risks, such as tumor seeding and bleeding, have been reduced through improving the experience of operators and perfecting those techniques (24) (**fig 1**). Moreover, an international panel has recommended RTB before any ablative treatment (25).

Imaging methods

Accurate preprocedural imaging study is crucial for a proper diagnosis, preoperative planning, and postoperative follow-up (26-28). Though the application of MRI is growing in the field of interventional radiology, most procedures are performed under fluoroscopic, ultrasound, and CT imaging guidance (19, 29-39). Percutaneous biopsy can be performed under CT or US guidance, but critical benefits and disadvantages have to be considered. Ultrasonography has the advantages to offer a real-time view during needle placement, which allows to avoid vascular structures; furthermore, US is a low-cost technique and allows multiplanar imaging (40). However, US does not allow an accurate visualization of all renal mass, thus requiring contrast media administration (41).

CT is frequently used, with a step-and-shoot approach or as CT-fluoroscopy, allowing a better and less operator-dependent target detection. CT approach is characterized by high spatial resolution and a large field of view, enabling multiplanar reconstruction (MPR) to obtain an adequate visualization of the path of the needle (19) (**fig 2**). The main disadvantages are related to the more difficult positioning of the needle due to the patient's respiratory movement, as well as the side effects related to ionizing radiation.

The technique

There are two primary modalities for performing a percutaneous biopsy: fine-needle aspiration biopsy (FNAB) and core needle biopsy (CNB) (42, 43).

FNAB is a cytologic technique involving the use of a small needle (18-25G) equipped with an inner stylet. Once in the target, the stylet is removed, and a syringe is connected.

Individual cells for cytological evaluation could be obtained after creating a vacuum and moving gently and repeatedly back-and-forth the system.

CNB involves devices with larger needles (usually 16-18G) and different mechanisms to obtain the

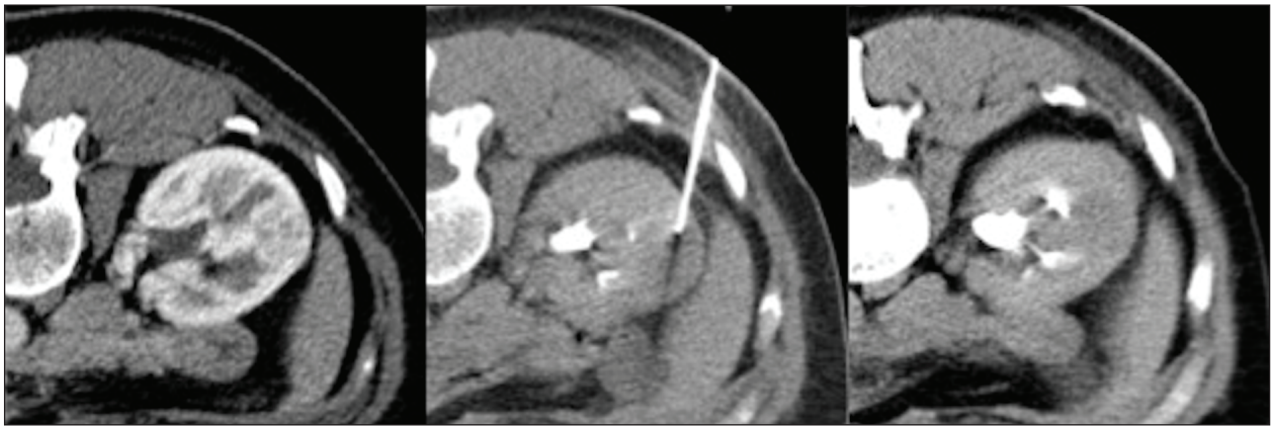

Figure 1. A core needle biopsy is performed on a single lesion in the para-hilar region of the right kidney. The lesion is in the proximity of important vascular and urinary system structures. The choice of a correct approach prevents post procedural complications such as bleeding and urinary tract lesions.

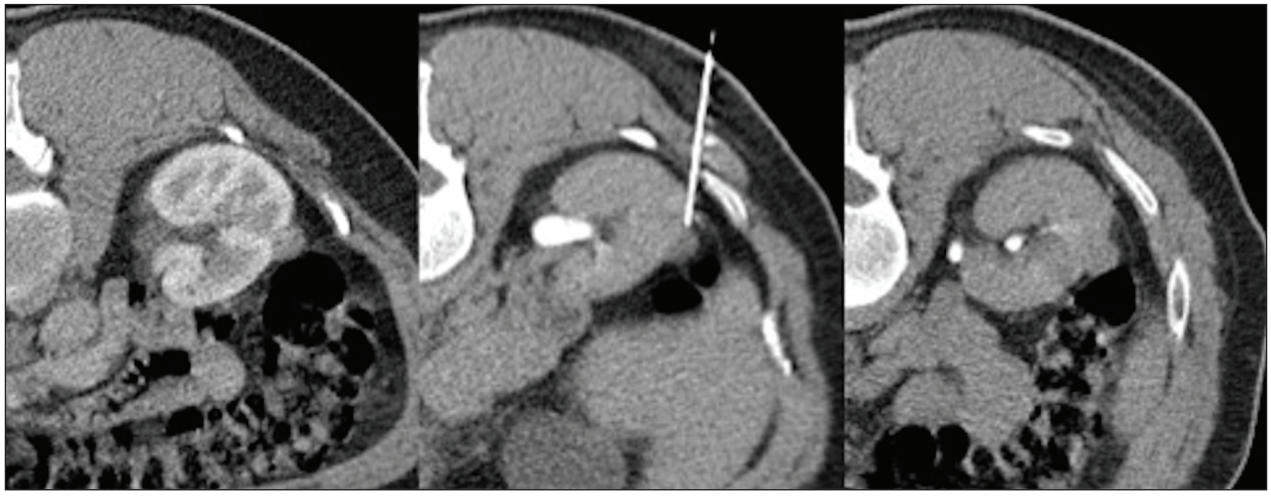

Figure 2. A single, small lesion at the middle third of the right kidney in the nearby of the ascending colon. Choosing the best approach, thanks to the large field of view and multiplanarity offered by CT, a fine needle aspiration biopsy is performed without any post-procedural complication.

specimen (manually or automatically cutting systems) (44). CNB is usually preferred to fine-needle aspiration (FNA) due to sample quality. Coaxial needle technique is a safe and proven technique consisting in the use of a guide needle (9-19G), previously advanced towards the target, in which the biopsy needle could be inserted to retrieve multiple specimens in a single puncture. Multiple cores allow a better assessment of tissue architecture and histologic subtype (22). Moreover, CNB does not increase the recurrence of complications and could decrease the tumor cells seeding risk along the needle path (45, 46). The sensitivity (97,5% - 99,7%) and specificity (96,2% - 99,1%), as reported in two large meta-analyses, are very high, allowing to consider RTB a highly accurate test in the detection of malignancy (47). When performing a percutaneous biopsy in nephritic or nephrotic syndrome, the target is usually the lower pole of the kidney. In lesions suspected for malignancy, the location should be chosen on the basis of the tumor size: in large tumors (>4cm), necrotic phenomena can occur, especially into the center of the lesion, making that site inappropriate for the sample quality (**fig 3**). In such lesions, to improve sensitivity and accuracy, a multi-quadrant technique is useful: obtaining multiple

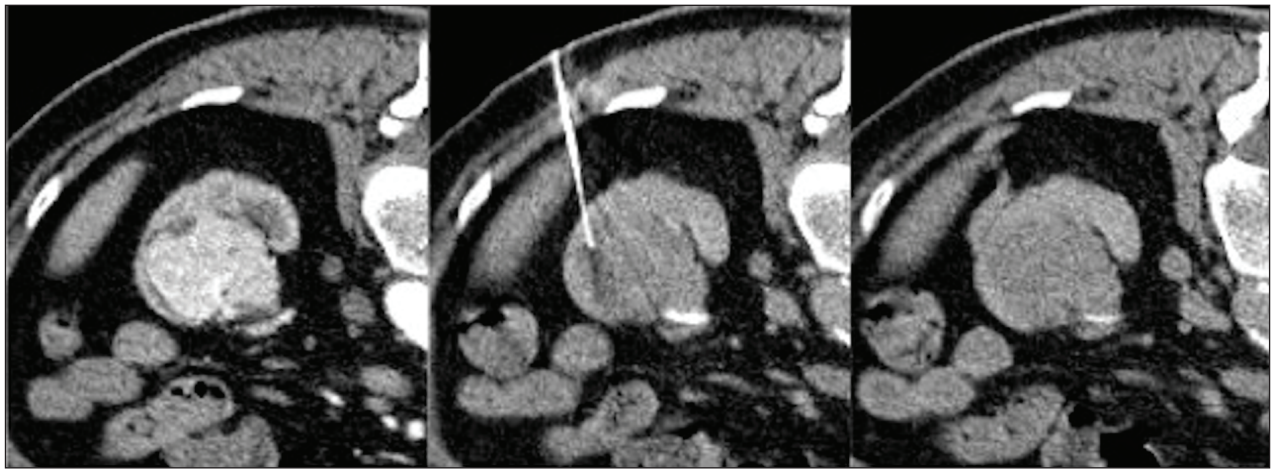

Fig 3. A large, hyperenhancing focal lesion at the lower third of the left kidney in the first scan (on the left). CT guided fine needle aspiration biopsy is performed with the patient in prone position. In such large lesions a peripheral approach is preferred in order to avoid the center of the lesion which could be necrotic and not useful for histologic characterization

cores from different areas within the tumor has proven to better detect aggressive pathologic futures as sarcomatoid dedifferentiation (48). In that cases, occurring usually in metastatic RCC with a poor life expectancy in the long-term (49-51), the biopsy has shown to have an important role in avoiding cytoreductive nephrectomy in patients who are unlikely to benefit and selecting different strategies as systemic therapy.

In large lesions, despite only 6,3% of masses higher than 7cm are not RCC-tumors, the biopsy could be essential in directing the appropriate treatment. E.g., lymphoma requires chemotherapeutical treatment instead of surgery (52), as large sarcomas need presurgical radiation (53). Although the benefit of retroperitoneal lymph node dissection (RPLND) for RCC is debatable (54), several studies reported high-risk features for lymph node metastases (55-57), pointing out the utility of RTB in the selection of patients with not-clinically-evident metastases who may benefit from aggressive surgery with RPLND.

Contraindications and complications

Reported absolute contraindications are severe uncontrolled hypertension, poor patient compliance to undergo the procedure, solitary kidney, and uncontrollable bleeding diathesis. Relative contraindications are renal morphologic abnormalities, urinary tract infections, severe azotemia, and coagulation disorders (58).

Principal complications include bleeding diathesis, consisting in hematuria (1-10%), perinephric hematoma (10-90%) to major bleeding requiring transfusion (0,3% - 7,4%) and nephrectomy (0,1%-0,5%) (**fig 4**). The risk is higher in cases of clotting disorders, thrombocytopenia, pharmacological treatment with anticoagulants or antiplatelets. According to the SIR-guidelines, renal biopsy is considered a high bleeding risk technique and appropriate preprocedural coagulation tests should be obtained (suggested laboratory value thresholds: correct INR to within range of 1.5–1.8 or less and consider platelet transfusion if platelet count is < 50 × 10^9/L) (59).

Other, less frequent complications are pneumothorax (0,6%), clinically significant pain (1,2%), infection and arteriovenous fistula. Tumor seeding is considered a fearsome complication but is very rare and reported only in a few cases (24,43,60-65),

Conclusions

Renal biopsy is a safe and effective technique in the majority of patients, useful in the diagnosis and management of certain medical conditions. Renal biopsy has a pivotal role in the algorithm of small renal masses (SMRs), avoiding unnecessary surgeries for benign disease and selecting appropriate candidates for focal ablation or active surveillance.

The biopsy is very useful for choosing the best management strategy, especially for SRMs, that is still based on the clinical setting of the patient and on histological characteristic of the lesion, selecting between

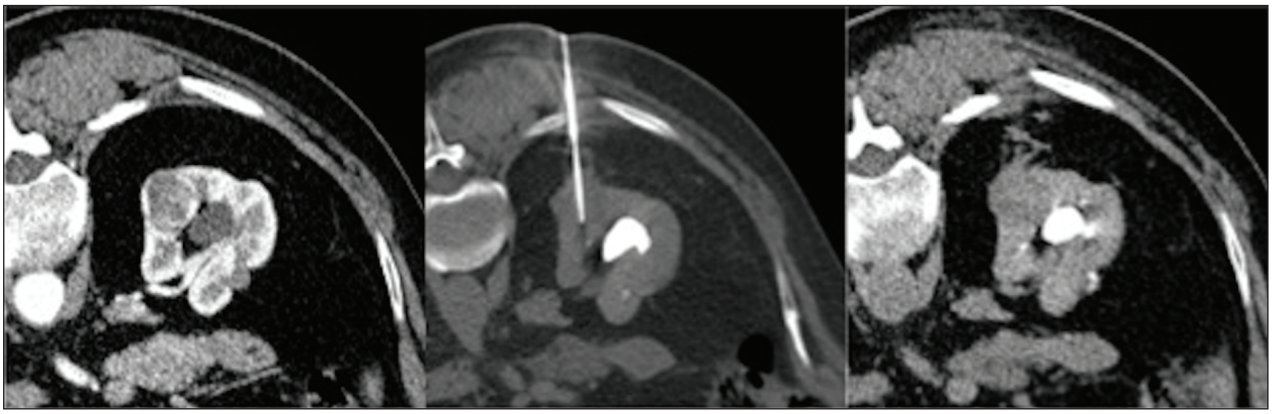

Fig 4. A core needle biopsy is performed on an exophytic lesion at the lower third of the right kidney; in the post-procedural scan (on the right) a minimal haematic suffusion of the pararenal tissue, along the needle path.

active surveillance, focal ablation, and surgical options. In tumors greater than 4cm and metastatic disease, the biopsy has a critical role in identifying patients that are unlikely to benefit from surgical operation or who may benefit from pre-nephrectomy systemic therapy, investigating the molecular and genetic information, and lymph node involvement in order to plan a different surgical approach, as the lymph node dissection.

Conflict of interest: Authors declare that they have no commercial associations (e.g. consultancies, stock ownership, equity interest, patent/licensing arrangement etc.) that might pose a conflict of interest in connection with the submitted article.

References

1. D'Amico G, Di Crescenzo V, Muto M, et al. [Cytological diagnosis of lymph nodes by instrumental guide: ultrasonography and CT]. Recenti Prog Med 2013; 104: 367-70.
2. Carrafiello G, Fontana F, Cotta E, et al. Ultrasound-guided thermal radiofrequency ablation (RFA) as an adjunct to systemic chemotherapy for breast cancer liver metastases. Radiol Med 2011; 116: 1059-66.
3. Carrafiello G, Lagana D, Nosari AM, et al. Utility of computed tomography (CT) and of fine needle aspiration biopsy (FNAB) in early diagnosis of fungal pulmonary infections. Study of infections from filamentous fungi in haematologically immunodeficient patients. Radiol Med 2006; 111: 33-41.
4. Belfiore G, Belfiore MP, Reginelli A, et al. Concurrent chemotherapy alone versus irreversible electroporation followed by chemotherapy on survival in patients with locally advanced pancreatic cancer. Med Oncol 2017; 34: 38.
5. Barile A, Quarchioni S, Bruno F, et al. Interventional radiology of the thyroid gland: critical review and state of the art. Gland Surg 2018; 7: 132-46.
6. Masciocchi C, Arrigoni F, La Marra A, Mariani S, Zugaro L, Barile A. Treatment of focal benign lesions of the bone: MRgFUS and RFA. Br J Radiol 2016; 89: 20150356.
7. Zoccali C, Rossi B, Zoccali G, et al. A new technique for biopsy of soft tissue neoplasms: a preliminary experience using MRI to evaluate bleeding. Minerva Med 2015; 106: 117-20.
8. Arrigoni F, Bruno F, Zugaro L, et al. Developments in the management of bone metastases with interventional radiology. Acta Biomed 2018; 89: 166-74.
9. Arrigoni F, Gregori LM, Zugaro L, Barile A, Masciocchi C. MRgFUS in the treatment of MSK lesions: a review based on the experience of the University of L'Aquila, Italy. Translational Cancer Research 2014; 3: 442-48.
10. Campobasso D, Marchioni M, Altieri V, et al. GreenLight Photoselective Vaporization of the Prostate: One Laser for Different Prostate Sizes. J Endourol 2020; 34: 54-62.
11. Castellani D, Cindolo L, De Nunzio C, et al. Comparison Between Thulium Laser VapoEnucleation and GreenLight Laser Photoselective Vaporization of the Prostate in Real-Life Setting: Propensity Score Analysis. Urology 2018; 121: 147-52.
12. Pavan N, Autorino R, Lee H, et al. Impact of novel techniques on minimally invasive adrenal surgery: trends and outcomes from a contemporary international large series in urology. World J Urol 2016; 34: 1473-9.
13. Greco F, Pini G, Alba S, Altieri VM, Verze P, Mirone V. Minilaparoendoscopic Single-site Pyeloplasty: The Best Compromise Between Surgeon's Ergonomy and Patient's Cosmesis (IDEAL Phase 2a). Eur Urol Focus 2016; 2: 319-26.
14. Floridi C, Radaelli A, Pesapane F, et al. Clinical impact of cone beam computed tomography on iterative treatment planning during ultrasound-guided percutaneous ablation of liver malignancies. Med Oncol 2017; 34: 113.
15. Nicolini D, Agostini A, Montalti R, et al. Radiological response and inflammation scores predict tumour recurrence in patients treated with transarterial chemoembolization before liver transplantation. World J Gastroenterol 2017; 23: 3690- 701.
16. Gwyn NB. Biopsies and the Completion of certain Surgical Procedures. Can Med Assoc J 1923; 13: 820-3.
17. Zhuo L, Wang H, Chen D, Lu H, Zou G, Li W. Alternative renal biopsies: past and present. Int Urol Nephrol 2018; 50: 475-79.
18. Carrafiello G, Fontana F, Mangini M, et al. Upper urinary tract biopsy: an old device for a new approach. Radiol Med 2012; 117: 1152-60.
19. Bevilacqua A, D'Amuri FV, Pagnini F, et al. Percutaneous needle biopsy of retroperitoneal lesions: technical developments. Acta Biomed 2019; 90: 62-67.
20. Bandari J, Fuller TW, Turner capital I UiURM, D'Agostino LA. Renal biopsy for medical renal disease: indications and contraindications. Can J Urol 2016; 23: 8121-6.
21. Marconi L, Dabestani S, Lam TB, et al. Systematic Review and Meta-analysis of Diagnostic Accuracy of Percutaneous Renal Tumour Biopsy. Eur Urol 2016; 69: 660-73.
22. Richard PO, Jewett MA, Bhatt JR, et al. Renal Tumor Biopsy for Small Renal Masses: A Single-center 13-year Experience. Eur Urol 2015; 68: 1007-13.
23. Richard PO, Martin L, Lavallee LT, et al. Identifying the use and barriers to the adoption of renal tumour biopsy in the management of small renal masses. Can Urol Assoc J 2018; 12: 260-66.
24. Volpe A, Finelli A, Gill IS, et al. Rationale for percutaneous biopsy and histologic characterisation of renal tumours. Eur Urol 2012; 62: 491-504.
25. Tsivian M, Rampersaud EN, Jr., del Pilar Laguna Pes M, et al. Small renal mass biopsy--how, what and when: report from an international consensus panel. BJU Int 2014; 113: 854-63.
26. Cortellini A, Bozzetti F, Palumbo P, et al. Weighing the role of skeletal muscle mass and muscle density in cancer

patients receiving PD-1/PD-L1 checkpoint inhibitors: a multicenter real-life study. Sci Rep 2020; 10: 1456.
27. Agliata G, Schicchi N, Agostini A, et al. Radiation exposure related to cardiovascular CT examination: comparison between conventional 64-MDCT and third-generation dualsource MDCT. Radiol Med 2019; 124: 753-61.
28. Agostini A, Mari A, Lanza C, et al. Trends in radiation dose and image quality for pediatric patients with a multidetector CT and a third-generation dual-source dual-energy CT. Radiol Med 2019; 124: 745-52.
29. Barile A, Arrigoni F, Bruno F, et al. Present role and future perspectives of interventional radiology in the treatment of painful bone lesions. Future Oncol 2018; 14: 2945-55.
30. Carrafiello G, Lagana D, Pellegrino C, et al. Ablation of painful metastatic bone tumors: a systematic review. Int J Surg 2008; 6 Suppl 1: S47-52.
31. Carrafiello G, Fontana F, Pellegrino C, et al. Radiofrequency ablation of abdominal wall endometrioma. Cardiovasc Intervent Radiol 2009; 32: 1300-3.
32. Arrigoni F, Napoli A, Bazzocchi A, et al. Magnetic-resonance- guided focused ultrasound treatment of non-spinal osteoid osteoma in children: multicentre experience. Pediatr Radiol 2019; 49: 1209-16.
33. Pagnini F, D'Amuri FV, Bevilacqua A, et al. Ultrasound-guided percutaneous irrigation of calcific tendinopathy: technical developments. Acta Biomed 2019; 90: 95-100.
34. Carrafiello G, Mangini M, Fontana F, et al. Microwave ablation of lung tumours: single-centre preliminary experience. Radiol Med 2014; 119: 75-82.
35. Carrafiello G, Ierardi AM, Duka E, et al. Usefulness of Cone- Beam Computed Tomography and Automatic Vessel Detection Software in Emergency Transarterial Embolization. Cardiovasc Intervent Radiol 2016; 39: 530-7.
36. Lagana D, Carrafiello G, Mangini M, et al. Indications for the use of the Amplatzer vascular plug in interventional radiology. Radiol Med 2008; 113: 707-18.
37. Mangini M, Lagana D, Fontana F, et al. Use of Amplatzer Vascular Plug (AVP) in emergency embolisation: preliminary experience and review of literature. Emerg Radiol 2008; 15: 153-60.
38. Cornelis FH, Borgheresi A, Petre EN, Santos E, Solomon SB, Brown K. Hepatic Arterial Embolization Using Cone Beam CT with Tumor Feeding Vessel Detection Software: Impact on Hepatocellular Carcinoma Response. Cardiovasc Intervent Radiol 2018; 41: 104-11.
39. Masciocchi C, Arrigoni F, Ferrari F, et al. Uterine fibroid therapy using interventional radiology mini-invasive treatments: current perspective. Med Oncol 2017; 34: 52.
40. Uppot RN, Harisinghani MG, Gervais DA. Imaging-guided percutaneous renal biopsy: rationale and approach. AJR Am J Roentgenol 2010; 194: 1443-9.
41. Israel GM, Bosniak MA. Pitfalls in renal mass evaluation and how to avoid them. Radiographics 2008; 28: 1325-38.
42. Gupta P, Rajwanshi A, Nijhawan R, et al. Fine needle aspiration in retroperitoneal lesions. APMIS 2017; 125: 16-23.
43. Tomozawa Y, Inaba Y, Yamaura H, et al. Clinical value of CT-guided needle biopsy for retroperitoneal lesions. Korean J Radiol 2011; 12: 351-7.
44. Misra RK, Mitra S, Jain RK, Vahikar S, Bundela A, Misra P. Image-guided fine needle cytology with aspiration versus non-aspiration in retroperitoneal masses: is aspiration necessary? J Pathol Transl Med 2015; 49: 129-35.
45. De Filippo M, Saba L, Rossi E, et al. Curved Needles in CT-Guided Fine Needle Biopsies of Abdominal and Retroperitoneal Small Lesions. Cardiovasc Intervent Radiol 2015; 38: 1611-6.
46. Pedote P, Gaudio F, Moschetta M, Cimmino A, Specchia G, Angelelli G. CT-guided needle biopsy performed with modified coaxial technique in the diagnosis of malignant lymphomas. Radiol Med 2010; 115: 1292-303.
47. Patel HD, Johnson MH, Pierorazio PM, et al. Diagnostic Accuracy and Risks of Biopsy in the Diagnosis of a Renal Mass Suspicious for Localized Renal Cell Carcinoma: Systematic Review of the Literature. J Urol 2016; 195: 1340-47.
48. Abel EJ, Heckman JE, Hinshaw L, et al. Multi-Quadrant Biopsy Technique Improves Diagnostic Ability in Large Heterogeneous Renal Masses. J Urol 2015; 194: 886-91.
49. Kyriakopoulos CE, Chittoria N, Choueiri TK, et al. Outcome of patients with metastatic sarcomatoid renal cell carcinoma: results from the International Metastatic Renal Cell Carcinoma Database Consortium. Clin Genitourin Cancer 2015; 13: e79-85.
50. Shuch B, Said J, La Rochelle JC, et al. Cytoreductive nephrectomy for kidney cancer with sarcomatoid histology--is up-front resection indicated and, if not, is it avoidable? J Urol 2009; 182: 2164-71.
51. Kassouf W, Sanchez-Ortiz R, Tamboli P, et al. Cytoreductive nephrectomy for metastatic renal cell carcinoma with nonclear cell histology. J Urol 2007; 178: 1896-900.
52. Kose F, Sakalli H, Mertsoylu H, et al. Primary renal lymphoma: report of four cases. Onkologie 2009; 32: 200-2.
53. Baldini EH, Wang D, Haas RL, et al. Treatment Guidelines for Preoperative Radiation Therapy for Retroperitoneal Sarcoma: Preliminary Consensus of an International Expert Panel. Int J Radiat Oncol Biol Phys 2015; 92: 602-12.
54. Barrisford GW, Gershman B, Blute ML, Sr. The role of lymphadenectomy in the management of renal cell carcinoma. World J Urol 2014; 32: 643-9.
55. Blute ML, Leibovich BC, Cheville JC, Lohse CM, Zincke H. A protocol for performing extended lymph node dissection using primary tumor pathological features for patients treated with radical nephrectomy for clear cell renal cell carcinoma. J Urol 2004; 172: 465-9.
56. Crispen PL, Breau RH, Allmer C, et al. Lymph node dissection at the time of radical nephrectomy for high-risk clear cell renal cell carcinoma: indications and recommendations for surgical templates. Eur Urol 2011; 59: 18-23.
57. Capitanio U, Suardi N, Matloob R, et al. Extent of lymph node dissection at nephrectomy affects cancer-specific survival and metastatic progression in specific sub-categories of patients with renal cell carcinoma (RCC). BJU Int 2014; 114: 210-5.

58. Clinical competence in percutaneous renal biopsy. Health and Public Policy Committee. American College of Physicians. Ann Intern Med 1988; 108: 301-3.
59. Patel IJ, Rahim S, Davidson JC, et al. Society of Interventional Radiology Consensus Guidelines for the Periprocedural Management of Thrombotic and Bleeding Risk in Patients Undergoing Percutaneous Image-Guided Interventions-Part II: Recommendations: Endorsed by the Canadian Association for Interventional Radiology and the Cardiovascular and Interventional Radiological Society of Europe. J Vasc Interv Radiol 2019; 30: 1168-84 e1.
60. Tomaszewski JJ, Uzzo RG, Smaldone MC. Heterogeneity and renal mass biopsy: a review of its role and reliability. Cancer Biol Med 2014; 11: 162-72.
61. De Filippo M, Bozzetti F, Martora R, et al. Radiofrequency thermal ablation of renal tumors. Radiol Med 2014; 119: 499-511.
62. De Filippo M, Saba L, Concari G, et al. Predictive factors of diagnostic accuracy of CT-guided transthoracic fine-needle aspiration for solid noncalcified, subsolid and mixed pulmonary nodules. Radiol Med 2013; 118: 1071-81.
63. De Filippo M, Saba L, Silva M, et al. CT-guided biopsy of pulmonary nodules: is pulmonary hemorrhage a complication or an advantage? Diagn Interv Radiol 2014; 20: 421-5.
64. De Filippo M, Gira F, Corradi D, Sverzellati N, Zompatori M, Rossi C. Benefits of 3D technique in guiding percutaneous retroperitoneal biopsies. Radiol Med 2011; 116: 407-16.
65. Blute ML, Jr., Drewry A, Abel EJ. Percutaneous biopsy for risk stratification of renal masses. Ther Adv Urol 2015; 7: 265-74.

Received: 20 May 2020
Accepted: 10 June 2020
Correspondence:
Massimo De Filippo
Department of Medicine and Surgery (DiMec),
Section of Radiology, University of Parma,
Maggiore Hospital, Parma, Italy
Via Gramsci 14, 43126, Parma, Italy
E-mail: massimo.defilippo@unipr.it

Acta Biomed 2020; Vol. 91, Supplement 8: 89-87 DOI: 10.23750/abm.v91i8-S.9975 © Mattioli 1885

Review

Predictive factors of volumetric reduction in lumbar disc herniation treated by O_2-O_3 chemiodiscolysis

Alberto Negro[1,2], Aldo Paolucci[3], Camilla Russo[4], Martina Di Stasi[4], Pasquale Guerriero[5], Francesco Arrigoni[6], Federico Bruno[6], Francesco Pagnini[7], Salvatore Alessio Angileri[8], Pierpaolo Palumbo[6], Carlo Masciocchi[6], Gianfranco Puoti[9], Fabio Tortora[4], Ferdinando Caranci[10]

[1] Ospedale del Mare – ASL NA1, Neuroradiology Unit, Naples, Italy; [2] Dipartimento di Scienze Mediche, Chirurgiche, Neurologiche, Metaboliche e dell'invecchiamento, University of Campania "Luigi Vanvitelli", Naples, Italy; [3] Ospedale Maggiore Policlinico Milano, Milan, Italy; [4] Advanced Biomedical Sciences Department University of Naples "Federico II", Napoli, Italy; [5] Department of Medicine and Health Sciences "V. Tiberio", University of Molise, Campobasso, Italy; [6] Department of Biotechnology and Applied Clinical Sciences, University of L'Aquila, L'Aquila, Italy; [7] Department of Medicine and Surgery, Unit of Radiology, University of Parma, Parma, Italy; [8] Operative Unit of Radiology, Fondazione IRCCS Ca' Granda Ospedale Maggiore Policlinico di Milano, Milan University, Via Francesco Sforza, 35, 20122, Milan, Italy; [9] Second Division of Neurology. Department of Advanced Medical and Surgical Sciences, Universityof Campania "Luigi Vanvitelli", Naples, Italy; [10] Department of Precision Medicine, University of Campania Luigi Vanvitelli, Naples, Italy

Summary. *Purpose:* Aim of this study is to assess the effectiveness of O_2-O_3 percutaneous chemiodiscolysis by evaluating volumetric changes in lumbar disc herniation on magnetic resonance imaging, in order to identify possible pre-treatment factors affecting such changes *Methods:* Between January 2014 and December 2017, a total of 87 patients with low back pain and 103 lumbar disc herniations with MRI confirmation were considered for O_2-O_3 chemiodiscolysis. The volume of each herniated disc was determined before and after the treatment. *Results:* Multiple linear regression analysis showed a strong correlation between post-treatment LDH volume percent change and both pre-treatment LDH volume and pre-treatment EQ-VAS (p<0.05), while age showed only a weak positive correlation with post-treatment LDH volume percent change (p<0.1). No association was found for other factors, such as sex and herniation disc level. *Conclusions:* In conclusion, age, baseline LDH volume and self-assessed disease severity score could represent three easy accessible outcome predictive parameters to consider when intradiscal O_2-O_3 chemiodiscolysis is envisaged. Better results after intradiscal O_2-O_3 chemiodiscolysis were obtained in older patients with higher pre-treatment LDH volume and low-moderate pre-treatment EQ-VAS. (www.actabiomedica.it)

Keywords: Lumbar Disc Herniation, Magnetic Resonance Imaging, Chemiodiscolysis, Minimally Invasive Surgery, Oxygen-Ozone Therapy

Abbreviations

Lumbar Disc Herniation = LDH; Magnetic Resonance Imaging = MRI; EuroQol Visual Analogue Scale = EQ-VAS; Cross Sectional Area = CSA; Diffusion-Weighted Imaging = DWI; Apparent Diffusion Coefficient = ADC.

Introduction

Degenerative disease of the intervertebral disc presenting as symptomatic lumbar disc herniation represents one of the most frequent causes of low back pain and functional limitation in adult population, with variable onset (ranging from acute to chronic) and symptoms intensity . Magnetic resonance imag-

ing is one of the most largely used imaging tool in many diagnostic and interventional settings thanks to its intrinsic excellent soft tissue contrast and the absence of ionizing radiation compared to CT (1-9).

Despite disc herniation can resorb spontaneously and associated symptoms can be relieved by conservative therapy, indications for surgical approach should be considered in case of drug-resistant persistent pain. At present the most appropriate surgical choice remains unclear, with recent evidences suggesting that minimally invasive techniques can be adopted prior to invasive surgery. Among these techniques, percutaneous intradiscal ozone injection has successfully and safely been used, with encouraging results in different clinical trials on large and representative populations (10, 11). Indeed ozone, a gas normally present in the atmosphere, can be used in combination with oxygen (O_2-O_3) at low concentrations for chemiodiscolysis; its main indication is low back pain (independently from radicular pain) refractory to 4-6 weeks of conservative therapy, in absence of motor deficits. Percutaneous CT-guided intradiscal injection is performed with thin needle (18-22gauge), and it is usually complemented by peri-ganglionic injection of corticosteroids and anaesthetics (12). This combination ensures immediate pain relief and allows for ozone to display its beneficial effects, including reversion of local venous stasis, anti-inflammatory effect and anti-nociceptor analgesic activity. O_2-O_3 chemiodiscolysis is a cost-effective procedure, with low complication rate and the possibility of being repeated in the same patient without precluding recourse to different surgical techniques in case of failure. However, despite its many advantages, O_2-O_3 chemiodiscolysis still raises some concerns in patients' selection and outcome optimization. Aim of this study is to assess the effectiveness of O_2-O_3 percutaneous chemiodiscolysis by evaluating volumetric changes in lumbar disc herniation (LDH) on magnetic resonance imaging (MRI), in order to identify possible pre-treatment factors affecting such changes.

Materials and Methods

Patients' selection

Between January 2014 and December 2017 we prospectively recruited 146 patients (86 males, 58,9%; 60 females, 41,1%; mean age 54,6y, DS±13,9y, range 24–83y) with low back pain following a dermatomal distribution and MRI confirmation of single- or multiple-level LDH, who were considered for O_2-O_3 chemiodiscolysis; 14 patients presented with disc herniation at two levels, while 3 patients at three levels. Patients referred to our department for well-discriminated persistent dermatomal pain with positive Lasègue test. The inclusion criteria were: single- or multiple-level LDH at MRI examination; 3-months long conservative treatment failure; age >18y and <85y. Exclusion criteria were: significant structural deformity of the spine, severe vertebral osteoarthrosis, fractures or calcified hernias (13); neurological motor deficit or cauda equina syndrome; infectious, inflammatory or neoplastic bone lesions (14-16); former contraindications to undergo MRI examination; absolute contraindications to CT-guided procedure, including allergy to proposed drugs and pregnancy (17). The presence of bleeding disorders, glucose-6-phosphate dehydrogenase deficiency, hyperthyroidism, severe anaemia, myasthenia, recent myocardial infarction and history of mental disorders were considered relative contraindications, therefore evaluated on a case-by-case basis. Finally, 87 patients (48 males, 55,2%; 39 females, 44,8%; mean age 53,7y, DS±13,1y, range 24–83y) were eligible for chemiodiscolysis, and a total number of 103 LDH were considered for statistical purposes (L5 n=25; L4 n=56; L3 n=15; L2 n=7). Before minimally invasive treatment, each patient was asked to rate disease severity by using the self-reported EuroQol Visual Analogue Scale (EQ-VAS) for pain intensity measurement. After therapy, all patients undergone chemiodiscolysis performed a follow-up lumbar spine MRI examination within 6 months from treatment (mean interval 19,7w; DS±7,2w; range 10-29w). The study was formerly approved by local Institutional Board, and written informed consent was preliminarily obtained from each patient.

Intradiscal O_2-O_3 chemiodiscolysis

Intradiscal O_2-O_3 chemiodiscolysis is carried out in a one-day surgery regimen; preliminary CT examination is performed to identify the infiltration

point and measure the distance from the conjugate foramen. The patient is placed on the imaging bed in prone position, with a cushion to reduce the physiological lumbar lordosis. CT scans are focused on the level to be treated and the entry point is marked with demographic pencil; the needle is introduced with an angle of 45° from the skin plane under CT guidance. Treatment consisted of 15ml O_2-O_3 injection (concentration: 30μg/ml), partly injected directly into the herniated disc (3-4ml) and partly in the periradicular/paravertebral soft tissues (11-12ml); using the same needle, the procedure is concluded with intraforaminal injection of corticosteroid (1mL, 40mg methylprednisolone) and local anaesthetic (1mL, 0.5% marcaine). A final CT scan to check gas distribution was also performed in order to exclude possible complications.

MRI examination and volume changes assessment

Pre- and post-operative lumbar spine MRI examinations carried on a 1.5T scanner included a sagittal TSE-T2w sequence (TE=100ms; TR=3000ms; NA=3; FA=90; slice thickness=3mm; spacing between slices=0), along with other axial and sagittal conventional T1w and T2w sequences. Two experienced neuroradiologists in consensus, different from the ones of team that performed the chemiodiscolysis, provided LDH measurements on raw MRI images. Lateral insertion positions of LDH were defined as the points showing the greatest contrast between the structures, while intervertebral disc height was defined as the distance between the middle portions of each endplate at the level of the affected disc. The contained affected disc was defined as the material located in the intervertebral space behind the intervertebral height line; conversely, the outer disc herniation was included until its borders became visually indistinguishable. Disc signal intensity and type of disc herniation (protruded, contained, extruded, sequestered, free fragment and migrated disc herniation) were also considered. For both time-points (pre- and post-operative MRI examination), LDH volume was assessed by hand-drawing height and cross sectional area (CSA) of the herniated disc located between the lateral margins of the vertebral pedicles (18), and computed by using the OsiriX "Compute Volume Tool". An example of LDH measurements before and after intradiscal O_2-O_3 chemiodiscolysis is shown in **Figure 1**.

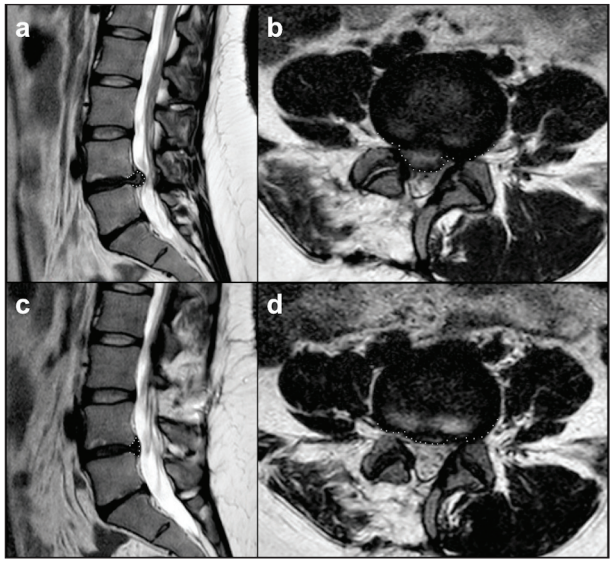

Figure 1 Sagittal and axial TSE-T2w MRI images on the most representative level, showing an example of LDH measurements before (**a-b**) and after (**c-d**) intradiscal O_2-O_3 chemiodiscolysis.

Statistical analysis

Multiple linear regression analysis was used to describe the relationship between LDH volume variation after intradiscal O_2-O_3 chemiodiscolysis and independent variables including age, sex, disc level, LDH volume at MRI diagnosis and pre-treatment self-assessed score of disease severity (EQ-VAS). To explain variation in treatment response that can be attributed to each explanatory variable, linear regression analysis was then applied; goodness of fit of regression was analysed using R^2 along with *p*-value. All statistical analysis was performed using XLSTAT software v.2019.1 (Addinsoft).

Results

LDH mean volume before treatment at baseline MRI examination was 0,58cm^3(DS±0,29cm^3), versus 0,43cm^3(DS±0,23cm^3) after treatment at MRI follow-up (mean variation -0,15±0,19; -20,4%, DS±44,6%); in 87,2% cases a reduction in LDH volumes was computed, in 10,9% cases there was a slight

increase in LDH size, while in the remaining 1,9% cases no significant variation was observed. Concerning self clinical assessment, mean EQ-VAS at baseline was 23,4 (DS±18,1), versus 59,2 (DS±25,1) after treatment (mean difference +35,7±30,9); 81,4% patients experiences an improvement in perception of disease severity, 9,7% patients complained a worsening in clinical symptoms, while the remaining 8,9% patients did not referred significant variation.

Multiple linear regression analysis showed a strong correlation between post-treatment LDH volume percent change and both pre-treatment LDH volume and pre-treatment EQ-VAS (p<0.05), while age showed only a weak positive correlation with post-treatment LDH volume percent change (p<0.1). Adjusted R^2 was 0.114 for the regression equation "Y= -0.112810 -0.392345X_1 +0.00580527X_2" (with Y=volume percent change; X_1= pre-treatment LDH volume; X_2= pre-treatment EQ-VAS). No correlation was found for sex and herniation disc level. Multiple linear regression analysis results are shown in **Table 1**. Linear correlation for bivariate data showed a significant negative correlation between post-treatment LDH volume percent change and pre-treatment LDH volume (p=0.013), as well as a significant positive correlation between post-treatment LDH volume percent change and pre-treatment EQ-VAS (p=0.021). Bivariate linear correlation analysis results are resumed in **Table 2**, and plotted in **Figure 2**.

Discussion

Back pain is one of the most common health problems affecting western population (19), and can be attributed to a wide range of disorders recognizing different aetiologies (8, 20-23). Among the possible aetiologies, LDH represents the most common cause (up to half cases of low back pain associated to sciatic symptoms are generated by disc herniation) (13, 16). The mechanism underlying low back radicular pain is multifactorial. Beyond the clinical evaluation, imaging plays a fundamental role in the initial assessment and cost-effective patient management; CT and MR imaging are considered the modality of choice, as in the study of other pathologies (24-34).

Indeed, LDH determine both variable direct compression of nerve root/dorsal root ganglion and indirect compression on perineural vessels, causing local venous stasis and ischemia. Moreover the injured herniated disc determines focal inflammation with subsequent involvement of facet capsule, epidural tissue surrounding nerve root and nerve root itself; the subsequent inflammatory cascade sensitizes neural no-

Table 1 Multiple linear regression analysis results of patients' variables (pre-treatment LDH volume, age and pre-treatment EQ-VAS, respectively) with post-treatment LDH volume percent change (p<0.05)

	Post-treatment LDH volume percent change			
Patients' variables	**b**	***p*-value**	**95% CI**	
		Lower limit	**Upper limit**	
Pre-treatment LDH volume	-0.394368	0.008 (p<0.05)	-0.682803	-0.105933
Age	-0.00551925	0.088 (p>0.05)	-0.0118802	0.000841720
Pre-treatment EQ-VAS	0.00526179	0.026 (p<0.05)	0.000651827	0.00987176

Legend: LDH=lumbar disc herniation; b=regression coefficient; CI=confidence interval; EQ-VAS=EuroQol Visual Analogue Scale.

Table 2 Bivariate linear correlation analysis results of patients' pre-treatment variables with post-treatment LDH volume percent change (p<0.05).

	Post-treatment LDH volume percent change		
Patients' variables	**r**	**R2**	***p*-value**
Pre-treatment LDH volume	-0.243	0.059	0.013
Age	-0.187	0.035	0.057
Pre-treatment EQ-VAS	0.226	0.051	0.021

Legend: LDH=lumbar disc herniation; r=correlation coefficient; R2=R-squared; EQ-VAS=EuroQol Visual Analogue Scale.

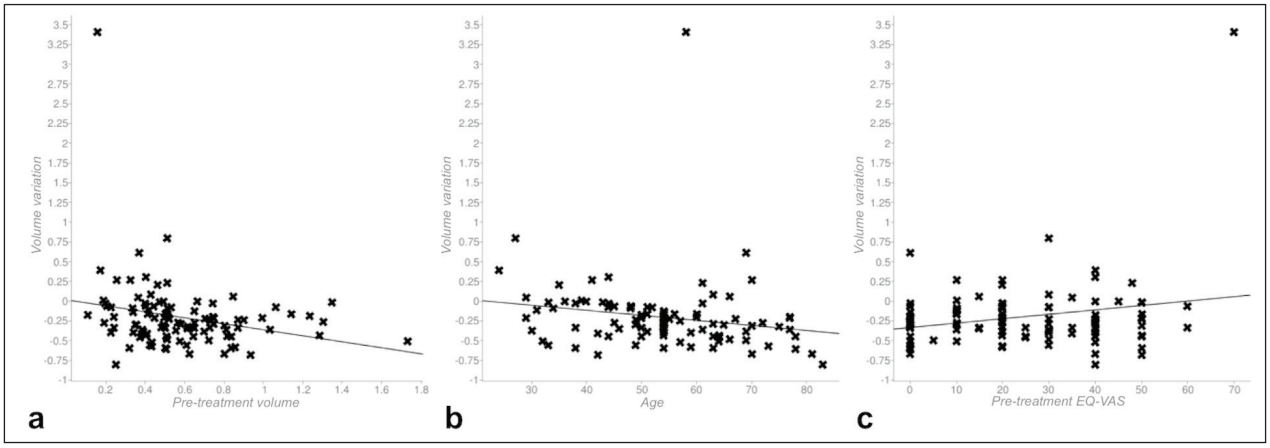

Figure 2 Bivariate linear correlation showing: (**a**) significant inverse correlation between post-treatment LDH volume percent change and pre-treatment LDH volume; (**b**) lack of significant association between post-treatment LDH volume percent change and patients' age; (**c**) significant positive correlation between post-treatment LDH volume percent change and pre-treatment EQ-VAS.

ciceptors and reduces pressure pain threshold (14, 16, 35).

LDH natural history is variable, and it is well known that disc herniation can resorb spontaneously and associated symptoms can be relieved by conservative therapy only (18). Therefore indications for surgical approach should be considered in case of drug-resistant persistent pain, when symptoms of LDH are refractory to initial conservative management (36, 37). However, before resorting to invasive surgery, minimally invasive approaches are often envisaged as a viable alternative to the more conventional open surgical techniques as they offer patients several benefits (including minor tissue trauma, reduced pain, and prompt recovery). Among these techniques, intradiscal O_2-O_3 chemiodiscolysis is one of the most used due to the beneficial antiseptic, immunomodulating, analgesic and anti-inflammatory ozone properties (38). However at present literature evidences from O_2-O_3 chemiodiscolysis compared to conventional surgical techniques are still controversial, with surgical treatment providing faster and greater relief from back pain in patients with LDH (despite no significant difference in results stability over time was observed at mid-term and long-term follow-up) (37). This variability in O_2-O_3 therapy outcome can be at least in part attributed to a challenging patient selection (39).

In this study we analysed potentially predictive factors of LDH volumetric reduction in order to improve patient selection and intradiscal O_2-O_3 chemiodiscolysis results, highlighting the possible role of age, baseline LDH volume and EQ-VAS score in predicting treatment outcome.

On the one hand, our results showed a strong correlation between post-treatment LDH volume percent change and both pre-treatment LDH volume and pre-treatment EQ-VAS (p<0.05). Inverse correlation between post-treatment LDH volume percent change and pre-treatment LDH volume suggest that O_2-O_3 chemiodiscolysis is more effective on larger disc herniation, probably when trans-ligamentous extension and posterior longitudinal ligament disruption makes unlikely an eventual spontaneous reduction (40). At the same time, positive correlation between post-treatment LDH volume percent change and pre-treatment EQ-VAS suggest that O_2-O_3 chemiodiscolysis should be preferred in case of mild clinical symptoms and moderate functional limitations, reserving more invasive approaches to patients with higher disease severity who experiment only limited benefits from minimally-invasive strategies. However it should always be considered that self-rating scales underlie some possible limitations regarding the interpretation of the results, which are mainly related to difficulties in determining how large a change in a certain score should be before it can be considered relevant for the patient.

On the other hand, age showed only a weak positive correlation with post-treatment LDH volume percent change (p<0.1). In recent times age was proposed as one of the factors influencing LDH resorption (41);

indeed herniated disc in older patients is supposed to be more fibrotic and dehydrated compared to the one of younger patients, negatively influencing spontaneous resorption. It is already known that, when considering acute disc herniation typical of younger patients, disc material is hyperintense on T2w sequences in more than 70% cases, with higher tendency to resolution (16). Conversely, when acute symptoms appear in a context of chronic disc herniation, inflammatory response is more involved as chronically damaged disc tissue elicits intense inflammatory changes when exposed to epidural fat/vasculature (42). According to this finding, in our sample the large majority of LDHs in older patients showed a low T2w-hyperintensity (presumably related to poor water content) (14, 15). Probably due to this difference, the LDH volume percent change after intradiscal O_2-O_3 chemiodiscolysis was more satisfying in older patients, where analgesic and anti-inflammatory ozone properties played a prominent role over direct disc dehydration.

Our experience further confirms the pivotal role of MRI in providing crucial data regarding pre-treatment patients' stratification based on LDH morphological features, thus not limiting this technique to simple diagnostic purposes. To this purpose recent evidences also suggested a possible role for diffusion-weighted imaging (DWI) and relative apparent diffusion coefficient (ADC) maps, already commonly used in different clinical settings to predict disease evolution and clinical outcome of various central nervous system disorders (43-45). In particular, LDH with lower ADC values were associated to poor improvement in clinical symptoms after O_2-O_3 chemiodiscolysis (30, 46). However DWI sequences were not available for our patients, therefore further studies are required to assess the possible role of pre-treatment ADC values for patients' selection. Some more limitations to the study should also be considered. First the results are referring to a 6-months long follow-up, and LDH volume reduction stability over time should be monitored on a mid/long-term follow-up; moreover, some additional risk factors that could somehow influence symptoms relapse (including for example weight fluctuations or work/professional activity) should also be considered in future analysis. Finally, it would be useful to assess the reproducibility of the presented results with different minimally invasive therapies other than intradiscal O_2-O_3 chemiodiscolysis**.**

In conclusion the flourishing of non-surgical therapeutic strategies for LDH should benefit of a more precise patients' selection based on clinical data and imaging features, in order to optimize treatment results. Age, baseline LDH volume and self-assessed disease severity score could represent three easy and rapidly accessible outcome predictive parameters to consider when intradiscal O_2-O_3 chemiodiscolysis is envisaged, with better outcome after intradiscal O_2-O_3 chemiodiscolysis in older patients with higher pre-treatment LDH volume and low-moderate pre-treatment EQ-VAS.

Conflict of interest: Authors declare that they have no commercial associations (e.g. consultancies, stock ownership, equity interest, patent/licensing arrangement etc.) that might pose a conflict of interest in connection with the submitted article.

References

1. Arrigoni F, Bruno F, Zugaro L, et al. Developments in the management of bone metastases with interventional radiology. Acta Biomed 2018; 89: 166-74.
2. Masciocchi C, Arrigoni F, La Marra A, Mariani S, Zugaro L, Barile A. Treatment of focal benign lesions of the bone: MRgFUS and RFA. The British journal of radiology 2016; 89: 20150356-56.
3. Tortora F, Cirillo M, Belfiore MP, et al. Spontaneous regression of dilated virchow-robin spaces. A case report. Neuroradiol J 2012; 25: 40-4.
4. Giordano AV, Arrigoni F, Bruno F, et al. Interventional Radiology Management of a Ruptured Lumbar Artery Pseudoaneurysm after Cryoablation and Vertebroplasty of a Lumbar Metastasis. Cardiovasc Intervent Radiol 2017; 40: 776-79.
5. Michelini G, Corridore A, Torlone S, et al. Dynamic MRI in the evaluation of the spine: state of the art. Acta Biomed 2018; 89: 89-101.
6. Cazzato RL, Arrigoni F, Boatta E, et al. Percutaneous management of bone metastases: state of the art, interventional strategies and joint position statement of the Italian College of MSK Radiology (ICoMSKR) and the Italian College of Interventional Radiology (ICIR). Radiol Med 2019; 124: 34-49.
7. Perri M, Grattacaso G, di Tunno V, et al. T2 shine-through phenomena in diffusion-weighted MR imaging of lumbar discs after oxygen-ozone discolysis: a randomized, double-blind trial with steroid and O2-O3 discolysis versus steroid only. Radiol Med 2015; 120: 941-50.

8. de Divitiis O, Elefante A. Cervical spinal brucellosis: a diagnostic and surgical challenge. World Neurosurg 2012; 78: 257-9.
9. Carrafiello G, Fontana F, Mangini M, et al. Initial experience with percutaneous biopsies of bone lesions using XperGuide cone-beam CT (CBCT): technical note. Radiol Med 2012; 117: 1386-97.
10. Giurazza F, Guarnieri G, Murphy KJ, Muto M. Intradiscal O2O3: Rationale, Injection Technique, Short- and Longterm Outcomes for the Treatment of Low Back Pain Due to Disc Herniation. Can Assoc Radiol J 2017; 68: 171-77.
11. Murphy K, Muto M, Steppan J, Meaders T, Boxley C. Treatment of Contained Herniated Lumbar Discs With Ozone and Corticosteroid: A Pilot Clinical Study. Can Assoc Radiol J 2015; 66: 377-84.
12. Shanthanna H, Busse JW, Thabane L, et al. Local anesthetic injections with or without steroid for chronic non-cancer pain: a protocol for a systematic review and meta-analysis of randomized controlled trials. Syst Rev 2016; 5: 18.
13. Kelsey JL, White AA, 3rd. Epidemiology and impact of low-back pain. Spine (Phila Pa 1976) 1980; 5: 133-42.
14. Bozzao A, Gallucci M, Masciocchi C, Aprile I, Barile A, Passariello R. Lumbar disk herniation: MR imaging assessment of natural history in patients treated without surgery. Radiology 1992; 185: 135-41.
15. Yasuma T, Arai K, Yamauchi Y. The histology of lumbar intervertebral disc herniation. The significance of small blood vessels in the extruded tissue. Spine (Phila Pa 1976) 1993; 18: 1761-5.
16. Matsubara Y, Kato F, Mimatsu K, Kajino G, Nakamura S, Nitta H. Serial changes on MRI in lumbar disc herniations treated conservatively. Neuroradiology 1995; 37: 378-83.
17. Teplick JG, Haskin ME. Spontaneous regression of herniated nucleus pulposus. AJR Am J Roentgenol 1985; 145: 371-5.
18. Seo JY, Roh YH, Kim YH, Ha KY. Three-dimensional analysis of volumetric changes in herniated discs of the lumbar spine: does spontaneous resorption of herniated discs always occur? Eur Spine J 2016; 25: 1393-402.
19. Patrick N, Emanski E, Knaub MA. Acute and chronic low back pain. Med Clin North Am 2014; 98: 777-89, xii.
20. Shah MK, Stewart GW. Sacral stress fractures: an unusual cause of low back pain in an athlete. Spine (Phila Pa 1976) 2002; 27: E104-8.
21. Demir MK, Yilmaz B, Toktas ZO, Akakin A, Eksi MS, Konya D. An unusual cause of low back pain in a young adult: myxopapillary ependymoma of the filum terminale. Spine J 2016; 16: e321-2.
22. Leon Salinas JP, Albertz Arevalo N, Belloch Ramos E, Guerrero Espejo A. An unusual cause of low back pain in a patient with sepsis. Enferm Infecc Microbiol Clin 2017; 35: 538-40.
23. Elefante A, Caranci F, Del Basso De Caro ML, et al. Paravertebral high cervical chordoma. A case report. Neuroradiol J 2013; 26: 227-32.
24. Bruno F, Arrigoni F, Palumbo P, et al. New advances in MRI diagnosis of degenerative osteoarthropathy of the peripheral joints. Radiol Med 2019; 124: 1121-27.
25. Arrigoni F, Napoli A, Bazzocchi A, et al. Magnetic-resonance- guided focused ultrasound treatment of non-spinal osteoid osteoma in children: multicentre experience. Pediatr Radiol 2019; 49: 1209-16.
26. Cortellini A, Bozzetti F, Palumbo P, et al. Weighing the role of skeletal muscle mass and muscle density in cancer patients receiving PD-1/PD-L1 checkpoint inhibitors: a multicenter real-life study. Sci Rep 2020; 10: 1456.
27. Carrafiello G, Lagana D, Pellegrino C, et al. Ablation of painful metastatic bone tumors: a systematic review. Int J Surg 2008; 6 Suppl 1: S47-52.
28. Reginelli A, Silvestro G, Fontanella G, et al. Validation of DWI in assessment of radiotreated bone metastases in elderly patients. International Journal of Surgery 2016; 33: S148-S53.
29. Splendiani A, D'Orazio F, Patriarca L, et al. Imaging of post-operative spine in intervertebral disc pathology. Musculoskelet Surg 2017; 101: 75-84.
30. Perri M, Grattacaso G, Di Tunno V, et al. MRI DWI/ADC signal predicts shrinkage of lumbar disc herniation after O2-O3 discolysis. Neuroradiol J 2015; 28: 198-204.
31. Bruno F, Smaldone F, Varrassi M, et al. MRI findings in lumbar spine following O2-O3 chemiodiscolysis: A longterm follow-up. Interv Neuroradiol 2017; 23: 444-50.
32. Patriarca L, Letteriello M, Di Cesare E, Barile A, Gallucci M, Splendiani A. Does evaluator experience have an impact on the diagnosis of lumbar spine instability in dynamic MRI? Interobserver agreement study. Neuroradiol J 2015; 28: 341-6.
33. Splendiani A, Bruno F, Patriarca L, et al. Thoracic spine trauma: advanced imaging modality. Radiol Med 2016; 121: 780-92.
34. Barile A, Arrigoni F, Bruno F, et al. Present role and future perspectives of interventional radiology in the treatment of painful bone lesions. Future Oncol 2018; 14: 2945-55.
35. Weinstein JN, Lurie JD, Tosteson TD, et al. Surgical vs nonoperative treatment for lumbar disk herniation: the Spine Patient Outcomes Research Trial (SPORT) observational cohort. JAMA 2006; 296: 2451-59.
36. Chen BL, Guo JB, Zhang HW, et al. Surgical versus nonoperative treatment for lumbar disc herniation: a systematic review and meta-analysis. Clin Rehabil 2018; 32: 146-60.
37. Gugliotta M, da Costa BR, Dabis E, et al. Surgical versus conservative treatment for lumbar disc herniation: a prospective cohort study. BMJ Open 2016; 6: e012938.
38. Boos N, Weissbach S, Rohrbach H, Weiler C, Spratt KF, Nerlich AG. Classification of age-related changes in lumbar intervertebral discs: 2002 Volvo Award in basic science. Spine (Phila Pa 1976) 2002; 27: 2631-44.
39. Dall'Olio M, Princiotta C, Cirillo L, et al. Oxygen-ozone therapy for herniated lumbar disc in patients with subacute partial motor weakness due to nerve root compression. Interv Neuroradiol 2014; 20: 547-54.

40. Ahn SH, Ahn MW, Byun WM. Effect of the transligamentous extension of lumbar disc herniations on their regression and the clinical outcome of sciatica. Spine (Phila Pa 1976) 2000; 25: 475-80.
41. Lee J, Kim J, Shin JS, et al. Long-Term Course to Lumbar Disc Resorption Patients and Predictive Factors Associated with Disc Resorption. Evid Based Complement Alternat Med 2017; 2017: 2147408.
42. Jinkins, Whittemore AR, Bradley WG. The anatomic basis of vertebrogenic pain and the autonomic syndrome associated with lumbar disk extrusion. American Journal of Roentgenology 1989; 152: 1277-89.
43. van Veluw SJ, Lauer A, Charidimou A, et al. Evolution of DWI lesions in cerebral amyloid angiopathy: Evidence for ischemia. Neurology 2017; 89: 2136-42.
44. Elefante A, Cavaliere M, Russo C, et al. Diffusion weighted MR imaging of primary and recurrent middle ear cholesteatoma: an assessment by readers with different expertise. Biomed Res Int 2015; 2015: 597896.
45. Rapalino O, Mullins ME. Intracranial Infectious and Inflammatory Diseases Presenting as Neurosurgical Pathologies. Neurosurgery 2017; 81: 10-28.
46. Niu X-K, Bhetuwal A, Yang H-F. Diffusion-Weighted Imaging for Pretreatment Evaluation and Prediction of Treatment Effect in Patients Undergoing CT-Guided Injection for Lumbar Disc Herniation. Korean journal of radiology 2015; 16: 874-80.

Received: 20 May 2020
Accepted: 10 June 2020
Correspondence:
Fabio Tortora, MD, Associate Professor
Advanced Biomedical Sciences Department
Università degli Studi di Napoli "Federico II"
Via Sergio Pansini 5 – 80131 Napoli
Tel. 0039 081 74623001
Office: +39 071 5964085
E-mail: fabio.tortora@unina.it

Acta Biomed 2020; Vol. 91, Supplement 8: 98-106 DOI: 10.23750/abm.v91i8-S.10007

Review

Advanced diagnostic imaging and intervention in tendon diseases

Federico Bruno[1], Pierpaolo Palumbo[1], Francesco Arrigoni[2], Silvia Mariani[2], Giacomo Aringhieri[3], Marina Carotti[4,5], Raffaele Natella[6], Marcello Zappia[7], Paola Cipriani[1], Roberto Giacomelli[1], Ernesto Di Cesare[8], Alessandra Splendiani[1], Carlo Masciocchi[1], Antonio Barile[1]

[1] Department of Biotechnology and Applied Clinical Sciences, University of L'Aquila, L'Aquila, Italy; [2] Emergency Radiology, San Salvatore Hospital, L'Aquila, Italy; [3] Diagnostic and Interventional Radiology, Department of Translational Research and of New Technologies in Medicine and Surgery, University of Pisa, Pisa, Italy; [4] Division of Special and Pediatric Radiology, Department of Radiology, University Hospital "Umberto I – Lancisi – Salesi", Ancona, AN, Italy; [5] Department of Clinical, Special and Dental Sciences, University Politecnica delle Marche, Ancona, AN, Italy; [6] Department of Precision Medicine, University of Campania "L. Vanvitelli", Naples, Italy; [7] Department of Medicine and Health Sciences, University of Molise, Campobasso, Italy; [8] Department of Life, Health and Environmental Sciences, University of L'Aquila, L'Aquila, Italy

Summary. Degenerative tendon pathology represents one of the most frequent and disabling musculoskeletal disorders. Diagnostic radiology plays a fundamental role in the clinical evaluation of tendon pathologies. Moreover, several minimally invasive treatments can be performed under imaging guidance to treat tendon disorders, maximizing the efficacy and reducing procedural complications. In this review article we describe the most relevant diagnostic features of conventional and advanced US and MRI imaging in tendon disorders, along with the main options for image-guided intervention. (www.actabiomedica.it)

Keywords: tendon, tendinosis, MRI, T2 mapping, ultrasound elastography

Introduction

Together with osteochondral (1-4) and synovial pathology (5-11), tendon pathology represents one of the main musculoskeletal disorders, with traumatic and - above all - degenerative pathology (12). Imaging plays a fundamental role in the clinical evaluation of tendon pathologies, as an accurate and timely diagnosis is crucial to allow the establishment of conservative measures, to reduce or delay the need for surgery (13-20). Moreover, several minimally invasive MSK interventional treatments can be performed under imaging guidance to maximize efficacy and reduce procedural complications (21,22).

This article aims to review the relevant diagnostic features of conventional and advanced imaging in tendon disorders – namely the degenerative pathology - and the main options for image-guided intervention.

Histology of tendon diseases and imaging correlates

Tendons are made up of dense fibrous connective tissue, mainly represented by multiple subunits of collagen fibers. This three-dimensional structure allows adequate transmission of mechanical force preventing damage and disruption of the fibers under stress. Tendons can be affected by different types of diseases that differ both macroscopically and microscopically (23).

Tendinosis, the main degenerative tendon alteration, is characterized histologically by collagen disorientation, fiber disorganization, and separation due to increased mucoid ground substance, increased cellularity and vascular spaces with or without neovascularization, focal necrosis, and calcifications (24). In more advanced stages, partial tendon rupture may show the superimposed presence of tears, including fibroblastic and myofibroblastic proliferation, hemorrhage, and

organizing granulation tissue. Together with degenerative changes, reactive inflammatory changes in the tendon sheaths and paratenonium (tendonitis/paratenonitis) are often associated (25).

MRI and ultrasound are potent tools for the assessment of tendon anatomy. The imaging appearance correlates with the histological tendon structure and the changes that occur during pathologic processes (26).

Thanks to its availability (27-29), low cost (30, 31), absence of ionizing radiation (32-35), and the ability to study superficial anatomical structures (36-39), ultrasound is often the first imaging method of approach to the evaluation of tendons. The ultrasound appearance of tendinopathy generally shows tendon thickening with loss of the normal fibrillar structure, and increased spacing of the hyperechoic fibrillar lines with reduced tendon echogenicity; calcifications may also be detected, usually near tendon insertion. Doppler study may also reveal the proliferation of neovessels and increased vascularization in case of inflammation. In severe tendinosis/partial rupture, anechoic fluid may be visible inside the tear in acute/subacute stages; in more chronic phases, the echogenicity may increase, making the differentiation with the tendon less evident. Dynamic imaging during muscle contraction or passive movement is often useful to unveil small tendon gaps. Doppler imaging may also be useful to distinguish small intrasubstance tears from vessels that have developed in the tendinopathic tendon. Regarding the localization, degenerative changes are more frequent in the midportion and areas of critical vascularization, while tendon anomalies in spondyloarthritis tend to be more closely related to fibrocartilaginous enthesis (40-42).

Being more panoramic (43, 44) and multiparametric (45-50), magnetic resonance imaging (MRI) is the other imaging modality of choice for the evaluation of tendon diseases, including tendinopathies. The tendon structure plays a critical role in determining the appearance in magnetic resonance imaging. The water and collagen in the tendon are aligned, reducing the T2 and T1 relaxation time. Along with tendon thickening, an increase in signal intensity in T2-weighted imaging sequences is often the first sign of tendon anomaly at MRI. Although the appearance of a complete or partial tear is variable, the main finding is the T2-hyperintense fluid signal at the tear site and in surrounding tissues; however, in late stages, intermediate signal scar tissue can obscure this finding. The fibroadipose involution of the myotendinous junction is another typical finding of chronic lesions (26, 34).

Advanced diagnostic imaging in tendon diseases

T2 mapping

As mentioned above, conventional MRI sequences can detect morphologic changes occurring in tendinopathy. However, the sensitivity and specificity of MRI to determine disease grading have proven to be variable with the evaluation of the signal intensity alone (35). Furthermore, the diagnosis and monitoring of post-surgical tendon healing remain primarily subjective. In recent years, advanced MRI sequences capable of identifying and showing structural and biochemical tissue changes have been implemented. Among them, T2 mapping was developed to exploit the sensitivity of magnetic resonance imaging to the biophysical properties of numerous tissues. In musculoskeletal pathology applications, T2 mapping demonstrated to be sensitive to structural and biochemical composition in the cartilage matrix (2). In particular, T2 relaxation time mapping correlates with the changes in collagen matrix integrity and cartilage water content that occur during the pathophysiology of degenerative osteoarthritis. Paralleling cartilage histology, biochemical and degenerative changes in tendons are related to proteoglycan loss and disorganization of the collagen matrix, which becomes less elastic, allowing increased mobility of water and consequentially increased levels of H_2O proton content; this leads to an increase of T2 relaxation values compared to normal levels. Both T2 and T2* mapping sequences can detect biochemical changes that occur in the early stage of tendinopathy, namely the change of collagen orientation, and the collagen and water content (35).

Although the experiences in literature are limited, focused mainly on Achilles and supraspinatus tendon, early evidence shows that T2 mapping values

are significantly higher in tendons tears, compared to tendinosis and healthy tendons (36). Some works also confirm the validity of this sequence in identifying and monitoring tendon healing after surgery (37). From our unpublished experience, T2 mapping sequences may also be valid for identifying changes in tendon structure after percutaneous minimally invasive tendon treatment, such as tendon needling and Platelet-rich-plasma injections (fig.1).

Sonoelastography

Elastography is an US method for quantitative imaging of the distribution of biological tissue strains and elasticity, that has been evaluated in various settings in clinical radiology as a reliable and useful complementary modality to conventional ultrasound in the evaluation of lesions in the liver, spleen, breast, thyroid, and prostate (38).

Over the past years, the number of studies on elastography in tendon pathologies has risen considerably, and several studies in vitro and in vivo have tried to provide answers regarding the normal and pathologic biomechanical and structural properties of tendons (39). However, they have also aimed to assess the reliability of elastography and the prospects offered by this technique in daily clinical practice. There are several techniques of elastosonography, the most used being:

- *Quasi-static elastography (QSE)*. The operator exerts, through the US probe handheld compression, slow mechanical stress (strain) on tissues that induce tissue displacement. Comparing the position of the structures at rest and under compression, the displacement generated by the stress can be estimated. The degree

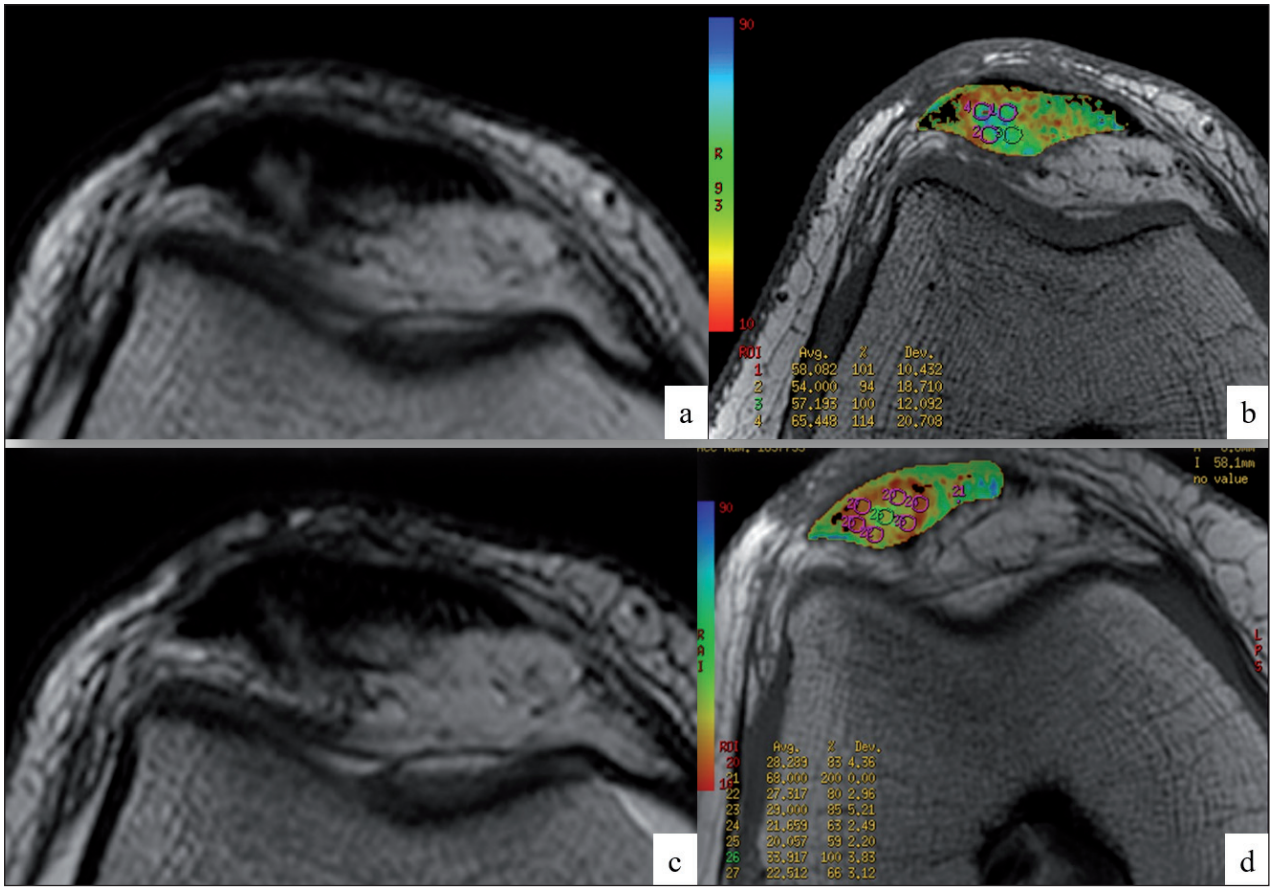

Figure 1. Axial images of standard T2 (a, c) and T2 mapping (b, d) sequences in a patellar tendon, before (a, b) and six months after (c, d) percutaneous US-guided intratendinous PRP injection treatment. Note the reduction of mean T2 relaxation values of circular ROIs within the most tendinopathic area (visible as a hyperintense intrasubstance alteration on standard imaging) after treatment, consistent with signs of tendon healing

of stiffness is represented in a color scale that identifies the "softest" and "hardest" tissue areas (38, 40).

- *Shear wave elastography (SWE)*. By generating several near-simultaneous pushes moved through the medium at supersonic speed, the device creates high-intensity shear waves that move through the medium transversely relative to the initial radiation force. Shear waves cause particulate moves recorded with high-frequency imaging (5000 to 30,000 Hz), from which the system calculates color elastograms in real-time (quantitative analysis) (41).

The literature on the application of elastosonography to the study of tendons has been focused mainly on the Achilles tendon in most studies (fig. 2). In QSE, the strain ratio (tendon/Kager's fat) was found to be higher and the tendon softer in case of tendinopathy, when compared to healthy subjects. QSE could also be a reliable tool in monitoring Achilles tendon after surgical repair: one research revealed that after percutaneous tenorrhaphy, tendons tend to stiffen progressively for at least a year, reflecting the abnormal collagen composition during scar formation. QSE was also used to detect small partial tears of the supraspinatus tendon (fig.3) and to evaluate structural and biomechanical changes of the Achilles tendon in metabolic diseases such as diabetes, acromegaly, severe renal insufficiency (38, 42, 43).

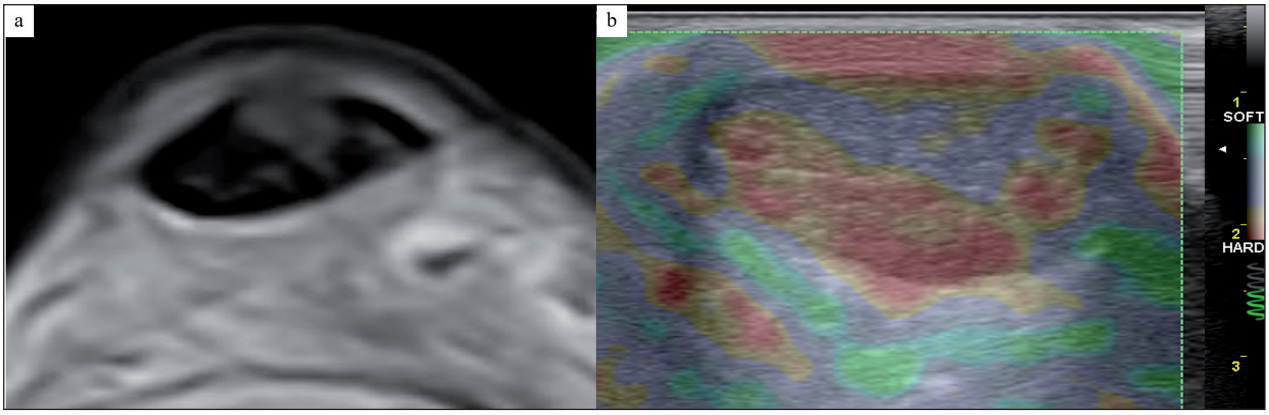

Figure 2. Axial T2-weighted image (a) and short-axis compression US elastography image (b) of an Achilles tendon. Note the intrasubstance hyperintense area of tendinosis within the tendon, evident at a "softer" area (in purple) at US compression elastogram

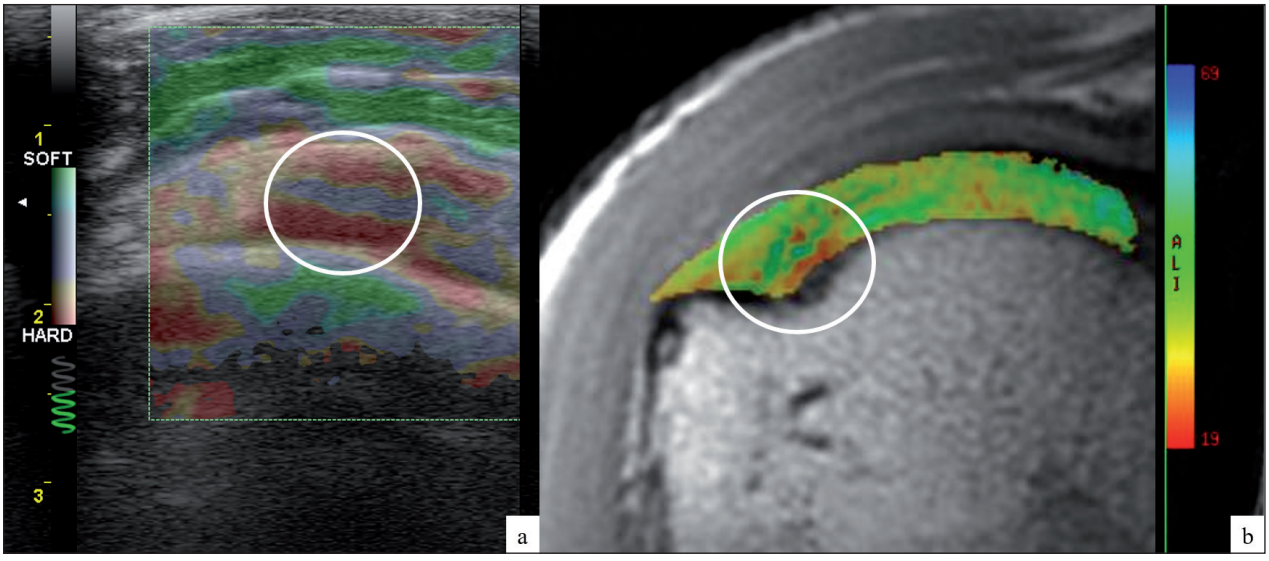

Figure 3. Concordance of US compression elastogram (a) and T2 mapping colorimetric scale (b) in a supraspinatus tendon tendinosis at the insertion area (white circle)

Interventional radiology procedures in tendon diseases

Several intervention have been introduced for the conservative treatment of tendinosis, including rest, oral and topical analgesics, and physical therapy (cryotherapy, stretching, eccentric strengthening, taping, bracing, extracorporeal shock-wave therapy) (44). Few of these treatments have been shown to be effective, and corticosteroid injections, once a mainstay of tendinopathy treatment, have been found to be harmful to tendons. Consequently, clinicians have sought safer and more effective interventions for the treatment of this condition.

In recent years, the indications for interventional radiology procedures have expanded thanks to the use of all diagnostic methods (45-50). With the use of US, the specific location of a tendon pathology can be accurately delineated, and this also allows to target many percutaneous minimally invasive treatments (51, 52). Among them, the most popular ones include percutaneous needle tenotomy (PNT), high-volume injection (HVI), and orthobiologic interventions, such as intratendinous injection of Platelet-rich Plasma (PRP) (53).

Percutaneous needle tenotomy (PNT), also termed needling, consists in the repeated passing of a needle (16-22 gauge) through the tendon, to disrupt the chronic degenerative process (including scar tissue), induce localized bleeding and fibroblast proliferation, which can lead to growth factor release, collagen formation, and ultimately healing. The number of needle passes (usually from 20 to 40) may vary based on numerous factors, such as patient characteristics, severity, and size of the tendinopathic area, presence or absence of tears, operator experience, and comfort level. This technique can be used alone or in combination with the injection of orthobiologic products. There is considerable variability in postprocedural care, such as the use of anti-inflammatory medications, the use of bracing, rehabilitation protocols, and return-to-activity guidelines. Most publications in literature are limited series on gluteus tendons, hamstring tendons, tensor fascia lata tendon, common extensor tendon of the elbow, rotator cuff tendons, Achilles and patellar tendon. Almost all studies showed improvement in clinical symptoms and reported rare complications (54-56).

High-volume injection (HVI) treatment focuses on using high volumes of injectate (about 10 mL of 0.5% bupivacaine, 25mg of hydrocortisone, and between 12-40 mL of normal saline) to disrupt neovessels and neonerves, which may reduce neurogenic inflammation and pain, and promote healing. This technique has mainly been studied in patellar and Achilles tendinopathy, where most neovessels and neonerves are sonographically observed between the affected tendon and an adjacent fat pad. US-guided HVI for the treatment of patellar and midportion Achilles tendinopathy has shown promise in improvement of both pain and functional scores, with positive effects persisting for up to 15 months. No significant complications have been reported. Another potential advantage of this procedure is that, because the tendon is not mechanically debrided, rehabilitation and return to activity may progress at a faster rate than with PNT (57, 58).

In the last decade, the use of biological therapies for the treatment of musculoskeletal diseases has increased significantly. Among them, *platelet-rich plasma (PRP)* is one of the most used compounds in regenerative musculoskeletal medicine, in particular for tendinopathies and degenerative joint pathologies, namely osteoarthritis. PRP is the blood-derived plasma fraction and contains high concentrations of platelets that release several growth factors with a critical role in tissue healing, such as platelet-derived growth factor, transforming growth factor-beta, and vascular endothelial growth factor. There are many studies and authors who report an intensification of the healing of tendinopathies treated with PRP. Several trials showed that PRP is an effective treatment for lateral epicondylitis, with short-term and long-term (up to 24 months) efficacy compared to steroids. Best available evidence suggests explicitly that LR-PRP (leucocyte-rich PRP) should be the treatment of choice. Only two trials of high-quality evidence – though with limited follow-up of 6 months - support the use of PRP in chronic refractory patellar tendinopathy, and recommended LR-PRP over LP-PRP (leucocyte-poor PRP). Concerning Achilles tendinopathy, one clinical trial reported efficacy of 4 LP-PRP injections, but also found similar results for high-volume injection of anesthetic, corticosteroid, and saline, perhaps suggesting the benefit may be due to mechanical volume effects (59, 60).

Although there remains a paucity of evidence to recommend PRP injections for rotator cuff tendinopathy routinely, PRP may be a safe and effective alternative to corticosteroid injections in conservative treatment of rotator cuff tendinopathy. PRP injections are an effective treatment for improving pain and function in chronic plantar fasciitis and may be superior to corticosteroids, especially considering the complications of multiple corticosteroid injections that are not associated with PRP. Nevertheless, there is substantial evidence that corticosteroids can be useful in chronic tendinopathy at relieving pain, reducing swelling, and improving function in the short term (61).

Recently, the anti-inflammatory and lubrication properties of *hyaluronic acid* have drawn the scientific community's interest to treat tendinopathies. Some in vitro and animal in vivo studies demonstrate encouraging results in terms of the ability of hyaluronic acid to facilitate tendon gliding, as well as creating better tendon structural organization. Moreover, the injection of hyaluronic acid may limit the proinflammatory effect by restoring viscoelasticity and by stimulating the endogenous synthesis of hyaluronic acid (62, 63).

Conclusions

In conclusion, diagnostic and interventional radiology are nowadays a matter of fact in all clinical settings (64-70). Tendon evaluation has improved with advances in ultrasound technology and MRI sequences. Beyond the anatomical changes detected with conventional imaging, MRI T2 mapping sequences and ultrasound elastography can provide information about the biochemical changes in tendon tissue and the consequent mechanical alteration induced by tendinopathy, giving reliable quantitative data for the diagnosis, staging, and follow-up.

The significant advancements in the use of musculoskeletal US for interventional purposes have played a critical role in the development of minimally invasive interventions to treat tendon diseases.

Conflict of interest: Authors declare that they have no commercial associations (e.g. consultancies, stock ownership, equity interest, patent/licensing arrangement etc.) that might pose a conflict of interest in connection with the submitted article.

References

1. Bruno F, Arrigoni F, Palumbo P, et al. The Acutely Injured Wrist. Radiol Clin North Am 2019; 57: 943-55.
2. Bruno F, Arrigoni F, Palumbo P, et al. New advances in MRI diagnosis of degenerative osteoarthropathy of the peripheral joints. Radiol Med 2019; 124: 1121-27.
3. Bruno F, Barile A, Arrigoni F, et al. Weight-bearing MRI of the knee: a review of advantages and limits. Acta Biomed 2018; 89: 78-88.
4. Zoccali C, Arrigoni F, Mariani S, Bruno F, Barile A, Masciocchi C. An unusual localization of chondroblastoma: The triradiate cartilage; from a case report a reconstructive technique proposal with imaging evolution. J Clin Orthop Trauma 2017; 8: S48-s52.
5. Giacomelli R, Gorla R, Trotta F, et al. Quality of life and unmet needs in patients with inflammatory arthropathies: results from the multicentre, observational RAPSODIA study. Rheumatology (Oxford) 2015; 54: 792-7.
6. Giacomelli R, Afeltra A, Alunno A, et al. Guidelines for biomarkers in autoimmune rheumatic diseases - evidence based analysis. Autoimmun Rev 2019; 18: 93-106.
7. Giacomelli R, Ruscitti P, Shoenfeld Y. A comprehensive review on adult onset Still's disease. J Autoimmun 2018; 93: 24-36.
8. Cipriani P, Di Benedetto P, Ruscitti P, et al. Perivascular Cells in Diffuse Cutaneous Systemic Sclerosis Overexpress Activated ADAM12 and Are Involved in Myofibroblast Transdifferentiation and Development of Fibrosis. J Rheumatol 2016; 43: 1340-9.
9. Giacomelli R, Liakouli V, Berardicurti O, et al. Interstitial lung disease in systemic sclerosis: current and future treatment. Rheumatol Int 2017; 37: 853-63.
10. Di Geso L, Zardi EM, Afeltra A, et al. Comparison between conventional and automated software-guided ultrasound assessment of bilateral common carotids intimamedia thickness in patients with rheumatic diseases. Clin Rheumatol 2012; 31: 881-4.
11. Salaffi F, Carotti M, Di Carlo M, Farah S, Gutierrez M. Adherence to Anti-Tumor Necrosis Factor Therapy Administered Subcutaneously and Associated Factors in Patients With Rheumatoid Arthritis. J Clin Rheumatol 2015; 21: 419-25.
12. Carotti M, Salaffi F, Di Carlo M, Giovagnoni A. Relationship between magnetic resonance imaging findings, radiological grading, psychological distress and pain in patients with symptomatic knee osteoarthritis. Radiol Med 2017; 122: 934-43.
13. Pogliacomi F, De Filippo M, Paraskevopoulos A, Alesci M, Marenghi P, Ceccarelli F. Mini-incision direct lateral approach versus anterior mini-invasive approach in total hip replacement: results 1 year after surgery. Acta Biomed 2012; 83: 114-21.
14. De Filippo M, Pesce A, Barile A, et al. Imaging of postoperative shoulder instability. Musculoskelet Surg 2017; 101: 15-22.

15. Barile A, Bruno F, Arrigoni F, et al. Emergency and Trauma of the Ankle. Semin Musculoskelet Radiol 2017; 21: 282-89.
16. Barile A, Bruno F, Mariani S, et al. Follow-up of surgical and minimally invasive treatment of Achilles tendon pathology: a brief diagnostic imaging review. Musculoskelet Surg 2017; 101: 51-61.
17. Zoccali C, Rossi B, Zoccali G, et al. A new technique for biopsy of soft tissue neoplasms: a preliminary experience using MRI to evaluate bleeding. Minerva Med 2015; 106: 117-20.
18. Di Pietto F, Chianca V, de Ritis R, et al. Postoperative imaging in arthroscopic hip surgery. Musculoskelet Surg 2017; 101: 43-49.
19. Barile A, Bruno F, Mariani S, et al. What can be seen after rotator cuff repair: a brief review of diagnostic imaging findings. Musculoskelet Surg 2017; 101: (Suppl1): 3-14
20. Patriarca L, Letteriello M, Di Cesare E, Barile A, Gallucci M, Splendiani A. Does evaluator experience have an im pact on the diagnosis of lumbar spine instability in dynamic MRI? Interobserver agreement study. Neuroradiol J 2015; 28: 341-6
21. Arrigoni F, Napoli A, Bazzocchi A, et al. Magnetic-resonance- guided focused ultrasound treatment of non-spinal osteoid osteoma in children: multicentre experience. Pediatr Radiol 2019; 49: 1209-16.
22. Cazzato RL, Arrigoni F, Boatta E, et al. Percutaneous management of bone metastases: state of the art, interventional strategies and joint position statement of the Italian College of MSK Radiology (ICoMSKR) and the Italian College of Interventional Radiology (ICIR). Radiol Med 2019; 124: 34-49.
23. Putz R, Muller-Gerbl M. [Anatomy and pathology of tendons]. Orthopade 1995; 24: 180-6.
24. Nakagaki K, Ozaki J, Tomita Y, Tamai S. Magnetic resonance imaging of rotator cuff tearing and degenerative tendon changes: Correlation with histologic pathology. J Shoulder Elbow Surg 1993; 2: 156-64.
25. Backman C, Boquist L, Friden J, Lorentzon R, Toolanen G. Chronic achilles paratenonitis with tendinosis: an experimental model in the rabbit. J Orthop Res 1990; 8: 541-7.
26. Weinreb JH, Sheth C, Apostolakos J, et al. Tendon structure, disease, and imaging. Muscles Ligaments Tendons J 2014; 4: 66-73.
27. Piccolo CL, Galluzzo M, Ianniello S, et al. Pediatric musculoskeletal injuries: role of ultrasound and magnetic resonance imaging. Musculoskelet Surg 2017; 101: 85-102.
28. Perrotta FM, Astorri D, Zappia M, Reginelli A, Brunese L, Lubrano E. An ultrasonographic study of enthesis in early psoriatic arthritis patients naive to traditional and biologic DMARDs treatment. Rheumatol Int 2016; 36: 1579-83.
29. Zappia M, Reginelli A, Russo A, et al. Long head of the biceps tendon and rotator interval. Musculoskelet Surg 2013; 97 Suppl 2: S99-108.
30. Zytoon AA, Eid H, Sakr A, El Abbass HA, Kamel M. Ultrasound assessment of elbow enthesitis in patients with seronegative arthropathies. J Ultrasound 2014; 17: 33-40.
31. Syha R, Springer F, Ketelsen D, et al. Achillodynia - radiological imaging of acute and chronic overuse injuries of the achilles tendon. Rofo 2013; 185: 1041-55.
32. Gurgenidze T, Mizandari MG, Gadeliia GT. [Normal sonoanatomy and ultrasound diagnosis of achilles tendon pathology]. Georgian Med News 2009; 119-25.
33. Cortellini A, Bozzetti F, Palumbo P, et al. Weighing the role of skeletal muscle mass and muscle density in cancer patients receiving PD-1/PD-L1 checkpoint inhibitors: a multicenter real-life study. Sci Rep 2020; 10: 1456.
34. Weber J, Buchhorn T. [Midportion Achilles tendinopathy]. Unfallchirurg 2017; 120: 1038-43.
35. Anz AW, Lucas EP, Fitzcharles EK, Surowiec RK, Millett PJ, Ho CP. MRI T2 mapping of the asymptomatic supraspinatus tendon by age and imaging plane using clinically relevant subregions. Eur J Radiol 2014; 83: 801-5.
36. Bachmann E, Rosskopf AB, Gotschi T, et al. T1- and T2*-Mapping for Assessment of Tendon Tissue Biophysical Properties: A Phantom MRI Study. Invest Radiol 2019; 54: 212-20.
37. Ganal E, Ho CP, Wilson KJ, et al. Quantitative MRI characterization of arthroscopically verified supraspinatus pathology: comparison of tendon tears, tendinosis and asymptomatic supraspinatus tendons with T2 mapping. Knee Surg Sports Traumatol Arthrosc 2016; 24: 2216-24.
38. Fusini F, Langella F, Busilacchi A, et al. Real-time sonoelastography: principles and clinical applications in tendon disorders. A systematic review. Muscles Ligaments Tendons J 2017; 7: 467-77.
39. Klauser AS, Miyamoto H, Tamegger M, et al. Achilles tendon assessed with sonoelastography: histologic agreement. Radiology 2013; 267: 837-42.
40. Tan S, Kudas S, Ozcan AS, et al. Real-time sonoelastography of the Achilles tendon: pattern description in healthy subjects and patients with surgically repaired complete ruptures. Skeletal Radiol 2012; 41: 1067-72.
41. Ooi CC, Malliaras P, Schneider ME, Connell DA. "Soft, hard, or just right?" Applications and limitations of axial-strain sonoelastography and shear-wave elastography in the assessment of tendon injuries. Skeletal Radiol 2014; 43: 1-12.
42. Busilacchi A, Olivieri M, Ulisse S, et al. Real-time sonoelastography as novel follow-up method in Achilles tendon surgery. Knee Surg Sports Traumatol Arthrosc 2016; 24: 2124-32.
43. Tudisco C, Bisicchia S, Stefanini M, Antonicoli M, Masala S, Simonetti G. Tendon quality in small unilateral supraspinatus tendon tears. Real-time sonoelastography correlates with clinical findings. Knee Surg Sports Traumatol Arthrosc 2015; 23: 393-8.
44. Lopez-Royo MP, Gomez-Trullen EM, Ortiz-Lucas M, et al. Comparative study of treatment interventions for patellar tendinopathy: a protocol for a randomised controlled trial. BMJ Open 2020; 10: e034304.
45. Carrafiello G, Dionigi G, Ierardi AM, et al. Efficacy, safety and effectiveness of image-guided percutaneous microwave

ablation in cystic renal lesions Bosniak III or IV after 24 months follow up. Int J Surg 2013; 11 Suppl 1: S30-5.
46. Ierardi AM, Piacentino F, Fontana F, et al. The role of endovascular treatment of pelvic fracture bleeding in emergency settings. Eur Radiol 2015; 25: 1854-64.
47. Ierardi AM, Tsetis D, Ioannou C, et al. Ultra-low profile polymer-filled stent graft for abdominal aortic aneurysm treatment: a two-year follow-up. Radiol Med 2015; 120: 542-8.
48. Carrafiello G, Ierardi AM, Duka E, et al. Usefulness of Cone-Beam Computed Tomography and Automatic Vessel Detection Software in Emergency Transarterial Embolization. Cardiovasc Intervent Radiol 2016; 39: 530-7.
49. Arrigoni F, Bruno F, Zugaro L, et al. Developments in the management of bone metastases with interventional radiology. Acta Biomed 2018; 89: 166-74.
50. Floridi C, Pesapane F, Angileri SA, et al. Yttrium-90 radioembolization treatment for unresectable hepatocellular carcinoma: a single-centre prognostic factors analysis. Med Oncol 2017; 34: 174.
51. Peck E, Jelsing E, Onishi K. Advanced Ultrasound-Guided Interventions for Tendinopathy. Phys Med Rehabil Clin N Am 2016; 27: 733-48.
52. Adler RS, Sofka CM. Percutaneous ultrasound-guided injections in the musculoskeletal system. Ultrasound Q 2003; 19: 3-12.
53. Barile A, La Marra A, Arrigoni F, et al. Anaesthetics, steroids and platelet-rich plasma (PRP) in ultrasound-guided musculoskeletal procedures. Br J Radiol 2016; 89: 20150355.
54. Hung CY, Chang KV. Ultrasound-Guided Percutaneous Needle Tenotomy with Platelet-Rich Plasma Injection for an Uncommon Case of Proximal Gluteus Medius Tendinopathy. J Med Ultrasound 2019; 27: 111-12.
55. Mattie R, Wong J, McCormick Z, Yu S, Saltychev M, Laimi K. Percutaneous Needle Tenotomy for the Treatment of Lateral Epicondylitis: A Systematic Review of the Literature. PM R 2017; 9: 603-11.
56. Hopkins J, Sampson M. Percutaneous tenotomy: Development of a novel, percutaneous, ultrasound-guided needle-cutting technique for division of tendons and other connective tissue structures. J Med Imaging Radiat Oncol 2014; 58: 327-30.
57. Maffulli N, Spiezia F, Longo UG, Denaro V, Maffulli GD. High volume image guided injections for the management of chronic tendinopathy of the main body of the Achilles tendon. Phys Ther Sport 2013; 14: 163-7.
58. Crisp T, Khan F, Padhiar N, et al. High volume ultrasound guided injections at the interface between the patellar tendon and Hoffa's body are effective in chronic patellar tendinopathy: A pilot study. Disabil Rehabil 2008; 30: 1625-34.
59. Kaux JF, Libertiaux V, Dupont L, et al. Platelet-rich plasma (PRP) and tendon healing: comparison between fresh and frozen-thawed PRP. Platelets 2020; 31: 221-25.
60. Yuan T, Zhang CQ, Wang JH. Augmenting tendon and ligament repair with platelet-rich plasma (PRP). Muscles Ligaments Tendons J 2013; 3: 139-49.
61. Rees JD, Stride M, Scott A. Tendons--time to revisit inflammation. Br J Sports Med 2014; 48: 1553-7.
62. Kaux JF, Samson A, Crielaard JM. Hyaluronic acid and tendon lesions. Muscles Ligaments Tendons J 2015; 5: 264-9.
63. Abate M, Schiavone C, Salini V. The use of hyaluronic acid after tendon surgery and in tendinopathies. Biomed Res Int 2014; 2014: 783632.
64. Bruno F, Smaldone F, Varrassi M, et al. MRI findings in lumbar spine following O2-O3 chemiodiscolysis: A long term follow-up. Interventional neuroradiology : journal of peritherapeutic neuroradiology, surgical procedures and related neurosciences 2017; 23: 444-450
65. Bruno F, Arrigoni F, Palumbo P, et al. New advances in MRI diagnosis of degenerative osteoarthropathy of the peripheral joints. Radiol Med 2019; 124: 1121-27.
66. Mariani S, La Marra A, Arrigoni F, et al. Dynamic measurement of patello-femoral joint alignment using weight-bearing magnetic resonance imaging (WB-MRI). European journal of radiology 2015; 84: 2571-8.
67. Masciocchi C, Arrigoni F, Ferrari F, et al. Uterine fibroid therapy using interventional radiology mini-invasive treatments: current perspective. Med Oncol 2017; 34: 52.
68. Masciocchi C, Arrigoni F, La Marra A, Mariani S, Zugaro L, Barile A. Treatment of focal benign lesions of the bone: MRgFUS and RFA. The British journal of radiology 2016; 89: 20150356-20150356.
69. Salvati F, Rossi F, Limbucci N, Pistoia ML, Barile A, Masciocchi C. Mucoid metaplastic degeneration of anterior cruciate ligament. The Journal of sports medicine and physical fitness 2008; 48: 483-487.
70. Zappia M, Castagna A, Barile A, Chianca V, Brunese L, Pouliart N. Imaging of the coracoglenoid ligament: a third ligament in the rotator interval of the shoulder. Skeletal Radiol 2017; 46: 1101-11.

Received: 20 May 2020
Accepted: 10 June 2020
Correspondence:
Federico Bruno
Department of Biotechnology and Applied Clinical Sciences, University of L'Aquila, L'Aquila, Italy
Via Vetoio 1, 67100 – L'Aquila (Italy)
Tel: +393313240926
E-mail: federico.bruno.1988@gmail.com

Acta Biomed 2020; Vol. 91, Supplement 8: 107-115 DOI: 10.23750/abm.v91i8-S.9993

Review

Diagnostic and interventional radiology fundamentals of synovial pathology

Chiara Acanfora[1], Federico Bruno[1], Pierpaolo Palumbo[1], Francesco Arrigoni[1], Raffaele Natella[2], Maria Antonietta Mazzei[3], Marina Carotti[4], Piero Ruscitti[1], Ernesto Di Cesare[5], Alessandra Splendiani[1], Roberto Giacomelli[1], Carlo Masciocchi[1], Antonio Barile[1]

[1] Department of Biotechnology and Applied Clinical Sciences, University of L'Aquila, L'Aquila, Italy; [2] Department of Precision Medicine, University of Campania "L. Vanvitelli", Naples, Italy; [3] Unit of Diagnostic Imaging, Department of Radiological Sciences, Azienda Ospedaliero-Universitaria Senese, Department of Medicine, Surgery and Neuroscience, University of Siena, Siena, Italy; [4] Department of Radiology - Division of Special and Pediatric Radiology, University Hospital "Umberto I - Lancisi - Salesi", Ancona, Italy; [5] Department of Life, Health and Environmental Sciences, University of L'Aquila, L'Aquila, Italy

Summary. The synovial membrane is a specialized mesenchymal tissue that lines the diarthrodial joints surfaces, bursae, and tendon sheaths of the body. This article aims to provide an overview of the fundamentals of synovial tissue, with particular regard to the imaging findings of the main pathologic processes that can affect the synovia and the role of image-guided interventions. (www.actabiomedica.it)

Keywords: synovia, knee, MRI, ultrasound, CEUS, joint injection

Synovial anatomy, physiology, and pathophysiology

Normal synovium is made up of two layers, the synovial intima, and subsynovial tissue. The synovial intima is formed by a layer of loosely connected synovial cells, while the subsynovial tissue widely varies in the structure based on its location, and it may be mainly fibrous, areolar, or adipose. The subsynovium is characterized by the presence of a vascular and lymphatic network; through this capillary network, fluid enters into the joint cavity as an ultrafiltrate of blood plasma. Synovial membrane roles are the production of synovial fluid, the removal of articular debris, and the facilitation of the sliding between the articular surfaces (1).

Synovial tissue reacts to the numerous kinds of stresses it may be subjected in a fast but stereotypical manner, and the pathogenesis of the majority of the synovial disorders routes into a final and common anatomopathological pathway. The initial fast response is characterized by the increase of blood flow that causes edema, alteration of the synovial matrix, and intra-articular effusion. The process proceeds inducing synovial proliferation accompanied by mononuclear infiltration; this leads to synovial hyperplasia that encroaches upon the articular surface. In the chronic phases, fibrotic changes may also occur (2, 3).

As in most anatomical districts, although the first step of the approach to synovial pathology is clinical evaluation, this can often have low sensitivity and specificity. Diagnostic imaging modalities, uniquely if integrated, are reliable support to diagnosis by demonstrating the type of anatomic alteration, approaching - in most cases - the final pathologic diagnosis, and being a noninvasive follow-up tool (4-20).

Synovial effusion

Synovial effusion is defined as the increase of the normal quantity of fluid on the articular cavity: its distribution is specific for each joint and follows the capsule anatomy. The normal synovium is barely percepti-

ble at MR imaging. Visualization of the synovium, in facts, suggests the presence of underlying pathologic changes. However, this is a nonspecific finding as it can be associated with traumatic, degenerative, overload, inflammatory and neoplastic pathology (21). So, effusion can be considered a sensitive indicator of joint pathology, but it may occur in either the presence or absence of proliferative synovitis. Due to the release of pluripotent cells (mainly fibroblasts), the synovial membrane undergoes to hyperplasia and/or hypertrophy that can be less or more fibrous, depending on the kind and the time lasting of the stress. Synovial thickening or proliferation can be challenging to detect in the presence of a joint effusion since both reveal themselves as an increased signal intensity on fluid-sensitive (T2-weighted) images. During the subacute stage of the pathology, in case of repeated stress, synovial thickening becomes more prominent and so more detectable from the synovial fluid. Additional morphologic findings may help in the differential diagnosis between synovial effusion and synovial thickening, such as the presence of scalloping or truncation of the prefemoral fat pad, defects of Hoffa's fat pad and the non-visualization or irregular margins of the quadriceps fat pad, that have been described as signs of synovial proliferation. The administration of intravenous gadolinium can be considered highly accurate in differentiating proliferative synovium from joint effusion (**fig. 1**). Besides being highly sensitive in the detection of the presence of joint effusions and synovitis, MR imaging is a reliable tool in quantifying synovial and effusion volumes. Its ability to quantify these synovial processes has important clinical implications: assessment of disease severity and response to therapy. Several studies have shown how MR imaging with the use of advanced quantitative evaluation of synovial hypertrophy and synovial fluid is an essential tool in the diagnostic and follow-up stages of many degenerative and inflammatory conditions (22, 23). Even if MR imaging remains the gold standard in the evaluation of synovial disorders of the knee, ultrasounds technique has been considered to find correlative accuracy in measurement of synovial thickness, vascularization, and effusion, most of all for its simple,

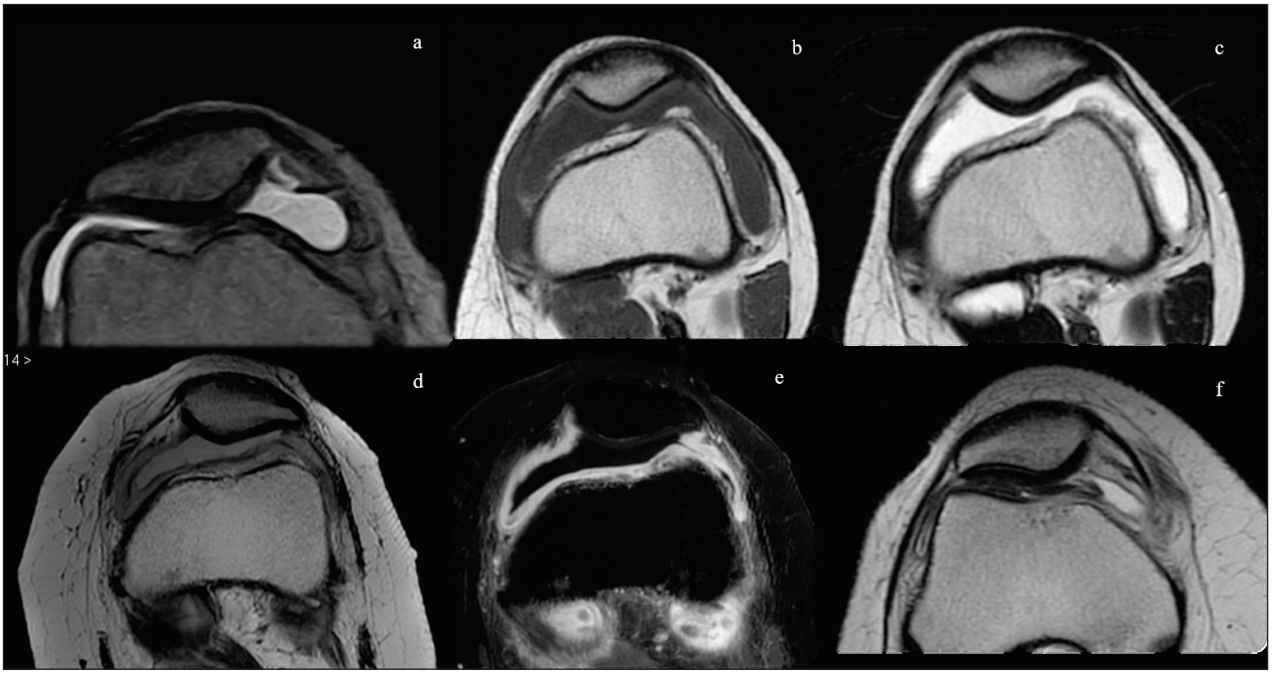

Figure 1. Imaging features of synovial effusion. In the acute phases (a), there is an increase of joint fluid, with the typical T2-hyperintensity and T1-hypointensity. In the subacute stages (b), the thickened synovial lining can be appreciated. Progressively, synovial hyperplasia and hypertrophy can be differentiated by the synovial effusion as it is clearly thickened, with villous appearance (c, d). The distinction is even more evident with the administration of gadolinium, where only the active synovial thickening enhances (e). In the chronic stages (f), the joint fluid can be less prominent and fibrotic aspects may occur

inexpensive, and beneficial properties. At US, synovial hyperplasia and hypertrophy are evident as a thickening of the synovial lining hyperechoic compared to the intra-articular effusion. Depending on the degree and chronicity of inflammation, it can have a smooth, irregular, villous/villonodular profile. Power-doppler and Color-doppler sampling are useful for documenting the degree of proliferation of neovessels within the hypertrophic synovial tissue (24). In several studies, the evaluation with contrast-enhanced ultrasound (CEUS) showed higher sensitivity (95%) for synovitis detection than CE-MRI (82%), power Doppler US (64%), or grayscale US (58%) (24, 25).

Inflammatory arthritis

The synovia is typically involved, as a prime pathophysiological process, in a wide range of inflammatory arthritis. Among them, the most frequent are represented by rheumatoid arthritis (RA) and psoriatic arthritis (PsA) (26-36). Though bone involvement has typical different pathologic and imaging patterns, all inflammatory arthritis are progressive inflammatory disorders, primarily affecting the synovium (37-40). Articular tumefaction reflects the synovial inflammation that is the primary target of the pathological process. The earliest anatomopathological alteration is the exudative synovitis characterized by increased vascularization and permeability, synovial effusion, and inflammatory infiltration (41, 42). Synovitis is an early phase of the process, and together with the bone edema is an important predictive factor of bone lesions. Synovitis can be exudative or proliferative, and MR imaging is crucial for its differentiation. MR imaging has become a central tool in the evaluation of inflammatory arthritis because of its superior soft-tissue contrast, its ability to detect and quantify synovial thickening/volume, and the fact that these measurements correlate highly with synovial inflammatory activity. Fat-suppressed T1-weighted 3D gradient-echo images offer an excellent differentiation of cartilage and joint fluid in patients with RA (43, 44). However, it is recognized that gadolinium-enhanced MR images offer superior differentiation of enlarged or hyperplastic synovium from the adjacent joint fluid. Synovitis is described as an area in the synovial compartment that shows an increased contrast enhancement after intravenous administration of gadolinium (45). For this reason, the administration of gadolinium turns out to be essential to obtain information about vascularization and – consequently- the activity stage of the disease; this, furthermore, allows both qualitative and quantitative evaluations (45, 46). For quantitative evaluation, dynamic imaging is used in order to appreciate the synovial enhancement and to obtain values of signal intensity according to acquisition time (47). The rate of early enhancement (30 to 60 seconds following injection) correlates highly with microscopic evidence of active inflammation (vessel proliferation and mononuclear leukocyte infiltration). The distinction between synovium and joint fluid is most reliable in the first 10 minutes following injection of gadolinium contrast, because the gadolinium diffuses into the joint, thereby obscuring the border between synovium and effusion. Synovitis can be evaluated by US as well and, as MR imaging, can be considered highly reliable and accurate when used to follow disease progression and monitor response to therapy (48). The thickened intra-articular synovial pannus can show Doppler signal, according to its increased vascularization. The Doppler signal intensity relates to the quantity of neo-formed vessels and thus with the severity of the inflammation (49, 50).

Osteoarthritis

Osteoarthritis (OA) is the most common form of arthritis and a major cause of joint pain and disability (51, 52). Traditionally, OA has been considered primarily a disease of hyaline cartilage with associated bone involvement, caused by overload or overuse; hover, the pathophysiology of OA development is now appreciated to be more complex. The newest evidence suggests that synovitis and the resultant pro-inflammatory mediators have a major and early role in the pathogenesis of OA, with secondary effects on articular cartilage. In light of this, MRI imaging and US have been used to assess the presence of "macroscopic" inflammation and have supported the role of synovitis as an active component of the OA process, associated with both pain and structural progression

(53-55). The histological pattern of synovium involvement in OA patients is characterized by synovial lining hyperplasia, sublining fibrosis, and stromal vascularization. Synoviocytes react by producing pro-inflammatory mediators, which in turn attract immune cells, increase angiogenesis, and induce a phenotypic shift in chondrocytes. A vicious cycle follows as chondrocytes produce additional cytokines and proteolytic enzymes that eventually increase cartilage degradation and induce further synovial inflammation (55). At the "macroscopic" level, MRI provides valuable insights into synovitis and can visualize synovial hypertrophy, synovial fluid volume, and level of synovial enhancement after intravenous injection of contrast agent. Several studies also demonstrated how MRI inflammation measures correlate well with histological inflammation and clinical symptoms.

Interventional radiology

Interventional radiology can propose a wide range of therapeutic procedures also in musculoskeletal pathology through ultrasound, CT, and MRI guidance (56-64). Based on the evidence reported above, the synovia – and namely synovial inflammation – has become one of the main therapeutic targets not only for inflammatory arthropathies but also in degenerative osteoarthritis. Corticosteroids are undoubtedly the most used anti-inflammatory drugs. The possibility, through image guidance, of direct intraarticular drug injection, is the key to maximize the therapeutic effects while minimizing the known systemic side effects (65). In addition to intra-articular administration, ultrasound imaging guidance is beneficial for intrabursal and peritendinous administration, where corticosteroids can have anti-inflammatory action on synovial tissue. The imaging guide also allows minimizing other risks of unguided infiltration of corticosteroids, such as tendon rupture. Hyaluronic acid (HA) injection is another interventional radiology procedure aimed at degenerative joint pathology (namely osteoarthritis) but primarily aimed at the synovium. Hyaluronic acid is a glycosaminoglycan consisting of highly hydrophilic chains of D-glucuronic acid and N-acetylglucosamine. There are numerous types of hyaluronic acid on the market, which mainly distinguish themselves by their molecular weight. Those with low molecular weight, able to bind to binding proteins (hyaladerine) and CD44 receptor, act mainly with a biological effect of viscoinduction (i.e., stimulating the endogenous production of HA) (66-68). Those with high molecular weight, on the other hand, have a lower biological effect, while performing a powerful viscosupplementation action, thanks to their rheological properties. Even if metanalysis highlight the heterogeneity of the available studies, intraarticular HA injections appear effective in the treatment of arthritic pain (mild-moderate OA) both at the level of the knee and the hip. The size of the effect on pain varies according to the studies, with a peak at 8 weeks (higher than corticosteroids). Cross-linked products (high molecular weight) have greater pain efficacy than linear HA, and there are evidences to support HA efficacy also concerning functional improvement (level 1B). In all guidelines, the use is recommended for the management of osteoarthritis as a second-line treatment in symptomatic patients after conservative therapy (NSAID) (69). Platelet-rich plasma injection is another therapeutic tool we can consider. This product, consisting of a platelet ultrafiltrate, performs its action through the release of several growth factors (PDGF, TGF-B, EGF, CTGF) with anti-inflammatory activity and trophic action on different joint tissues. There are several in vitro and clinical evidences that intraarticular PRP injection may exert a positive influence in patients affected by knee cartilage degeneration and OA and that it may have higher and longer efficacy than HA in improving pain and articular function (70, 71).

Synovial tumors and pseudotumors

Synovial cysts and ganglia

Synovial cysts are fluid-filled masses lined with synovium located within or about joints. They can be intraneural, extraneural, or between or within muscles. The distinction between a synovial cyst and ganglion cyst is made primarily based on the histological nature of the lining of the cyst, the contents of the cyst, and the presence/absence of communication with the joint

(72, 73). Ganglion cysts are lined by spindle-shaped cells and are characterized by myxoid contents. Because true synovial cysts are, by definition, lined by synovial cells, they manifest disease and are affected by the same disease processes as other synovial structures. They are most commonly encountered about the knee and occur with synovial inflammatory disorders, rheumatologic and otherwise, as a result of trauma, and in conjunction with osteoarthritis. Synovial cysts can arise from different causes (degenerative articular processes, chronic microtrauma soft tissue/bursae, or reflect anatomical remnants), and knowledge of the most relevant localizations, pathological and radiological picture is helpful for a correct diagnosis (74).

Pigmented villonodular synovitis (PVNS)

Pigmented villonodular synovitis (PVNS) is a rare, benign synovial proliferative process whose distribution is usually monoarticular. The disorder is idiopathic with two primary forms, localized and diffuse, either intraarticular or extra-articular (75-77). Although any synovial joint may be involved, the knee is the most frequently affected. Patients usually present with nonspecific symptoms such as monoarticular pain and decreased range of motion. The disease is characterized by the presence of abundant hemosiderin-laden macrophage deposition into a bulky, mass-like synovium. MR imaging is the imaging method of choice for the diagnosis, surgical planning, and evaluation of recurrence (75). Clumps of hemosiderin-laden macrophage deposits demonstrate low signal intensity on T1- and T2-weighted images due to the paramagnetic effects of the iron in the ferric state, and this is the most reliable diagnostic feature (**fig. 2**). A large amount of joint effusion is usually present, but not specific. The pathological equivalent at the level of the tendon sheaths is the giant cell tumor of the tendon sheaths (GCTTS) (77).

Lipoma arborescens

Lipoma arborescens, or villous lipomatous proliferation of the synovial membrane, is a rare intra-articular lesion that usually involves the knee. It is characterized by villous proliferation of the synovium and extensive replacement of the subsynovial tissue by mature adipose cells. It is usually a monoarticular condition. MR imaging shows a frond-like morphology with high signal intensity (isointense to subcutaneous fat) on T1-weighted images (78, 79). Lack of enhancement after injection of intravenous contrast material excludes the diagnosis of other synovial inflammatory or neoplastic processes (**fig. 3**).

Synovial chondromatosis

Idiopathic synovial osteochondromatosis is a non-neoplastic, proliferative, and metaplastic disorder of the synovium characterized by the presence of multiple cartilaginous or osteocartilaginous bodies

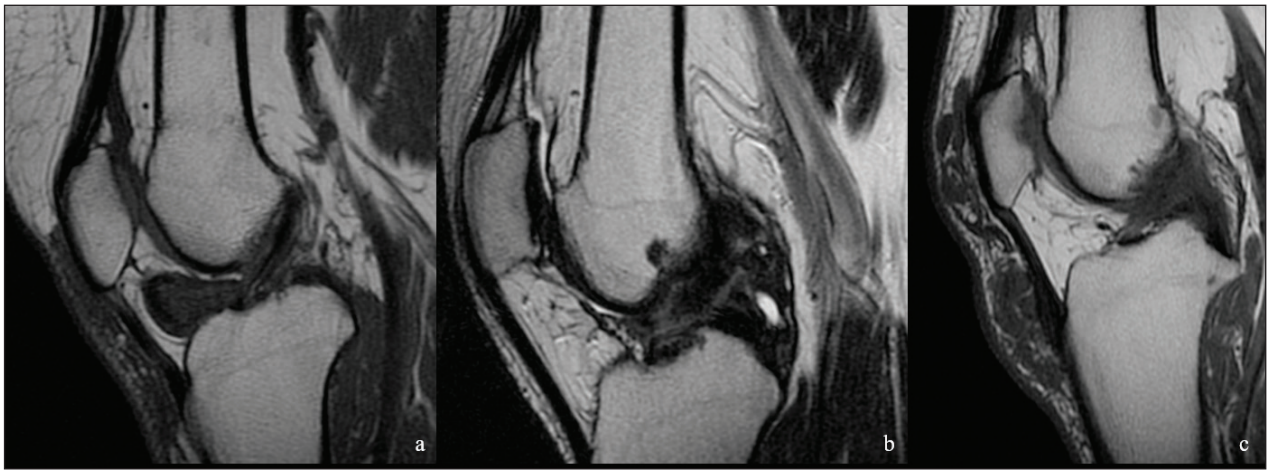

Figure 2. Imaging features of pigmented villonodular synovitis (PVNS) in solitary (a), diffuse (b), and extraarticular form. Note the low signal intensity on both T1- and T2-weighted sequences

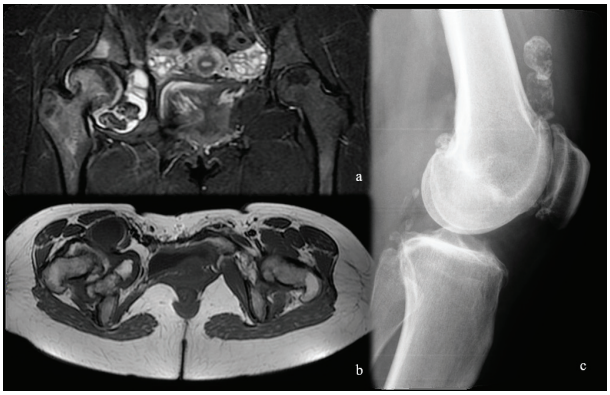

Figure 3. Imaging features of synovial chondromatosis. In a and b, note the right hip joint effusion with intraarticular osteocartilaginous bodies with signs of ossification. In c, a plain film of the knee with secondary synovial chondromatosis showing osteocartilaginous bodies distributed in the joint recesses

within an articulation or adjacent synovial lined structure (80). Two forms of the condition occur, primary and secondary osteochondromatosis. The secondary one is more common and characterized by the presence of intraarticular osteocartilaginous bodies against a backdrop of degenerative joint disease. The second type, primary synovial osteochondromatosis, is relatively uncommon. The condition is usually progressive, leading to early osteoarthritis. The MR imaging characteristics depend on the presence and extent of calcification and or ossification in the bodies. In the case of intra-articular bodies composed primarily of cartilage, the bodies are lobulated in appearance with intermediate to low signal intensity on T1-weighted sequences with high signal intensity on fluid-sensitive sequences. In the case of calcified intraarticular bodies, the signal characteristics are described as foci of low signal intensity on both T1-weighted and fluid-sensitive sequences (81). Marrow-containing bodies will show the high signal intensity of the marrow within the bodies on T1-weighted images (**fig. 4**). Heterogeneous enhancement of cartilaginous bodies can be seen after the administration of intravenous contrast material.

Conclusions

Imaging is a central piece of the complex puzzle of synovial diseases; the role of multimodal imaging is crucial in many aspects regarding the management of these disorders from the very beginning of the diagnosis, going through the follow-up and the treatment as well.

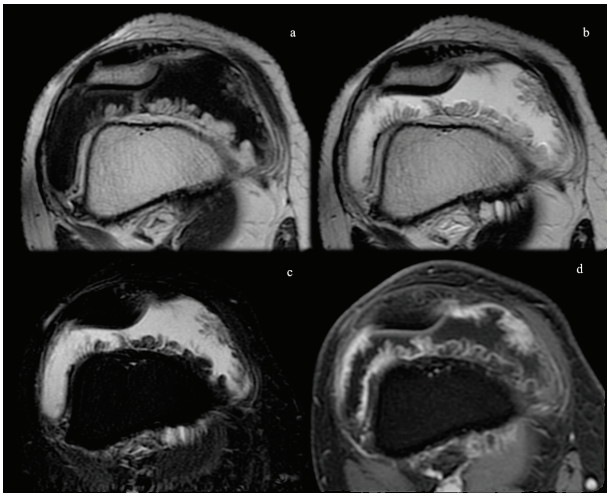

Figure 4. MRI imaging features of a lipoma arborescens of the knee. Note the typical frond-like thickening of the synovium in the supra-patellar recess showing signal intensity of fat (T1- and T2-hyperintense in a-b and hypointense in the fs-T2 sequence in c). After gadolinium administration (d) there is enhancement only of the superficial synovial lining

Conflict of interest: Authors declare that they have no commercial associations (e.g. consultancies, stock ownership, equity interest, patent/licensing arrangement etc.) that might pose a conflict of interest in connection with the submitted article.

References

1. Broeren MGA, Waterborg CEJ, Wiegertjes R, et al. A threedimensional model to study human synovial pathology. ALTEX 2019; 36: 18-28.
2. Frick MA, Wenger DE, Adkins M. MR imaging of synovial disorders of the knee: an update. Radiol Clin North Am 2007; 45: 1017-31, vii.
3. Chung CB, Boucher R, Resnick D. MR imaging of synovial disorders of the knee. Semin Musculoskelet Radiol 2009; 13: 303-25.
4. Reginelli A, Silvestro G, Fontanella G, et al. Validation of DWI in assessment of radiotreated bone metastases in elderly patients. Int J Surg 2016; 33 Suppl 1: S148-53.
5. Reginelli A, Zappia M, Barile A, Brunese L. Strategies of imaging after orthopedic surgery. Musculoskelet Surg 2017; 101: 1.
6. Barile A, Bruno F, Mariani S, et al. What can be seen after rotator cuff repair: a brief review of diagnostic imaging findings. Musculoskelet Surg 2017; 101: (Suppl1): 3-14
7. Cortellini A, Bozzetti F, Palumbo P, et al. Weighing the

role of skeletal muscle mass and muscle density in cancer patients receiving PD-1/PD-L1 checkpoint inhibitors: a multicenter real-life study. Sci Rep 2020; 10: 1456.
8. Piccolo CL, Galluzzo M, Ianniello S, et al. Pediatric musculoskeletal injuries: role of ultrasound and magnetic resonance imaging. Musculoskelet Surg 2017; 101: 85-102.
9. Zappia M, Capasso R, Berritto D, et al. Anterior cruciate ligament reconstruction: MR imaging findings. Musculoskelet Surg 2017; 101: 23-35.
10. Bruno F, Arrigoni F, Palumbo P, et al. The Acutely Injured Wrist. Radiol Clin North Am 2019; 57: 943-55
11. Salvati F, Rossi F, Limbucci N, et al. Mucoid metaplastic-degeneration of anterior cruciate ligament. The Journal of sports medicine and physical fitness 2008; 48: 483-487
12. Zappia M, Castagna A, Barile A, et al. Imaging of the coracoglenoid ligament: a third ligament in the rotator interval of the shoulder. Skeletal Radiology 2017; 46: 1101-1111
13. Mariani S, La Marra A, Arrigoni F, et al. Dynamic measurement of patello-femoral joint alignment using weight-bearing magnetic resonance imaging (WB-MRI). European journal of radiology 2015; 84: 2571-8
14. De Filippo M, Pesce A, Barile A, et al. Imaging of postoperative shoulder instability. Musculoskelet Surg 2017; 101: 15-22.
15. Pogliacomi F, De Filippo M, Paraskevopoulos A, Alesci M, Marenghi P, Ceccarelli F. Mini-incision direct lateral approach versus anterior mini-invasive approach in total hip replacement: results 1 year after surgery. Acta Biomed 2012; 83: 114-21.
16. Barile A, Bruno F, Mariani S, et al. Follow-up of surgical and minimally invasive treatment of Achilles tendon pathology: a brief diagnostic imaging review. Musculoskelet Surg 2017; 101: 51-61.
17. Zoccali C, Arrigoni F, Mariani S, Bruno F, Barile A, Masciocchi C. An unusual localization of chondroblastoma: The triradiate cartilage; from a case report a reconstructive technique proposal with imaging evolution. J Clin Orthop Trauma 2017; 8: S48-s52.
18. Bruno F, Barile A, Arrigoni F, et al. Weight-bearing MRI of the knee: a review of advantages and limits. Acta Biomed 2018; 89: 78-88.
19. Zappia M, Reginelli A, Russo A, et al. Long head of the biceps tendon and rotator interval. Musculoskelet Surg 2013; 97 Suppl 2: S99-108.
20. Di Pietto F, Chianca V, de Ritis R, et al. Postoperative imaging in arthroscopic hip surgery. Musculoskelet Surg 2017; 101: 43-49.
21. Bredella MA, Tirman PF, Wischer TK, Belzer J, Taylor A, Genant HK. Reactive synovitis of the knee joint: MR imaging appearance with arthroscopic correlation. Skeletal Radiol 2000; 29: 577-82.
22. Perry TA, Gait A, O'Neill TW, et al. Measurement of synovial tissue volume in knee osteoarthritis using a semi-automated MRI-based quantitative approach. Magn Reson Med 2019; 81: 3056-64.
23. Wang Y, Teichtahl AJ, Pelletier JP, et al. Knee effusion volume assessed by magnetic resonance imaging and progression of knee osteoarthritis: data from the Osteoarthritis Initiative. Rheumatology (Oxford) 2019; 58: 246-53.
24. Liu H, Huang C, Chen S, et al. Value of contrast-enhanced ultrasound for detection of synovial vascularity in experimental rheumatoid arthritis: an exploratory study. J Int Med Res 2019; 47: 5740-51.
25. Fiocco U, Stramare R, Coran A, et al. Vascular perfusion kinetics by contrast-enhanced ultrasound are related to synovial microvascularity in the joints of psoriatic arthritis. Clin Rheumatol 2015; 34: 1903-12.
26. Cipriani P, Ruscitti P, Carubbi F, Liakouli V, Giacomelli R. Methotrexate in rheumatoid arthritis: optimizing therapy among different formulations. Current and emerging paradigms. Clin Ther 2014; 36: 427-35.
27. Giacomelli R, Gorla R, Trotta F, et al. Quality of life and unmet needs in patients with inflammatory arthropathies: results from the multicentre, observational RAPSODIA study. Rheumatology (Oxford) 2015; 54: 792-7.
28. Ruscitti P, Ursini F, Cipriani P, et al. Poor clinical response in rheumatoid arthritis is the main risk factor for diabetes development in the short-term: A 1-year, single-centre, longitudinal study. PLoS One 2017; 12: e0181203.
29. Ruscitti P, Cipriani P, Masedu F, et al. Increased Cardiovascular Events and Subclinical Atherosclerosis in Rheumatoid Arthritis Patients: 1 Year Prospective Single Centre Study. PLoS One 2017; 12: e0170108.
30. Ruscitti P, Cipriani P, Liakouli V, et al. Subclinical and clinical atherosclerosis in rheumatoid arthritis: results from the 3-year, multicentre, prospective, observational GIRRCS (Gruppo Italiano di Ricerca in Reumatologia Clinica e Sperimentale) study. Arthritis Res Ther 2019; 21: 204.
31. Giacomelli R, Ruscitti P, Shoenfeld Y. A comprehensive review on adult onset Still's disease. J Autoimmun 2018; 93: 24-36.
32. Ruscitti P, Iacono D, Ciccia F, et al. Macrophage Activation Syndrome in Patients Affected by Adult-onset Still Disease: Analysis of Survival Rates and Predictive Factors in the Gruppo Italiano di Ricerca in Reumatologia Clinica e Sperimentale Cohort. J Rheumatol 2018; 45: 864-72.
33. Ruscitti P, Cipriani P, Ciccia F, et al. Prognostic factors of macrophage activation syndrome, at the time of diagnosis, in adult patients affected by autoimmune disease: Analysis of 41 cases collected in 2 rheumatologic centers. Autoimmun Rev 2017; 16: 16-21.
34. Cipriani P, Di Benedetto P, Ruscitti P, et al. Perivascular Cells in Diffuse Cutaneous Systemic Sclerosis Overexpress Activated ADAM12 and Are Involved in Myofibroblast Transdifferentiation and Development of Fibrosis. J Rheumatol 2016; 43: 1340-9.
35. Giacomelli R, Liakouli V, Berardicurti O, et al. Interstitial lung disease in systemic sclerosis: current and future treatment. Rheumatol Int 2017; 37: 853-63.
36. Di Cesare E, Battisti S, Di Sibio A, et al. Early assessment of sub-clinical cardiac involvement in systemic sclerosis (SSc) using delayed enhancement cardiac magnetic resonance (CEMRI). Eur J Radiol 2013; 82: e268-73.

37. Salaffi F, Carotti M, Di Carlo M, Farah S, Gutierrez M. Adherence to Anti-Tumor Necrosis Factor Therapy Administered Subcutaneously and Associated Factors in Patients With Rheumatoid Arthritis. J Clin Rheumatol 2015; 21: 419-25.
38. Di Geso L, Zardi EM, Afeltra A, et al. Comparison between conventional and automated software-guided ultrasound assessment of bilateral common carotids intima-media thickness in patients with rheumatic diseases. Clin Rheumatol 2012; 31: 881-4.
39. Salaffi F, Carotti M, Bosello S, et al. Computer-aided quantification of interstitial lung disease from high resolution computed tomography images in systemic sclerosis: correlation with visual reader-based score and physiologic tests. Biomed Res Int 2015; 2015: 834262.
40. Vitali C, Carotti M, Salaffi F. Is it the time to adopt salivary gland ultrasonography as an alternative diagnostic tool for the classification of patients with Sjogren's syndrome? Comment on the article by Cornec et al. Arthritis Rheum 2013; 65: 1950.
41. Giacomelli R, Afeltra A, Alunno A, et al. Guidelines for biomarkers in autoimmune rheumatic diseases - evidence based analysis. Autoimmun Rev 2019; 18: 93-106.
42. Cipriani P, Berardicurti O, Masedu F, et al. Biologic therapies and infections in the daily practice of three Italian rheumatologic units: a prospective, observational study. Clin Rheumatol 2017; 36: 251-60.
43. Dakkak YJ, Boer AC, Boeters DM, Niemantsverdriet E, Reijnierse M, van der Helm-van Mil AHM. The relation between physical joint examination and MRI-depicted inflammation of metatarsophalangeal joints in early arthritis. Arthritis Res Ther 2020; 22: 67.
44. Barendregt AM, Bray TJP, Hall-Craggs MA, Maas M. Emerging quantitative MR imaging biomarkers in inflammatory arthritides. Eur J Radiol 2019; 121: 108707.
45. Cimmino MA, Parodi M, Barbieri F, et al. Dynamic Contrast- Enhanced MRI Confirms Rapid And Sustained Improvement Of Rheumatoid Arthritis Induced By Tocilizumab Treatment: An Italian Multicentre Study. Biologics 2020; 14: 13-21.
46. Cimmino MA, Innocenti S, Livrone F, Magnaguagno F, Silvestri E, Garlaschi G. Dynamic gadolinium-enhanced magnetic resonance imaging of the wrist in patients with rheumatoid arthritis can discriminate active from inactive disease. Arthritis Rheum 2003; 48: 1207-13.
47. Yi J, Lee YH, Song HT, Suh JS. Double-inversion recovery with synthetic magnetic resonance: a pilot study for assessing synovitis of the knee joint compared to contrast-enhanced magnetic resonance imaging. Eur Radiol 2019; 29: 2573-80.
48. Perrotta FM, Astorri D, Zappia M, Reginelli A, Brunese L, Lubrano E. An ultrasonographic study of enthesis in early psoriatic arthritis patients naive to traditional and biologic DMARDs treatment. Rheumatol Int 2016; 36: 1579-83.
49. Ostergaard M, Court-Payen M, Gideon P, et al. Ultrasonography in arthritis of the knee. A comparison with MR imaging. Acta Radiol 1995; 36: 19-26.
50. El-Miedany YM, Housny IH, Mansour HM, Mourad HG, Mehanna AM, Megeed MA. Ultrasound versus MRI in the evaluation of juvenile idiopathic arthritis of the knee. Joint Bone Spine 2001; 68: 222-30.
51. Bruno F, Arrigoni F, Palumbo P, et al. New advances in MRI diagnosis of degenerative osteoarthropathy of the peripheral joints. Radiol Med 2019; 124: 1121-27.
52. Carotti M, Salaffi F, Di Carlo M, Giovagnoni A. Relationship between magnetic resonance imaging findings, radiological grading, psychological distress and pain in patients with symptomatic knee osteoarthritis. Radiol Med 2017; 122: 934-43.
53. de Vries BA, van der Heijden RA, Poot DHJ, et al. Quantitative DCE-MRI demonstrates increased blood perfusion in Hoffa's fat pad signal abnormalities in knee osteoarthritis, but not in patellofemoral pain. Eur Radiol 2020; 30: 3401-08.
54. Oo WM, Linklater JM, Bennell KL, et al. Are OMERACT knee osteoarthritis ultrasound scores associated with pain severity, other symptoms, radiographic and MRI findings? J Rheumatol 2020;
55. Shakoor D, Demehri S, Roemer FW, Loeuille D, Felson DT, Guermazi A. Are contrast-enhanced and non-contrast MRI findings reflecting synovial inflammation in knee osteoarthritis: a meta-analysis of observational studies. Osteoarthritis Cartilage 2020; 28: 126-36.
56. Barile A, Arrigoni F, Bruno F, et al. Present role and future perspectives of interventional radiology in the treatment of painful bone lesions. Future Oncol 2018; 14: 2945-55.
57. Masciocchi C, Arrigoni F, Ferrari F, et al. Uterine fibroid therapy using interventional radiology mini-invasive treatments: current perspective. Med Oncol 2017; 34: 52 69.
58. Ierardi AM, Piacentino F, Fontana F, et al. The role of endovascular treatment of pelvic fracture bleeding in emergency settings. Eur Radiol 2015; 25: 1854-64.
59. Masciocchi C, Arrigoni F, La Marra A, et al. Treatment of focal benign lesions of the bone: MRgFUS and RFA. The British journal of radiology 2016; 89: 20150356-56 71.
60. Carrafiello G, Ierardi AM, Duka E, et al. Usefulness of Cone- Beam Computed Tomography and Automatic Vessel Detection Software in Emergency Transarterial Embolization. Cardiovasc Intervent Radiol 2016; 39: 530-7.
61. Perri M, Grattacaso G, di Tunno V, et al. T2 shine-through phenomena in diffusion-weighted MR imaging of lumbar discs after oxygen-ozone discolysis: a randomized, double-blind trial with steroid and O2-O3 discolysis versus steroid only. Radiol Med 2015; 120: 941-50.
62. Cazzato RL, Arrigoni F, Boatta E, et al. Percutaneous management of bone metastases: state of the art, interventional strategies and joint position statement of the Italian College of MSK Radiology (ICoMSKR) and the Italian College of Interventional Radiology (ICIR). Radiol Med 2019; 124: 34-49.
63. Arrigoni F, Barile A, Zugaro L, et al. Intra-articular be-

nign bone lesions treated with Magnetic Resonance-guided Focused Ultrasound (MRgFUS): imaging follow-up and clinical results. Med Oncol 2017; 34: 55.
64. Zoccali C, Rossi B, Zoccali G, et al. A new technique for biopsy of soft tissue neoplasms: a preliminary experience using MRI to evaluate bleeding. Minerva Med 2015; 106: 117-120
65. Barile A, La Marra A, Arrigoni F, et al. Anaesthetics, steroids and platelet-rich plasma (PRP) in ultrasound-guided musculoskeletal procedures. Br J Radiol 2016; 89: 20150355.
66. De Lucia O, Murgo A, Pregnolato F, et al. Hyaluronic Acid Injections in the Treatment of Osteoarthritis Secondary to Primary Inflammatory Rheumatic Diseases: A Systematic Review and Qualitative Synthesis. Adv Ther 2020; 37: 1347-59.
67. Henrotin Y, Lambert C, Richette P. Importance of synovitis in osteoarthritis: evidence for the use of glycosaminoglycans against synovial inflammation. Semin Arthritis Rheum 2014; 43: 579-87.
68. Ayhan E, Kesmezacar H, Akgun I. Intraarticular injections (corticosteroid, hyaluronic acid, platelet rich plasma) for the knee osteoarthritis. World J Orthop 2014; 5: 351-61.
69. Deseyne N, Conrozier T, Lellouche H, et al. Hip Inflammation MRI Scoring System (HIMRISS) to predict response to hyaluronic acid injection in hip osteoarthritis. Joint Bone Spine 2018; 85: 475-80.
70. Paterson KL, Hunter DJ, Metcalf BR, et al. Efficacy of intraarticular injections of platelet-rich plasma as a symptom- and disease-modifying treatment for knee osteoarthritis - the RESTORE trial protocol. BMC Musculoskelet Disord 2018; 19: 272.
71. Raeissadat SA, Ghorbani E, Sanei Taheri M, et al. MRI Changes After Platelet Rich Plasma Injection in Knee Osteoarthritis (Randomized Clinical Trial). J Pain Res 2020; 13: 65-73.
72. Telischak NA, Wu JS, Eisenberg RL. Cysts and cystic-appearing lesions of the knee: A pictorial essay. Indian J Radiol Imaging 2014; 24: 182-91.
73. Bermejo A, De Bustamante TD, Martinez A, Carrera R, Zabia E, Manjon P. MR imaging in the evaluation of cystic-appearing soft-tissue masses of the extremities. Radiographics 2013; 33: 833-55.
74. Beaman FD, Peterson JJ. MR imaging of cysts, ganglia, and bursae about the knee. Magn Reson Imaging Clin N Am 2007; 15: 39-52.
75. Falek A, Niemunis-Sawicka J, Wrona K, et al. Pigmented villonodular synovitis. Folia Med Cracov 2018; 58: 93-104.
76. Willimon SC, Busch MT, Perkins CA. Pigmented Villonodular Synovitis of the Knee: An Underappreciated Source of Pain in Children and Adolescents. J Pediatr Orthop 2018; 38: e482- e85.
77. Gouin F, Noailles T. Localized and diffuse forms of tenosynovial giant cell tumor (formerly giant cell tumor of the tendon sheath and pigmented villonodular synovitis). Orthop Traumatol Surg Res 2017; 103: S91-S97.
78. Nambiar M, Onggo JR, Jacobson A. Lipoma arborescens: a rare cause of clicking in the knee. BMJ Case Rep 2019; 12:
79. Minami S, Miyake Y, Kinoshita H. Lipoma arborescens arising in the extra-articular bursa of the knee joint. SICOT J 2016; 2: 28.
80. Padhan P, Ahmed S. Synovial Chondromatosis. N Engl J Med 2019; 381: 1364.
81. Derek Stensby J, Fox MG, Kwon MS, Caycedo FJ, Rahimi A. Primary synovial chondromatosis of the subtalar joint: case report and review of the literature. Skeletal Radiol 2018; 47: 391-96.

Received: 20 May 2020
Accepted: 10 June 2020
Correspondence:
Federico Bruno
Department of Biotechnology and Applied Clinical Sciences, University of L'Aquila, L'Aquila, Italy
Via Vetoio 1, 67100 – L'Aquila (Italy)
E-mail: federico.bruno.1988@gmail.com

Acta Biomed 2020; Vol. 91, Supplement 8: 116-124 DOI: 10.23750/abm.v91i8-S.9942

Review

Clinical utility of dual energy computed tomography in gout: current concepts and applications

Marina Carotti[1], Fausto Salaffi[2], Emilio Filippucci[2], Giacomo Aringhieri[3], Federico Bruno[4], Sabrina Giovine[5], Francesco Gentili[6], Chiara Floridi[7], Alessandra Borgheresi[1], Massimo De Filippo[6], Carlo Masciocchi[4], Antonio Barile[4], Andrea Giovagnoni[1]

[1] Department of Radiology – Division of Special and Pediatric Radiology, University Hospital "Umberto I – Lancisi –Salesi"-University Politecnica Marche – Ancona, Italy; [2] Rheumatological Clinic, Department of Molecular and Clinical Sciences, University Politecnica Marche – Ancona, Italy; [3] Radiologia Diagnostica ed Interventistica, Dipartimento di ricercar Traslazionale e Nuove Tecnologie in Medicina e Chirurgia, Università di Pisa, Pisa, Italy; [4] Department of Biotechnology and Applied Clinical Science, University of L'Aquila, L'Aquila, Italy; [5] Department of Radiology, SG Moscati Hospital, ASL Caserta, Aversa, Caserta, Italy; [6] Department of Medicine and Surgery (DiMec), Section of Radiology, University of Parma, Maggiore Hospital, Parma, Italy; [7] Department of Clinical, Special and Dental Sciences, University Politecnica delle Marche, Ancona, AN, Italy

Summary. Gout is the most common inflammatory arthritis and is increasing in prevalence and incidence in many countries worldwide. Dual Energy Computed Tomography (DECT) has a high diagnostic accuracy in established gout, but its diagnostic sensitivity is low in subjects with recent-onset gout. A meta-analysis of 17 studies showed a pooled sensitivity and specificity of 0.85 and 0.88, respectively. DECT is a useful diagnostic tool for patients with contraindications for joint aspiration or for those who refuse joint aspiration. This article aims to give an up to date review and summary of existing literature on the role and accuracy of DECT in the imaging of gout. (www.actabiomedica.it)

Keywords: gout, dual-energy computed tomography, ultrasonography, imaging, diagnosis, tophaceous gout, non-tophaceous gout

Introduction

Gout is a common inflammatory form of arthritis that develops after a history of hyperuricemia and subsequent deposition of monosodium urate (MSU) crystals in joints and soft tissues (1). Overall, the prevalence in the Italian general population increased from 6.7 per 1000 inhabitants in 2005 to 9.1 per 1000 inhabitants in 2009, while the incidence was stable (respectively, 0.93 and 0.95 per 1000 person-years) (2). Clinical manifestations include acute arthritis (typically, first affecting the foot or the ankle), recurrent and chronic arthritis, tophi, bursitis, urolithiasis and renal disease. Tophaceous gout has been associated with relevant structural damage of joints and peri-articular tissues. In a recent international survey of more than 600 patients with gout, the presence of gouty tophi was associated with impairments to quality of life, productivity, and increased healthcare resource use (3). Gout is also associated with increased cardiovascular (CV) morbidity and mortality (4). Demonstrating MSU crystals in the joint fluid or an in tophus is the gold standard for gout diagnosis. However, many health care providers do not perform arthrocentesis and the identification of MSU crystals can be challenging, especially in early disease, since the treatment is distinctly different from that of other types of inflammatory arthritis. However, characteristic radiographic findings are only seen late

in the disease, including "punched-out" erosions with overhanging edges and sclerotic margins, often in association with asymmetric soft tissue masses (5). Various advanced imaging techniques are being utilized, including ultrasonography (US) with power Doppler, magnetic resonance imaging (MRI), and conventional computed tomography (CT).

CT, US and MRI are valuable diagnostic tools for the diagnosis and the guidance of interventional procedures in a wide range of organs (6-28).

Each has its unique advantages and disadvantages. However, none are specific enough to confirm a diagnosis of gout. Dual Energy Computed Tomography (DECT) is a relatively new imaging modality which shows great promise in the diagnosis of gout. It has been considered a good noninvasive alternative to the synovial fluid aspiration to detect MSU crystals. DECT has been reported to have higher sensitivity and specificity than the other techniques for gout diagnosis (29, 30), and is incorporated in the 2015 American College of Rheumatology (ACR) and the European League Against Rheumatism (EULAR) classification criteria (31). In this article, we will review techniques in image acquisition, processing and interpretation, diagnostic value and clinical significance, pitfalls and artifacts of DECT, as a valuable and accurate imaging modality in patients with gout.

Basic principles of DECT

DECT or spectral imaging is a revolutionary imaging method, and its use has had an increase in the last decade in many clinical applications, such as in the field of neuroradiology and chest, cardiovascular, abdominal and musculoskeletal systems. Dual-source scanners are equipped with two independent X-ray tubes, coupled with two independent detectors; each set is mounted within the same gantry with an angular offset of about 90°. DECT data are acquired by the two tubes which operate at different voltages (70 kV and 150 kVp), allowing simultaneous acquisition of images at these two different energy levels. The use of two X-ray tubes makes it possible to extract information and characterizes the chemical composition of material, based on the different degrees of the X-ray beam, absorption and attenuation, according to the atomic weight electron density of the compounds. High atomic number materials, such as calcium, have a greater difference in attenuation when exposed to X-rays of two different energy levels.

In comparison, materials of lower atomic number such as MSU have a smaller difference in attenuation at different X-ray energy levels. This characteristic allows differentiating some substances such as iodine, calcium, uric acid crystals, gadolinium, and xenon. These compounds are then color-coded and displayed as an overlay on a standard DECT grayscale image, for a simultaneous display of anatomy and localization of urate deposits. Although color coding can vary between manufacturers, green is the most common color assigned to MSU crystals, lavender to cortical bone, and pink to trabecular bone (29). Dedicated software allows automated volume evaluation of urate deposition.

Clinical characteristics and DECT findings - a structural approach

Deposits of MSU crystals and tophi have been identified both adjacent to and within tendons and also at the tendon-bone interface using histology (32), US (33), CT (34), and DECT (35). Tophus infiltration into tendons has also been observed during surgery (36). A recent DECT analysis in the feet of patients with tophaceous gout has demonstrated that tendon involvement in gout is much more common than previously thought (Figure 1). In this study, 10.8 % of the tendon/ligament sites analyzed had MSU crystals present (35).

Diagnosing gout by DECT

ACR-EULAR gout classification criteria

In an attempt to achieve a more uniform system for reporting and comparing studies on gout, the ACR and the EULAR formulated criteria in 2015 for the classification of gout (31). The entry criterion for the new classification criteria is the occurrence of at least

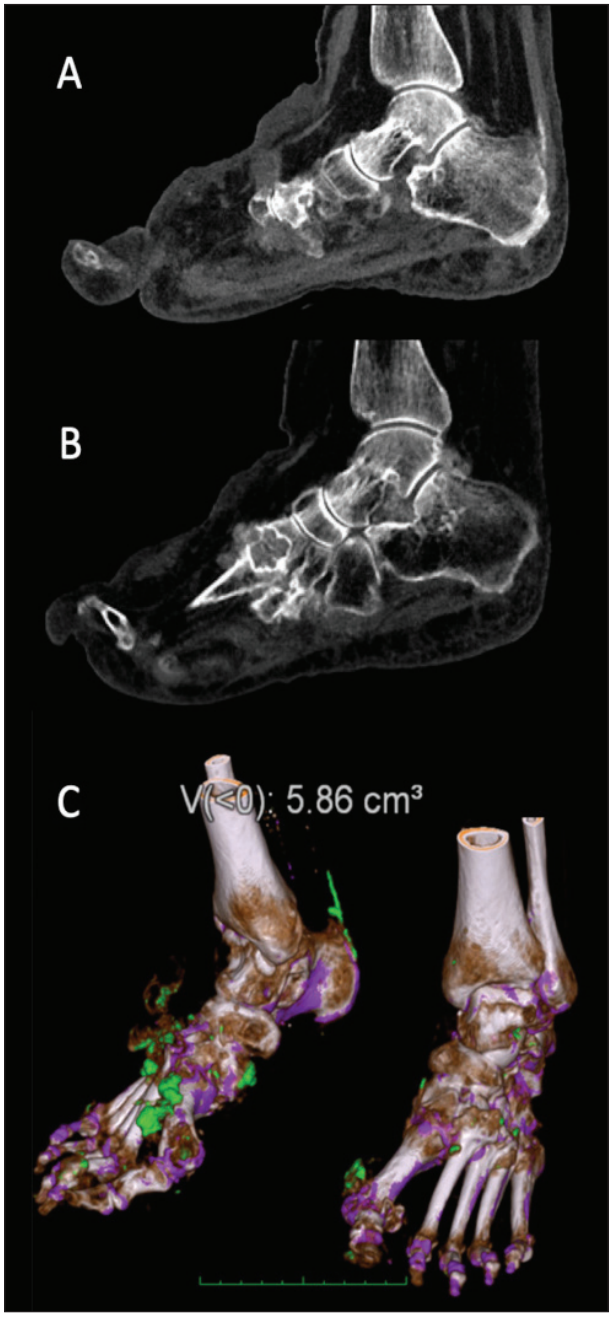

Figure 1. Dual-energy CT. A-B: sagittal multiplanar reformatted grayscale images of ankles/feet showing large bone erosions and severe joint damage at the tarso-metatarsal joints of both feet, with high-attenuating material adjacent to the erosions and along the distal end of the right Achilles tendon (A) representing monosodium urate deposition. C: corresponding volume-rendered color-coded dual-energy image of ankles/feet showing urate deposits (depicted in green) at the tarsometatarsal, metatarsophalangeal and interphalangeal joints and along the distal end of the right Achilles tendon. Automated quantification of urate volume is displayed at the top of the image.

one episode of peripheral joint or bursal swelling, pain, or tenderness. The presence of MSU crystals in synovial fluid (SF) of symptomatic joint/bursa or in a tophus is a sufficient criterion for classification of the subject as having gout and does not require further assessment. The new classification criteria include 4 clinical, 2 laboratories (serum urate and SF analysis) and 2 imaging (DECT OR US, and conventional radiography) criteria (31). The maximum possible score of the criteria is 23. A score of ≥8 classifies an individual as having gout.

Diagnostic accuracy of DECT in gout

The Outcomes Measures in Rheumatology (OMERACT) gout working group suggested that DECT is superior in the quantification of urate burden when compared to other modalities (37). A meta-analysis of 11 studies by Ogdie et al. (38) showed a pooled sensitivity of 0.87 (95% CI 0.79–0.93) and specificity of 0.84 (95% CI 0.75–0.90), compared with the reference standard of crystal identification by means of polarised light microscopy. More recently, Lee and Song performed a meta-analysis on the diagnostic accuracy of DECT in gout diagnosis. Of the eight studies analyzed, which included 510 patients and 268 controls, the pooled specificity and sensitivity of DECT were 93.7% and 84.7%, respectively. The authors concluded that DECT is highly accurate in the diagnosis of gout (30). In a prospective study by Choi et al. (39) investigating 40 crystal proven gout patients (17 tophaceous) and 40 controls with other arthritic conditions, the specificity and sensitivity of DECT for gout were 0.93 (95% CI 0.80– 0.98) and 0.78 (95% CI 0.62–0.89), respectively, with near-perfect inter- and intra-observer intraclass correlation coefficients for DECT volume measurements. In the present review, we pooled data from 17 studies and performed analyses to provide clinically more applicable data for clinicians; in person-based evaluations, the pooled (95% CI) sensitivity and specificity were 0.85 (0.70 to 0.90) and 0.88 (0.77 to 0.94), respectively. Details of the performance of the 17 included studies are presented in Figure 2.

DECT, generally, has good diagnostic accuracy in established gout and is regarded as a critical appliance to diagnose gout patients. However, DECT has lower

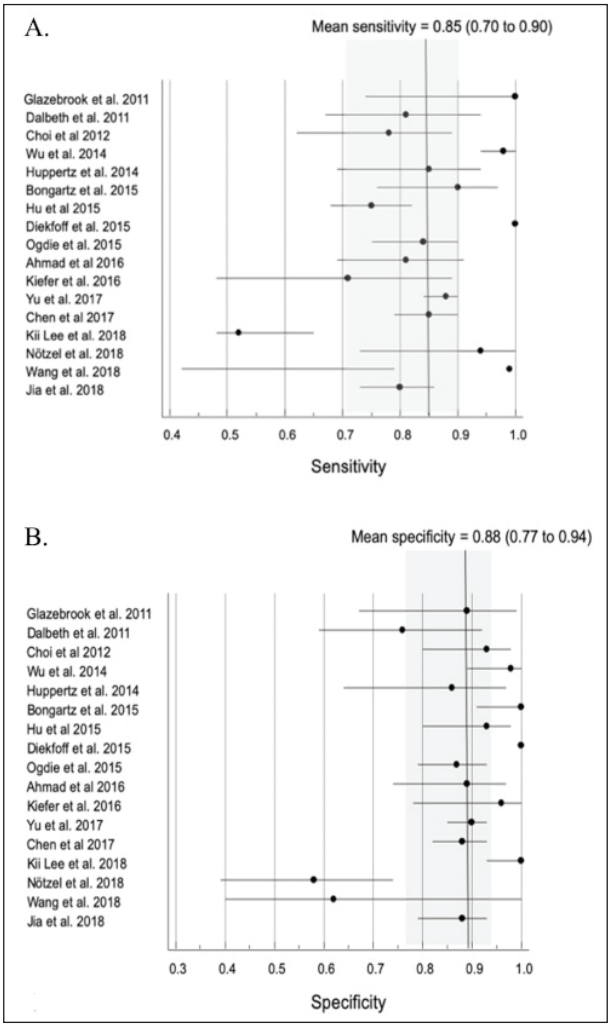

Figure 2. Sensitivity (A) and specificity (B) estimates for dual-energy computed tomography for the diagnosis of gout. Circles and lines represent point estimates and 95% confidence intervals, respectively.

sensitivity when restricted to individual crystal-proven gouty joints in non-tophaceous disease or in individual with short disease duration, especially in the first onset patients (40). The detection of MSU deposits by DECT depends on their size and density and the detection parameters of the DECT scanner (41). Several studies have reported that some patients with asymptomatic hyperuricemia have subclinical MSU crystal deposits. In a study of 25 patients with asymptomatic hyperuricemia (sUA ≥9 mg/dL), 24% had DECT-identified MSU crystal deposits in joints and tendons (42). In a cross-sectional study of 46 patients with asymptomatic hyperuricemia (sUA levels ≥6.5 mg/dL), 15% of patients with asymptomatic hyperuricemia had subclinical MSU crystal deposits on foot/ankle DECT scans (43).

Comparison between DECT and ultrasound in the diagnosis of gout

According to a recent systematic review, DECT and US have similar sensitivity and specificity in diagnosing gout in patients with crystal proven disease, being US more sensitive and DECT more specific (44). However, a comprehensive analysis aiming at comparing DECT with US in the diagnosis of gout should include not only their diagnostic accuracy in the detection of MSU crystal deposits, but also the main intrinsic properties and characteristics of these imaging techniques. Different diagnostic performances reported in the literature should be interpreted in the light of the following key aspects: standard reference for diagnosing gout (i.e., definitive diagnosis of gout fulfilling international criteria, MSU crystals identified using synovial fluid analysis); disease duration; and anatomic sites to scan (i.e., the clinically involved joints, a defined core set of the most frequently involved structures) (45, 46). In 2015, the OMERACT US working group finalized a process to obtain international consensus-based definitions on US elementary abnormalities indicative of MSU crystal deposition (i.e., double contour sign, tophi and aggregates) (47). Of note, double contour sign was included in the imaging domain of the ACR/EULAR gout classification criteria as sonographic evidence of urate deposition (31).

Moreover, US allows for the detection of not specific abnormalities, including synovial effusion, and helps to obtain synovial fluid to be assessed by polarized microscopy, improving the rate of successful aspirations guiding the needle to reach difficult targets such as small or deep fluid collections (48). These issues together with the US characteristics of being safe, not invasive, well accepted by patients, with low running costs, and increasingly available and portable, explain why several authors agree in considering US as a first-line imaging technique to screen the presence of MSU crystal deposition, especially in the early stages of the disease, and a suitable tool for monitoring changes in-

duced by urate-lowering therapy. However, despite the efforts of the OMERACT US working group a scoring system for the assessment of MSU crystal deposits is currently not available yet (49). Hence, US potential is underused in follow-up assessments and mainly based on the presence/absence of US findings.

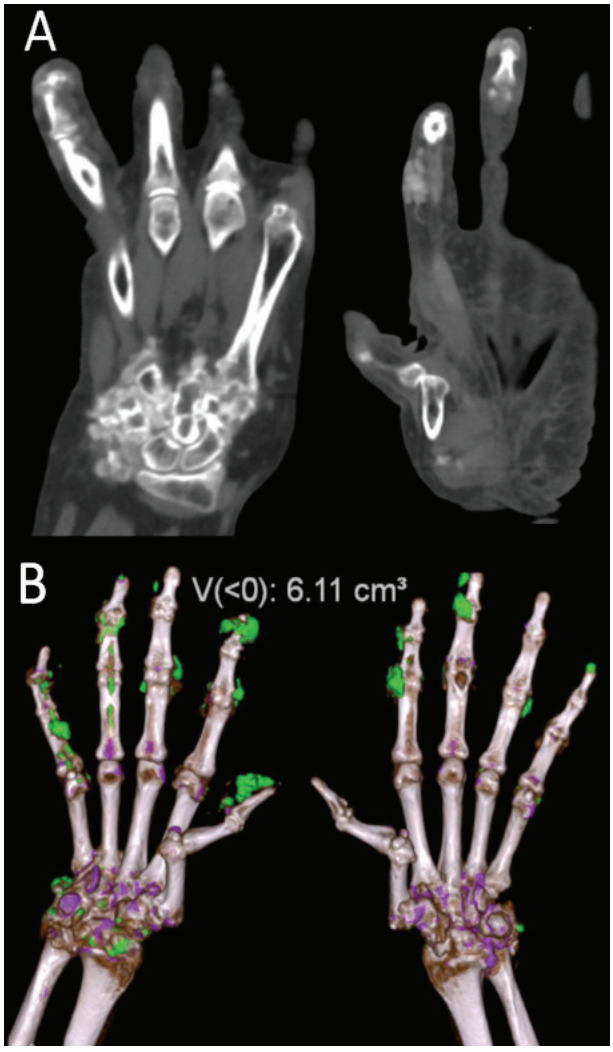

Figure 3. Dual-energy CT. A: coronal multiplanar reformatted grayscale images of hands/wrists showing bone erosions at left wrist and fingers of both hands, with high-attenuating material adjacent to the erosions and along the metacarpophalangeal and proximal and distal interphalangeal joints, indicative of monosodium urate deposits. B: corresponding volume-rendered color-coded dual-energy image of wrists/hands showing numerous urate deposits (depicted in green) along the metacarpophalangeal and proximal and distal interphalangeal joints and in the both wrists. Bilateral dislocation of first metacarpophalangeal joints can also be observed. Automated quantification of urate volume is displayed at the top of the image.

On the other hand, one of the advantages of DECT is to display the extent of the MSU crystal deposits in a single 3D image, which facilitates the estimation of their amount (Figure 3). Taking into account its high specificity, DECT should be used especially in cases with no clear diagnosis and in patients with high clinical suspicion and negative US findings (45).

Role of DECT in monitoring disease activity and damage – response to treatment

Beyond the clinical evaluation essential for all rheumatic diseases (50-58), imaging plays a fundamental role in the initial assessment and follow up of many pathologies in the musculoskeletal field and other organs (59-65).

DECT has shown to be of value in burden quantification and treatment monitoring and continues to be actively investigated in these roles. DECT also allows for the accurate and reproducible quantification of MSU deposits using automated software techniques (Figure 4), which calculates the volume of MSU deposits independent of the volume of hyperdense or calcified soft tissue. Furthermore, the quantitative software automation of DECT is valuable because visual analysis of

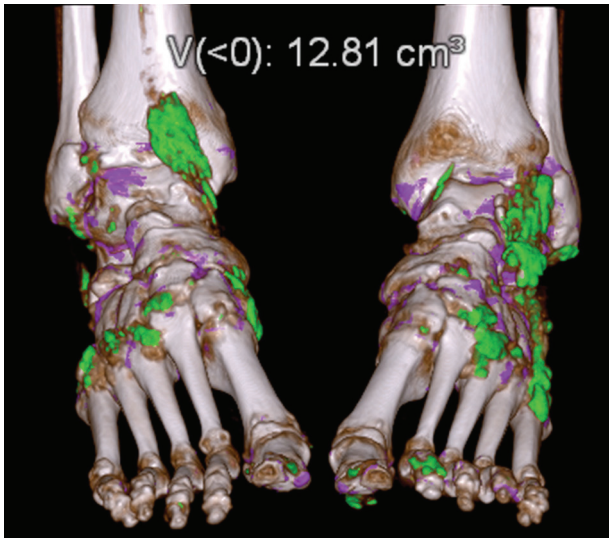

Figure 4. Dual-energy CT. Volume-rendered color-coded dual-energy image of ankles/feet showing urate deposits (depicted in green). Automated quantification of urate volume is displayed at the top of the image.

the gout burden after treatment may not discern small decreases in MSU crystal volume. This is helpful for follow-up imaging for assessing the reduction in volume of MSU deposits as a marker of treatment response in serial DECT scans without dependence on operator-defined margins of perceived tophi used in other methods of assessment. Overall, the level of evidence was low with one report of two randomized controlled trials, two non-randomized studies and 69 case series and reports. The review concluded that treatment with urate-lowering therapy including allopurinol and/or benzbromarone, febuxostat or pegloticase, can lead to a reduction in tophi. Finkenstaedt et al. (66) evaluated the diagnostic impact of DECT in patients with known hyperdense soft-tissue deposits on radiographs or conventional CT images, so patients with high suspicion for gout. This study showed that the therapy was changed in 23/43 (53%) of the patients, with a low incidence of gouty attacks in the following year. Dalbeth et al. (51) examined whether dose escalation of allopurinol to achieve serum urate target can influence bone erosion or MSU crystal deposition as measured by DECT in patients with gout. It provides evidence that long-term urate-lowering therapy using a treat to serum urate target strategy can influence structural damage and reduce urate crystal deposition. These findings are consistent with prospective studies conducted in gouty patients receiving urate-lowering therapy (31). Araujo et al. (67) investigated the effect of intensive lowering of serum uric acid (SUA) levels by pegloticase on the resolution of tophi in patients with refractory gout. In this paper, Araujo et al. described the ability of DECT to show the reduction of MSU deposits in responders. While DECT was superior for identifying total (including occult) urate deposition and assessing the volume of deposits, other modalities, such as Vernier calipers, photographs and musculoskeletal ultrasound, may permit better assessment of non-urate tophus components.

Pitfalls and problems in DECT

Interpretation of DECT in patients with suspicion of gout, particularly non-tophaceous gout, can be complicated by artifacts that are color-coded similar to MSU crystals, leading to false-positive results. False-positive color coding can be seen in nails, nailbeds, skin, callus, and vasculature. The most frequently reported artifact by far, is the nail bed artifact, which can be seen in 76% of imaged feet. Nail bed artifact may be due to the overlap of DECT values of MSU crystals and the keratinous nail bed. Skin artifacts may also be present in callused or thickened skin of the feet, such as the heel or toes, due to keratin content within these regions. Increased noise can also give rise to artifacts in the dual-energy data set. Urate-like pixellations in vascular calcification has also been described, although it remains unclear if this is due to real MSU deposition or an artifact. Urate deposition has been implicated as a factor in endothelial dysfunction in patients with gout and cardiovascular disease, but this has not been corroborated in necropsied cases so far. The sources of image noise are numerous, but two of the most common are using too low of an x-ray tube current or an inappropriate reconstruction algorithm. Patient motion during the scan can also result in image distortion and artifacts. Ensuring patient comfort and immobilization of the target anatomic site (e.g., via the use of taping or cradling devices) can help limit the occurrence of this artifact.

Conclusion

In conclusion, gout is becoming increasingly more relevant to properly identify and treat due to its association with metabolic syndrome. Various inflammatory arthritides such as pseudogout, rheumatoid arthritis, psoriatic arthritis, septic arthritis can mimic gout. DECT allows for highly accurate detection and quantification of MSU crystal deposits and should be implemented on a larger scale. This is especially true in all those situations where synovial fluid analysis is not feasible. However, several common artifacts can occur with DECT imaging. Knowledge of these artifacts is crucial for accurate qualitative and quantitative assessment of MSU crystals using DECT in patients with gout.

Conflict of interest: Authors declare that they have no commercial associations (e.g. consultancies, stock ownership, equity interest, patent/licensing arrangement etc.) that might pose a conflict of interest in connection with the submitted article.

References

1. Dalbeth N, Merriman TR, Stamp LK. Gout. Lancet (London, England) 2016; 388: 2039-2052.
2. Trifiro G, Morabito P, Cavagna L, et al. Epidemiology of gout and hyperuricaemia in Italy during the years 2005-2009: a nationwide population-based study. Annals of the rheumatic diseases 2013; 72: 694-700.
3. Scire CA, Manara M, Cimmino MA, et al. Gout impacts on function and health-related quality of life beyond associated risk factors and medical conditions: results from the KING observational study of the Italian Society for Rheumatology (SIR). Arthritis research & therapy 2013; 15: R101.
4. Clarson LE, Hider SL, Belcher J, Heneghan C, Roddy E, Mallen CD. Increased risk of vascular disease associated with gout: a retrospective, matched cohort study in the UK clinical practice research datalink. Annals of the rheumatic diseases 2015; 74: 642-7.
5. McQueen FM, Chhana A, Dalbeth N. Mechanisms of joint damage in gout: evidence from cellular and imaging studies. Nature reviews. Rheumatology 2012; 8: 173-81.
6. Agliata G, Schicchi N, Agostini A, et al. Radiation exposure related to cardiovascular CT examination: comparison between conventional 64-MDCT and third-generation dual-source MDCT. La Radiologia medica 2019; 124: 753-761.
7. Agostini A, Mari A, Lanza C, et al. Trends in radiation dose and image quality for pediatric patients with a multidetector CT and a third-generation dual-source dual-energy CT. La Radiologia medica 2019; 124: 745-752.
8. Mariani S, La Marra A, Arrigoni F, et al. Dynamic measurement of patello-femoral joint alignment using weight-bearing magnetic resonance imaging (WB-MRI). European journal of radiology 2015; 84: 2571-8
9. Di Pietto F, Chianca V, de Ritis R, et al. Postoperative imaging in arthroscopic hip surgery. Musculoskeletal surgery 2017; 101: 43-49.
10. Perrotta FM, Astorri D, Zappia M, Reginelli A, Brunese L, Lubrano E. An ultrasonographic study of enthesis in early psoriatic arthritis patients naive to traditional and biologic DMARDs treatment. Rheumatology international 2016; 36: 1579-1583.
11. Bruno F, Barile A, Arrigoni F, et al. Weight-bearing MRI of the knee: a review of advantages and limits. Acta bio-medica : Atenei Parmensis 2018; 89: 78-88.
12. Cazzato RL, Arrigoni F, Boatta E, et al. Percutaneous management of bone metastases: state of the art, interventional strategies and joint position statement of the Italian College of MSK Radiology (ICoMSKR) and the Italian College of Interventional Radiology (ICIR). La Radiologia medica 2019; 124: 34-49.
13. Michelini G, Corridore A, Torlone S, et al. Dynamic MRI in the evaluation of the spine: state of the art. Acta Biomed 2018; 89: 89-101
14. Zoccali C, Arrigoni F, Mariani S, Bruno F, Barile A, Masciocchi C. An unusual localization of chondroblastoma: The triradiate cartilage; from a case report a reconstructive technique proposal with imaging evolution. Journal of clinical orthopaedics and trauma 2017; 8: S48-s52.
15. Di Geso L, Zardi EM, Afeltra A, et al. Comparison between conventional and automated software-guided ultrasound assessment of bilateral common carotids intima-media thickness in patients with rheumatic diseases. Clinical rheumatology 2012; 31: 881-4.
16. Salvati F, Rossi F, Limbucci N, et al. Mucoid metaplastic-degeneration of anterior cruciate ligament. The Journal of sports medicine and physical fitness 2008; 48: 483-487
17. Salaffi F, Carotti M, Bosello S, et al. Computer-aided quantification of interstitial lung disease from high resolution computed tomography images in systemic sclerosis: correlation with visual reader-based score and physiologic tests. BioMed research international 2015; 2015: 834262.
18. Salaffi F, Carotti M, Di Carlo M, Farah S, Gutierrez M. Adherence to Anti-Tumor Necrosis Factor Therapy Administered Subcutaneously and Associated Factors in Patients With Rheumatoid Arthritis. Journal of clinical rheumatology : practical reports on rheumatic & musculoskeletal diseases 2015; 21: 419-25.
19. Zappia M, Castagna A, Barile A, et al. Imaging of the coracoglenoid ligament: a third ligament in the rotator interval of the shoulder. Skeletal Radiology 2017; 46: 1101-1111
20. Masciocchi C, Arrigoni F, Ferrari F, et al. Uterine fibroid therapy using interventional radiology mini-invasive treatments: current perspective. Med Oncol 2017; 34: 52
21. Zoccali C, Rossi B, Zoccali G, et al. A new technique for biopsy of soft tissue neoplasms: a preliminary experience using MRI to evaluate bleeding. Minerva Med 2015; 106: 117-120
22. Bruno F, Arrigoni F, Palumbo P, et al. The Acutely Injured Wrist. Radiol Clin North Am 2019; 57: 943-55
23. Arrigoni F, Bruno F, Zugaro L, et al. Developments in the management of bone metastases with interventional radiology. Acta Biomed 2018; 89: 166-74
24. De Filippo M, Pesce A, Barile A, et al. Imaging of postoperative shoulder instability. Musculoskeletal surgery 2017; 101: 15-22.
25. Pogliacomi F, De Filippo M, Paraskevopoulos A, Alesci M, Marenghi P, Ceccarelli F. Mini-incision direct lateral approach versus anterior mini-invasive approach in total hip replacement: results 1 year after surgery. Acta bio-medica : Atenei Parmensis 2012; 83: 114-21.
26. Giordano AV, Arrigoni F, Bruno F, et al. Interventional Radiology Management of a Ruptured Lumbar Artery Pseudoaneurysm after Cryoablation and Vertebroplasty of a Lumbar Metastasis. Cardiovasc Intervent Radiol 2017; 40: 776-79
27. Carrafiello G, Ierardi AM, Duka E, et al. Usefulness of Cone- Beam Computed Tomography and Automatic Vessel Detection Software in Emergency Transarterial Embolization. Cardiovascular and interventional radiology 2016; 39: 530-7.
28. Perri M, Grattacaso G, di Tunno V, et al. T2 shine-through phenomena in diffusion-weighted MR imaging of lumbar

discs after oxygen-ozone discolysis: a randomized, double blind trial with steroid and O2-O3 discolysis versus steroid only. Radiol Med 2015; 120: 941-50
29. Bongartz T, Glazebrook KN, Kavros SJ, et al. Dual-energy CT for the diagnosis of gout: an accuracy and diagnostic yield study. Annals of the rheumatic diseases 2015; 74: 1072-7.
30. Lee YH, Song GG. Diagnostic accuracy of dual-energy computed tomography in patients with gout: A meta-analysis. Seminars in arthritis and rheumatism 2017; 47: 95-101.
31. Neogi T, Jansen TL, Dalbeth N, et al. 2015 Gout classification criteria: an American College of Rheumatology/European League Against Rheumatism collaborative initiative. Annals of the rheumatic diseases 2015; 74: 1789-98.
32. Chhana A, Callon KE, Dray M, et al. Interactions between tenocytes and monosodium urate monohydrate crystals: implications for tendon involvement in gout. Annals of the rheumatic diseases 2014; 73: 1737-41.
33. Naredo E, Uson J, Jimenez-Palop M, et al. Ultrasound-detected musculoskeletal urate crystal deposition: which joints and what findings should be assessed for diagnosing gout? Annals of the rheumatic diseases 2014; 73: 1522-8.
34. Carotti M, Salaffi F, Ciapetti A. Computed Tomography in Tophaceous Gout. The Journal of Rheumatology 2010; 37: 1267-1268.
35. Dalbeth N, Kalluru R, Aati O, Horne A, Doyle AJ, McQueen FM. Tendon involvement in the feet of patients with gout: a dual-energy CT study. Annals of the rheumatic diseases 2013; 72: 1545-8.
36. Therimadasamy A, Peng YP, Putti TC, Wilder-Smith EP. Carpal tunnel syndrome caused by gouty tophus of the flexor tendons of the fingers: sonographic features. Journal of clinical ultrasound : JCU 2011; 39: 463-5.
37. Grainger R, Dalbeth N, Keen H, et al. Imaging as an Outcome Measure in Gout Studies: Report from the OMERACT Gout Working Group. J Rheumatol 2015; 42: 2460-4.
38. Ogdie A, Taylor WJ, Weatherall M, et al. Imaging modalities for the classification of gout: systematic literature review and meta-analysis. Annals of the rheumatic diseases 2015; 74: 1868-74.
39. Choi HK, Burns LC, Shojania K, et al. Dual energy CT in gout: a prospective validation study. Annals of the rheumatic diseases 2012; 71: 1466-71.
40. Jia E, Zhu J, Huang W, Chen X, Li J. Dual-energy computed tomography has limited diagnostic sensitivity for short-term gout. Clinical rheumatology 2018; 37: 773-777.
41. Baer AN, Kurano T, Thakur UJ, et al. Dual-energy computed tomography has limited sensitivity for non-tophaceous gout: a comparison study with tophaceous gout. BMC musculoskeletal disorders 2016; 17: 91.
42. Dalbeth N, House ME, Aati O, et al. Urate crystal deposition in asymptomatic hyperuricaemia and symptomatic gout: a dual energy CT study. Annals of the rheumatic diseases 2015; 74: 908-11.
43. Wang P, Smith SE, Garg R, et al. Identification of monosodium urate crystal deposits in patients with asymptomatic hyperuricemia using dual-energy CT. RMD open 2018; 4: e000593.
44. Chen J, Liao M, Zhang H, Zhu D. Diagnostic accuracy of dual-energy CT and ultrasound in gouty arthritis : A systematic review. Zeitschrift fur Rheumatologie 2017; 76: 723-729.
45. Wang Y, Deng X, Xu Y, Ji L, Zhang Z. Detection of uric acid crystal deposition by ultrasonography and dual-energy computed tomography: A cross-sectional study in patients with clinically diagnosed gout. Medicine 2018; 97: e12834.
46. Klauser AS, Halpern EJ, Strobl S, et al. Gout of hand and wrist: the value of US as compared with DECT. European radiology 2018; 28: 4174-4181.
47. Terslev L, Gutierrez M, Christensen R, et al. Assessing Elementary Lesions in Gout by Ultrasound: Results of an OMERACT Patient-based Agreement and Reliability Exercise. J Rheumatol 2015; 42: 2149-54.
48. Di Matteo A, Filippucci E, Cipolletta E, et al. Hip Involvement in Patients With Calcium Pyrophosphate Deposition Disease: Potential and Limits of Musculoskeletal Ultrasound. Arthritis care & research 2019; 71: 1671-1677.
49. Bayat S, Baraf HSB, Rech J. Update on imaging in gout: contrasting and comparing the role of dual-energy computed tomography to traditional diagnostic and monitoring techniques. Clinical and experimental rheumatology 2018; 36 Suppl 114: 53-60.
50. Cortellini A, Bozzetti F, Palumbo P, et al. Weighing the role of skeletal muscle mass and muscle density in cancer patients receiving PD-1/PD-L1 checkpoint inhibitors: a multicenter real-life study. Scientific reports 2020; 10: 1456.
51. Dalbeth N, Billington K, Doyle A, et al. Effects of Allopurinol Dose Escalation on Bone Erosion and Urate Volume in Gout: A Dual-Energy Computed Tomography Imaging Study Within a Randomized, Controlled Trial. Arthritis & rheumatology (Hoboken, N.J.) 2019; 71: 1739-1746.
52. Cipriani P, Ruscitti P, Carubbi F, Liakouli V, Giacomelli R. Methotrexate in rheumatoid arthritis: optimizing therapy among different formulations. Current and emerging paradigms. Clinical therapeutics 2014; 36: 427-35.
53. Giacomelli R, Gorla R, Trotta F, et al. Quality of life and unmet needs in patients with inflammatory arthropathies: results from the multicentre, observational RAPSODIA study. Rheumatology (Oxford, England) 2015; 54: 792-7.
54. Giacomelli R, Afeltra A, Alunno A, et al. Guidelines for biomarkers in autoimmune rheumatic diseases - evidence based analysis. Autoimmunity reviews 2019; 18: 93-106.
55. Giacomelli R, Ruscitti P, Shoenfeld Y. A comprehensive review on adult onset Still's disease. Journal of autoimmunity 2018; 93: 24-36.
56. Ruscitti P, Iacono D, Ciccia F, et al. Macrophage Activation Syndrome in Patients Affected by Adult-onset Still Disease: Analysis of Survival Rates and Predictive Factors in the Gruppo Italiano di Ricerca in Reumatologia Clinica e Sperimentale Cohort. J Rheumatol 2018; 45: 864-872.
57. Ruscitti P, Cipriani P, Ciccia F, et al. Prognostic factors of macrophage activation syndrome, at the time of diagnosis,

in adult patients affected by autoimmune disease: Analysis of 41 cases collected in 2 rheumatologic centers. Autoimmunity reviews 2017; 16: 16-21.
58. Cipriani P, Di Benedetto P, Ruscitti P, et al. Perivascular Cells in Diffuse Cutaneous Systemic Sclerosis Overexpress Activated ADAM12 and Are Involved in Myofibroblast Transdifferentiation and Development of Fibrosis. J Rheumatol 2016; 43: 1340-9.
59. Carotti M, Salaffi F, Di Carlo M, Giovagnoni A. Relationship between magnetic resonance imaging findings, radiological grading, psychological distress and pain in patients with symptomatic knee osteoarthritis. La Radiologia medica 2017; 122: 934-943.
60. Russo S, Lo Re G, Galia M, et al. Videofluorography swallow study of patients with systemic sclerosis. La Radiologia medica 2009; 114: 948-59.
61. Bruno F, Arrigoni F, Palumbo P, et al. New advances in MRI diagnosis of degenerative osteoarthropathy of the peripheral joints. La Radiologia medica 2019; 124: 1121-1127.
62. Arrigoni F, Napoli A, Bazzocchi A, et al. Magnetic-resonance- guided focused ultrasound treatment of non-spinal osteoid osteoma in children: multicentre experience. Pediatric radiology 2019; 49: 1209-1216.
63. Carrafiello G, Lagana D, Pellegrino C, et al. Ablation of painful metastatic bone tumors: a systematic review. International journal of surgery (London, England) 2008; 6 Suppl 1: S47- 52.
64. Barile A, Arrigoni F, Bruno F, et al. Present role and future perspectives of interventional radiology in the treatment of painful bone lesions. Future oncology (London, England) 2018; 14: 2945-2955.
65. Reginelli A, Silvestro G, Fontanella G, et al. Validation of DWI in assessment of radiotreated bone metastases in elderly patients. International journal of surgery (London, England) 2016; 33 Suppl 1: S148-53.
66. Finkenstaedt T, Manoliou A, Toniolo M, et al Gouty arthritis: the diagnostic and therapeutic impact of dual-energy CT. 2016 Eur Radiol:1–11
67. Araujo EG, Bayat S, Petsch C, et al. Tophus resolution with pegloticase: a prospective dual-energy CT study. RMD open 2015; 1: e000075

Received: 20 May 2020
Accepted: 10 June 2020
Correspondence:
Marina Carotti, MD
Department of Radiology – Division of Special and Pediatric Radiology, University Hospital "Umberto I – Lancisi –Salesi"-Universiy Politecnica Marche
Via Conca 71, 60126 Ancona, AN, Italy.
Tel. +39 071 5964085
Email: marina.carotti@gmail.com

Acta Biomed 2020; Vol. 91, Supplement 8: 125-135 DOI: 10.23750/abm.v91i8-S.9994

Review

Diagnostic and interventional management of infective spine diseases

Pierpaolo Palumbo[1], Federico Bruno[1], Francesco Arrigoni[1], Marcello Zappia[2], Anna Maria Ierardi[3], Giuseppe Guglielmi[4], Luigi Zugaro[5], Marina Carotti[6], Ernesto Di Cesare[7], Alessandra Splendiani[1], Luca Brunese[2], Carlo Masciocchi[1], Antonio Barile[1]

[1] Department of Biotechnology and Applied Clinical Sciences, University of L'Aquila, L'Aquila, Italy, [2] Department of Medicine and Health Sciences "V. Tiberio", University of Molise, Campobasso, Italy; [3] Radiology Department, Fondazione IRCCS Cà Granda, Ospedale Maggiore Policlinico, Milan, Italy; [4] Department of Clinical and Experimental Medicine, University of Foggia, Foggia, Italy; [5] Department of Emergency Radiology, San Salvatore Hospital, L'Aquila, Italy; [6] University Department of Radiology - Division of Special and Pediatric Radiology Hospital "Umberto I - Lancisi - Salesi", Ancona, Italy; [7] Department of Life, Health and Environmental Sciences, University of L'Aquila, L'Aquila, Italy

Summary. Spondylodiscitis (SD) is one of the main causes of back pain. Although the low mortality, high morbidity is related to spondilodiscitys, leading spine instability, chronic pain or neurological deficit. Diagnostic imaging plays a primary role in diagnosing spondylodiscitis. However different accuracy is highlighted by different diagnostic tool, depending also on timing of disease which represents a cardinal element for the phenotypic manifestation of the disease, beyond spatial resolution and tissue characterization proper of specific modality imaging. Conventional Radiology (CR), Computed Tomography (CT) and MRI (Magnetic Resonance Imaging) all have proven to be of primary importance in the approach to spondylodiscitis, although magnetic resonance imaging has demonstrated the greatest advantage in identifying the disease from its earliest stages, demonstrating high sensitivity and specificity (92% and 96%, respectively). This review focus on the role of different imaging modality in the approach to the spondylodiscitis, also addressing the role of interventional radiology that is pivotal not only for a diagnosis of certainty through biopsy, but also for a minimally-invasive treatment of paravertebral abscesses spondylodiscitis-related. (www.actabiomedica.it)

Keywords: spondylodiscitis, spine infection disease, MRI, CT, CR, interventional radiology

Introduction

Spondylodiscitis (SD) is one of the main causes of back pain (1-6). The relative low incidence (5-5.3/10^6 per year; M>F) is unfortunately increasing as a consequence of wide-spread chronic and degenerative spine pathologies, spinal surgery, use of immunosuppressive therapies, vascular device, or extensive use of intravenous substances of abuse (7-12). SD refers to an infection involving the vertebral bodies (spondylitis) and intervertebral disc (discitis). Though the low mortality (2-4%), SD is related to a high morbidity, leading to spine instability, chronic pain or neurological deficit (13).

Different pathogenic mechanics and pathogens are identified as responsible for SD. Hematogenous diffusion, contamination by contiguity or direct inoculation are the leading mechanism of SD. Hematogenous diffusion is the main cause of SD (60-80%), mainly via arteriosus system. Primary discitis is a typical mechanism of infection only in children due to the high vascularization of the disc, while vascular anas-

tomoses with the intradiscal vessels are involuted in adulthood. Direct inoculation is responsible for the 15-40% of cases, related mainly to spinal procedures, including the minimally invasive ones. Diffusion of the infection by contiguity from adjacent structures, such as abscesses or after aortic grafts, remains an infrequent cause (approximately 3%) (14).Pyogenic [S. aureus (60%), Enterobacter (30%), E. coli, Salmonella, Pseudomonas aeruginosa, Klebsiella pneumoniae (10%)] and granulomatous infection (m. tuberculosis, brucellosis) are differentiated, the latter less frequent. Pyogenic SD mainly involve the lumbar spine (58%), less frequent thoracic (30%) and cervical (11%) spine, reflecting their different vascularization; conversely, tuberculous SD primarily affect the thoracic spine, with an involvement of more than two levels often, a sign characteristic of tuberculous SD compared to the pyogenic ones.

Clinical considerations

Symptoms for SD are often non-specific, as laboratory testing generally used in clinical practice both for diagnosis and follow-up, which unfortunately show only a moderate diagnostic accuracy. Main symptom of SD is pain and, less frequent, fever. Non-specific pain occurs in 90% of cases, often as first symptom. Pain generally worsens during the night, often radiates to the abdomen, lower limbs, scrotum and perineum, and it could be exacerbated by movements (15). Fever can be present in 48% of patients with pyogenic spondylodiscitis and 17% of cases with tuberculous type. Neurological complications occur in approximately 12% of cases, related to spinal cord or nerve root compression, or meningitis. Paraspinal or epidural abscesses is found in 44% of cases of patient with neurological complications. White blood cell counts are often normal and can increase in 35% of patients without exceeding 12,000 cells / mm^3 (4). Erythrocyte Sedimentation Rate (ESR) and C-Reactive Protein (CRP) are sensitive markers with low specificity, although the latter is often considered the best marker for follow-up (16). Procalcitonin also is considered a highly specific and sensitive marker for the diagnosis and control of the effectiveness of the treatment, even higher than CRP. Blood cultures could be positive in approximately 50% of cases with hematogenous diffusion. Considering non-specificity of symptoms and laboratory testing, 2015 Infectious Diseases Society of America (IDSA) Clinical Practice Guidelines for the Diagnosis and Treatment of Native Vertebral Osteomyelitis in Adults outline specific consideration for a clinical suspicion of SD. Therefore, a progression of nuchal or back pain, or a back pain of recent onset with fever, increase in ESR and CRP and evidence of infection with hematogenous spread or endocarditis, is a strong recommendation for potential SD. Conversely, a patient with fever and neurological symptoms of recent onset, with or without pain, or a patient with nuchal or back pain of recent onset after a recent sepsis from S. aureus infection, is a weak recommendation (17).

Radiology in SD

Cross-sectional imaging (MRI, CT and CR) techniques, gained large application in standard practice, also on spine pathologies (18-26). Diagnostic imaging plays therefore a primary role in diagnosing of spondylodiscitis, advised MRI, CT and CR as first line techniques in the diagnosis, staging and follow-up. However, different techniques have an obvious different capability in detecting specific alteration SD-related. Moreover, timing of the disease represents a cardinal element for the phenotypic manifestation of the disease and thus consequently for the different techniques to detect specific SD findings.

Conventional Radiology (CR)

Conventional radiology is a low sensitive and specific technique (82% and 57%, respectively) (27) especially in the early diagnosis of spondylodiscitis, although conventional x-ray is often used for the first approach to the back pain. Notably, conventional radiology is capable in identifying later bone alterations which can occur from 3-6 weeks after the infection, as subchondral erosion, that is considered the first identifiable CR sign (15). With the progression of disease, some alterations become more evident, with possible fragmentation or erosion of the anterior angle of the

vertebral plate, reduction of intervertebral space, loss of physiological lordosis and structural deformity. Later manifestation (about 8-12 weeks after) include reactive sclerosis and bony bridge formation between different soma. In case of effective treatment, the fusion of the vertebral bodies can be appreciated, while in case of ineffective treatment, a complete somatic collapse can occur (fig. 1).

Computed Tomography (CT)

CT also is insensitive in detecting early SD alteration. More of SD-related CT-findings occur after 2 weeks from infection, and they could be identified in about one half of the patients. CT, indeed, could be useful mainly in identifying, describing and estimating the extension of osteolysis, or in showing an involvement of paravertebral tissue with a thickening of adipose tis-

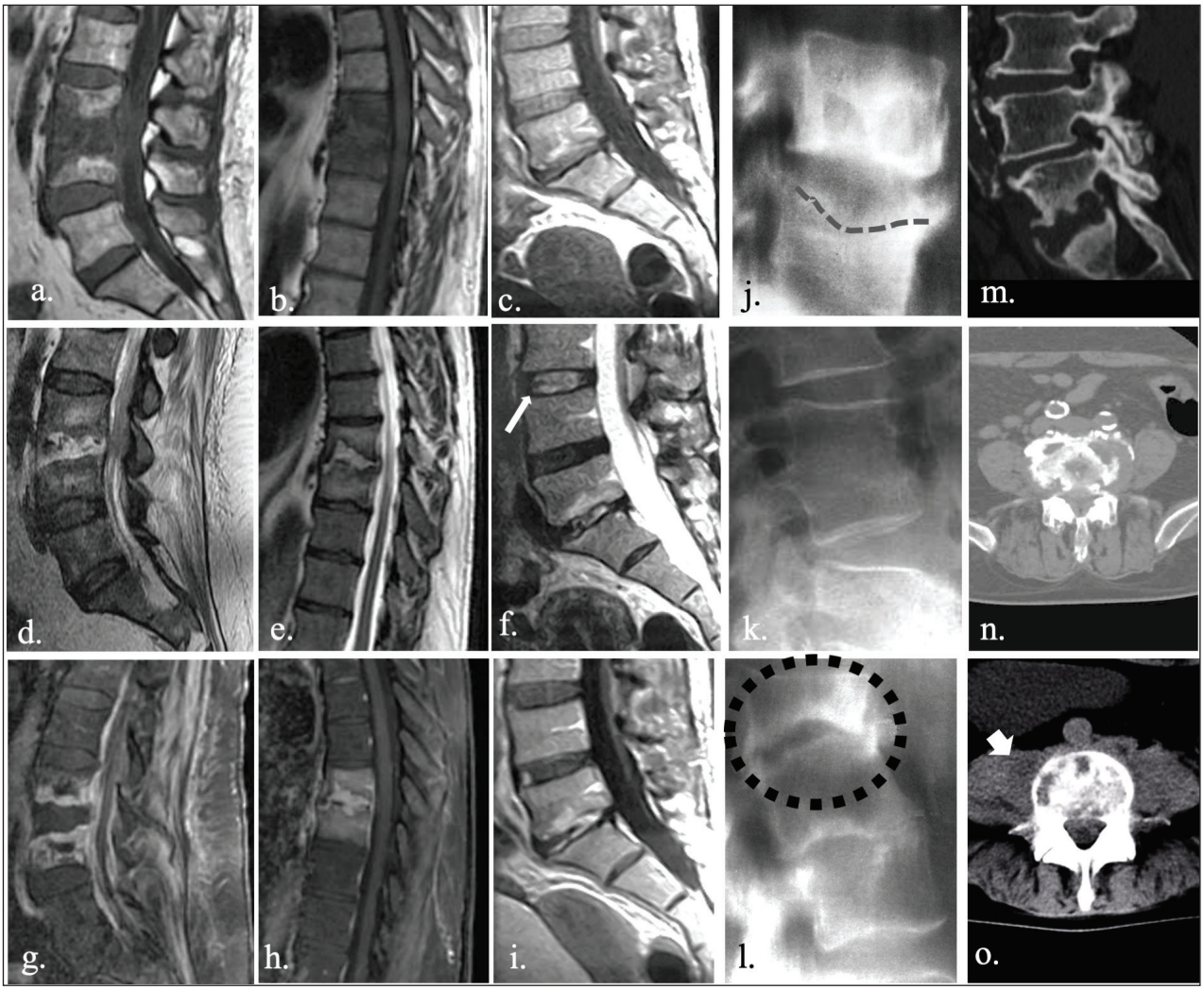

Figure 1. MRI is an accurate tool in diagnosing spondylodyscitis. Typical presentation includes low T1 (a., b., c.) and high T2 (d., e., f.) signal intensity involving both disc and vertebral endplate. Structural alterations within the disc allow for a loss of typical intranuclear cleft (f., white arrow), which represents normal fibrous tissue within the nucleus polposus. Post-inflammatory vascularization and granulomatous tissue could be responsible for a sever enhancement after injection of contrast media (g., h., i.). Conversly, CR and CT are insensitive especially in the early stages of the infection. First CR sign is represented by subchondral erosion (j., dashed line), observable from 3-6 weeks after the infection. Fusion of vertebral bodies (k.) or complete somatic collapse (l., blak dots) could be observed in later stages, in case of effective or ineffective treatment, respectively. CT could be useful mainly in estimating the entity of osteolysis (m., n.), allowing also to evaluate the extension to perivertebral tissue (o. large arrow).

sue. However, CT contribution within the diagnostic process is very poor and its role is mainly limited to a preoperative planning of spinal procedures or as an alternative in case of contraindication to MRI (14)(fig. 1).

Magnetic Resonance Imaging (MRI)

MRI, thanks to its excellent soft tissue contrast and multiplanar capability, is the primary imaging tool for a variety of conditions and diseases both for diagnostic and interventional purpose, especially in the neuroradiological field (28-33). Currently, MRI is the gold standard in the diagnosis of SD, with a high sensitivity and specificity (92% and 96%, respectively) especially in the early stages of diseases due to the excellent tissue characterization and ability in identifying bone edema and areas with anomalous vascularization (7, 27). Bone edema, indeed, is observed since the early phase of disease which is characterized by infiltration of inflammatory cells and thus by an increase of extracellular space. Increase in water content determines low T1-signal intensity of bone tissue and hyperintensity on T2-weighted sequences; moreover, highly water content within the disc is responsible for the loss a typical disc appearance known as "intranuclear" cleft (13)(fig.1). Some authors suggest also high accuracy of high T2 signal intensity of psoas muscles as very-early sign of lumbar SD (34). Moreover, enhancement of disco-somatic structures can be observed in response to inflammatory alterations, potentially extended to adjacent structures. MRI shows high accuracy also in identifying later or post-infection alterations which include replacement of necrotized tissue with vascularized fibrous tissue, yellow marrow transformation, subchondral fibrosis and osteosclerosis.

Since etiologic characterization of SD is crucial for an adequate treatment, MRI could offer some advantages especially in differentiating between non-pyogenic forms (e.g., tubercular or brucellosis SD).

Differential diagnosis

Other conditions can mimic SD radiological feature and symptomatology. Osteochondritis, also known as discovertebritis or aseptic spondylodiscitis, is one of the great mimes of SD. Modic I or vascular pattern, indeed, often observed in presence of degenerative alteration of spine, is characterized by bony inflammation with low T1 and high T2 signal intensity of endplates, similar to SD (7)(fig. 2). Though disc alterations often permit an adequate differentiation,

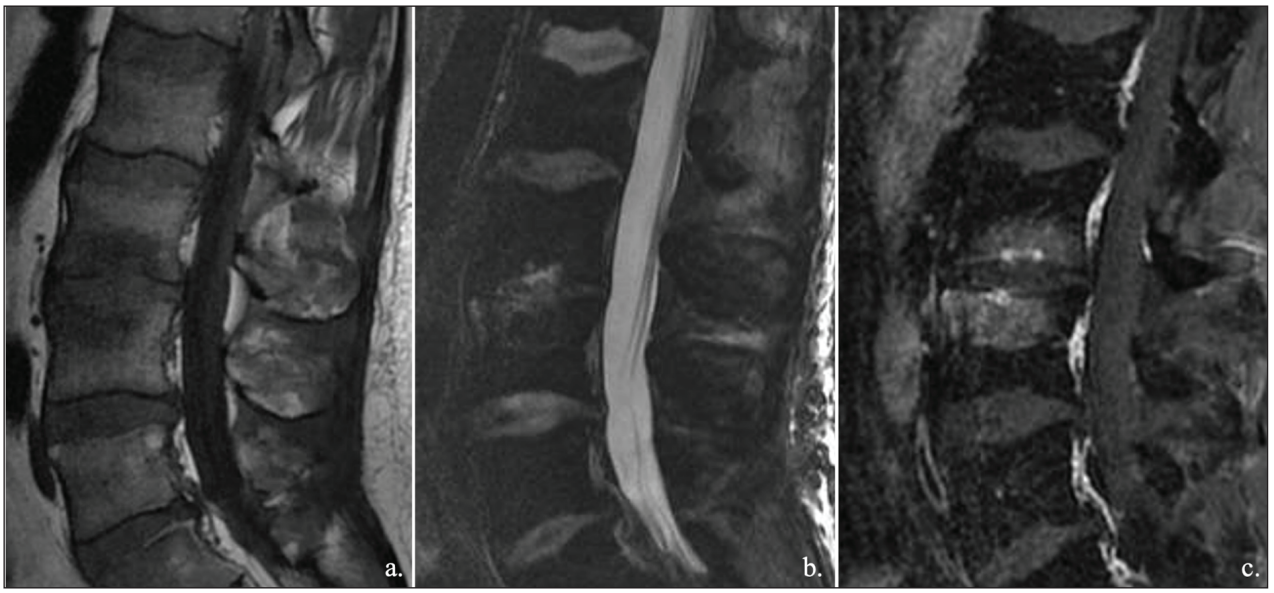

Figure 2. Osteochondritis, also known as discovertebritis or aseptic spondylodiscitis, is one of the great mimes of spondylodyscitis. Inflammation mainly involved the vertebral endplates, with increase in water content and vascular granulation tissue, and consequently bone edema. Intervetebral disc often is degenerated.

sometime the two forms are overlapped, especially between symptomatic forms, and biopsy remain the main discriminator. Although the poor representation of anatomical details, 18-FDG PET, also as hybrid methods (PET/MRI, mainly) has shown high efficacy in differentiating between degenerative and infectious disease. PET technique, indeed, has shown a good correlation with histological finding of infection severity and with the involvement of extraspinal structures (7). CRMO (Chronic Recurrent Multifocal Osteomyelitis) also has to be considered for a proper differential diagnosis of SD. CRMO is a migrant forms characterized by litic lesion with a well-defined sclerotic hem. CRMO often involves different soma with bone edema and vertebral collapse. Spinal involvement is not so rare in CRMO (35)(fig. 3).

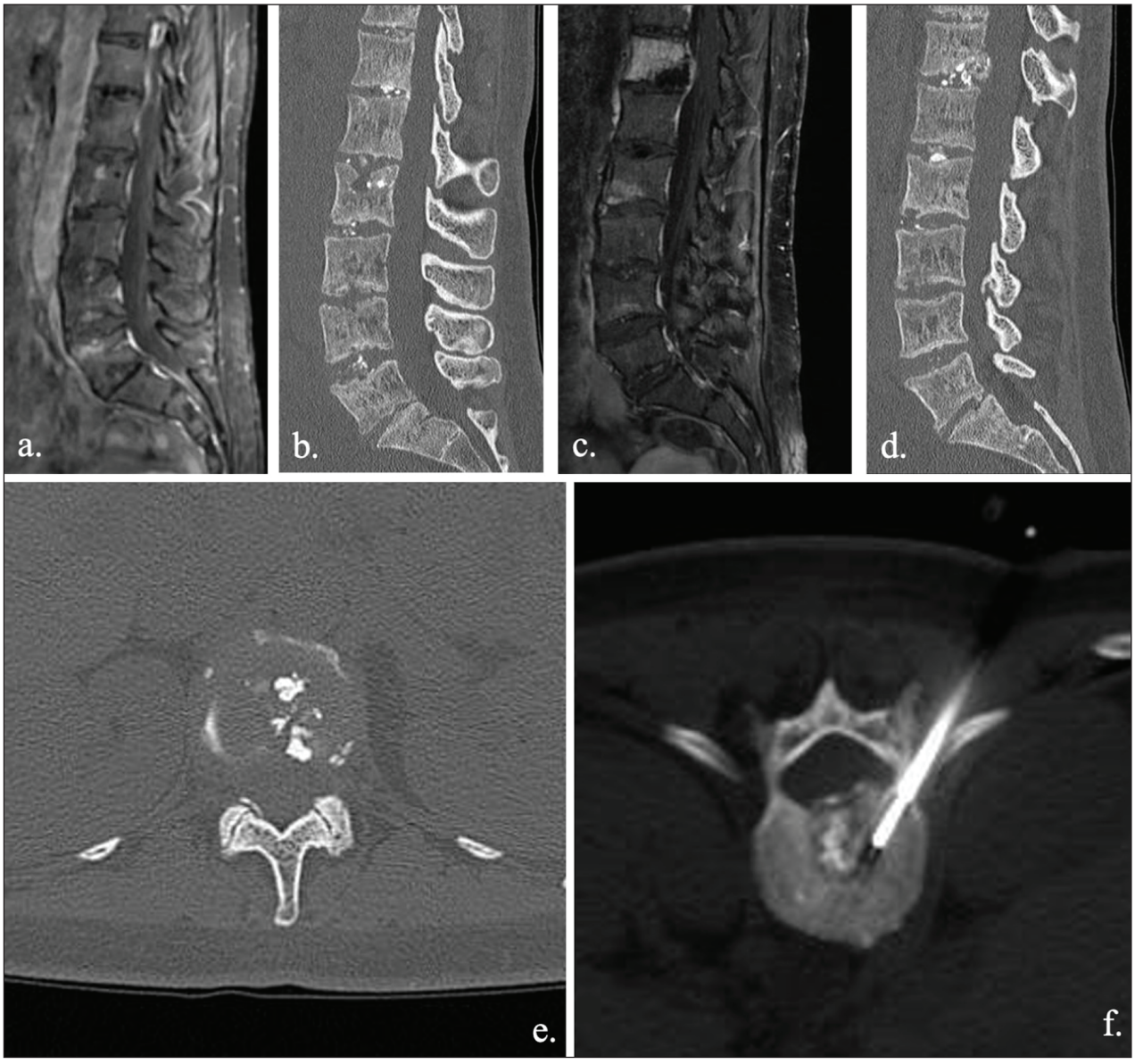

Figure 3. Spinal involvement in CMRO is rare. Migrant erosion involved different soma with bone edema and vertebral collapse. Radiological evolution can occur within few months (a.-b. diagnostic imaging acquired in March; c.-d. diagnostic imaging acquired in July), with a rapid worsening of clinical status mainly related to severe pain. Bone biopsy (e., f.,) is commonly required in CMRO in order to exclude infection, neoplasia or histiocytosis, since the diagnosis of CRMO is made by exclusion.

Biopsy

Multidisciplinary approach has high sensitivity and specificity in detecting SD. However, identification of the specific pathogen remains the key point for a proper treatment and thus for setting up an adequate antibiotic therapy, especially for atypical or tuberculous pathogens (36). In this regard, blood cultures have a limited role, because of only the 50% of cases results positive if an hematogenous spread, other that they do not always correlate with the pathogen found at site of infection. For these reasons, biopsy plays a crucial role in the etiological diagnosis of SD. Open and percutaneous techniques could be performed, with a higher prevalence for the percutaneous one although the high variability showed in literature, ranging from 36% to 91% (37). CT-guided biopsy is the most performed percutaneous technique, indicated as soon as possible in patients with no neurological deficits, instability/deformity or sepsis. Otherwise, the surgery approach is recommended. Empirical antibiotic therapy is recommended only in high risk patients as with sepsis or medullar compression, neutropenia or in a neurologically compromised patient. A double specimen should be taken for cultural and histologic examinations. If coltural examination is of prior importance for the identification of the specific pathogen, histologic examination could be useful for distinguishing granulomatous forms (38). Potential complications of CT-guided biopsy are vascular or nervous damage, hematoma or non-target biopsy. In order to limit time and radiation dose exposure of procedure and avoid non-target region, lately CT navigation with volumetric acquisition has shown high advantages (39, 40). Specimen could be taken from bone or discal region, with costo-vertebral or transpeduncolar access depending on different thoracic or lumbar target respectively, or instead from paravertebral tissue if involved (fig. 4). Several reasons are responsible for high variability of percutaneous biopsies, as inadequate specimen or representation of pathogen within the specimen, or when an empirical therapy is administered before the biopsy. However, in patient with a non-diagnostic specimen, a second biopsy is recommended when other contraindication are absent.

As mentioned, the main indication to the "open" biopsy is the presence of severe neurological deficits due to structural damage. Open technique should be recommended also after a second inadequate percutaneous attempt, without further improvement after antibiotic therapy, or when the percutaneous technique is technically contraindicated. The "open" technique has shown an efficacy of about 75%, especially in the diagnosis of lumbar forms. However, diagnostic yield of open technique drops to similar percutaneous technique validity after empirical antibiotic therapy.

Treatment

Goals of the treatment in SD are eradication of the infection, stabilization of spine and recovery of potential neurological deficits. Although no standard therapeutic approach are defined, antibiotic therapy, immobilization of the spine and spinal decompression are of great importance for an effective treatment that allows a complete recovery. Generally, conservative and surgical therapies could be considered. Conservative therapy is often the primary option especially for elderly patients or in patients with a physical decay (41). Antibiotic strategies mainly depend on specific etiological definition. As a general rule, it is advisable to administer intravenous antibiotics for at least 2/4 weeks to improve bioavailability, although the treatment should be more prolonged in high risk patients. Therapy for tuberculous spondylodiscitis should be carried out for at least 18-24 months to allow a complete healing and avoid recurrence. Broad-spectrum antibiotic therapy should be considered in patients with sepsis or fulminant SD. Conversely, surgical approach aims to physically remove the septic focus, allowing also the collection of samples for microbiological testing. Primary advantage offered by surgical approach is the spinal decompression in case medullar extension with stabilization and recovery of the infected column segment. Compared to conservative therapy, this approach allows for safer and faster treatment, with earlier mobilization (42). Recently, new scoring system has been developed to simplify decisional algorithm in order to identify when surgical intervention may be required (43).

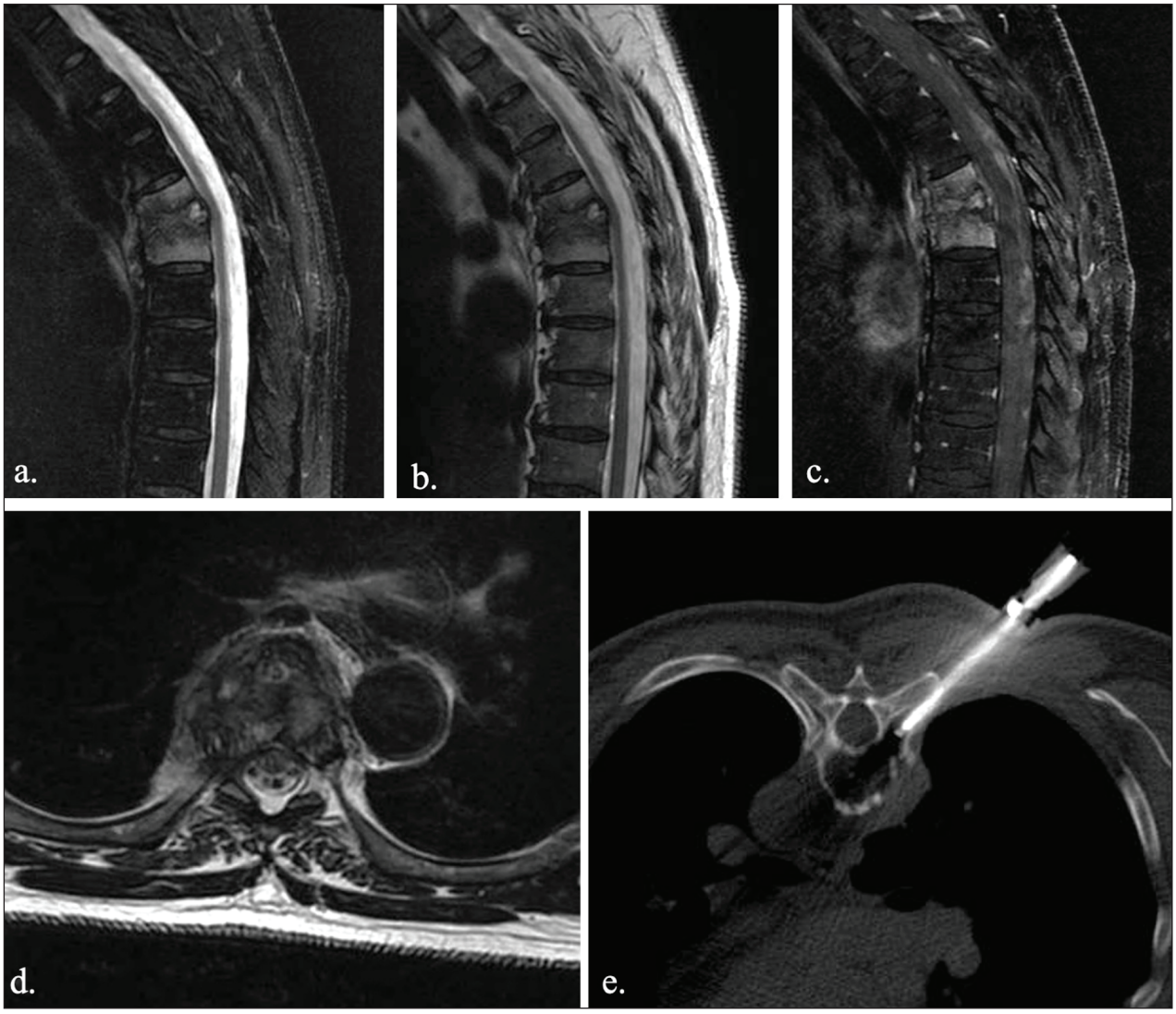

Figure 4. Bone biopsy plays a crucial role in the etiological diagnosis of spondylodyscitis. CT-guided biopsy is the most performed percutaneous technique. MRI shows thoracic spondylodyscitis (a., b., c.). A costo-vertebral approach (e.) was preferred in thoracic spine biopsy

Interventional radiology

The interventional radiology plays a key role both in diagnosing and treatment also in SD (44-45).

As mentioned CT-guided biopsy are considered of primary importance in the clinical setting of SD patients. CT, indeed, is a valuable diagnostic tool for the diagnosis and the guidance of interventional procedures in a wide range of organs (46-51). Moreover, interventional approach is of primary importance also for the treatment of psoas muscle abscess, which is a potentially life-threatening infection. Mortality rate in psoas pyogenic abscess ranges from 50% to 100%. Death is usually due to inadequate / delayed treatment, with mortality close to 100% in septic patients. In the acute phase, in the presence of psoas muscle abscess, this procedure has the purpose of draining the collection and possibly injecting local antibiotic. When the abscess is drained, the patient's pain gradually decreases as the pressure inside the collection decreases with consequent relief of the symptoms. The procedure is performed with aseptic precautions under local anesthesia with the patient usually in a prone position, performed with a CT or a US guide. Contraindica-

tions for percutaneous treatment are represented by coagulopathies and lack of patient's collaboration (52).

Follow-up

The 2015 the American Society of Infectious Diseases (IDSA) guidelines suggest that persistent pain, residual neurological deficits, unchanged or increased inflammation markers and radiographic findings do not necessarily indicate a failure of therapy (17). MRI is not recommended routinely and should not be performed in the follow-up of patients with good clinical-laboratory response, since CRP values have been shown to improve in patients with vertebral infection and are closely related to the clinic. Moreover, MR-signs of inflammation, included post-contrastographic enhancement, could be detected after several time after the infection, even in case of effective therapy (53). In the case of clinical suspicion of treatment failure, systemic follow-up of markers and MRI are recommended to confirm the suspicion and highlights the presence of abscesses or column instability that could benefit from specific treatments. Particular attention during the follow-up of MRI must be paid to the paravertebral and epidural tissues, for possible involvement and therefore progression of the pathology. CT and MRI can highlight severe forms of non-typical inflammation, involvement of two discs or paravertebral extension. CT, compared to MRI, can be useful in distinguishing advanced stages in which bone destruction can be achieved (54).

Conclusion

Multidisciplinary approach is of primary importance in diagnosis and intervention of traumatic, tumoral and infectious MSK diseases (55-59). MRI plays a primary role in diagnosing spondylodiscitis with a high sensitivity and specificity. However, the biopsy currently represents the ultimate diagnostic level, essential for the identification of the specific pathogen responsible of the infection and thus for the setting of a specific therapeutic strategy. MRI is recommended during the follow only with clinical and laboratory findings indicative of ineffective treatment or neurological complication.

Conflict of interest: Authors declare that they have no commercial associations (e.g. consultancies, stock ownership, equity interest, patent/licensing arrangement etc.) that might pose a conflict of interest in connection with the submitted article.

References

1. Bruno F, Smaldone F, Varrassi M, et al. MRI findings in lumbar spine following O2-O3 chemiodiscolysis: A long-term followup. Interv Neuroradiol 2017; 23: 444-50.
2. Splendiani A, Bruno F, Patriarca L, et al. Thoracic spine trauma: advanced imaging modality. Radiol Med 2016; 121: 780-92.
3. Perri M, Grattacaso G, di Tunno V, et al. T2 shine-through phenomena in diffusion-weighted MR imaging of lumbar discs after oxygen-ozone discolysis: a randomized, double-blind trial with steroid and O2-O3 discolysis versus steroid only. Radiol Med 2015; 120: 941-50.
4. Michelini G, Corridore A, Torlone S, et al. Dynamic MRI in the evaluation of the spine: state of the art. Acta Biomed 2018; 89: 89-101.
5. Bruno F, Palumbo P, Tommasino E, et al. Evaluation of intervertebral disc using T2 mapping sequences in patients undergoing O2-O3 chemiodiscolysis: an instrumental study with clinical correlation. Neuroradiology 2020; 62: 55-61.
6. Splendiani A, Bruno F, Marsecano C, et al. Modic I changes size increase from supine to standing MRI correlates with increase in pain intensity in standing position: uncovering the "biomechanical stress" and "active discopathy" theories in low back pain. Eur Spine J 2019; 28: 983-92.
7. Fahnert J, Purz S, Jarvers JS, et al. Use of Simultaneous 18FFDG PET/MRI for the Detection of Spondylodiskitis. J Nucl Med 2016; 57: 1396-401.
8. Cipriani P, Berardicurti O, Masedu F, et al. Biologic therapies and infections in the daily practice of three Italian rheumatologic units: a prospective, observational study. Clin Rheumatol 2017; 36: 251-60.
9. Giacomelli R, Afeltra A, Alunno A, et al. Guidelines for biomarkers in autoimmune rheumatic diseases - evidence based analysis. Autoimmun Rev 2019; 18: 93-106.
10. Giacomelli R, Liakouli V, Berardicurti O, et al. Interstitial lung disease in systemic sclerosis: current and future treatment. Rheumatol Int 2017; 37: 853-63.
11. Cipriani P, Di Benedetto P, Ruscitti P, et al. Perivascular Cells in Diffuse Cutaneous Systemic Sclerosis Overexpress Activated ADAM12 and Are Involved in Myofibroblast Transdifferentiation and Development of Fibrosis. J Rheumatol 2016; 43: 1340-9.
12. Salaffi F, Carotti M, Di Carlo M, Farah S, Gutierrez M. Adherence to Anti-Tumor Necrosis Factor Therapy Administered Subcutaneously and Associated Factors in Patients With Rheumatoid Arthritis. J Clin Rheumatol 2015; 21: 419-25.
13. Duarte RM, Vaccaro AR. Spinal infection: state of the art and management algorithm. Eur Spine J 2013; 22: 2787-99.

14. Sans N, Faruch M, Lapegue F, Ponsot A, Chiavassa H, Railhac JJ. Infections of the spinal column--spondylodiscitis. Diagn Interv Imaging 2012; 93: 520-9.
15. Skaf GS, Domloj NT, Fehlings MG, et al. Pyogenic spondylodiscitis: an overview. J Infect Public Health 2010; 3: 5-16.
16. Gouliouris T, Aliyu SH, Brown NM. Spondylodiscitis: update on diagnosis and management. J Antimicrob Chemother 2010; 65 Suppl 3: iii11-24.
17. Berbari EF, Kanj SS, Kowalski TJ, et al. Executive Summary: 2015 Infectious Diseases Society of America (IDSA) Clinical Practice Guidelines for the Diagnosis and Treatment of Native Vertebral Osteomyelitis in Adults. Clin Infect Dis 2015; 61: 859-63.
18. Reginelli A, Silvestro G, Fontanella G, et al. Validation of DWI in assessment of radiotreated bone metastases in elderly patients. Int J Surg 2016; 33 Suppl 1: S148-53.
19. Bruno F, Arrigoni F, Palumbo P, et al. New advances in MRI diagnosis of degenerative osteoarthropathy of the peripheral joints. Radiol Med 2019; 124: 1121-1127
20. Bruno F, Arrigoni F, Palumbo P, et al. The Acutely Injured Wrist. Radiol Clin North Am 2019; 57: 943-55
21. D'Orazio F, Splendiani A, Gallucci M. 320-Row Detector Dynamic 4D-CTA for the Assessment of Brain and Spinal Cord Vascular Shunting Malformations. A Technical Note. Neuroradiol J 2014; 27: 710-7
22. Mariani S, La Marra A, Arrigoni F, et al. Dynamic measurement of patello-femoral joint alignment using weight-bearing magnetic resonance imaging (WB-MRI). European journal of radiology 2015; 84: 2571-8
23. Splendiani A, D'Orazio F, Patriarca L, et al. Imaging of postoperative spine in intervertebral disc pathology. Musculoskelet Surg 2017; 101: 75-84
24. Agostini A, Mari A, Lanza C, et al. Trends in radiation dose and image quality for pediatric patients with a multidetector CT and a third-generation dual-source dual-energy CT. Radiol Med 2019; 124: 745-52
25. Zappia M, Maggialetti N, Natella R, et al. Diagnostic imaging: pitfalls in rheumatology. Radiol Med 2019; 124: 1167-74.
26. Salaffi F, Carotti M, Bosello S, et al. Computer-aided quantification of interstitial lung disease from high resolution computed tomography images in systemic sclerosis: correlation with visual reader-based score and physiologic tests. Biomed Res Int 2015; 2015: 834262.
27. Herren C, Jung N, Pishnamaz M, Breuninger M, Siewe J, Sobottke R. Spondylodiscitis: Diagnosis and Treatment Options. Dtsch Arztebl Int 2017; 114: 875-82.
28. Carotti M, Salaffi F, Di Carlo M, Giovagnoni A. Relationship between magnetic resonance imaging findings, radiological grading, psychological distress and pain in patients with symptomatic knee osteoarthritis. Radiol Med 2017; 122: 934-43.
29. De Filippo M, Pesce A, Barile A, et al. Imaging of postoperative shoulder instability. Musculoskelet Surg 2017; 101: 15-22.
30. Pogliacomi F, De Filippo M, Paraskevopoulos A, Alesci M, Marenghi P, Ceccarelli F. Mini-incision direct lateral approach versus anterior mini-invasive approach in total hip replacement: results 1 year after surgery. Acta Biomed 2012; 83: 114-21.
31. Zoccali C, Arrigoni F, Mariani S, Bruno F, Barile A, Masciocchi C. An unusual localization of chondroblastoma: The triradiate cartilage; from a case report a reconstructive technique proposal with imaging evolution. J Clin Orthop Trauma 2017; 8: S48-s52.
32. Masciocchi C, Arrigoni F, La Marra A, Mariani S, Zugaro L, Barile A. Treatment of focal benign lesions of the bone: MRg- FUS and RFA. Br J Radiol 2016; 89: 20150356.
33. Di Pietto F, Chianca V, de Ritis R, et al. Postoperative imaging in arthroscopic hip surgery. Musculoskelet Surg 2017; 101: 43-49.
34. Ledbetter LN, Salzman KL, Shah LM. Imaging Psoas Sign in Lumbar Spinal Infections: Evaluation of Diagnostic Accuracy and Comparison with Established Imaging Characteristics. AJNR Am J Neuroradiol 2016; 37: 736-41.
35. Hospach T, Langendoerfer M, von Kalle T, Maier J, Dannecker GE. Spinal involvement in chronic recurrent multifocal osteomyelitis (CRMO) in childhood and effect of pamidronate. Eur J Pediatr 2010; 169: 1105-11.
36. Spira D, Germann T, Lehner B, et al. CT-Guided Biopsy in Suspected Spondylodiscitis--The Association of Paravertebral Inflammation with Microbial Pathogen Detection. PLoS One 2016; 11: e0146399.
37. Nam KH, Song GS, Han IH, Choi BK, Cha SH. Diagnostic Value of Biopsy Techniques in Lumbar Spondylodiscitis: Percutaneous Needle Biopsy and Open Biopsy. Korean J Spine 2011; 8: 267-71.
38. Michel SC, Pfirrmann CW, Boos N, Hodler J. CT-guided core biopsy of subchondral bone and intervertebral space in suspected spondylodiskitis. AJR Am J Roentgenol 2006; 186: 977-80.
39. Carrafiello G, Fontana F, Mangini M, et al. Initial experience with percutaneous biopsies of bone lesions using XperGuide cone-beam CT (CBCT): technical note. Radiol Med 2012; 117: 1386-97.
40. Carrafiello G, Lagana D, Nosari AM, et al. Utility of computed tomography (CT) and of fine needle aspiration biopsy (FNAB) in early diagnosis of fungal pulmonary infections. Study of infections from filamentous fungi in haematologically immunodeficient patients. Radiol Med 2006; 111: 33-41.
41. Zarghooni K, Rollinghoff M, Sobottke R, Eysel P. Treatment of spondylodiscitis. Int Orthop 2012; 36: 405-11.
42. Homagk L, Homagk N, Klauss JR, Roehl K, Hofmann GO, Marmelstein D. Spondylodiscitis severity code: scoring system for the classification and treatment of non-specific spondylodiscitis. Eur Spine J 2016; 25: 1012-20.
43. Appalanaidu N, Shafafy R, Gee C, et al. Predicting the need for surgical intervention in patients with spondylodiscitis: the Brighton Spondylodiscitis Score (BSDS). Eur Spine J 2019; 28: 751-61.
44. Ierardi AM, Piacentino F, Fontana F, et al. The role of endo-

vascular treatment of pelvic fracture bleeding in emergency settings. Eur Radiol 2015; 25: 1854-64.
45. Arrigoni F, Napoli A, Bazzocchi A, et al. Magnetic-resonance- guided focused ultrasound treatment of non-spinal osteoid osteoma in children: multicentre experience. Pediatric radiology 2019; 49: 1209-1216
46. Lagana D, Carrafiello G, Mangini M, et al. Indications for the use of the Amplatzer vascular plug in interventional radiology. Radiol Med 2008; 113: 707-18.
47. Carrafiello G, Lagana D, Pellegrino C, et al. Ablation of painful metastatic bone tumors: a systematic review. Int J Surg 2008; 6 Suppl 1: S47-52.
48. Carrafiello G, Piffaretti G, Lagana D, et al. Endovascular treatment of ruptured abdominal aortic aneurysms: aorto-uni-iliac or bifurcated endograft? Radiol Med 2012; 117: 410-25.
49. Carrafiello G, Mangini M, Fontana F, et al. Suprarenal inferior vena cava filter implantation. Radiol Med 2012; 117: 1190-8.
50. Carrafiello G, Ierardi AM, Duka E, et al. Usefulness of Cone- Beam Computed Tomography and Automatic Vessel Detection Software in Emergency Transarterial Embolization. Cardiovasc Intervent Radiol 2016; 39: 530-7.
51. Cazzato RL, Arrigoni F, Boatta E, et al. Percutaneous management of bone metastases: state of the art, interventional strategies and joint position statement of the Italian College of MSK Radiology (ICoMSKR) and the Italian College of Interventional Radiology (ICIR). Radiol Med 2019; 124: 34-49.
52. Arrigoni F, Bruno F, Zugaro L, et al. Developments in the management of bone metastases with interventional radiology. Acta Biomed 2018; 89: 166-74.
53. Dave BR, Kurupati RB, Shah D, Degulamadi D, Borgohain N, Krishnan A. Outcome of percutaneous continuous drainage of psoas abscess: A clinically guided technique. Indian J Orthop 2014; 48: 67-73.
54. Cottle L, Riordan T. Infectious spondylodiscitis. J Infect 2008; 56: 401-12.
55. Foreman SC, Schwaiger BJ, Meyer B, et al. Computed Tomography and Magnetic Resonance Imaging Parameters Associated with Poor Clinical Outcome in Spondylodiscitis. World Neurosurg 2017; 104: 919-26 e2.
56. Barile A, Conti L, Lanni G, Calvisi V, Masciocchi C. Evaluation of medial meniscus tears and meniscal stability: weightbearing MRI vs arthroscopy. Eur J Radiol 2013; 82: 633-9.
57. Ruscitti P, Cipriani P, Liakouli V, et al. Subclinical and clinical atherosclerosis in rheumatoid arthritis: results from the 3-year, multicentre, prospective, observational GIRRCS (Gruppo Italiano di Ricerca in Reumatologia Clinica e Sperimentale) study. Arthritis research & therapy 2019; 21: 204.
58. Ruscitti P, Cipriani P, Masedu F, et al. Increased Cardiovascular Events and Subclinical Atherosclerosis in Rheumatoid Arthritis Patients: 1 Year Prospective Single Centre Study. PloS one 2017; 12: e0170108.
59. Zappia M, Castagna A, Barile A, Chianca V, Brunese L, Pouliart N. Imaging of the coracoglenoid ligament: a third ligament in the rotator interval of the shoulder. Skeletal radiology 2017; 46: 1101-1111.

Received: 20 May 2020
Accepted: 10 June 2020
Correspondence:
Pierpaolo Palumbo
Department of Biotechnology and Applied Clinical Sciences, University of L'Aquila, L'Aquila, Italy
Via Vetoio, 1 – 67100 – L'Aquila, Italy
E-mail: palumbopierpaolo89@gmail.com

Acta Biomed 2020; Vol. 91, Supplement 8: 136-144 DOI: 10.23750/abm.v91i8-S.9976

Review

Diagnosis and management of intralabyrinthine schwannoma: case series and review of the literature

Antonella Miriam Di Lullo[1,2], Aldo Paolucci[3] ,Sergio Motta[1], Elena Cantone[1], Emiliano Barbieri[4], Domenico Cicala[5], Roberta Grassi[6], Federico Bruno[7], Alessandra Splendiani[7], Fabio Tortora[8], Michele Cavaliere[1], Luca Brunese[4]

[1]Department of Neuroscience, Reproductive and Odontostomatologic Sciences, University of Naples "Federico II", Naples, Italy; [2]CEINGE- Advanced Biotechnology, Naples, Italy; [3]Ospedale Maggiore Policlinico Milano, Milan, Italy; [4]Department of Medicine and Health Sciences "V. Tiberio", University of Molise, Campobasso, Italy; [5]Department of Neurosciences, "Santobono-Pausilipon" Pediatric Hospital, Naples, Italy; [6]Department of Precision Medicine, University of Campania Luigi Vanvitelli, Naples, Italy; [7]Department of Biotechnological and Applied Clinical Sciences, University of L'Aquila, L'Aquila,Italy; [8]Department of Advanced Biomedical Sciences, University of Naples "Federico II", Naples, Italy

Summary. Intralabyrinthine schwannoma (ILS) is a rare benign tumor affecting cochlear and vestibular nerves, whose symptoms are generally unspecific and frequently responsible for a late diagnosis. Radiological examinations, with particular reference to magnetic resonance imaging (MRI), represent the only diagnostic technique to identify ILS. On computed tomography ILS can only be indirectly suspected by the presence of surrounding bone remodeling, whereas MRI provides direct visualization of the neoplasm as a filling defect within the labyrinth with vivid contrast enhancement. At the same time, MRI is also helpful in defining ILS anatomical extension into adjacent structures and in planning therapeutic management. Here we report three representative cases of ILS with new pictorial imaging features to improve ILS early detection and optimize subsequent therapeutic management. (www.actabiomedica.it)

Keywords: Schwannoma, Labyrinth, Magnetic Resonance Imaging, Differential Diagnosis

Introduction

Intralabyrinthine schwannoma (ILS) was first described by Meter in 1917 as a rare benign tumor, affecting cochlear and vestibular nerves (1). Most tumors show a modification in intracellular pathways (2-8). It can variably involve vestibule, cochlea, or semi-circular canals (9). Its symptoms are generally unspecific due to the slow growth pattern, frequently causing a late diagnosis. In most cases, it occurs with unilateral progressive sensorineural hearing loss (95%); more inconstant symptoms include tinnitus (51%), imbalance (35%), vertigo (22%), or fullness (2%), alone or in combination (1, 10). Magnetic Resonance Imaging (MRI) and Computed Tomography (CT) are the primary imaging tool for a variety of conditions and diseases, both for diagnostic and interventional purposes, especially in the neuroradiological field (11,12).

The most common differential diagnoses include Menière's disease and vestibular neuritis (1), and neuroradiological investigation with magnetic resonance imaging (MRI) (13-18) represents the reference method to identify ILS diagnostic features.

CT imaging, indeed, could only raise the suspicion of ILS in the case of surrounding bone remodeling. Conversely, MRI shows a filling defect within the labyrinth with relatively high signal on T1w images, low signal on T2w, and vivid contrast enhancement

after contrast media administration. MRI is also helpful in defining ILS anatomical epicenter and extension into adjacent structures, as well as in planning therapeutic management (16, 19, 20). Here we report three representative cases with striking imaging features to improve ILS early diagnosis and optimize therapeutic management. All patients had written informed consent, and all the performed procedures were by the 1964 Helsinki declaration and its later Amendments.

Materials And Methods

A 29-year-old woman came to our observation for the first episode of subjective vertigo; she also complained about right-sided tinnitus and hearing loss in the last year. A previous audiometric examination had revealed right fluctuating sensorineural hearing loss with modest pan-tonal hypoacusia, classified ad suspected for Meniere's disease for which she was administered Betaistina 24mg/2die. ENT showed normal otoscopic findings, whereas audiometry revealed a worsening of the known sensorineural hearing loss for acute frequencies (moderate-to-severe), still limited to the right side (**Figure 1A**). An oral exam showed a right-sided slight reduction in detection threshold and alteration in word discrimination (15). Tympanogram was Type A bilaterally, while vestibular examination revealed a deficit on the right ear at Head Impulse Test (HIT). Contrast-enhanced MRI scan of the temporal bone was therefore performed, showing a small mass within the proper vestibule, reducing the regular representation of endocochlear fluids (**Figure 1B**). Homogeneous and intense enhancement was observed after contrast media administration (**Figure 1C**); thus the suspicion of ILS was raised. The patient refused to undergo surgery, so a wait-and-scan approach was decided. At present, after a 1-year follow-up, no significant lesion growth was observed. A 56-year-old man complained tinnitus and right-sided hearing loss persisted for 3 years. He underwent his first otoscopic examination was negative on both sides. Audiometric tests showed right-sided progressive (moderate-to-severe) sensorineural hearing loss for low frequencies (**Figure 2A**), with a slight reduction in detection threshold but no alteration in word discrimination. No spontaneous nystagmus was evoked at the vestibular examination; the Romberg test was negative, and neu-

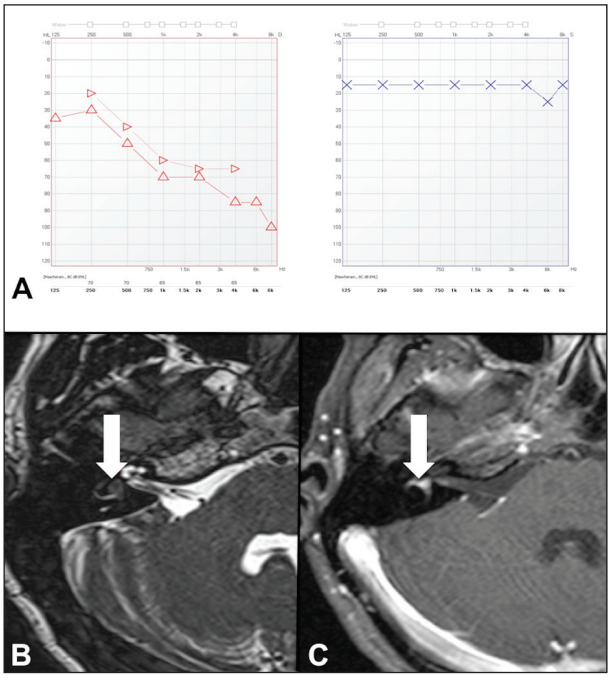

Figure 1. Audiometry results (A), axial volumetric T2w (B) and axial volumetric contrast-enhanced T1w image (C) of Patient#

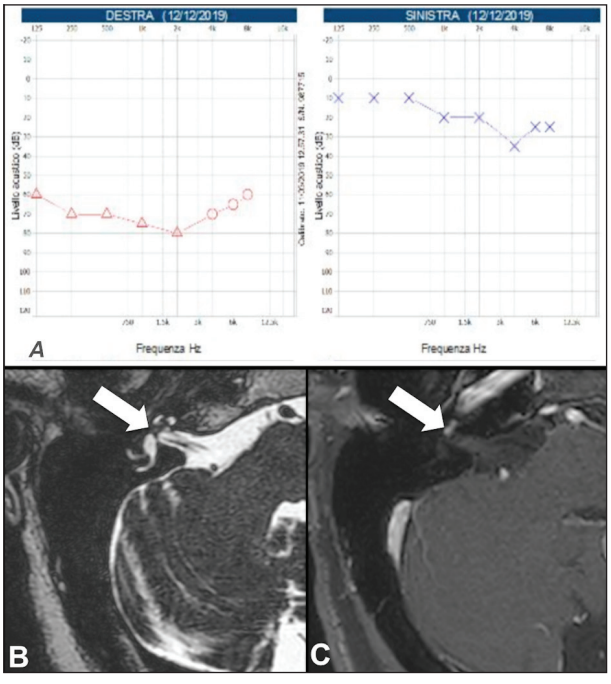

Figure 2. Audiometry results (A), axial volumetric T2w (B) and axial volumetric contrast-enhanced T1w image (C) of Patient#2

rological functions were normal. HIT showed slight hyporeflexia on the affected side. Subsequent contrast-enhanced MRI scan showed the presence of a right ear small intralabyrinthine mass limited to the vestibule without the involvement of the semi-circular canals and vivid enhancement (**Figure 2B-C**), accounting for the diagnosis of ILS. Due to the limited lesion volume and patient's refusal, surgery was temporarily excluded to avoid hearing loss; after a 2-years follow-up, neither audiometry deterioration nor ILS growth was observed. A 29-year-old man complaining recent onset of right ear hearing loss without tinnitus/vertigo came to our attention for ENT evaluation. Otoscopic examination revealed normal findings bilaterally. Audiometry showed right-sided deep pan-tonal sensorineural hearing loss (**Figure 3A**), while the vestibular examination was normal. The patient, therefore, underwent contrast-enhanced MRI showing a right intracochlear mass, involving medium and apical turns of the snail on T2w images (**Figure3B**) with intense contrast enhancement (**Figure 3C**); also in this case, the suspicion of ILS was raised, but the patient refused surgery. After a 3-years follow-up, audiometry confirmed a further deterioration of sensorineural hearing loss, but no significant ILS growth was observed at MRI examination, so wait-and-scan approach was continued.

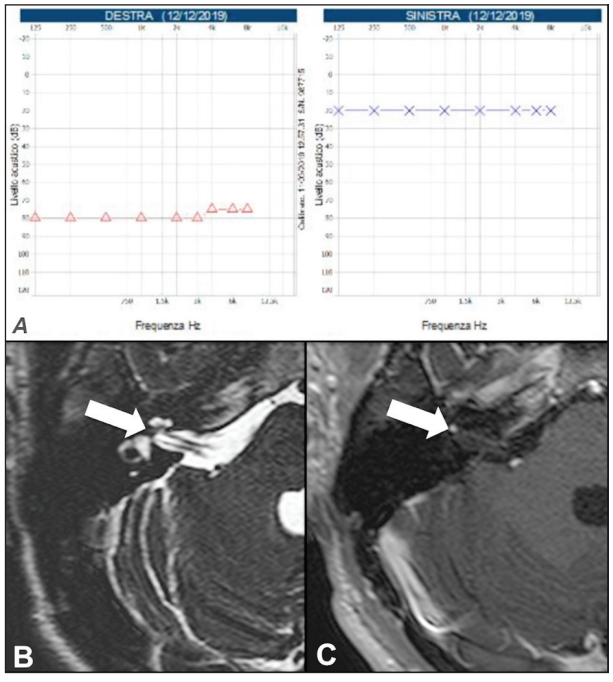

Figure 3. Audiometry results (A), axial volumetric T2w (B) and axial volumetric contrast-enhanced T1w image (C) of Patient#3

Discussion

Schwannoma is the most common benign neoplasm affecting the internal auditory canal and pontocerebellar angle (up to 6% of all intracranial tumors), rising from the ends of cochlear and vestibular nerves (21, 22). ILS is a subtype of schwannoma originating from the perineural Schwann cells of the vestibule-cochlear nerve proximal to the membranous labyrinth (cochlea and vestibule) without any outer extension (23). Although considered a rare disease, its prevalence is higher in some patients' subgroups (i.e., in patients with symptoms accounting for Meniere's disease who underwent MRI, ILS was found in 0.4% patients) (1, 23). A revision of all the ILS cases described in current scientific literature is reported in **Table 1**. Kennedy et al. (21, 22) further classified ILS into 7 categories according to anatomical localization (**Table 2**): intra-cochlear, when confined to the cochlear loops; intra-vestibular, when confined to the vestibule with or without extension into semi-circular canals; vestibule-cochlear, when involving both vestibule and cochlea; trans-macular, when extending from the vestibule to IAC through the lamina cribrosa; trans-modiolar, when extending through the modiolus into the inner auditory canal; tympano-labyrinthine; trans-otic, when involving posterior labyrinth, IAC, and middle ear. In 2013 Van Abel et al. identified 2 more types, respectively, trans-labyrinthine and trans-otic variant into a cerebellopontine angle (1, 10) (**Table 2**).

In recent years, the ILS incidence has increased thanks to the use of more accurate and advanced imaging techniques (14, 19, 22).

In this regard, imaging techniques have assumed a primary role in the study and treatment planning of numerous pathologies (24-27). In particular, MRI represents the golden standard for the diagnosis of ILS, ensuring an accurate depiction of dimension, shape, margins, signal intensity and relation with adjacent structures (21); moreover, MRI is important in pre-surgical planning, as well as in follow-up when a

Table 1. Literature review of intralabyrinthine schwannoma cases reported in current scientific literature

Author	Year	n	Clinical picture	Location
Lee et al.	2019	16	Progressive HL, vertigo	37.5% intracochlear 18.75% intravestibular 18.75% intravestibular-cochlear 12.5% transmodiolar 6.25% transmacular 6.25% nc
Withers et al.	2019	1	Bilateral HL	Intracochlear
Venkatasamy et al.	2019	3	Progressive hearing loss, vertigo	
Pan et al.	2019	1	Unilateral HL, vertigo	
Park et al.	2019	1	HL, vertigo	Intravestibular-cochlear
Thapa et al.	2019	30	72% gradual HL 51% tinnitus 21% dizziness 9% facial nerve paresthesia 12% SNHL	
Marchioni et al.	2018	8	100% HL 62.5% vertigo 75% tinnitus	62.5% intracochlear 12.5% intravestibular 25% transmodiolar
Marinelli et al.	2018	14	29% sudden HL 36% vertigo 29% aural fullness 21% neurofibromatosis type 2	
Bae et al.	2018	9		
Mazzoni et al.	2017	8	Severe HL, vertigo	37.5% transmodiolar 12.5% transotic + CPA 25% transmacular transmodiolar 12.5% transmacular 12.5% intracochlear
Plontke et al. [35]	2017	12	100% hearing loss	
Covelli et al.	2017	1	Hearing fluctuating, vertigo	
Fukushima et al.	2017	1	Sudden hearing loss	
Plontke et al.	2017	1	Sudden hearing loss	
Sabatino et al.	2017	1	Rapidly progressive hearing loss, vertigo	
Jerin et al.	2016	5	40% progressive hearing loss 40% sudden hearing loss 20% vertigo	
Shupak et al.	2016	7	95% progressive hearing loss	
Gosselin et al.	2015	66	No description	50.9% intracoclear 38.2% intravestibular 10.9% intravestibulocochlear
Lee et al.	2015	1	Sudden hearing loss, vertigo	
Dubernard et al.	2014	110	94.5% progressive hearing loss 59.1% vertigo	50% intracochlear 19.2% intravestibular 14.5% transmodiolar 11.8% intravestibulocochlear 2.7% transmacular 1.8% tympanolabyrinthine
Bittencourt et al.	2014	1	Hearing fluctuating and tinnitus	
Kim et al.	2013	1	Sudden hearing loss	
Schutt et al.	2013	1	Hearing fluctuating, ear fullness and vertigo	

Table 1. Literature review of intralabyrinthine schwannoma cases reported in current scientific literature

Author	Year	n	Clinical picture	Location
Van Abel et al.	2013	234	84% progressive hearing loss 3% hearing fluctuation 43% vertigo	51% intracochlear 29% intravestibular 9% intravestibulocochlear 5% transmodiolar 1% transmacular 1% translabyrinthine
Salzaman et al.	2012	45	60% progressive hearing loss 31.11% sudden hearing loss 8.89% hearing fluctuating 35.56% vertigo	31.11% intracochlear 28.88% transmodiolar 15.55% intravestibular 11.11% intravestibulocochlear 8.88% transmacular 4.47% transotic
Gordts et al.	2011	1	Hearing fluctuating and tinnitus	
Magliulo et al.	2009	1	Sudden hearing loss and vertigo	
Brozek-Madry et al.	2009	1	Sudden hearing loss and vertigo	
Tieleman et al.	2008	52	83.67% progressive hearing loss 14.28% sudden hearing loss 19.23% vertigo	80.7% intracochlear 13.5% intravestibular 5.8% intravestibulocochlear
Jia et al.	2008	4	75% progressive hearing loss 25% sudden hearing loss 75% vertigo	
Nishimura et al.	2008	1	Sudden hearing loss and tinnitus	
Lella et al.	2007	7	71.42% progressive hearing loss 28.5% sudden hearing loss 57.14% vertigo	
Kennedy et al.	2004	28	61% progressive hearing loss 32% sudden hearing loss 7% hearing fluctuating 71% tinnitus 29% vertigo	32% intracochlear 21% intravestibular 32% transmodiolar 11% transmacular 4% transotic
Green et al.	1999	4	75% progressive hearing loss 25% sudden hearing loss 75% vertigo	
Deux et al.	1998	3	Progressive hearing loss, tinnitus, vertigo	
Weed et al.	1994	1	Progressive hearing loss, tinnitus	
De Lozier et al.[35]	1979	2	Progressive hearing loss, vertigo	

Table 2. Kennedy's classification of ILSs (modified by Van Abel*)

Class	Areas of ear involved
Intra-vestibular (IV)	Vestibule ± semi-circular canal (SCC)
Intra-cochlear (IC)	Cochlea
Vestibulo-cochlear	Vestibule and cochlea
Trans-modiolar (TMO)	Cochlea and IAC
Trans-macular (TMA)	Vestibule and IAC
Trans-otic	Middle ear and vestibule/cochlea and IAC
Tympano-labyrinthine	Middle ear and vestibule/cochlea
Trans-labyrinthine *	Vestibule and/or SCC + cochlea + Internal auditory meatus (IAM)
Trans-otic variant into CPA *	CPA ± cochlea ± vestibule and/or SCC ± IAM ± Middle ear

"watch-an-wait" strategy is preferred (28). However, for diagnostic purposes, MRI is also crucial in providing imaging clues for differential diagnosis from other causes of vertigo, tinnitus, and hearing loss with negative otoscopic findings (29). E.g., when acute labyrinthitis is suspected MRI shows less pronounced enhancement that gradually decreases and progressively disappears at follow-up (23), whereas schwannoma enhancement does not change over time. In more challenging cases, such as intralabyrinthine extension of otomastoiditis or cholesteatoma, MRI can provide differential diagnosis by the use of diffusion-weighted techniques (30-32). Conversely, only in rare cases, CT can be more informative than MRI, as it happens in case of suspected labyrinthitis ossificans (33).

ILS management options primarily include the "wait and scan" approach, surgical removal, and radiotherapy (34). The "wait and scan" approach, based on longitudinal MRI examinations, relies on the slow growth rate of ILS and on the preservation of inner ear functions (1). The surgical removal is reserved to a limited number of cases (about 3% cases) (10), mostly depending on patients' compliance, tumor size, localization, and growth pattern, and mainly on the presence of intractable symptoms refractory to medical treatment. Surgical ablative treatment results in total hearing loss in 100% of cases; moor inconstant consequences also include facial nerve palsy (4%), cerebrospinal fluid leakage (5.4%), and meningeal inflammation (1.8%) (1, 34). At present only few cases of ILS stereotactic radiosurgery have been reported (1), generally reserved to patients who cannot undergo surgery due to systemic counter-indications and intractable symptoms; however, no significant effect on vertigo was observed, whereas the probability of neurological side-effects and malignant tumor transformation was increased (1). Finally, recent studies reported some cases of ILS treatment by trans-tympanic steroid and intra-tympanic gentamicin injections, improving clinical outcomes in those cases were vestibular impairment was relatively more prominent than hearing loss (1, 35).

In conclusion, although ILS is a very rare pathology, its incidence has increased in recent years due to the availability of more accurate imaging techniques. As well documented in both neurological and other clinical specialties, diagnostic investigations and interventional radiology represent a fundamental integration to clinical evaluation. MRI is the gold standard both for ILS diagnosis and preoperative management, also allowing for differential diagnosis between ILS and possible mimickers. Several algorithms for ILS management have been proposed, but no consensus concerning the best therapeutic strategy was reached. At present, a tailored therapeutic approach based on the multidisciplinary evaluation of every single case should be considered the best option to be pursued.

Conflict of interest: Authors declare that they have no commercial associations (e.g. consultancies, stock ownership, equity interest, patent/licensing arrangement etc.) that might pose a conflict of interest in connection with the submitted article.

References

1. Covelli E, Volpini L, Filippi C, et al. Intralabyrinthine Vestibular Schwannoma Responsive to Intratympanic Gentamicin Treatment. J Int Adv Otol 2017; 13: 285-88.
2. Moccia F, Zuccolo E, Poletto V, et al. Targeting Stim and Orai Proteins as an Alternative Approach in Anticancer Therapy. Curr Med Chem 2016; 23: 3450-80.
3. Zuccolo E, Dragoni S, Poletto V, et al. Arachidonic acide-voked Ca(2+) signals promote nitric oxide release and proliferation in human endothelial colony forming cells. Vascul Pharmacol 2016; 87: 159-71.
4. Zuccolo E, Lim D, Kheder DA, et al. Acetylcholine induces intracellular Ca(2+) oscillations and nitric oxide release in mouse brain endothelial cells. Cell Calcium 2017; 66: 33-47.
5. Zuccolo E, Kheder DA, Lim D, et al. Glutamate triggers intracellular Ca(2+) oscillations and nitric oxide release by inducing NAADP- and InsP3 -dependent Ca(2+) release in mouse brain endothelial cells. J Cell Physiol 2019; 234: 3538-54.
6. Coppola N, Perna A, Lucariello A, et al. Effects of treatment with Maraviroc a CCR5 inhibitor on a human hepatic stellate cell line. J Cell Physiol 2018; 233: 6224-31.
7. Perna A, Lucariello A, Sellitto C, et al. Different Cell Cycle Modulation in SKOV-3 Ovarian Cancer Cell Line by Anti-HIV Drugs. Oncol Res 2017; 25: 1617-24.
8. Esposito T, Lucariello A, Hay E, et al. Effects of curcumin and its adjuvant on TPC1 thyroid cell line. Chem Biol Interact 2019; 305: 112-18.
9. Doyle KJ, Brackmann DE. Intralabyrinthine schwannomas. Otolaryngol Head Neck Surg 1994; 110: 517-23.
10. Van Abel KM, Carlson ML, Link MJ, et al. Primary inner ear schwannomas: a case series and systematic review of the literature. Laryngoscope 2013; 123: 1957-66.

11. Gibelli D, Cellina M, Gibelli S, Oliva AG, Termine G, Sforza C. Anatomical variants of sphenoid sinuses pneumatisation: a CT scan study on a Northern Italian population. Radiol Med 2017; 122: 575-80.
12. Cellina M, Fetoni V, Baron P, Orsi M, Oliva G. Unusual primary central nervous system lymphoma location involving the fourth ventricle and hypothalamus. Neuroradiol J 2015; 28: 120-5.
13. Striano P, Tortora F, Evoli A, et al. Periodic myoclonus due to cytomegalovirus encephalitis in a patient with good syndrome. Arch Neurol 2007; 64: 277-9.
14. Cocozza S, Russo C, Pontillo G, et al. Is advanced neuroimaging for neuroradiologists? A systematic review of the scientific literature of the last decade. Neuroradiology 2016; 58: 1233-39.
15. Ottaviano G, Cantone E, D'Errico A, et al. Sniffin' Sticks and olfactory system imaging in patients with Kallmann syndrome. Int Forum Allergy Rhinol 2015; 5: 855-61.
16. Tortora F, Prudente M, Cirillo M, et al. Diagnostic accuracy of short-time inversion recovery sequence in Graves' Ophthalmopathy before and after prednisone treatment. Neuroradiology 2014; 56: 353-61.
17. Varrassi M, Cobianchi Bellisari F, Bruno F, et al. High-resolution magnetic resonance imaging at 3T of pituitary gland: advantages and pitfalls. Gland Surg 2019; 8: S208-s15.
18. D'Orazio F, Splendiani A, Gallucci M. 320-Row Detector Dynamic 4D-CTA for the Assessment of Brain and Spinal Cord Vascular Shunting Malformations. A Technical Note. Neuroradiol J 2014; 27: 710-7.
19. Tieleman A, Casselman JW, Somers T, et al. Imaging of intralabyrinthine schwannomas: a retrospective study of 52 cases with emphasis on lesion growth. AJNR Am J Neuroradiol 2008; 29: 898-905.
20. Plontke SK, Rahne T, Pfister M, et al. Intralabyrinthine schwannomas : Surgical management and hearing rehabilitation with cochlear implants. Hno 2017; 65: 136-48.
21. Kennedy RJ, Shelton C, Salzman KL, Davidson HC, Harnsberger HR. Intralabyrinthine schwannomas: diagnosis, management, and a new classification system. Otol Neurotol 2004; 25: 160-7.
22. Salzman KL, Childs AM, Davidson HC, Kennedy RJ, Shelton C, Harnsberger HR. Intralabyrinthine schwannomas: imaging diagnosis and classification. AJNR Am J Neuroradiol 2012; 33: 104-9.
23. Sabatino L, Greco F, Quattrocchi CC, Salvinelli F, Casale M. "Canalolabyrinthine Schwannoma," A Rare Variant of Intralabyrinthine Schwannoma: A Case Report. J Int Adv Otol 2017; 13: 140-42.
24. Cappabianca S, Colella G, Russo A, et al. Maxillofacial fibrous dysplasia: personal experience with gadoliniumenhanced magnetic resonance imaging. Radiol Med 2008; 113: 1198-210.
25. Bonomo P, Desideri I, Loi M, et al. Elderly patients affected by head and neck squamous cell carcinoma unfit for standard curative treatment: Is de-intensified, hypofractionated radiotherapy a feasible strategy? Oral Oncology 2017; 74: 142-47.
26. Conforti R, Marrone V, Sardaro A, Faella P, Grassi R, Cappabianca S. From anatomy to image: The cranial nerves at MRI. Recenti Progressi in Medicina 2013; 104: 308-13.
27. Desideri I, Francolini G, Carta GA, et al. Efficacy and tolerability of cyberknife stereotactic robotic radiotherapy for primary or secondary orbital lesions: A single-center retrospective experience. Technology in Cancer Research and Treatment 2019; 18:
28. Choudhury B, Carlson ML, Jethanamest D. Intralabyrinthine Schwannomas: Disease Presentation, Tumor Management, and Hearing Rehabilitation. J Neurol Surg B Skull Base 2019; 80: 196-202.
29. Bykowski J, Mafee MF. Intralabyrinthine pathology: Role of imaging. Operative Techniques in Otolaryngology-Head and Neck Surgery 2014; 25: 29-35.
30. Patel KM, Almutairi A, Mafee MF. Acute otomastoiditis and its complications: Role of imaging. Operative Techniques in Otolaryngology-Head and Neck Surgery 2014; 25: 21-28.
31. Elefante A, Cavaliere M, Russo C, et al. Diffusion weighted MR imaging of primary and recurrent middle ear cholesteatoma: an assessment by readers with different expertise. Biomed Res Int 2015; 2015: 597896.
32. Cavaliere M, Di Lullo AM, Caruso A, et al. Diffusion-weighted intensity magnetic resonance in the preoperative diagnosis of cholesteatoma. ORL J Otorhinolaryngol Relat Spec 2014; 76: 212-21.
33. Buch K, Baylosis B, Fujita A, et al. Etiology-Specific Mineralization Patterns in Patients with Labyrinthitis Ossificans. AJNR Am J Neuroradiol 2019; 40: 551-57.
34. Grayeli AB, Fond C, Kalamarides M, et al. Diagnosis and management of intracochlear schwannomas. Otol Neurotol 2007; 28: 951-7.
35. Iseri M, Ulubil SA, Topdag M, Oran A. Hearing loss owing to intralabyrinthine schwannoma responsive to intratympanic steroid treatment. J Otolaryngol Head Neck Surg 2009; 38: E95-7.

Received: 20 May 2020
Accepted: 10 June 2020
Correspondence:
Fabio Tortora, MD, Associate Professor
Department of Advanced Biomedical Sciences
University of Naples "Federico II", Naples, Italy
Via Pansini, 5 - 80131 Naples - Italy
Tel: 0039 333 7050711
E-mail: fabio.tortora@unina.it